UNIVERSIDADE DE LISBOA

FACULDADE DE FARMÁCIA

DEPARTAMENTO DE FARMÁCIA GALÉNICA E TECNOLOGIA FARMACÊUTICA

Production and mechanistic evaluation of the stability of polymorphic olanzapine in solid dosage forms

Maria de Castro Paisana

Orientador: Professor Doutor João F. Pinto
Co-orientador: Professor Doutor Martin A. Wahl

Tese especialmente elaborada para obtenção do grau de Doutor em Farmácia
(Tecnologia Farmacêutica)

Lisboa, 2016

UNIVERSIDADE DE LISBOA

FACULDADE DE FARMÁCIA

DEPARTAMENTO DE FARMÁCIA GALÉNICA E TECNOLOGIA FARMACÊUTICA

U

LISBOA

UNIVERSIDADE
DE LISBOA

Production and mechanistic evaluation of the stability of polymorphic olanzapine in solid dosage forms

Maria de Castro Paisana

Orientador: Professor Doutor João F. Pinto

Co-orientador: Professor Doutor Martin A. Wahl

Tese especialmente elaborada para obtenção do grau de Doutor em Farmácia
(Tecnologia Farmacêutica)

Júri:

<u>Presidente</u>:

Professora Doutora Matilde F. Castro

<u>Vogais</u>:

Professor Doutor João José M. Simões de Sousa

Professor Doutor Chris Vervaet

Professora Doutora Helena M. Cabral Marques

Professora Doutora Maria Helena A. R. Amaral

Professor Doutor Luís F. P. Gouveia

Lisboa, 2016

UNIVERSIDADE DE LISBOA

FACULDADE DE FARMÁCIA

DEPARTAMENTO DE FARMÁCIA GALÉNICA E TECNOLOGIA FARMACÊUTICA

Production and mechanistic evaluation of the stability of polymorphic olanzapine in solid dosage forms

Tese especialmente elaborada para obtenção do grau de Doutor em Farmácia
(Tecnologia Farmacêutica)

Lisboa, 2016

À minha família,

Ao Luís,

"Onde há uma vontade, há um caminho"
George Bernard Shaw

x

Acknowledgments

Table of Contents

Abstract (670 words)

Research related to drug polymorphism is an important aspect in drug product development since the properties of a formulated product, such as its stability and bioavailability, are often directly related to the physicochemical properties of the existing polymorph in the formulation. Olanzapine (OLZ) belongs to a new generation of benzodiazepines for the treatment of schizophrenia and other related psychoses and may exist in several crystalline forms, including polymorphic anhydrates, hydrates and solvates. Consequently, the physical treatments and technological processes undergone by the drug may have an impact on its solid-state, which in turn may affect its performance in terms of dissolution rate, absorption and therapeutic activity and response. OLZ Form I is the form used in marketed tablets and the most stable form at room temperature.

The work presented in this Thesis aimed to provide an in-depth understanding of the conversion of olanzapine polymorphic forms into hydrated forms when exposed to different processing conditions. To perform this study we used several techniques, such as a combination of thermal analysis (differential scanning calorimetry (DSC), thermogravimetry (TGA) and hot stage microscopy (HSM)) with spectroscopic (infrared spectroscopy – DRIFT; FTIR), diffraction analysis (XRPD) and surface measurements (contact angle and surface free energy). Dissolution performance and impact of polymorphism on the mechanical characteristic of solid dosage forms was also evaluated.

At first, a thorough investigation of the solid state stability of olanzapine forms I and II was performed. Aspects such as the interaction with water and the conversion of both forms into different dihydrates were fully explored. This allowed the successful clarification of the higher hygroscopic nature and easier ability of olanzapine Form II to undergo hydrate formation. On the other hand, Form I showed to hydrate into the lowest soluble form of olanzapine - dihydrate D – when subjected to high RH environments. The interaction of Form I with humidity and excipients was fully investigated. Form I was found to hydrate at different rates depending on the excipients in which it is formulated. Polymers such as polyethylene glycol (PEG) and hydroxypropyl cellulose (HPC) could induce hydrate transformation at lower relative humidity (75%), whereas PVP could avoid hydrate conversions at 93% RH. PEG, when physically mixed with olanzapine, showed to accelerate hydrate conversion, especially when the materials were subjected to a tableting process before storage. This study showed an interesting interplay between the polymer's choice, load and chemistry that could further be used to maintain the stability of olanzapine in solid-dosage products.

Transformations of olanzapine during processing, namely during the rapid expansion of supercritical solutions (RESS) and rapid expansion of supercritical solutions into aqueous solutions (RESSAS) processes were also taken into consideration. These technologies enabled

the production of nanoparticles and nanosuspensions of olanzapine, respectively. During the RESSAS process the selection of the right excipients was imperative to produce stable nanosuspensions before and after freeze drying the products.

Microcrystalline cellulose and polymers (PEG, PVP and HPC) were used in the process of extrusion and spheronisation of olanzapine. The transformations which occur during processing (wet environments are involved) and during dissolution of the pellets were taken into consideration. During the extrusion process olanzapine showed to hydrate into a mixture of different hydrates when extruded in the presence of microcrystalline cellulose. The addition of polymers such as PVP and HPC to the formulation allowed olanzapine to remain anhydrous during processing and dissolution, which showed to significantly influence the dissolution of the drug. PEG, on the other hand, could not avoid the hydrate formation of olanzapine, having this transformation an impact on the physical and mechanical characteristics of the pellets, as well as an impact on the drug performance. The impact of the polymer content and molecular weight into olanzapine stabilization during wetting were also taken into consideration.

In conclusion, the research carried out contributed to a better understanding of the complex characterization of solid state olanzapine and formulated products prepared by different technologies. In detail, it showed the impact of polymorphic/pseudopolymorphic changes on OLZ's technological performance and dissolution, which highlighted the importance of this study during preformulation and formulation studies.

Resumo (803 palavras)

O estudo do polimorfismo de fármacos é uma área científica importante no desenvolvimento de formas farmacêuticas sólidas, uma vez que as propriedades de um produto formulado, tais como estabilidade e biodisponibilidade, estão muitas vezes diretamente relacionadas com as propriedades físico-químicas dos polimorfos existentes na formulação. A olanzapina (OLZ) pertence a uma nova geração de benzodiazepínicos para o tratamento da esquizofrenia e outras psicoses relacionadas. Este fármaco pode existir em várias formas cristalinas, incluindo formas anidras, hidratadas e solvatadas. Por conseguinte, os tratamentos físicos e processos tecnológicos sofridos pelo fármaco podem ter um impacto na estabilidade da forma polimórfica escolhida para o produto final. Consequentemente, estes processamentos podem afetar o seu desempenho em termos de taxa de dissolução, absorção e, finalmente, atividade terapêutica. A olanzapina Forma I é a forma usada nos comprimidos existentes no mercado e é a forma polimórfica mais estável à temperatura ambiente.

O trabalho apresentado nesta tese teve como objetivo obter uma compreensão aprofundada da conversão de formas polimórficas de olanzapina em formas hidratadas quando expostas a diferentes condições de processamento. Para tal, neste trabalho foram utilizadas diversas técnicas, tais como uma combinação de análise térmica (DSC, TGA, HSM) com espectroscópica (DRIFT; FTIR), análise de difração (XRPD) e energia de superfície (medições de ângulo de contacto e energia livre de superfície). Foi também avaliada a dissolução e o impacto do polimorfismo nas características mecânicas das formas farmacêuticas sólidas.

Primeiramente foi realizada uma investigação completa sobre a estabilidade das formas cristalinas anidras I e II. Aspetos como o estudo da estabilidade das formas quando em presença de diferentes humidades relativas e caracterização dos hidratos formados foram explorados. Este estudo permitiu concluir que a Forma cristalina II é mais higroscópica, hidratando mais rapidamente e a menores humidades relativas do que a Forma I. A forma I, por outro lado, mostrou hidratar numa forma hidratada – dihidrato D – que apresenta uma velocidade de dissolução inferior às outras formas hidratadas da olanzapina, alertando para a necessidade de um armazenamento apropriado para este fármaco. Visto que os excipientes podem alterar as cinéticas de hidratação, estes podem fazer com que esta forma hidratada da olanzapina apareça a humidades mais reduzidas e com maior velocidade. Assim sendo, foram investigadas a interação da forma I com humidade e excipientes. Estando descrito que os excipientes poliméricos poderão ter maior impacto no processo de hidratação, 3 polímeros foram escolhidos para o estudo. A Forma I mostrou hidratar a velocidades diferentes, dependendo dos excipientes em que foi formulada. Polímeros, tais como PEG e HPC, mostraram induzir a transformação no hidrato D a uma humidade relativa baixa (75% RH), enquanto a PVP mostrou evitar quaisquer conversões, mesmo a humidades relativas de 93%. O PEG quando misturado fisicamente com

olanzapina, mostrou acelerar a conversão em hidrato, especialmente se estas misturas físicas tenham sido pressionadas (submetidas a um processo compactação) antes do armazenamento. Este estudo mostrou que deve ser feito um balanço quando é feita a escolha dos polímeros a serem usados no processo de formulação, nomeadamente tendo em conta a quantidade usada e a sua estrutura química, de forma a manter a estabilidade da olanzapina em formas farmacêuticas sólidas.

As transformações da olanzapina durante o processo RESS / RESSAS foram igualmente estudadas. Estas tecnologias permitiram produzir nanopartículas e nanossuspensões de olanzapina, respetivamente. Durante o processo de RESSAS a seleção dos excipientes estabilizadores das suspensões formadas mostrou ser imperativa para produzir nanossuspensões estáveis antes e após o processo de secagem por congelação.

A celulose microcristalina, bem como os diferentes polímeros utilizados neste trabalho (PVP, PEG, HPC) foram usados no processo de extrusão e esferonização da olanzapina. Foram estudadas as transformações que ocorreram durante o processamento (ambientes húmidos estão envolvidos) e durante a dissolução dos esferóides. Durante a extrusão a olanzapina mostrou hidratar numa mistura de diferentes hidratos apenas quando em presença da celulose microcristalina. A adição de polímeros à formulação, tais como o PVP e a HPC, permitiram a manutenção da olanzapina na sua forma anidra I tanto durante o processamento como durante a dissolução, o que mostrou influenciar de forma significativa a dissolução da mesma. O PEG, por outro lado, mostrou ser incapaz de estabilizar a olanzapina. Os hidratos formados durante o processo de extrusão mostraram afetar as características físicas e mecânicas dos *pellets*, bem como a dissolução do fármaco. Os diferentes polímeros usados, os seus pesos moleculares e as suas proporções nas formulações revelaram ter impacto na estabilização da olanzapina durante o processo de extrusão, nomeadamente durante a fase de malaxagem.

Em conclusão, a investigação feita no âmbito desta Tese contribuiu para uma melhor compreensão da caracterização das alterações polimórficas e pseudopolimórficas da olanzapina durante o seu processamento e armazenamento. Permitiu ainda perceber em pormenor o impacto das alterações polimórficas e pseudopolimórficas na performance tecnológica e na dissolução da olanzapina, alertando para a importância do seu estudo nas fases de pré-formulação e formulação.

List of Tables

List of Figures

List of Abbreviations & Symbols

API	Active pharmaceutical ingredient
DRIFT	Diffuse reflectance infrared Fourier transform
DSC	Differential scanning calorimetry
FTIR	Fourier transform infra-red
HPC	Hydroxypropyl cellulose
HPMC	Hydroxypropylmetyl cellulose
HSM	Hot stage microscopy
MCC	Microcrystalline cellulose
mDSC	Modulated temperature DSC
MW	Molecular weight
OLZ	Olanzapine
PbS	Polysorbate
PEG	Polyethylene glycol
PM	Physical mixture
PVP	Polyvinylpyrrolidone
RH	Relative humidity
Rpm	Rotation per minute
SD	Standard deviation
SEM	Scanning electron microscope
T_g	Glass transition temperature
TGA	Thermogravimetric analysis
T_m	Melting temperature
UV	Ultraviolet
XRPD	X-ray powder diffraction

Motivation and Objectives

The studies on pre-formulation of drugs are part of the official requirements for the investigation and development of new drugs and new drug applications, since these studies assess the physicochemical properties and the biopharmaceutical performance of the APIs.

Pharmaceutical companies have been paying special attention to research on phase transformations of the APIs because such transformations could lead to complications on the bioavailability, manufacturability and stability of the formulated product. Therefore, the study of polymorphic and pseudopolymorphic transformations of the drugs, alone or in the presence of excipients during processing and storage, has to be undertaken since an incomplete characterization of a drug substance can lead to problems on the manufacturability and bioavailability of the final product.

The aim of this research was the production and characterization of different olanzapine crystal forms (polymorphs and pseudopolymorphs), assessing the stability of each crystal form during storage and processing, always with the clear objective of understanding the impact of processing on the technological properties, particularly on the dissolution rate of the drug.

This goal was reached by:

– Controlled production and characterization of defined polymorphic forms;

– Understanding the polymorphic transitions to allow the anticipation of stability of each polymorph as a raw material or as a component of an extrudate;

– Understanding the potential interactions between the API and the excipients, namely the stabilization effect that the excipient might have on the polymorph;

– The identification of environmental conditions that affect the stability of polymorphs (e.g. humidity, in the air or in the excipients while being processed, and temperature, both room and processing temperatures on drying);

– Study of the impact of particle size reduction techniques, namely SCF technology, on the technological properties and dissolution of olanzapine;

– The identification of polymorphic forms at each moment of the manufacturing of extrudates and tablets, as well as the identification of the advantages / disadvantages on using a particular polymorph of the API on the preparation of an extrudate or tablet

Thesis overview

This thesis is divided into 8 chapters. Since olanzapine has a high capacity to interact with water molecules and form hydrates, firstly it was aimed to understand the role of water on the stability of olanzapine. Then we decided to mix olanzapine with certain excipients which are known to affect the water absorption capability of drugs when physically mixed or processed with them. Two pharmaceutical processes involving the utilization of water were studied, namely, rapid expansion of supercritical solutions into aqueous solutions and wet extrusion. Hence, the organization and objectives of each chapter can be briefly summarized, as follows:

Chapter 1 – Describes the state of the art and provides the main concepts necessary to understand and discuss the work presented in the subsequent chapters;

Chapter 2 – Summarizes the materials used, namely the API and excipients, throughout the thesis. The different technologies considered for producing and characterizing the different polymorphs of olanzapine and dosage forms are referred in this chapter, together with a short description of the characteristics of the equipments used.

Chapter 3 – Provides a thorough investigation of the different olanzapine forms (anhydrates and hydrates) considered in the thesis. Differentiation on the physical stability of 2 anhydrous forms and their ability to form hydrates, as function of different relative humidity, is studied.

Research question: Can anhydrous olanzapine hydrate in the presence of high humidity environments? What is the impact of the hydrate conversions on the dissolution performance of this drug?

Chapter 4 – Explores the relative humidity conditions that could lead to the hydrate formation of olanzapine Form I (the most stable form) when physically mixed with different excipients (as powders or compacts) that present different crystallinities and moisture uptake abilities.

Research question: May excipients have a role on hydrate conversion kinetics of olanzapine over storage? What is the impact of compaction of olanzapine and excipients on the pseudopolymorphic transformations of olanzapine?

Chapter 5 – Gives an insight into the role of polymers on stabilization of olanzapine Form I (the most stable form) in aqueous environments.

Research question: How polymers may stabilize anhydrous olanzapine in aqueous suspensions?

Chapter 6 – Provides an evaluation of the effect of particle size reduction of olanzapine by supercritical fluid (SCF) technology on the solid-state form of olanzapine.

Research question: Can SCF technology reduce the particle size of olanzapine without affecting its crystal structure? Can SCF technology produce olanzapine particles with a submicron size and increased dissolution rate? What is the impact of excipients in the stabilization of submicron particles of OLZ?

Chapter 7 – Identifies the impact of the extrusion/spheronisation process on the polymorphic transformation of olanzapine, with a special focus on the impact of those transformations on the mechanical properties of the final product (pellets).

Research question: Can the process of extrusion lead to hydrate changes of olanzapine solid-state form, with an impact on physical and mechanical properties of the extrudates?

Chapter 8 – Explores how excipients used in extrusion/ spheronisation of wet masses of olanzapine can avoid pseudopolymorphic changes of olanzapine, with an impact on dissolution.

Research question: May excipients have a role on the stabilization of olanzapine during wet extrusion? What is the impact of hydrate conversion on the final dissolution of olanzapine from the pellets?

Chapter 9 – Presents the main conclusions and suggests future work.

Hypothesis

Polymorphic/pseudopolymorphic changes of olanzapine which occur during storage and processing with impact on drug's performance can be identified, characterized and prevented.

CHAPTER 1

Chapter 1 - Introduction

1.1 Introduction to solid-state properties of materials used in pharmacy

The majority of drug entities are encountered in the solid state (1). A full characterization of the solid characteristics of an active pharmaceutical ingredient (API) is recognized as an essential part of pre-formulation research, in order for the quality of the manufacturing process, the drug's performance and its bioavailability are maintained in its final dosage form (2). A solid state API can be classified based upon the order of its molecular packing into 2 major groups: the crystalline and the amorphous states.

1.1.1 Amorphous State

An amorphous structure has a short-range molecular order (3). The increased free volume, molecular mobility and the enthalpy of the amorphous state results in a structure with higher solubility, chemical reactivity and water vapor sorption when compared to the crystalline state (4). The higher solubility of an amorphous API, for example, is an advantage when rapid dissolution and absorption rates are required to obtain an increase of the bioavailability of the drug (5). However, the amorphous state is in a non-equilibrium state, thus an amorphous API may crystallize during storage or during a manufacturing process (6). The most used methods for large-scale production of amorphous materials at the moment are freeze-drying, spray-drying and melt extrusion, being freeze-drying the most popular method, resulting from the easy control of operation parameters throughout the production of amorphous materials. Usually, excipients are added to the formulations to improve the stability of amorphous drug formulations (7).

1.1.2 Crystalline state

A crystalline state requires an ideal crystal, which is composed of atoms, ions or molecules arranged in a periodic 3-dimensionl pattern. The 3-dimensional array is called a lattice. The smallest periodic volume is defined as a unit cell (Figure 1.1). The unit cell has an orientation and shape defined by the translational vectors, a, b, and c and therefore has a definite volume, V, that contains the atoms and molecules necessary to form the crystal (8).
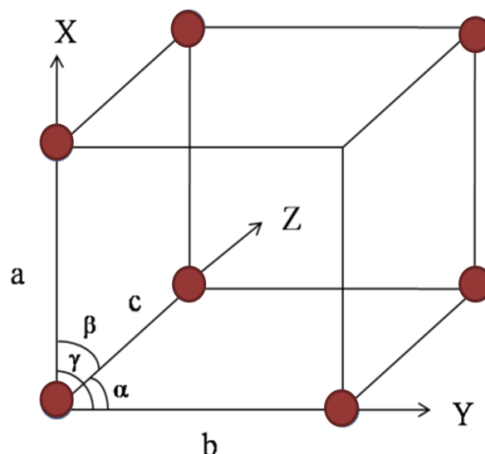
Figure 1.1 – Crystal unit cell and its dimensions.

There are seven possible crystal systems (cubic, tetragonal, orthorhombic, rhombohedral, hexagonal, monoclinic, triclinic) which are described by the relationships between the axis lengths, *a*, *b*, and *c*, of the unit cell and between the angles, α, β, and γ of the unit cell (8, 9). For instance, if the three edge lengths are identical and all corner angles are 90º, then the crystal belongs to the cubic system.
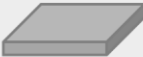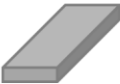
In any kind of repeating pattern, it is useful to have a convenient way of specifying the orientation elements relative to the unit cell. This is carried out by assigning to each element a set of integer numbers, known as Miller index. Miller indices are a notation for describing directions and labelling planes in lattices and crystals. The basis for determining the index is the unit cell (the smallest three-dimensional volume element from which the crystal can be constructed). Each face is designated with three integers, *h, k and l,* which are the inverse of intersections of that face with the crystallographic axes *a, b* and *c*. Faces that are parallel to a crystal axis are given the Miller index of 0.

The external shape of a crystal, also termed habit, form or morphology, is determined by its internal structural symmetry. In practice, crystal morphology is usually described in terms of length, width and thickness. Six basic crystal shapes have been reported and crystals having these shapes can occur in any of the seven systems (10). In the pharmaceutical area the classifications of crystal shapes adopted by either British Standard (BS 2955:1993) or the US Pharmacopoeia (monograph 776, Table 1.1) (11) are often used for routine microscopic studies of solid materials (12-14).

The faces that can potentially develop into a crystal are determined by the symmetry properties of the underlying lattice, but the sizes of the faces that actually develop under specific conditions – and thus the overall shape of the crystal – are determined by the relative growth rate of the various faces. The slower the growth rate the larger the face.

Powders that have been milled may not present any evidence of the original shapes of the crystal, and the particles are likely to be irregularly shaped and have angular fragments (10).

Table 1.1 – Classification of common crystal morphologies for pharmaceutical solids accepted by the US Pharmacopoeia.

Morphology	Description	Diagram
Equant	Crystal with similar length, width and thickness	
Flakes	Thin, flat crystals of similar width and length	
Plates	Flat, tabular crystals with similar width and length but thicker than flakes	
Laths	Elongated, thin and blade-like crystals	
Needles	Acicular, thin and highly elongated crystals having similar width and breadth	
Columnar	Elongated, prismatic crystals with greater width and thickness than needles	

1.2 Polymorphism

A crystalline substance has polymorphism (from Greek: *poly*-multiple, *morfe*-shape) when it can crystallize in different crystal packing arrangements and/or different conformations (15). Polymorphism in molecular crystals can be divided into two categories: conformational and packing polymorphism. In conformational polymorphism, the molecules are flexible and can adopt more than one conformation in the solid state (16). Since pharmaceutical compounds generally contain flexible moieties in their molecular structures, there are numerous examples of conformational polymorphs. Two well-known examples of drugs that exhibit this type of conformational polymorphism are the antidepressant venlafaxine hydrochloride (17) and the antipsychotic olanzapine (18). Packing polymorphism emerge from different possible packing arrangements in the three dimensional space of conformational rigid molecules. Forms I and II of acetaminophen are the best known example of packing polymorphs (19, 20).

Polymorphs have different relative intermolecular and/or inter atomic distances, or unit cells, resulting in different physical and chemical properties, as shown in Table 1.2 (21).

Table 1.2 – Properties that can be altered by choosing different polymorphic forms (21)

Thermodynamic properties	Kinetic properties
- Melting and sublimation temperatures - Enthalpy, entropy and heat capacity - Free energy - Solubility	- Dissolution rate - Rates of solid state reaction - Physical/chemical stability - Rate of nucleation/ crystal growth
Packing Properties	**Surface properties**
- Molar volume and density - Refractive index - Particle morphology - Hygroscopicity - Color	- Surface free energy - Interfacial tensions - Habit
Mechanical properties	
- Hardness - Compactibility and tableting - Cleavage	- Tensile strength - Handling, flow - Blending

The different properties of a polymorph can have an impact in the drug's pharmaceutical properties such as bioavailability, processability and manufacturability. Some of the most important properties during drug discovery and development are solubility in water, dissolution and bioavailability. For a drug whose absorption into the body is only limited by its dissolution, differences in the apparent solubility of the various polymorphic forms are likely to affect the bioavailability of the drug (22). It is the goal of pre-formulation scientists to understand and characterize polymorphs of a pharmaceutical solid and select a form with the best combination of desired properties to proceed to the formulation stage (23). Furthermore, regulatory agencies declare that the understanding and controlling of the physical forms of a polymorphic drug substance have to be controlled, especially if drug bioavailability is affected by its polymorphism (24) (25).

1.2.1 Polymorphic systems

The term "polymorphic transition" refers to the interconversion between polymorphic forms. The stability relationship between a pair of polymorphs can be categorized as Monotropic or Enantiotropic, depending on their stability with respect to a range of temperatures and pressures. When one polymorph is stable at all temperatures and pressures below the melting point and all other polymorphs are unstable, the polymorphic system is

referred as Monotropic. If one of the polymorphs is stable (i.e., has lower free energy and solubility) over a certain temperature range and pressure while the other polymorph is stable over a different temperature range and pressure, then the two polymorphs are said to be Enantiotropes (Figure 1.2) (6, 26). Therefore, understanding thermodynamic and interconversion relationships between polymorphs is paramount to solid state characterization.
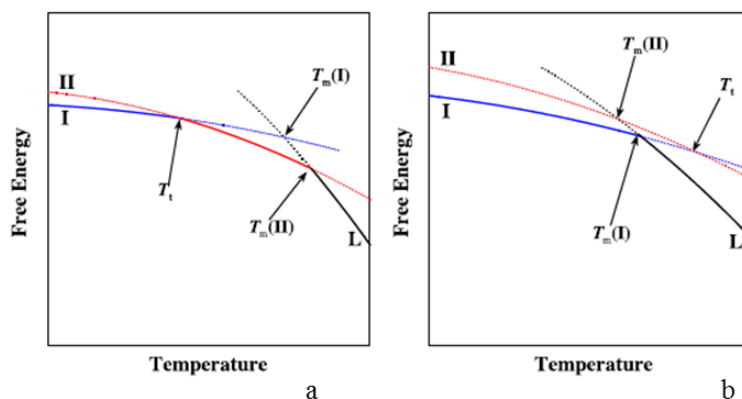
Figure 1.2 – Free energy phase diagrams for Enantiotropic System (a) and Monotropic System (b) (6).

The question that still needs to be addressed is why and how polymorphs do form. Like most chemical processes, crystallization in polymorphic systems is governed by a combination of thermodynamic and kinetic factors.

1.2.2 Thermodynamics

Systems tend to move toward a thermodynamically equilibrated state, i.e., in the polymorphic systems the metastable forms are eventually going to transform into the most stable state. Thermodynamics provides information about the relative thermodynamic stability between different polymorphic forms and the conditions and the direction in which a transformation can occur. The main approaches used to assess thermodynamic stability relationships of polymorphs are based on thermodynamic rules (distinguishes between monotropic and enantiotropic systems) (26) and free energy change–temperature diagrams (also allows for calculation of the transition temperature) (27, 28).

The relative thermodynamic stability of solids and the driving force for a transformation at constant temperature and pressure depends on the difference in Gibbs free energy (ΔG) between the different forms. When the difference is negative, the transformation may occur spontaneously and a change has the potential to continue to occur as long as the free energy of the system decreases, unless blocked by a kinetic barrier. If ΔG is equal to zero the system is at equilibrium with respect to the transformation and the Gibbs energy of the two phases is the same. In systems where the difference in Gibbs energy is positive then the transformation is not possible under the specific conditions

The thermodynamic conditions to either have equilibrium between phases or different transformations at constant pressure for a single component system that exists in both amorphous and crystalline states are shown in the Gibbs free energy plot (Figure 1.3). This diagram shows that polymorph C is more stable than A, since $\Delta G = G_C - G_A$ is lower than 0, thus allowing for a transformation from polymorph A to C. Amorphous or disordered solids of the same compound have a higher free energy than the crystalline states because of the higher enthalpy and entropy of the glass (28) .

In the G versus T diagram, the intersection points show phases that coexist in equilibrium, crystal and liquid states corresponding to melting temperatures, crystalline states at transition temperatures, and both amorphous and supercooled liquid states at glass transition temperatures.
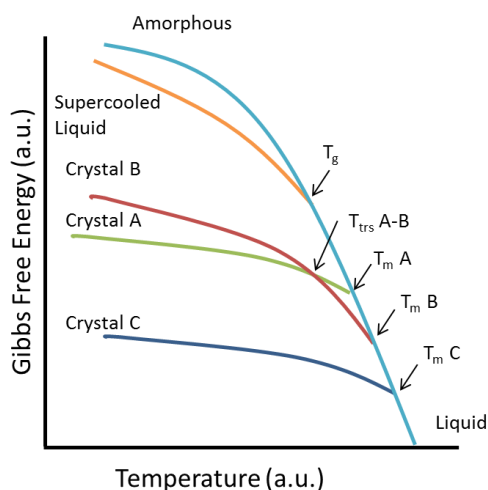
Figure 1.3 – Gibbs free energy curves for a component system that presents crystalline and amorphous phase transitions. Monotropic systems (A and C), enantiotropic systems (A and B) with a transition temperature (T_t), and an amorphous and supercooled liquid with a glass transition temperature (T_g). Melting points (T_m), for the crystalline phases are represented by the intersection of the curves for the crystalline and liquid states (28).

1.2.3 Kinetics

Thermodynamic theory, as referred before, refers that crystallization must result in an overall decrease in the free energy of the system. This means that, in general, the crystal structures that appear will be those with the larger (negative) lattice (free) energies. However, the routes to the final stable state are dependent on the kinetics as well as other factors as shown below (29).
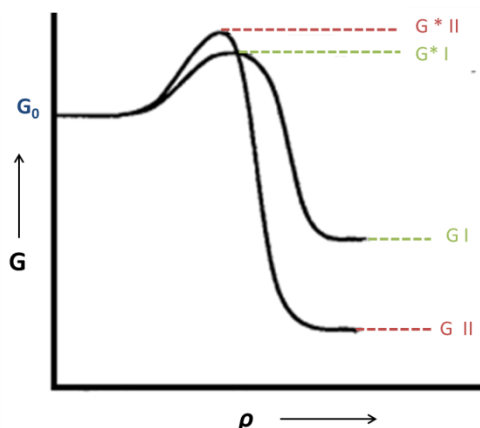
Figure 1.4 – Schematic representation of the reaction coordinate ρ for crystallization in a dimorphic system to show the activated barriers for the formation of polymorphs I and II.

The traditional energy-reaction diagram (Figure 1.4) shows the kinetic factors involved in the nucleation process. This diagram represents G_0 (the free energy per mole of a solute) in a supersaturated fluid which transforms by crystallization into one of two crystalline products, I or II, in which II is the more stable (GI>GII).

A transition from the initial state G0 to state I or II will depend on the energy barrier and according to the reaction pathway in Figure 1.4, the height of the energy barrier for structure II ($G^*II - G_0$) is higher than that for B (G^* I- G_0). Since the rate of nucleation is related to the height of the energy barrier on the reaction path, I will nucleate at a faster rate than II (29).

In general one can say that the probability of appearance of a particular Form I is given by equation (Eq. 1.1) in which ΔG is the free energy for forming the polymorph i and R is the rate of the kinetic process associated with the formation of a crystal by molecular aggregation. Following the above argument one could equate the rate process with the rate of nucleation (J) of Form I. If all polymorphs have the same rates of nucleation, then their appearance probability would be restrained to the relative free energies of the possible crystal structures.

$$P\ (i) = f(\Delta G, R) \qquad \textbf{Eq. 1.1}$$

According to the classical expression of Volmer (30), the rates of nucleation are related to various thermodynamic and physical properties of the system, such as, the bulk and surface free energies (γ), temperature (T), degree of supersaturation (σ) or solubility (hidden in the pre-exponential factor A) which will not be the same for each structure but will correctly reflect the balance between changes in bulk and surface free energies during nucleation. This effect is shown in Equation 1.3 (2), which relates the rate of nucleation to the above parameters (ν is the molecular volume).

$$J = A_n \, exp \left[-\frac{16\pi\gamma^3 v^2}{3k^3 T^3 \sigma^2} \right] \qquad \textbf{Eq 1.2}$$

Therefore, the tradeoff between kinetics and thermodynamics is not absolutely obvious. Figure 1.5 shows a schematic solubility diagram for a monotropic dimorphic system. It is noted that, for the occurrence given by solution compositions and temperatures that lie between the Form I and II solubility curves, only polymorph II can crystallize. Nevertheless, the outcome of an isothermal crystallization that follows the crystallization pathway indicated by the blue vector in Figure 1.5 is not so clear. In this case, the initial solution is now supersaturated with respect to both polymorphic structures, with thermodynamics favoring Form II (29).
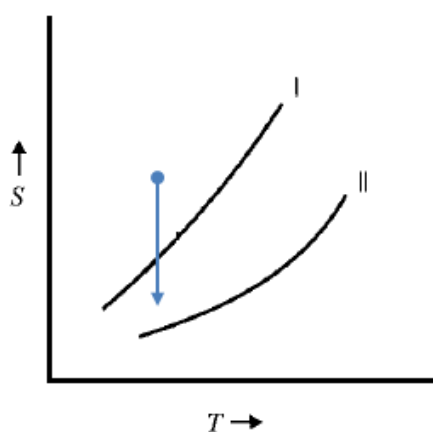
Figure 1.5 – Schematic solubility diagram for a dimorphic system (polymorphs I and II) showing a hypothetical crystallization pathway at constant temperature.

In the 19th century, authors working in the area of science of crystallization, observed that compounds could be obtained in more than one solid state form and a vast number of cases were documented about the fact that a metastable form of a compound tended to first crystallize prior to transformation into a more stable form. These observations led Ostwald in 1897 to propose the *Law of Stages,* where he stated that crystallization from melts and solutions yields an initial metastable form which is ultimately replaced by a stable form. This means that when a given compound leaves its initial metastable state it does not seek out the most stable state, but transforms instead into the nearest metastable one, that is, the one that can be reached without loss of free energy (28).

Later, Stranski and Totomanov (31) provided an explanation for this phenomenon developed in terms of the kinetics of transformation. In this model, the determining factors are the relative rates of nucleation and crystal growth for the stable and metastable forms. The differences between the various parameters may be theoretically justified by the fact that, at a specific working temperature, the rate of nucleation is higher for the metastable product. This situation would cause the metastable phase to preferentially nucleate. In a distinct scenario, the

rates of nucleation may be more or less the same for the two forms, but if the metastable phase has a higher rate of growth, then this form would eventually predominate in the isolated product (32). Figure 1.6 shows the rates of nucleation as functions of supersaturation for a dimorphic system. As it can be seen in Figure 1.6, the rate of nucleation of the metastable Form I is never higher over the entire supersaturation ranges. This indicates that there may be conditions in which the nucleation rates of the two forms are similar hence their appearance probabilities are nearly equal. Under such conditions we might expect the polymorphs to crystallize concomitantly (29).
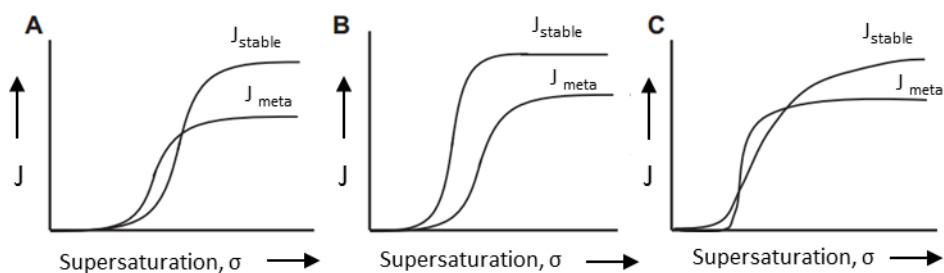
Figure 1.6 – The rates of nucleation as functions of supersaturation for a dimorphic system. Note that both solutions A and C allow for simultaneous nucleation of the forms at supersaturation levels corresponding to the crossover of the curves (29).

1.3 A comprehensive understanding of crystallization

Crystallization is defined as a phase change that leads to the formation of a crystalline solid (33). The most frequent type of crystallization is crystallization from solution, in which a material that is a crystalline solid at a temperature of interest is dissolved in a solvent while crystallization is induced by changing the state of the system in some way that reduces the solubility of the solute in the solvent. Commonly, this kinetic process is described in terms of two distinct steps: nucleation and crystal growth. The properties of the crystals obtained are the result of the kinetic relationship between these two processes. This sub-section aims on the introduction of the basic concepts of nucleation and crystal growth from solution and impact of these phenomena on the properties of pharmaceutical materials, including the parameters that can influence crystallization.

1.3.1 Driving force for crystallization

Crystallization can occur over the concentration range limited by the equilibrium composition of the system at specified conditions (Figure 1.7). Thermodynamic equilibrium is achieved when the solution is saturated with respect to the solute, that is, the concentration of the solution represents the solubility value for that solid phase. Under these conditions the rates of dissolution and crystallization are equal. When the solute concentration is below the

saturation limit (solid line) a solution is termed under-saturated and the existing crystals will dissolve. The system must be carried into a non-equilibrium state where the concentration of the solute exceeds its equilibrium concentration (i.e., the solution is supersaturated) for the crystallization to occur. The driving force for crystallization is going to be the degree of supersaturation, which is defined as the difference between solution concentration and saturation concentration at a specific temperature. Commonly, the methods which are used to create supersaturation in a solution are: temperature change, solvent evaporation, chemical reaction, pH change, and changes in solvent composition (34).

Supersaturation leads to the creation of metastable (far from equilibrium) liquid state and crystallization provides a means to reduce the free energy of the system to the most stable state (equilibrium) (35). The metastable limit determines the compositions at which spontaneous crystallization occurs. The region between the saturation limit and the metastable limit is named metastable zone. The metastable zone width varies depending on the purity of the system, the thermal history of solution and the density of foreign particles present in the solution. It is, therefore, important to know the metastable zone since it defines the working area for designed crystallizations (34). In order to produce just the required product, the concentration and temperature of the crystallization medium must be narrowly controlled within this zone. If the solubility line is crossed to the left, the seed crystals will dissolve and if the metastable zone limit is crossed to the right, spontaneous nucleation will take place and could result in unwanted crystal forms (34, 36). The kinetics of nucleation and crystal growth are strongly dependent on supersaturation (37, 38).

The metastable zone specifies the default region for operating an industrial crystallization process to avoid uncontrolled sizes (36). The solution has to achieve a certain concentration-temperature point where spontaneous nucleation occurs – this is the limit of the metastable zone.
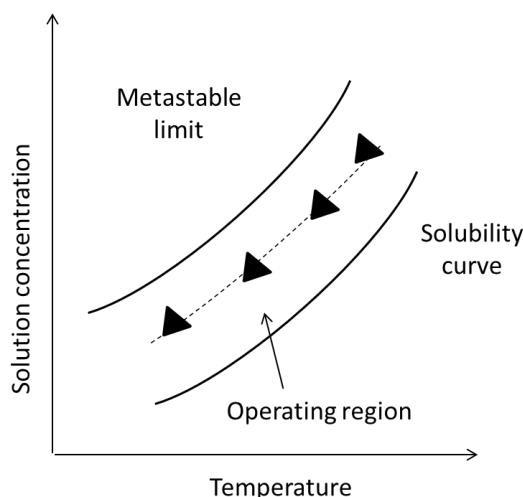
Figure 1.7 – Schematic solubility/ supersolubility diagram. The metastable zone specifies the default region for operating an industrial crystallization process. The operating region of batch crystallization is bound by the solubility curve and the metastable limit. The concentration temperature profile (control trajectory, dashed line) lies within this region (36).

1.3.2 Nucleation

The step between the generation of supersaturation and initiation of nucleation is called the induction period. The length of this period depends on temperature, pressure, presence of impurities or seeds, and mechanical disturbances. The presence of seeds and increased supersaturation decrease the length of the induction period (39).

Crystal nucleation encompasses the aggregation of dissolved molecules in the supersaturated solution into organized clusters (embryos) thus developing a surface that detach them from the environment. Nucleation can be either homogeneous or surface catalysed (Figure 1.8). Homogeneous nucleation which occurs spontaneously in bulk solutions seldom occurs in volumes larger than 100 μl, as most solutions contain random impurities that may induce nucleation, so it is the usual mechanism in small scales (40, 41). Surface catalysed nucleation can be promoted by surfaces of the crystallizing solute (secondary nucleation) or by surface/interface of different composition than the solute may induce nucleation (heterogeneous nucleation) by decreasing the energy barrier for the formation of nuclei (35).

Surfaces that promote heterogeneous nucleation may be introduced into the crystallization solution intentionally (with the goal of controlling crystal form of the product) (28) or unintentionally (dust and other impurities), or they can be an inevitable part of the process (crystallization vessel, vessel-solution interface and the solution-air interface). Heterogeneous nucleation is of practical importance in drug formulations, as excipients may provide the surfaces or interfaces necessary to promote nucleation. Moreover, heterogeneous nucleation happens at low driving forces and the favourable dissolution properties of the metastable drug may be lost due to the fast nucleation of the stable form (42).

```
                        ┌─────────────────┐
                        │   Nucleation    │
                        └─────────────────┘
                 ┌───────────────┴──────────────┐
        ┌─────────────────┐            ┌─────────────────┐
        │ Surface Catalyzed│           │  Homogeneous    │
        └─────────────────┘            └─────────────────┘
```

Heteogeneous

Catalyzed by interfaces or surfaces
other than the crystallizing solute

Secondary

Catalyzed by surfaces of the
crystallizing solute
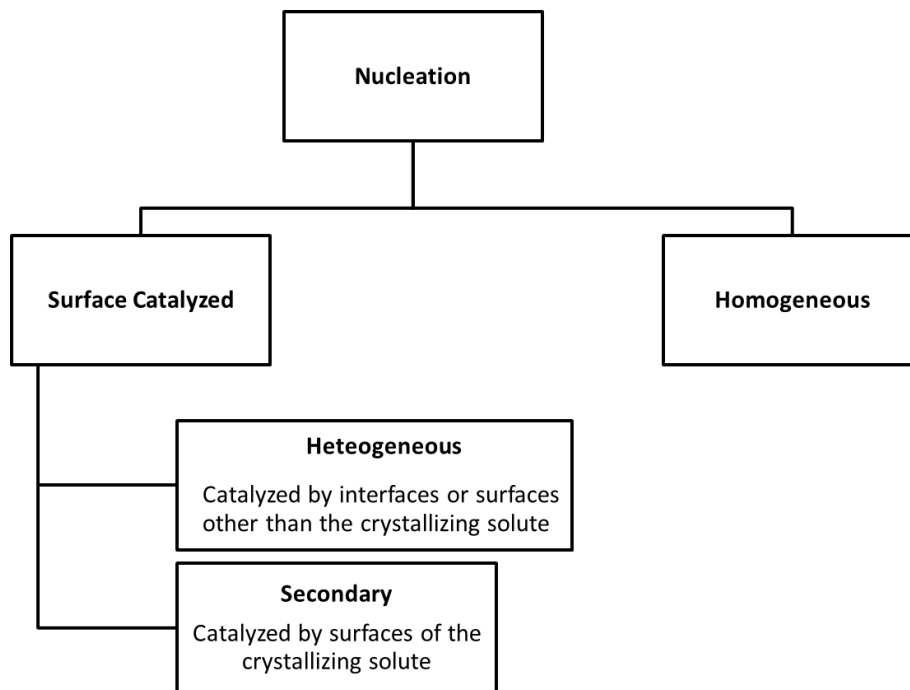
Figure 1.8 – Mechanisms for crystal nucleation.

The intentional addition of surfaces that catalyse nucleation, into crystallization solutions, is known as "seeding". Commonly, seeding is carried out by introducing crystals of the solute that have the desired crystal structure that is preferred to obtain in the final product (43). Seeding techniques can be performed with different goals, namely, to initiate crystallization, to control particle size (normally when larger crystals with uniform size distribution are required), to control a polymorphic form, to obtain crystals of high purity and perfection, desired orientation and with a sufficient size for crystal structure determination by X-ray diffraction (34).

1.3.3 Crystal Growth

When a nucleus overcomes a certain critical cluster size it becames stable enough to grow into macroscopic crystals. The process of crystal growth is a multi-step process which includes, (i) transport of the growth units to the impingement site, which may not be the final growth site, (ii) adsorption of the growth units at the impingement site, (iii) diffusion of the growth units from the impingement site to the growth site, and (iv) incorporation into the space lattice to form the crystal structure. The mechanism of crystal growth can be volume-diffusion controlled or surface-integration controlled. In particular, the surface-integration can occur as continuous or by layers crystal growth. The three dimensional structure and crystal defects can also influence the growth rates and thus determine the interaction between surface and solution at a molecular level (44).

1.3.4 Factors that influence nucleation and crystal growth

Previous studies have established that several factors such as solvent, temperature, concentration, pH, agitation and surfaces area and type in contact with growth solutions may influence nucleation and growth of crystals (44, 45).

Solvents

Solvents have a strong influence on the habit of crystalline material because they can preferential adsorb onto the different surfaces or facets of crystals as they develop, in this way hindering the deposition of solute molecules differentially on the different surfaces. Solvents may change the interfacial tension, an increase in the interfacial tension leads to a decrease on the growth rate. During the removal of solvent molecules, the face where the solvent molecules are more adsorbed will grow slower than the faces where the solvent molecules are less strongly adsorbed (46).

Temperature

Temperature can control nucleation and crystal growth by manipulating the solubility and supersaturation of the material (47). When a certain compound is more soluble at high temperature, slow cooling is a commonly used approach for crystallization of saturated solutions. On the other hand, slow warming can be applied if the compound is less soluble at higher temperatures. The approach of slow cooling or warming allows the thermodynamically most stable polymorph to form under conditions where the selectivity is the highest for nucleation and growth of that most stable form. By opposition, rapid cooling frequently generates nucleation and growth of several different polymorphs, particularly when the solubilities of the different polymorphs are similar (48, 49).

Concentration

The period needed for crystals to nucleate and begin growth depends on the concentration and the rate at which solvent evaporates. To achieve the supersaturation point for a given solution to initiate crystallization, it is required a reduction of the solvent amount (e.g., evaporation of solvent) or a reduction on the solubility of the solute. Thus, evaporation of solvent is one of the more commonly used methods for crystallizing compounds. Ostwald showed that unstable polymorphic forms have a greater solubility than the more stable forms in a particular solvent (50). Thus, crystallization by slow evaporation results often in formation of the most stable polymorph.

pH

pH can affect crystallization and the appearance of polymorphs, mainly for protein crystallization. In aqueous solution, a protein with hydrophilic groups on its surface is covered

with surface-bond water molecules. Consequently the addition of ions to solution results in the elimination of some water molecules on the surface of the protein. Therefore, the protein is free to bind to other protein molecules. Aggregation of proteins and subsequent nucleation and growth of crystals often can be therefore promoted simply by changing the pH of the solution (51).

Agitation, mixing and stirring

In industry, mixing of crystallization solutions and crystal slurries is often necessary, to ensure homogeneity (heat transfer, dispersion of additives, uniformity of crystal suspension, avoidance of settling, etc.). Its impact on nucleation (primary and secondary) and crystal growth is quite complex. A non-stirred solution can, generally, be cooled before the onset of nucleation, once the main goal of mixing is a decrease in the width of the metastable zone. In a stirred solution at constant supersaturation, with no crystals yet present, mixing intensity can reduce induction time – the time elapsed before crystals first appear. Induction time decreases up to a critical speed and then remains unchanged (52, 53). Mixing actively may origin secondary nuclei through crystal-crystal, crystal-vessel and crystal-impeller impacts. A larger number of nuclei created in stirred systems leads to a decrease in the final crystal size of the product.

Addition of impurities and additives

Crystallization may be affected by impurities (unintentionally present components) and additives (intentionally added substance). Examples of additives employed for controlling polymorphic outcome of pharmaceuticals include structurally related (tailor-made) organic molecules (54), polymers (55) and surface-active agents (56). Polymers and surfactants can also act as crystallization or phase transformation inhibitors in pharmaceutical formulations (57-60). In the case of the polymers, these substances may get adsorbed in the crystal lattice of a growing crystal and disturb the regular and repeating arrangements of the crystal, creating defects and leading to polymorphic modifications. They can also inhibit crystal growth at certain crystal faces, resulting in crystal habit changes (61).

Polymeric crystallization inhibitors

Polymers are molecules that when fully solubilized in a given solvent, exist as random/extended coils. This extended coil conformation exists as a result of the relative rotational freedom of the polymer backbone and due to the numerous conformations that the polymeric material can adopt when it does not establish significant intramolecular interactions. When the polymer is in a presence of a poor solvent, the conformation is more contracted in order to minimize the contact with the solvent (39). The impact that the polymers may have on the enhancement of the solubility of drugs, should be considered when we are examining the mechanism of crystallization inhibition. For instance, the increase on the induction times for

crystallization in the presence of the polymer is often used to provide an indication of the most effective crystallization inhibitor. Therefore, when the polymer addition results in the increase of the drug solubility, the degree of supersaturation (a prerequisite for precipitation) may be reduced and possibly reduced below the level of saturation. Under these circumstances, crystallization will be inhibited, but due to a change to the system thermodynamics (i.e. equilibrium solubility) (39).

The increase of the saturation stability and therefore the reduction of the extent of supersaturation result from the formation of complexes between the polymer and the drug of interest. For the formation of the complexes, the polymers can interact with drug molecules via electrostatic bonds (i.e., ion-to-ion, ion-to-dipole and dipole-to-dipole bonds) but other types of forces, such as van der Waals' forces and hydrogen bridges, may frequently participate in the complex formation (62). In the literature one can find many examples of polymers showing to increase the equilibrium solubility of drugs. For instance, PVP showed to increase the solubility of acetazolamide and hydrocortisone (62), felodipine (63), and valdecoxib (64). The addition of polymers, even at low fractions, may also cause stabilization by increasing the local viscosity, impeding diffusion of drug molecules, and increasing thermodynamic and kinetic barriers (65). The ability of polymers to kinetically stabilize the supersaturated state is thought to result from intermolecular interactions between the drug and polymer in solution (e.g. via hydrogen bonding or hydrophobic interactions) and/or the ability of the polymer to sterically hinder the crystallization process (66).

In summary, polymers which inhibit crystallization may inhibit crystallization at both the nucleation and growth stages (kinetics and crystal habit). Several potential sites of action have been identified (39) (67):

- Changing the bulk solution properties such as surface tension (where decreasing surface tension moves crystallization from diffusion control to surface nucleation control) and solubility (where increasing solubility reduces supersaturation and the tendency for nucleation).

- Altering the adsorption layer at the crystal–solution interface, including the properties of the hydrodynamic boundary layer surrounding the crystal, potentially decreasing the rate of diffusion of drug molecules to the crystal nuclei, increasing the kinetic barrier to nucleation.

- Adsorbing to the crystal surface interface, by formation of hydrogen bonding between the polymer and the drug, blocking crystal growth by preventing the access of the solute molecules to the crystal terrace;

- Adsorbing onto the growth terraces and thereby disrupting the growth of steps across the surface, blocking access of adsorbed molecules to the terrace steps and/or kinks;

- Adsorbing into surface imperfections causing rough surfaces to become flat, therefore eliminating growth spots;

- Modifying the surface energy of the crystal face, potentially changing the level of solvation;

1.4 Solvatomorphism

The ability of a substance to form solvates is referred to as solvatomorphism.

In solvatomorphism, the formation of various crystals is a result of the incorporation of solvent molecules in the crystal lattice (68). Solvates may contain solvent molecules within the crystal structure, in either stoichometric or non-stoichometric proportions. The introduction of solvent molecules in a crystalline drug structure is going to originate differences in the physical and pharmaceutical properties. For this reason, the properties of solvates, such as density, solubility, dissolution rate and bioavailability are different from those of non-solvated species. These physical properties changes are analogous to those associated with polymorphism, and therefore solvates are often referred to as pseudopolymorphs (69) (70) to distinguish them from polymorphs. When the entrapped solvent in a solvate is water, the term <u>hydrate</u> is used (71, 72).

Regarding the prevalence of solvatomorphism among APIs, 29% of APIs have been reported to form hydrates and 10% to form other solvates (73). The ease to form and stabilize hydrates can be explained by the fact that molecules within the crystal will attempt to pack so that the amount of unoccupied space is minimized and the number of close contacts with neighboring molecules maximized (74). However, when large voids exist in the crystal structure, energetically favorable hydrogen bonds with solvents compensate for the loss of spatial efficiency and thus stabilize the crystal structure (75).

Steroids, antibiotics and sulfonamids have the particular ability to form solvates. This is related to the cavities or large channels that are often present in the crystal structures of these substances. The size and chemical environment of the cavity or channel establish the type of incorporated solvent molecule as well as the type of interaction between guest and host (76). When the solvent molecules are trapped, as in clathrates, the solvate is more stable than when the solvent molecules are located along channels in the lattice. Table 1.3 lists some examples of the effect of solvation on drugs and solid dosage forms.

Table 1.3 – Effects of solvation on drug activity (76)

API	Effect
Ampicillin	Anhydrate shows higher bioavailability compared to trihydrate.
Hydrocortisone	Hemiacetone solvates showed higher absorption compared to anhydrates.
Caffeine	Increased dissolution of anhydrous forms compared to hydrates.
Theophylline	Increased dissolution of anhydrous forms compared to hydrates.
Glutethimide	Increased dissolution of anhydrous forms compared to hydrates.
Prednisolone	Higher dissolution and activity of a solvate from pellets implanted.
Griseofulvin	Chloroformate solvate gives higher bioavailability compared to anhydrates, also solvation-desolvation results in increased surface area.
Citric acid	Hydrate used to provide mole of water as granulating agent in effervescent preparations.

1.4.1 Solvated systems

The stability of solvates depends on the pressure, temperature and partial pressure (*activity*) of the solvent of crystallization above the solid (77). Similarly to an energy diagram for polymorphic systems, the stability range of solvate and unsolvated form can be established using a van't Hoff plot (natural logarithm solubility versus reciprocal temperature plot) (78). The relationship between free energy and an ideal solubility of a solid is given by:

$$\Delta G = RT \ln X \qquad \text{Eq. 1.3}$$

or

$$\ln X = \frac{\Delta S_f}{R} - \frac{\Delta H_f}{R} * \frac{1}{T} \qquad \text{Eq. 1.4}$$

where, ΔS_f and ΔH_f are, respectively, the entropy and enthalpy of fusion, and R is the gas constant. A negative slope of a van't Hoff plot is equal to $\Delta H_f/R$, while the intercept yields $\Delta S_f/R$ for each phase. It is commonly accepted that a solvate is the most stable thus, the least soluble form in its own solvent. Therefore, the aqueous solubility (and hence stability) order for solvated systems is typically the following: stable hydrate < metastable hydrate < anhydrate < solvate with organic solvent (Figure 1.9).
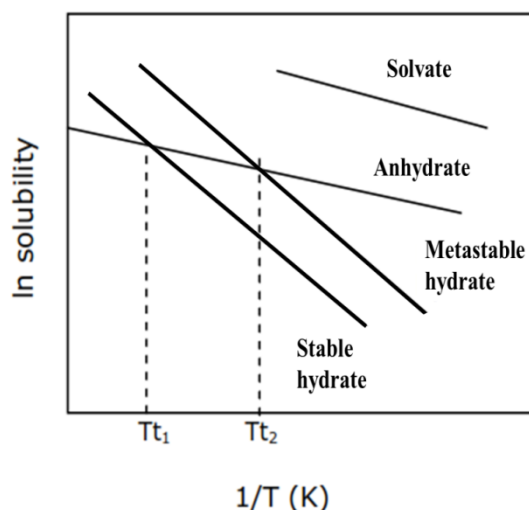
Figure 1.9 – Solubility diagram for a system of different solvates showing transition temperatures, T_{t1} and T_t, between the anhydrate and the hydrates (78).

1.4.2 Hydrates

Hydrates frequently readily crystallize due to the small size of water molecules that can easily fill structural voids and form multidirectional hydrogen bonding with the drug molecules forming stable crystal structures (69). It is the activity of water in the medium that will determine whether a given hydrate structure will form. In accordance to this, the determination of the physical stability of anhydrous forms as a function of water vapor pressure is of great importance in order to avoid a reduction on the pharmaceutical performance of the API. The formation of hydrates during manufacturing can affect the solubility and, consequently, the bioavailability of a drug compound (79, 80). The solubility and dissolution behavior of anhydrous and hydrated forms is different, anhydrous forms having commonly greater aqueous solubility and faster dissolution rates than the hydrates (81).

Crystalline hydrates have been classified either according to their structure or energetic related considerations. The classification of crystalline hydrates of pharmaceutical interest by their structural characteristics is the most common approach. Thus, depending on the structural characteristic of the hydrates, and the way how water molecules interact with drug molecules, the hydrates can be classified as:

Isolated site hydrates (Class I), which represents the structures where the water molecules have a well-defined isolated location, the hydrates of this class often being stoichiometric. The water molecules are kept from contacting with other water molecules directly in the lattice structure. Although water molecules exposed to the surface of crystals may be easily lost, once they are removed they do not give access to the water molecules inside the crystal lattice. The thermogravimetric analysis (TGA) and the differential scanning calorimetry

(DSC) for this class of hydrates show thermograms with sharp endotherms reflecting the sudden release of molecules. Cephradine dihydrate is an example of this class of hydrates (80).

Channel or planar hydrates (Class II) includes hydrates where water molecules form continuous channels or planes inside the crystalline structure, in a generally non-stoichiometric relationship. Special care should be taken with these hydrates, as inconsistencies in the moisture content as a result of absorption or desorption of water vapor may lead to variations in content uniformity in the drug product and may also result in materials with dissimilar powder properties. The TGA and DSC data show early-onset temperatures of dehydration and broad dehydration enthalpies. This is because the dehydration begins from the edges of the channels that are on the surface of the crystal. After water removal from the surface of the crystal, water molecules in the inner part of the crystal are continuously removed until all water molecules are eliminated through the channels. Some hydrates, called planar hydrates, have water molecules in a 2D space (80).

Ion-associated hydrate solids (Class III) contain metal-ion coordinated water. The interaction between the metal ions and water molecules is the major force in the structure of crystalline hydrates. Consequently, dehydration occurs at very high temperatures. These last hydrates can either be stoichiometric or non-stoichiometric. The TGA and DSC thermograms present very sharp peaks, expected at high temperatures, corresponding to dehydration of water bonded to metal ions (80).

1.5 Process-induced phase transformations

Throughout processing a drug is often exposed to temperature, pressure and humidity changes, which potentiate the occurrence of process-induced phase transformations. Special care should be taken with insoluble drugs, since their crystalline modifications can often lead to changes in solubility that will strongly affect the dissolution/ bioavailability of the drug in the final solid dosage forms. Process-induced phase transitions may lead to the formation of metastable polymorphs, amorphous forms, hydrates/solvates or desolvated forms depending on the drug and processing conditions. They can also induce changes in size and shape of the materials. Those transformations may be completed or not during the processing and may have crucial effects on the product quality (5). Furthermore, it can be difficult to predict and control them. It is then important to determine whether or not phase transformations do take place, in order to understand the mechanism and kinetics of phase transformations and factors that may influence them and finally, control them during manufacturing processes (82-84).

With the advances in pharmaceutical materials and processing, an improvement in the understanding and monitoring of each step from raw material qualification to final product is required (85). For this reason, with a close monitoring of the process, a new understanding, and knowledge of critical control points are provided, facilitating a better control and predictability

of process variations. This item in particular guarantees the high quality and performance attributes of raw materials and final products (86). For the monitoring of the process, several methods are used for characterizing and for routine off-line testing of pharmaceutical solid polymorphs: X-ray powder diffraction (XRPD), microscopy (SEM, OM), thermal analysis (TGA, DSC) and spectroscopy (FTIR, NIR).

1.5.1 Particle size reduction and particle engineering

Particle size reduction is one of the oldest strategies for improving the dissolution rate of the APIs. As the particle size becomes smaller, the surface area to volume ratio increases, thus increasing the surface area available for solvation. Particle size reduction technologies are therefore routinely used to increase the bioavailability of poorly soluble drugs (87). Many solid dosage forms in the pharmaceutical industry are made of microparticles. Dry powders are inhaled as aerosols into the lung, delivered to the nose, filled into capsules, or pressed into tablets for oral applications, or even delivered transdermally (88). Conventional size reduction of pharmaceuticals is accomplished by mechanical comminution such as crushing, grinding and milling of previously formed larger particles. This process involves shearing/cutting, compressing, impacting or attrition of drug particles which create mechanical stress and often heat. Accordingly, this process could lead to polymorphic transitions, dehydration and amorphization of the drug. Milling induced polymorphic changes have been observed in many small drug molecules, such as ranitidine hydrochloride and indomethacin (89, 90). In the case of ranitidine, it was suggested that the transformation from form 1 to form 2 during milling occurred via an intermediate amorphous form.

The supercritical fluid (SCF) technology comprises several applications for particle formation and design. It allows for a single step crystallization of particular pharmaceutical materials with precisely controlled characteristics, such as solid-state form, particle size, shape and crystallinity (91-93). This technology enables the tuning of the properties of the SCF (e.g. solvent ability) to target to a component in a complex matrix, or it can suddenly change these properties during the process due to changes in pressure and / or temperature, with the aim of achieving of very homogeneous supersaturation conditions, which in turn can lead to the production of fine powders with a narrow particle size distribution. In this work special attention will be given to this technology, with the aim of producing particles with reduced sizes and determining their solid-state characteristics.

Supercritical fluids (SCFs), i.e., gases and liquids at temperatures and pressures above their critical points, have liquid-like densities with gas-like transport properties and moderate solvent power, which can further be adjusted with changes in pressure and temperature (94) and addition of other materials (e.g. surfactants). SCFs work as solvents with adjustable viscosity, density, and solvation strength (95). In the pharmaceutical field, the most used SCF is carbon

dioxide due to its low critical temperature (31.1ºC), which is attractive for heat-sensitive materials (96). In the pharmaceutical field, precipitation from <u>supercritical solutions composed of SCF and solutes</u> (1) and <u>precipitation from saturated solutions using SCF as an antisolvent</u> (2) are the most commonly used modifications of the SCFs technology. In the first process, the solid product is solvated in the SCF forming a solution. This solution is rapidly depressurized through an adequate nozzle, causing an extremely rapid nucleation and particle formation. This process is termed Rapid Expansion of Supercritical Solutions (RESS). It is an attractive methodology due to the absence of organic solvents, as it is simple and relatively easy to implement. However, its application is restricted to the products that present a moderate solubility in the SCFs (e.g. low polarity compounds) (97). Due to RESS collisions during free jet expansion, particles at the organic-CO_2 interfaces are forced to grow. This growth may be inhibited by expanding into an aqueous solution with the use of surfactants as stabilizers, a process known as rapid expansion of supercritical solutions to aqueous solutions (RESSAS) (98). In this usage of the technology, the supercritical solution is expanded through an orifice or conical shaped nozzle into an aqueous solution containing a stabilizer to minimize particle aggregation throughout the free jet expansion. Various process parameters influence the properties of the final particles manufactured by RESS, such as the extraction (understood in this context dissolution or solubilization of the drug) temperature, the extraction pressure, the pre-expansion temperature, the spray distance, post expansion pressure and the nozzle configuration (length, diameter and geometry) (99). The surfactants may be introduced into the CO_2 phase, the aqueous phase or into both. During the expansion, the nuclei of the drug / material particles come in contact with an expanding CO_2 phase and an aqueous phase simultaneously. This process combines aspects of phase separation with interfacial stabilization. RESSAS may also be used to enhance the dissolution rate of poorly water soluble drugs (100). The reduction of particle size and, therefore, an increase in interfacial area, lead to an increase of dissolution rates in the gastrointestinal tract. Furthermore, coating drug particles with polymeric and low molar mass hydrophilic stabilizers to enhance wetting and solvation by intestinal fluids, may further increase the dissolution rates of such drug particles. Stable suspensions of submicrometer-sized particles of cyclosporine, a water insoluble drug, have been produced by RESSAS with an aqueous solution containing polysorbate-80 (100).

The second process referred previously (2) helps to overcome the solubility limitation of the SCF by dissolving the drug in a solvent. This process is based on the same concept of using antisolvents in solvent-based crystallization processes. It allows, throughout decompression, the efficient separation of the antisolvent from both the solvent and solid products (101). This process is named Supercritical Anti-Solvent (SAS). It is commonly used to prepare nanoparticles without the need for a grinding procedure. Some operating parameters such as

temperature, pressure, drug concentration have a great influence on particle size in the SAS process (102).

1.5.2 Wet granulation

During wet granulation, several different steps are involved, such as wetting, mechanical stress and sieving, which provide an ideal medium for the crystallization of new phases of the drug (83). The extent of conversion is dependent on the amount dissolved with time, which results from the solubility of the forms, volume of solvent (granulation fluid) and the dissolution rate. Considering the fact that hydrated forms are more stable than anhydrous forms in the wet material, hydration will be the most likely transformation to occur. In the case of poorly soluble drugs in contact with the granulating fluid, the anhydrous phase will tend to convert into a hydrate by a solvent-mediated mechanism. The analytic techniques used for the detection of those transformations will depend on the drug load in the granules and the potential interference from the excipients (6, 103).

The main question will be how that hydrate will behave in the subsequent drying process where the processing stress is due to the high temperature and the relatively low humidity. It has been described that a dehydration of a hydrated form can result in a metastable anhydrate, a lower hydrate, an amorphous form or a thermodynamically stable anhydrous form. The path of any transformation is kinetically controlled and dependent on the conditions for the duration of the wetting and drying steps, as well as on the duration of the process. Examples of the impact of such drying conditions on the formation of different crystal forms are phenobarbitone (104), chlorpromazine hydrochloride (105) and theophylline (106).

Drying kinetics in fluid bed dryers has been well studied. It has been studied that two main stages exist during the fluid-bed drying process of granulations for pharmaceutical applications. The first stage is limited by the heat-transfer which occurs during the moment when the water molecules at the surface or the ones loosely bounded are evaporating from the surface of particles. The relationship between moisture content and time is, in this stage, linear. The second stage of drying is diffusion dependent, where the water inside the granules must diffuse to the surface of the granule before it can be removed by the drying fluid. Here, for spherical particles, the relationship between moisture content and time is exponential (83).

1.5.3 Extrusion-spheronisation

Pelletization of drugs is a worldwide used technology to create multi-particulate solid dosage forms. Pellets are spherical or nearly spherical, free-flowing granules with a narrow size distribution, typically varying between 500 and 1500 μm for pharmaceutical applications (107). These formulations have multiple advantages in comparison to the conventional single-unit solid dosage forms. For instance, due to the fact that pellets are much smaller than tablets, they are more rapidly emptied out of the stomach, regardless of the feeding state of the patient.

Secondly, each small pellet-unit contains only a small amount of drug. There is consequently less risk of high local drug concentrations or irritation of the gastric and duodenal mucosa. The use of pellets also gives the advantage of being able to combine multiple drugs that otherwise would not be compatible in one dosage form. Once pellets have been made they can be compressed into tablets or filled into hard gelatin capsules (107, 108).

Among various methods of manufacturing pellets, the process of extrusion–spheronisation is of particular interest. Extrusion–spheronisation is a process organized in five unit operations: blending, wet massing, extrusion, spheronisation, and drying (109). The liquid phase (generally water) provides inter-particle cohesion, lubricates particle contacts, promotes wall slip and can also bear some of the stress generated during the forming process (110). Extrusion and spheronisation of wet masses includes the wetting and drying steps of the materials together with mechanical stresses, which are also likely to promote solid-state modifications of an API. Furthermore, the amount of wetting liquid used in this process is relatively high, when compared to other processes, namely fluidized bed granulation. Therefore, APIs to be included in pellets manufactured by extrusion of wet masses are more prone to undergo structural transformations than APIs manufactured by other drier and gentler technologies (111). The physical and chemical properties of the active pharmaceutical ingredient (API) are important in wet mass formulation: the solubility of the API in the liquid phase, its particle size characteristics and packing behavior can affect the amount of liquid necessary to obtain a wet mass with the required 'plasticity'. Particle size, specific surface area and packing behavior has been identified as key factors affecting the variation in process ability (112).

Extrusion–spheronisation produces well-densified pellets, offers a narrow particle-size distribution, yields low friability, ensures regular sphericity and maintains good flow properties. The properties of the final product depend on the physicochemical properties of the raw materials and the amount of each component in the formulation (113). Various process variables affect the quality of the pellets. These variables include: the type and quantity of solvent added to the powder mixture; mixing time and speed; type of extruder, design of the screen, and rate of extrusion; spheronisation speed, time, load, and plate design; and drying rate and time (108).

1.5.4 Tableting

The powders/granules may be subjected to compression forces as high as 40kN during tableting. Here, the pressure, temperature and mechanical stress may play a role. However, it may be difficult to know the contribution of each of these factors on solid-state transitions. Therefore, tableting may induce solid phase changes in either the drug or the excipients via the solid-state mechanism. Most of the data supports the idea that the transformations from one polymorphic form to another during tableting result from an intermediate amorphous phase. For

a form which resists to the mechanical stress it will be expected that the crystal behaves as predicted by its Pressure-Temperature phase diagram (83). Caffeine, sulfabenzamide and maprotiline hydrochloride have been reported to undergo polymorphic transformations during compression (114).

1.6 Storage: Moisture-induced phase transitions

The API and excipients in the formulation may have different moisture sorption properties. Hence, they can interact differently with moisture and produce unpredicted phase transitions. The study of the interaction of moisture with pharmaceutical solids is of practical interest since it allows a prediction of solid dosage form stability and shelf-life (4). Furthermore, the process of moisture sorption by amorphous and crystalline materials is different making their study important when designing new formulations and processes. The amorphous character is common to the polymeric molecules used as excipients. As a consequence of the higher mobility and ability to interact with moisture, amorphous substances are also more likely to undergo solid-state modifications. The highly hygroscopic characteristics of such substances can also have significant consequences for the stability of pharmaceutical formulations. The impact of the excipient's moisture present in the drug-excipient interaction, depends on its fraction in the formulation, as well as, the relative ability of each solid to uptake and retain water at a particular temperature and RH (6).

1.7 Mechanism of phase transformations occurring during processing and storage

Throughout the designing, development and manufacturing of a medicine it is essential to identify process-induced solid phase transitions of the API. For instance, for a drug which is sensitive to moisture or to a solvent, a process of dry granulation can be the appropriate process to manufacture this drug. Therefore, it is important to know the susceptibilities of each APIs, throughout an understanding of the mechanism(s) of phase transitions and the factors affecting their kinetics. These studies can provide an insight of such transitions during the manufacturing, allowing selection of a robust process to ensure consistent product manufacturing and performance (6, 34).

1.7.1 Solid-state pathway

Solid-state mechanism involves phase transitions that occur in the solid-state without passing through intervening transient liquid or vapor phases. The kinetics of phase transition via a solid-state mechanism is often induced by the environment (temperature, mechanical stress, vapor pressure, etc.), the presence of crystalline defects, particle size distribution and impurities. Phase transitions that occur through solid-state mechanisms are polymorphic transitions, hydration/dehydration, amorphous crystallization/ amorphisation (6).

1.7.2 Melt pathway

Phase transitions occur when a solid is heated above its melting point and then cooled to the ambient temperature. In these cases, the original solid phase may be altered as a result of a phase transition through this heating/cooling cycle. The factors that will determine the final solid phase are the relative rates of nucleation, the crystal growth and the cooling rates. Impurities or excipients can also affect the course of crystallization. Amorphisation and polymorphic transitions are the most likely phase transitions obtained through this pathway (6).

1.7.3 Solution pathway

A drug is commonly dissolved, or partially dissolved, in a solvent (typically water) during pharmaceutical processing. For example, the drug may partially dissolve in water during wet granulation, or it may completely dissolve in water during freeze-drying or spray drying processes. If the following solvent removal (drying) induces a transformation, it is said that it has occurred through a solution mechanism. The solid formed may not be the same crystal form as the original phase or it may consist of a mixture of phases. However, only the fraction of drug that is dissolved can undergo this transformation. The solid formed may be a single phase or a mixture of amorphous and crystal forms, depending on the rate of solvent removal, the ease of nucleation and the crystal growth rate of the crystal forms when exposed to particular processing conditions. The fraction of solid material that did not dissolve may act as seeds and direct the crystallization to the original crystal form or, together with the insoluble excipients can provide surfaces for heterogeneous nucleation of a different phase. Soluble excipients may also affect the nucleation and crystal growth of the drug (52). It is also important to notice that the transitions explained by this mechanism can either be from a metastable phase to a stable phase or vice-versa (6).

1.7.4 Solvent-mediated pathway

In formulation and processing the stable crystalline form is usually preferred to its metastable counterpart. However, a metastable solid phase, with larger thermodynamic activity, may be chosen due to its better biopharmaceutical performance. The disadvantage is that, since any system seeks to reach the thermodynamic equilibrium, a metastable form present in the formulation is liable to suffer a solvent-mediated transformation upon processing (e.g. wet granulation/ wet extrusion) and/or storage. This transformation is governed by the solubility difference between the two phases when the metastable phase is in contact with the saturated solution and allows for the transition from a metastable to the stable phase. Based on this, solvent mediated transformations are commonly used to produce the most stable polymorph (115).

The solvent-mediated pathway only permits the transition from a metastable phase to a stable one. This transformation takes place when the metastable phase contacts the saturated

solution. The solubility differences between both phases enable these types of transformations. Three steps are involved in those transformations (116, 117): (1) the initial dissolution of the metastable phase into the solution to reach and exceed the solubility of the stable phase; (2) nucleation of the stable phase; (3) crystal growth of the stable phase coupled with the continuous dissolution of the metastable phase. Steps 2 or 3 are usually the slowest steps (6). When step (2) is the rate-controlling step, the overall transformation is influenced by factors that affect nucleation (e.g. solubility and solubility differences between the phases, processing temperature, contact surfaces, agitation, and soluble excipients/impurities). When step (3) is the rate determining step, the kinetics of the conversion is determined by the solubility difference, solid/solvent ratio, agitation, processing temperature, particle size of the original phase, and soluble excipients/impurities (6). The crystalline transformation occurring in a suspension or during kneading of a wet mass for granulation, can be outlined according to the following scheme:

$$\text{Anhydrate} \xrightarrow[K_d]{\text{Dissolution}} \text{Supersaturated Solution} \xrightarrow[K_n]{\text{Nucleation}} \text{SS*} \xrightarrow[K_c]{\text{Crystal growth}} \text{Hydrate}$$

where, k_d is the dissolution coefficient constant, k_n is the nucleation rate constant and k_c is the crystal growth rate constant. The SS* is activated supersaturated solution containing enough nuclei to start the growth of the crystal. Thus, the crystal transformation followed consecutive reaction kinetics and contemplates an induction period (118).

This kind of transformation may also take place during solubility measurements, dissolution studies and accelerated stability tests in hydrated systems. The rate of transformation can be affected by the introduction of specific impurities that may delay the rate of dissolution of the less stable species (57).

1.8 Excipients

1.8.1 The importance of excipients selection

Excipients' proper characterization is paramount because variations in raw materials properties can lead to failures in production causing batch-to-batch variation and failed batches and/or dosage form performance (85).

Most APIs used for oral administration require formulations with excipients. In spite of excipients having traditionally been thought of as being inert it has been demonstrated that they can interact with a drug to affect its absorption and bioavailability (119). Some excipients can also be added to a formulation specifically to take advantage of the interaction between the API and that excipient, when it affects the bioavailability of the drug.

Instability of APIs and excipients may be broadly classified as chemical (e.g. hydrolysis or oxidation) or physical instability (like polymorphism or pseudopolymorphism) which may have a potential impact on the absorption and bioavailability of the drug. In particular, the formation of metastable crystalline polymorphs of the API can be dangerous, since they may be chemically less stable than crystalline stable forms (5). The main factors that could cause the molecular transformation of an API in formulation are <u>environmental</u> (e.g. water vapor and sunlight), <u>stresses during conversion to the dosage form</u> (e.g. compaction processes with interactions between adjacent molecules of API), <u>interactions between functional groups on the same molecules</u>. Optimizing the selection of excipients in the formulation could reduce problems during manufacturing and storage of final dosage forms. In addition, each excipient must be compatible with the other components in the formulation and perform efficiently its desired function in the final product (119). Accordingly, it is important that the processes of formulation design and development are properly integrated to obtain optimized drug delivery systems as early as possible (120). For this reason, in this study a special attention is paid to the interactions between the drug and excipients when they are exposed to <u>aqueous environments, humidity, temperature and pressure changes,</u> since they may potentiate or protect the occurrence of process-induced phase transformations.

1.8.2 The water sorption behavior of excipients

The interaction of moisture with pharmaceutical solids is crucial to an understanding of water-based processes, e.g. prediction of solid dosage form stability and shelf life.

Different excipients have different abilities to interact with moisture from the surrounding atmosphere during storage. In general, materials which are not affected by water vapor are termed non-hygroscopic, while those in a dynamic equilibrium with water in the atmosphere are called hygroscopic. Generally, crystalline excipients, because of the close packing and high degree of order of the crystal lattice, do not absorb water into their structures, contrasting with amorphous solids that can absorb significant amounts of moisture within the material. Furthermore, water absorbed into the amorphous regions can act as a plasticizer and increase molecular mobility due to the breakage of hydrogen bonds between molecules (121).

Water can interact with crystalline solids by different mechanisms: 1) adsorption on the surface of the particles; 2) incorporation into microporous regions by capillary condensation; 3) formation of crystal hydrate; and 4) deliquescence. The adsorption of water onto non-hydrating crystalline solids depends on the polarity of the surfaces and is proportional to surface area. When the specific surface area is large, e.g., very small or porous particles, the adsorption is particularly critical in affecting the properties of solids. The mechanism of water sorption into the solid depends on the crystal structure, water-solubility, porous structure and the ability to form crystal hydrates (58, 122). Crystalline excipients are commonly non-hygroscopic,

therefore, at low RH, water is adsorbed onto the surface of a crystalline material. As the RH increases, the water molecules become attached to the solid-vapor interface by weak interaction forces (e.g. van der Waals forces). Water interacts firstly with the polar groups on the crystalline surface, which is a surface effect. Thus, surface area, particle size and size distribution are important for the ability to adsorb moisture as a function of RH. As the RH is increased, some tendency for multilayer sorption is expected (123).

Several processes, such as grinding, spray drying, wet granulation and thermal treatments, may introduce significant fractions of amorphous domains into pharmaceutical crystals (124). Additionally, most pharmaceutical polymer excipients are substantially amorphous. The amount of water sorbed into amorphous materials is commonly proportional to the volume/weight of the amorphous solid and independent of the surface area of the solid. Amorphous materials take up significantly higher amount of water than their crystalline counterparts, which could cause physicochemical instability in their formulations (125). Therefore, it is very important to study the water sorption ability of amorphous materials.

Water absorbed into the amorphous regions can act as a plasticizer (depress the T_g) and could cause structural changes in amorphous materials (126). When the T_g is below the environmental temperature, the solid enters the rubbery or supercooled liquid state. Therefore, glass transition must be considered when accelerated stability tests (increased temperatures/humidity) are designed - the mobility of drug molecules would increase and the viscosity would decrease above the glass transition, which could lead to a significant increase in the crystallization rate (127).

CHAPTER 2

Chapter 2 - Materials and methods

2.1 Materials

2.1.1 Olanzapine

Olanzapine (OLZ), 2-methyl-4-(4-methyl-1-piperazinyl)-10*H*thieno[2,3-*b*][1,5]benzo-diazepine (Figure 2.1 A), belongs to a new generation of benzodiazepines for the treatment of schizophrenia and other related psychoses. It has structural and pharmacological properties resembling those of the atypical antipsychotic clozapine and an improved tolerability profile compared with the classical antipsychotic haloperidol (128). It is a yellow and crystalline powder. It is practically insoluble in water, freely soluble in methylene chloride and slightly soluble in ethanol (129).

Olanzapine can exist in several crystalline forms, including polymorphic anhydrates, dihydrates, solvates and one higher hydrate structure (18). Bhardwaj et al. have recently calculated the crystal energy landscape of different forms of olanzapine and observed that olanzapine molecules have a packing efficiency of no more than 70%, which explained the tendency to form solvated forms (130). .

OLZ is, therefore, a molecule with a certain degree of structural complexity. Consequently, the physical treatments and technological processes undergone by the drug may have an impact on its solid-state, which may affect its performance in terms of dissolution rate, absorption, and therapeutic activity and response. Moreover, the recommended daily oral olanzapine dose for schizophrenia ranges from 5 to 20 mg, which is a small amount, thus requiring a well-defined purity and an assessment of the nature of the active agent; the manufacturing process of solid olanzapine in practical terms can be complicated by its ability to form such different structures (131).
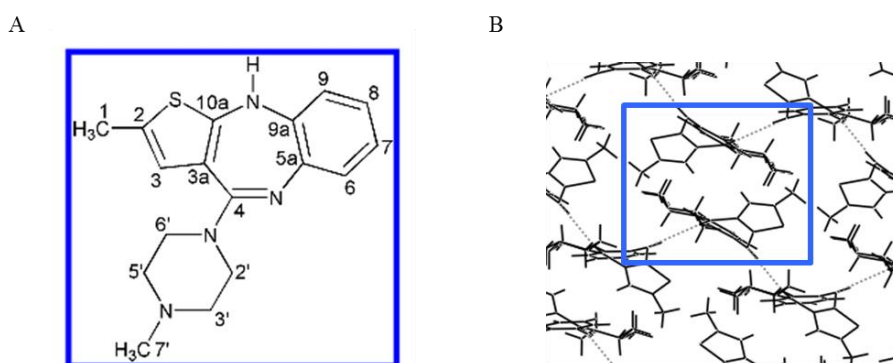
Figure 2.1 – Olanzapine molecule (A) and one example of packing (B).
Box in B shows two enantiomers of olanzapine.

All olanzapine crystalline forms present a structural building block which is composed by a dimeric unit (racemic pair), which is quite "rigid" irrespective of the packing environment, in spite of the weak interactions involved in its stability (Figure 2.1 B). These racemic pairs connect to each other through NH⋯N hydrogen bonds in anhydrous forms or by solvate-mediated interactions (18). The system used for numbering the known olanzapine forms is sometimes confusing in the previous art disclosures. Thus, it was decided to follow SM Reutzel-Edens et al. (18) nomenclature for both anhydrous and hydrated forms.

Olanzapine raw material revealed to be in the anhydrous Form I and was used to prepare the different olanzapine forms (Chapter 3). Form I is an anhydrous form and the most stable crystalline form of olanzapine. Its chemical structure and main physicochemical properties are presented below in Table 2.1.

Table 2.1 – Physicochemical properties of olanzapine Form I (18, 132-134)

Properties	Olanzapine Form I
IUPAC Name	2-methyl-4-(4-methylpiperazin-1-yl)-5H-thieno [3,2-c][1,5]benzodiazepine
Chemical Formula	$C_{17}H_{20}N_4S$
General Designation	Anhydrate Form I
Molecular weight (MW)	312.43 g/mol
Density (ρ)	1.30 g/cm^3 (18)
Entries in the CSD	UNOGIN UNOGIN01 (18, 133)
Recrystallization from solvents	Can be recrystallised from anhydrous solvents such as ethyl acetate toluene, propyl acetate, isopropyl acetate, butyl acetate, tetrahydrofuran and acetone. Furthermore, it can be obtained from desolvation of several low alcohol solvates viz., methanol, ethanol and propanol and from dihydrates B, D and E (18)

2.1.1.1 Olanzapine Anhydrous forms

The first reported anhydrous form of olanzapine (herein referred to as Form II) revealed to be metastable and undergoes discoloration on exposure to air and moist environments (135). The second anhydrous polymorph to be reported (herein referred to as Form I) showed to have a higher stability and is therefore well adapted for commercial use (136). However, during its production, the stress created by temperature, mechanical treatment and the use of certain solvents may result in the concomitant appearance of both anhydrous polymorphic forms I and II as a final product (132). Olanzapine Form II is commonly prepared from de-solvation of methanol solvate and crystallized from acetonitrile and dichloromethane (18).

Many studies have been conducted on anhydrous forms I (most stable anhydrous form) and II (metastable form), for example, thermal behavior, vibrational spectroscopic and X-ray powder diffraction characterization (137-139). However, there is still a lack of information about how these anhydrous forms behave during processing and storage and how can they affect their pharmaceutical performance, being the latter one of the aims of the present work.

Regarding the thermal studies performed to both forms, it was observed that both forms presented endothermic peaks when heated, which reveled not to be related to their degradation. In Form I a endothermic transition was observed at a T_{onset} of about 194ºC, whereas Form II presented an endothermic peak at 177ºC, followed by an exothermal signal (recrystallization) superposed to the latter and, finally, an endothermic peak at about 194ºC (137). The superposed signs of the first endotherm and the exotherm reveled to be associated with the coexisting of Form II and Form I in the temperature range of 160-180ºC, when a X-ray powder diffraction diagram was taken to Form II in function of temperature (139). A satisfactory explanation for these facts was that the dimorphic monotropic relationship between both forms, where Form I is the most stable form at all temperatures below its melting point, and Form II is only converted into Form I after its melting due to the higher thermodynamic stability of Form I in relation to the melted Form II (137).

The vibrational spectroscopy study of both anhydrous forms revealed that the differences between forms I and II should be related with the atoms involved directly or indirectly with the NH intermolecular hydrogen bond, suggesting that weaker intermolecular interactions are present in Form II, explaining its lower density. These results provided additional support to the monotropic relationship proposed for the olanzapine forms (138).

Concerning the XRPD study carried out for both anhydrous forms, the powder pattern specific of each form was identified. The same study also developed a way to determine the amount of Form II olanzapine in Form I samples. However, the number of peaks, areas and preferred orientations showed to be strongly affected by the particle sizes (139).

2.1.1.2 Olanzapine dihydrates

Reutzel-Edens et al. (2003) (18) identified the structure of three OLZ dihydrates (B, D and E). Dihydrate D is considered to be the most stable, having a more organized crystal packing and therefore a higher dehydration temperature. Reference codes of the dihydrates of olanzapine found in the Cambridge Structural Database are: AQOMAU (dihydrate D), AQOMAU01 (dihydrate B) and AQOMAU02 (dihydrate E).

Both anhydrous and dihydrates of olanzapine present the olanzapine dimer that has been proposed to be the crystal building block (racemic pair) of olanzapine structures. The neighbor

dimers may come in contact with each other by the olanzapine hydrogen-bond donor – $N_{10}H$ and by the two good olanzapine acceptors - N_5 and $N_{4'}$.

While olanzapine Form I the NH-N_5 bond links the crystal building blocks with no participation of the piperidine $N_{4'}$, the hydrogen-bonding patterns in dihydrates B, D and E allow both N_5 and $N_{4'}$ to participate in hydrogen bondings due to the incorporation of water in their crystal forms. Therefore, the previously NH-N interaction in Form I is disrupted by bridging water molecules in hydrates- NH-O_w-H_w-O_w-N (Table 2.2).

Table 2.2 – Hydrogen-bond distances (Å) for different olanzapine crystal forms (18)

Forms	D-H···A	D···A
Form I	N10-H···N5	3.09
Dihydrate B	N10-H···O1	2.91
	O1-H_a···N4´	2.83
	O2-H_a···N5	2.99
	O1-H_b···O1	3.04
	O2-H_b···O1	2.94
Dihydrate D	N10-H···O1	2.86
	O2-H_a···N4´	2.82
	O2-H_a···N5	2.86
	O1-H_b···O2	2.85
	O1-H_b···O2	2.83
Dihydrate E	N10-H···O1	2.89
	O1-H_a···N4´	2.81
	O2-H_a···N5	3.06
	O1-H_b···O2	2.96
	O1-H_b···O1	2.96
Higher hydrate	N10-H···O1	2.90
	O1-H_a···N4´	2.79
	O2-H_a···N5	2.96
	O1-H_b···O2	2.78
	O1-H_b···O1	2.82
	O2-H_b···O3	2.61
	O3-H_b···O2	2.67

The water molecules of crystallization are positioned between the olanzapine dimers forming different olanzapine crystal building blocks. In dihydrates B and E the olanzapine building blocks are aligned in a herringbone motif while in dihydrate D they are aligned end-on-end and mounted directly on top of one another (Figure 2.2).
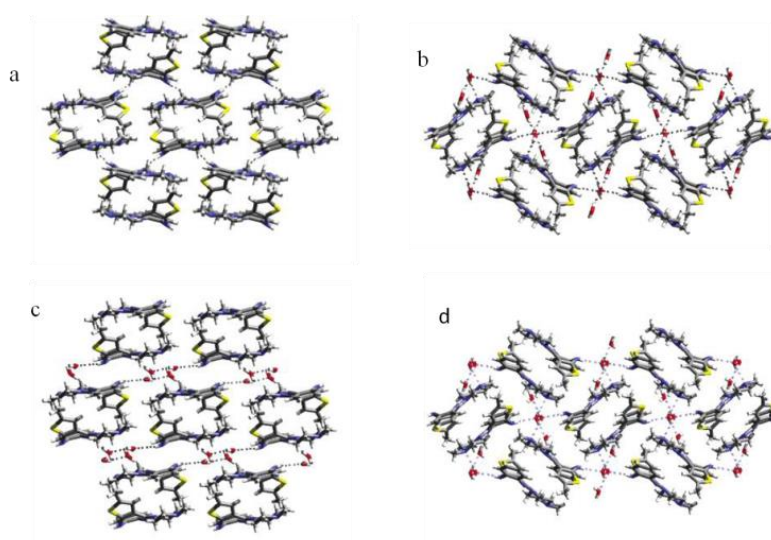
Figure 2.2 – Olanzapine crystal building blocks in (a) Form I, (b) dihydrate B, (c) dihydrate D and (d) dihydrate E [adapted from (18)]

The stability of the dihydrates can be well correlated with their densities (D: 1.285 > B: 1.278 > E: 1.239 g/cm^3), having the dihydrate D (the thermodynamically most stable form) the most efficient crystal packing.

2.1.1.3 Olanzapine higher hydrate

It is a metastable form containing 2-2.5 mol of water. It converts to dihydrate E within few minutes after being isolated from the crystallization solution. This Form is also reported in the CSD: AQOMEY. Crystallize from EtOAc-toluene-water mixtures at temperatures lower than 55 ^{o}C and dichloromethane-water mixtures.

2.1.2 Polyvinylpyrrolidone (PVP)

Polyvinylpyrrolidone or Povidone (PVP) has the following chemical formula: $(C_6H_9NO)_n$. It is a synthetic polymer consisting essentially of linear 1-vinyl-2-pyrrolidinone groups, the differing degree of polymerization of which results in polymers of various molecular weights.
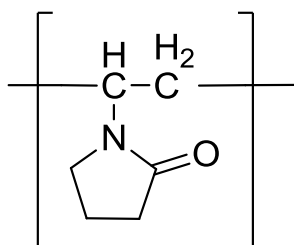
Figure 2.3 – Chemical structure of polyvinylpyrrolidone.

It is characterized by its viscosity in aqueous solution, relative to that of water, expressed as a K-value. Povidone is an amorphous powder and extremely hygroscopic, meaning

that significant amounts of moisture can be absorbed at low relative humidity. PVP's hygroscopic nature is attributed to the electronegative groups of the carbonyl group in the pyrrolidone structure which are able to establish hydrogen bonding with water (140).

Although povidone is used in a variety of pharmaceutical formulations, it is mainly used in solid-dosage forms. For instance, povidone solutions are used as binders in wet-granulation processes, or be added to powder blends in the dry form and granulated *in situ* by the addition of water, alcohol, or hydroalcoholic solutions. PVP has been shown to enhance dissolution of poorly soluble drugs from solid-dosage forms (141, 142), due to the presence of an hydrophilic lactam group and an hydrophobic vinyl in its molecular structure, which enables PVP to form amphiphilic micellar structures. The critical micelle concentration (CMC) of this polymer is 0.1% (m/v) (143, 144). A poorly soluble drug which is solubilized by PVP is present in the aqueous phase as individual, non-crystalline molecules, usually with a higher bioavailability. The mechanism of action of this polymer results on the large dipole moment of this polymer's side groups that are able to interact with any other dipole present in the system, forming complexes with the drug. PVP presents both hydrophilic and hydrophobic groups. Therefore, the polymer can interact with the poorly soluble drug and continuing to be water-soluble. The complex formation between the polymer and the drug is driven by entropy due to the release of water molecules previously bound to the polymer. However, the molecular interaction between the polymer and the drug resulting in a favorable enthalpy term is normally required for a good performance(145).

Povidone solutions may additionally be used as coating agents or as binders when coating active pharmaceutical ingredients on a support such as sugar beads. Furthermore, PVP can also be used as a suspending, stabilizing, or viscosity-increasing agent in a few of topical and oral suspensions and solutions. The solubility of a number of poorly soluble active drugs may be increased by mixing them with povidone (146).

When water is absorbed into the amorphous regions of PVP acts as a plasticizer, thus lowering the glass transition temperature (T_g) of the polymer (147).

2.1.3 Polyethylene glycol (PEG)

Polyethylene glycol (PEG) has the formula: $HOCH_2(CH_2OCH_2)_mCH_2OH$, where m represents the average number of oxyethylene groups. Alternatively, the general formula $H(OCH_2CH_2)_nOH$ may be used to represent polyethylene glycol, where n is the number m in the previous formula + 1 (146), as shown in Figure 2.4.
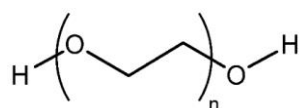
Figure 2.4 – Chemical structure of polyethylene glycol.

Polyethylene glycols are stable, hydrophilic and water-soluble. PEGs are commercially available from 200 to 10000000 g/mol molecular weight (MW), with MWs above 600 g/mol existing as semi-crystalline solids at room temperature. PEG has been widely used in pharmaceutical dosage forms, presenting low toxicity and cost (148).

In solid-dosage formulations, higher-molecular-weight polyethylene glycols can enhance the effectiveness of tablet binders and impart plasticity to granules. However, they have only limited binding action when used alone, and can prolong disintegration if present in concentrations greater than 5% w/w. Polyethylene glycols can also be used to enhance the aqueous solubility or dissolution characteristics of poorly soluble compounds by making solid dispersions with an appropriate polyethylene glycol (146).

PEG is a hygroscopic material. Cohen et al. (149) have shown a correlation between PEG MW and moisture sorption; however, these results were limited to a particular temperature and relative humidity (37ºC, 75% RH).

It was recently shown that semi-crystalline PEGs can undergo deliquescence at high relative humidity environments (148). Moisture sorption isotherms for PEG 1450, 3350, 6000, 8000 and 100000 showed that, at high relative humidities, PEG sorbs atmospheric moisture through the mechanism of deliquescence and that the deliquescence relative humidity (RH) decreased as PEG MW decreased (148).

2.1.4 Hydroxypropyl cellulose (HPC)

Hydroxypropyl Cellulose is a partially substituted poly(hydroxypropyl) ether of cellulose. Hydroxypropyl cellulose is commercially available in a number of different grades that have various solution viscosities.

$R = H$ or $CH_2CH(OH)CH_3$
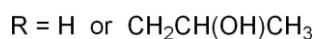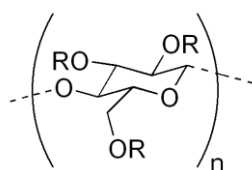
Figure 2.5 – Chemical structure of hydroxypropyl cellulose.

Molecular weight has a range of 50000–1250000. Hydroxypropyl cellulose is an ether of cellulose where some of the hydroxyl groups of the cellulose have been hydroxypropylated, forming $–OCH_2CH(OH)CH_3$ groups. HPC is often used in oral and topical pharmaceutical formulations. In oral products, hydroxypropyl cellulose is primarily used in tableting as a binder, film-coater and extended-release-matrix former. As an alternative technology to wet granulation, dry granulation and direct compression of HPC formulations have been reported to

exhibit acceptable tableting and flow characteristics for application in extended-release matrix tablets. Hydroxypropyl cellulose absorbs moisture from the atmosphere; the amount of water absorbed depends upon the initial moisture content and the temperature and relative humidity of the surrounding air. Typical equilibrium moisture content values at 25ºC are 4% w/w at 50% relative humidity (146).

Otsuka et al., (118) showed that HPC has an important role on the inhibition of the conversion between anhydrous and dihydrate forms of carbamazepine in aqueous solutions. They suggested that HPC altered the nucleation kinetics, and that this effect varied based on the grade and concentration of HPC.

2.1.5 Hydroxypropyl methylcellulose (HPMC)

HPMC is a partly O-methylated and O-(2-hydroxypropylated) cellulose. It is available in several grades that vary in viscosity and extent of groups substitution. Grades may be distinguished by appending a number indicative of the apparent viscosity, in mPa.s, of a 2% w/w aqueous solution at 20ºC. Molecular weight varies between 10.000–1.500.000. HPMC is widely used in oral, ophthalmic, nasal and topical pharmaceutical formulations. In oral products, HPMC is mainly used as a tablet binder, in film-coating and as a matrix for use in extended release tablet formulations. Concentrations between 2% and 5% w/w may be used as a binder in either wet- or dry-granulation processes. High-viscosity grades may be used to retard the release of drugs from a matrix at levels of 10–80% w/w in tablets or capsules. HPMC is hygroscopic.

The inhibiting effect of HPMC on polymorphic transformation kinetics was first addressed by Katzhendler et al. (150). These authors observed that the transformation of carbamazepine anhydrous into its dihydrate Form in aqueous solution was inhibited when using HPMC in a sustained release tablet. It was suggested that the inhibition was related to hydrogen bonding between HPMC and carbamazepine (151).

$R = H$ or CH_3 or $CH_2CH(OH)CH_3$
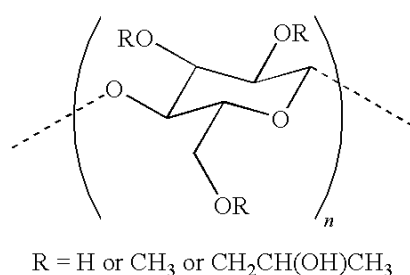
Figure 2.6 – Chemical structure of hydroxypropyl methylcellulose.

2.1.6 Microcrystalline cellulose (MCC)

Microcrystalline cellulose is commonly used in pharmaceuticals, primarily as a binder/diluent in oral tablet and capsule formulations where it is used in both wet-granulation and direct-compression processes (146).
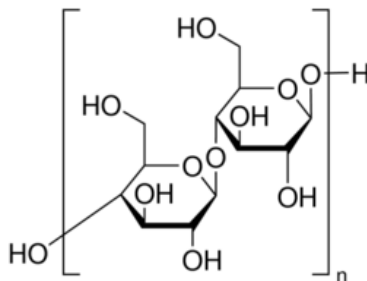
Figure 2.7 – Chemical structure of microcrystalline cellulose.

Furthermore, microcrystalline cellulose also has some lubricant and disintegrant properties that make it useful in tableting. MCC offers other advantages, including broad compatibility with APIs, physiological inertness, ease of handling and security of supply (146).

MCC is a white, odorless, tasteless, crystalline powder composed of porous particles. It is commercially available in different particle sizes and moisture grades that have different properties and applications. It is a hygroscopic material, which is related to the presence of abundant hydroxyl groups on cellulose chains. When exposed to 25°C and 50% relative humidity, its equilibrium moisture content is approximately 5%. However, different grades may contain varying amounts of water. The sorption mechanism involves water molecules tightly bound to accessible hydroxyl groups of the anhydroglucose units, followed by a second, less tightly bound layer, with further additional layers of water. Water is only sorbed in the amorphous regions of MCC, which are more hydrophilic than the crystalline regions. The crystallinity for microcrystalline cellulose showed to vary between 60−80%. Considering that the amorphous region is more hydrophilic, lower degrees of crystallinity should result in higher equilibrium moisture contents. Thus, it is proposed that the total amount of sorbed water is proportional to the fraction of amorphous material and is independent of the surface area (152).

2.1.7 Raw materials and raw materials suppliers

The raw materials used in the different experiments are listed in Table 2.3 with the respective suppliers

Table 2.3 – Raw materials and respective suppliers

Category	Substance	Supplier
APIs and Excipients	Olanzapine Form I	Pharmorgana (India)
	Olanzapine Form I	Vega Pharma (China)
	PVP K12, K25, K30 (Kollidon®)	BASF (Germany)
	HPC- LF (Klucel™)	Ashland (Germany)
	HPMC; Pharmacoat 615	Syntapharm (Germany)
	PEG 6000	Sigma Aldrich (Germany)
	PEG 40000	Sigma Aldrich (Germany)
	PEG 40000	Serva (Austria)
	Tricalcium Phosphate Tribasic	Sigma Aldrich (Germany)
	Polysorbate 80	Croda (Germany)
	MCC (Avicel® PH-101)	FMC corporation (USA)
	Sodium lauryl sulphate (Texapon K12 G)	Cognis (Germany)
	Lactose monohydrate (Granulac® 200)	Meggle Pharma(Germany)
Salts used for Stability Test	Lithium chloride	Sigma Aldrich (Germany)
	Magnesium Nitrate	Sigma Aldrich (Germany)
	Sodium Chloride	Sigma Aldrich (Germany)
	Potassium Nitrate	Sigma Aldrich (Germany)
Solvents	Methanol	Sigma Aldrich (Germany)
	Ethanol	Sigma Aldrich (Germany)
	Methylene chloride	Sigma Aldrich (Germany)
	Ethyl Acetate	Sigma Aldrich (Germany)
	Toluene	Sigma Aldrich (Germany)
Materials used to Prepare Dissolution Media	Hydrochloride Acid	Sigma Aldrich (Germany)
	Potassium Dihydrogen Orthophosphate	Fischer Scientific (UK)
	Sodium Phosphate Dibasic	Sigma Aldrich (Germany)
Gases	Nitrogen	Air Liquide (Portugal)
	Helium	Air Liquide (Portugal)
	Carbon Dioxide	Air Liquide (Germany)

2.2 Preparation of different polymorphic forms

2.2.1 Olanzapine anhydrous Form I (OLZ FI)

For the first study, where Form I and Form II were compared in terms of moisture sorption, olanzapine raw material (2 g) was recrystallized. It was suspended in ethyl acetate (20 ml). The stirred suspension was heated to 76 °C to dissolve the solids (18). The solution was then cooled to ambient temperature (25 °C) with formation of crystals (prismatic shape). The solid product was collected by filtration under vacuum and dried in an oven (50 °C/ 2 days) providing a dried powder, as shown by thermogravimetric evaluation (0.0% mass loss). The diffractogram pattern of the crystallized material was according to the Cambridge Structural Database (refcode: UNOGIN), identified as monoclinic, with a space group of P21/c (with a = 10.346 Å, b = 14.902 Å, c = 10.605 Å, β = 100.63°).

2.2.2 Olanzapine anhydrous Form II (OLZ FII)

Olanzapine Form II was obtained by recrystallization of raw olanzapine (1 g) from methylene chloride. Olanzapine was dissolved in 6 ml of methylene chloride and heated under reflux to assure dissolution of any remaining particles (70 °C/ 5 min). 0.1 g of a silica gel (37-63 μm) was added to remove undesirable impurities. The suspension formed was filtered (153). The filtrate was rapidly cooled to about 0 °C and the lath shaped crystals formed were filtered off and dried in an oven (40 °C / 2 days) showing no water present (thermogravimetry). The diffractogram obtained for this form was in accordance with Form II, which is described and characterized in many studies (137, 139, 153, 154). However, it must be pointed out the findings by Rajni et al. (2013) (130) who found that the metastable polymorph II is always contaminated with a closely related structure of a third polymorphic Form (III). Fortunately, these authors were able to extract one single crystal of Form II, from a mixture of both Forms II and III, enabling them to solve the structure. The powder pattern obtained from our dried crystals was indexed (*Appendix,* CELREF software) and consistent with the described Form II (monoclinic, space group P21/c, with a =9.8448 Å, b = 16.3409 Å, c = 9.9834 Å, β = 92.280°). However, 3 peaks were identified as contamination of Form III, namely at $2\Theta = 15.07°$, $19.28°$, $25.48°$. Based on the facts that the anhydrous Form II is never formed as a pure form, and the fraction of Form III is negligible, authors considered that the continuation of the study was justified and valid to enlighten and explain transformations during pharmaceutical production / crystallization of olanzapine polymorphs. For a better clarity of presentation, in this work the experimentally obtained Form II contaminated with traces of Form III, is referred to as Form II.

2.2.3 Olanzapine dihydrate B

Olanzapine (2.5 g) was suspended in ethyl acetate (25 ml) and toluene (2 ml) under stirring before heating (80 °C) for complete dissolution. Then, the solution was cooled down to 60 °C prior to the addition of water (30 ml) and further cooled down to room temperature, producing crystalline slurry. The crystals of the dihydrate B were collected by filtration under vacuum (18) (CSD refcode: AQOMAU01).

2.2.4 Olanzapine dihydrate D

Olanzapine (1 g) was suspended in water (10 ml) at room temperature for 7 days under stirring before filtration under vacuum for collection of the crystals formed (18) (CSD refcode: AQOMAU).

2.2.5 Olanzapine dihydrate E

Olanzapine (3g) was suspended in ethyl acetate (60ml) and toluene (3.6 ml). The suspension was stirred and heated to 80 °C for complete dissolution. The solution was then cooled to ambient temperature to produce a slurry. The suspension was filtered, washed with water and dried at room temperature (18) (CSD refcode: AQOMAU02).

2.3 Preparation of controlled humidity containers

To achieve the different relative humidity conditions, desiccators containing saturated salt solutions were prepared. Four different humidity containers were prepared using the following salts: lithium chloride (11.30 ± 0.27 %, referred in the text as 11 % RH), magnesium nitrate (52.89 ± 0.22 %, i.e., 53 % RH), sodium chloride (75.29 ± 0.12 %, i.e., 75 % RH) and potassium nitrate (93.48 ± 0.55 %, i.e., 93 % RH) (155).

2.4 Pelletization

Extruders can be divided into three main categories, according to their feed mechanism: screw feed (i.e., single- or twin-screw), gravity-feed (i.e., sieve, gear, cylinder, and basket) and ram extruders (108, 109).

In this work pellets were produced by ram extrusion. Ram extrusion is an example of a pumping mode process. A typical configuration is shown in Figure 2.8, where a moving ram compacts and extrudes a charge of paste through a die. Laboratory experiments usually feature a single-holed die plate, allowing the paste rheology to be characterized using capillary rheometry techniques (156). After the production of the extrudates they are spheronized and dried.
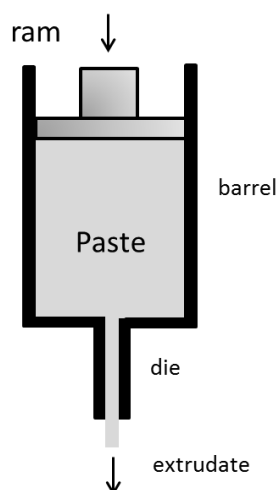
Figure 2.8 – Schematic representation of a ram extruder.

2.4.1 Equipment used for the extrusion/spheronisation of materials

In this work before the extrusion step powders were dry-mixed and kneaded in a planetary mixer (Chef, Kenwood, UK). Wet masses were extruded in a ram extruder (Lurga, Portugal) adjusted to a universal testing machine (LR 50K, Lloyds Instruments, UK) fitted with a load cell to allow the collection of data for the applied force to the ram and its displacement (200 mm/min). The wet masses were forced to pass through a die (Length/Diameter = 6) and, after extrusion, the extrudates were immediately placed in a spheroniser (radial friction plate rotating at 500 rpm, Caleva, UK). The wet pellets were dried in a fluid bed drier (Aeromatic-Fielder AG, Switzerland) at 45 ºC.

2.5 Preparation of nanoparticles by a technology using fluids in a supercritical state

A pilot scale unit designed for high-pressure extractions and RESS-technique (Sietec-Sieber, Switzerland) was used for particle design (Figure 2.9). Carbon dioxide was used as solvent in all experiments. The equipment comprises a tank, where the solvent is present in liquid state. Liquid CO_2 is then conveyed via a high-pressure pump into the extraction vessel with a volume of 5 l. After dissolution of the material placed inside the extraction vessel is completed, or an equilibrium between solid and dissolved material is reached, the supercritical solution is passed through a micro valve, which regulates the flow through the 150 μm nozzle. Upon passage of the nozzle, the supercritical solution is expanded inside the expansion chamber which is equipped with a paper filter to reduce the speed of the gas flow, thereby holding particles back in the chamber. To compensate for the cooling effect inside the expansion chamber, the mantle temperature was set to 70 °C for RESS experiments and to 55°C for RESSAS experiments. The pressure of the expansion chamber was kept at atmospheric

conditions (1 bar / 25 ºC). All RESS and RESSAS experiments were conducted during 1 h of expansion time with a medium CO_2 flow rate between 1.5 and 3.5 kg/h.

Figure 2.9 – Pilot unit designed for high-pressure extraction (RESS-technique).

2.6 Techniques considered for the characterization of materials and products

For each technique the principles of operation are highlighted, followed by the specification of the equipment used for the characterization of the materials.

2.6.1 Differential Scanning Calorimetry (DSC)

Differential scanning calorimetry (DSC) is a thermal analysis technique that looks at how a material's heat capacity (C_p) is affected by temperature. A sample of known mass is heated or cooled and the changes in its heat capacity are tracked as changes in the heat flow. This allows the detection of transitions such as melts, glass transitions and phase changes (157).

There are two types of DSCs: Heat flow DSC and Power compensation DSC. The DSC used in the experiments carried out (TA Instruments, USA) operates by heat flux and its descriptions are schematically represented in Figure 2.10. In heat flow DSC, both sample and reference are placed symmetrically inside the furnace and share a common heat source. The temperature difference between the sample and the reference is recorded (by thermocouples) and converted to a difference in heat flow rate to the sample and to the reference, using a suitable calibration factor (158).

Power compensation DSC involves two separated furnaces, one for the sample and a second one for the reference. The temperature difference between the two furnaces is kept similar by supplying an electric power to the sample furnace.
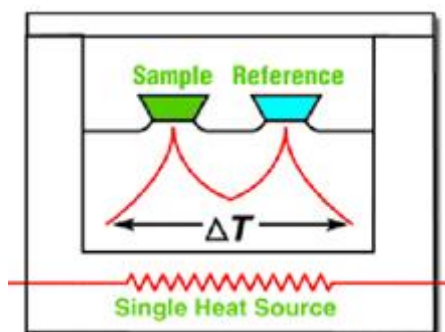
Figure 2.10 – Schematic representation of a heat flow DSC showing the sample and the reference pans location within the same furnace.

The differential heat flow measured during DSC experiments can be expressed by:

$$\frac{dQ}{dt} = \frac{\Delta T}{R}$$
Eq. 2.1

Where, *dQ/dt* represents the heat flow (where *Q* is heat and *t* is time); ΔT is the temperature difference between the furnace and the sample and *R* is the thermal resistance of the heat path between the furnace and the crucible.

When a given material is heated, the heat flow signal is determined by the heat capacity (C_p) of the material. Heat capacity can be described as the amount of energy required to raise the temperature of the sample by 1 K and can be expressed by:

$$\frac{dQ}{dt} = C_p \times \frac{dT}{dt}$$
Eq. 2.2

where *dT/dt* is the heating rate.

An inert atmosphere is essential in all DSC experiments which can be achieved by purging an inert gas into the cell. The selected gas is usually nitrogen however, helium can also be used. The purge gas provides more efficient heat transfer between the cell and the sample pan, helps to cool the cell, and allows the removing of moisture or oxygen which may accumulate and damage the cell over time.

To obtain accurate experimental results, routine calibrations processes and daily verification were carried out. The thermograms presented in this thesis were obtained with a Differential Scanning Calorimeter (TA instruments, Q200, USA). Dry N_2 was used as the purge gas (N45, Air Liquide, 50 ml/min).

2.6.2 Thermogravimetric Analysis (TGA)

Thermogravimetric analysis (TGA) is a technique of thermal analysis which measures changes in physical and chemical properties of materials as a function of increasing temperature (at a constant heating rate), or as a function of time (at a constant temperature and/or constant mass loss). TGA can provide information about physical phenomena, such as second-order phase transitions, including vaporization, sublimation, adsorption, absorption and desorption. Likewise, TGA can provide information about chemical phenomena including chemisorptions, desolvation (especially dehydration), decompositions and solid-gas reactions (e.g. oxidation/ reduction). TGA is commonly used to determine selected characteristics of materials that exhibit either mass loss or gain due to decomposition, oxidation or loss of volatiles (such as water).

All the thermogravimetric analyses in this work were carried out in a TGA (7, Perkin-Elmer, USA). The samples were placed in an open platinum crucible. The balance chamber was kept under a positive nitrogen flow (Air Liquide N45) of 38 $cm^3 \cdot min^{-1}$ and helium (Air Liquide N55) at a flow of 22.5 $cm^3 \cdot min^{-1}$ was used as sample purge gas. The mass scale of the instrument was calibrated with a standard 100 mg weight. The temperature calibration was based on the measurement of the Curie points (T_C) of alumel alloy (Perkin-Elmer, $T_C = 427.35$ K) and nickel (PerkinElmer; mass percentage 99.999%, $T_C = 628.45$ K) standard reference materials.

2.6.3 Scanning electron microscopy (SEM)

Olanzapine powders and pellets were analyzed by scanning electron microscopy. The samples were mounted on aluminum stubs and coated with gold by ion sputtering (JEOL JFC-1200 Fine Coater, Japan) and were observed under a scanning electron microscope (JSM-5200 LV, Japan).

2.6.4 Hot stage microscopy (HSM)

Hot-stage microscopy (HSM) is a technique widely used to visually examine thermal transitions of the materials when the sample is heated or cooled. This analytical technique enables the characterization of physical properties of materials such as melting, solid state transformations, recrystallizations, etc. as a function of temperature. High resolution color cameras and image manipulation software are nowadays powerful accessories of HSM that enable the recording of thermal events happening during the heating/cooling cycles of the sample (159).

In this thesis, the size and shape of different olanzapine forms were observed under a microscope with polarized light (Olympus BX51, Japan) fitted with a heating stage (Linkam THMS350V, UK).

2.6.5 Fourier transform infrared (FTIR)

Fourier transform infrared (FTIR) is a spectroscopic technique that provides information about the molecular composition, structure and interactions within a sample based on its chemical bonds. In infrared spectroscopy, IR radiation is passed through a sample. Some of the infrared radiation is absorbed by the sample and some of it is passed through it (transmitted). The resulting spectrum represents the molecular absorption and transmission, creating a molecular fingerprint of the sample. Like a fingerprint, no two unique molecular structures produce the same infrared spectrum. This makes infrared spectroscopy useful for several types of analysis, being commonly used for identification, characterization, quantification, structure elucidation, reaction monitoring, quality control and quality assurance (160).

In this technique, the samples are irradiated with a polychromatic light in the IR region (4000 to 400 cm^{-1}) and a photon of light is absorbed when the frequency (energy) of the absorbed light matches the energy required for a particular bond to vibrate within the sample. In order for a vibration to be IR active, the molecular dipole moment must change during the vibration. Any IR light that has not been absorbed is transmitted to the sample to a detector. The fraction of transmitted light allows the absorbed frequencies to be determined (161).

The FTIR spectroscopic analyses present in this thesis were performed in an IR Affinity-1 Shimadzu spectrophotometer (Japan). For the analyses, the samples were mixed with KBr. The mixtures (±200 mg) were compressed into a tablet of 12 mm diameter. The infrared spectra were measured at the absorption mode with 64 scans with a resolution of 2 cm^{-1}.

2.6.6 Diffuse Reflectance Infrared Fourier transform (DRIFT)

DRIFT is an infrared spectroscopy technique used on powder samples. In this technique the preparation of the sample does not involve the preparation of a KBr tablet, and, therefore, no compression is involved. The preparation of the sample is achieved by the simple dilution of the material with nonabsorbent KBr. The spectra are plotted in Kubelka-Munk units versus wavenumber. The Kubelka-Munk units plots can relate reflectance to concentration using a scaling factor.

In this work, the dilution of the sample in KBr powder was in appropriate weight proportions to obtain spectral absorbance in the range of applicability of the Kubelka–Munk transformation (162).

$$KM = F(R_\infty) = \frac{(1-R_\infty)^2}{2R_\infty} = \frac{k}{s} = \frac{\varepsilon c}{s} = \frac{2.303ac}{s} \qquad \text{Eq. 2.3}$$

where $F(R_\infty)$ is the Kubelka–Munk spectrum; (R_∞) is the absolute reflectance of the spectrum; s is the scattering factor, which is dependent on sample preparation; k is the absorption coefficient, equal to 2.303ac or εc; ε is the molar extinction coefficient of the analyte; a is the

absorptivity related to analyte species; and c is an analyte concentration. Therefore, *KM* intensity is linearly proportional to the concentration of the analyte if the scattering factor is controlled.

In this work the spectra in diffuse reflectance mode were collected by a Nicolet 6700 spectrometer (Thermo Electron Corp., Madison, USA) equipped with a deuterated triglycine sulfate (DTGS) detector (4000–400 cm^{-1}) and a Smart Diffuse Reflectance (SDR) kit (Thermo Electron Corp.). Spectra were obtained from 528 scans with a resolution of 2 cm^{-1} for the sample and background experiments. Data was acquired with the OMNIC 8.1 software (Thermo Fisher Scientific, USA).

2.6.7 Near Infrared spectroscopy

Near-infrared spectroscopy (NIRS) is a spectroscopic method that uses the near-infrared region of the electromagnetic spectrum from about 700 nm to 2500 nm. NIR can typically penetrate much farther into a sample than mid infrared radiation. Near-infrared spectroscopy is not a particularly sensitive technique, but it can be very useful in probing bulk material with little or no sample preparation. The molecular overtone and combination bands seen in the near-IR are commonly very broad, leading to complex spectra; it can be difficult to assign specific features to specific chemical components. Multivariate (multiple variables) calibration techniques (e.g., principal components analysis, partial least squares, artificial neural networks) are often used to extract and summarize the data.

A Thermo Scientific Antaris FTNIR spectrometer equipped with an InGaAs detector was used in this study. The spectrum was acquired with a reflectance probe (Sabir, Thermo Nicolet, USA) having an illumination area with a diameter of 0.5 cm. The equipment is controlled via the RESULTS software (Thermo Scientific, USA).

2.6.8 X-ray powder diffraction (XRPD)

X-ray powder diffraction (XRPD) is a rapid analytical technique primarily used for phase identification of a crystalline material and can provide information on unit cell dimensions.. X-rays are generated by a cathode ray tube which works as a source of electrons, which are then accelerated and strike a target (the anode) and produces a characteristic X-ray spectrum (163). When X-rays pass through the sample they interact with the electron cloud of atoms in the molecules and the intensity and position of the emergent X-rays are recorded by a detector. The interaction of the incident rays with the sample produces constructive interference (and a diffracted ray) when conditions satisfy Bragg's Law ($n\lambda=2d$ sin θ, where n is a positive integer and λ is the wavelength of incident wave). This law relates the wavelength of electromagnetic radiation to the diffraction angle and the lattice spacing in a crystalline sample. These diffracted X-rays are then collected, processed and counted. By scanning the sample through a range of 2θ angles, all possible diffraction directions of the lattice should be attained

due to the random orientation of the powdered material. The regularly spaced atoms (electrons) in a crystal solid can be described by imaginary planes and the distance between these planes is called the *d-spacing*. The intensity of the d-space pattern is directly proportional to the number of electrons (atoms) that are found in the imaginary planes. Every crystalline solid will have a unique pattern of *d-spacings* (known as the powder pattern). Therefore, XRPD is a gold standard technique in the characterization of pharmaceutical materials in the solid state. It is mainly used for fingerprinting and quantification analysis due to its high sensitivity to small chemical changes. Prior to the analysis of the material, it should be finely ground and homogenized and average bulk composition is determined.

In this work, XRPD analyses of solids were performed in two different equipment: Equipment 1: The X-ray powder diffractograms were recorded at room temperature by a diffractometer (Philips PW1730, Netherlands) with automatic data acquisition software (APD Philips v.35B, Netherlands) using a Cu Kα radiation source. The tube amperage was 30 mA and the tube voltage 40 kV. Equipment 2: The structural characterization of the samples was carried out by X-ray powder diffraction (XRPD) on an Analytical X'Pert PRO apparatus (Netherlands) set with a vertical PW 3050/60 goniometer (θ-2θ mode) equipped with X'Celerator detector and with automatic data acquisition (X'Pert Data Collector (v2.0b) software), using a monochromatized CuKa radiation as incident beam, 40 kV–30 mA. The scanning range was based on the characteristics peaks of each sample.

2.6.9 Dissolution testing

Dissolution testing of pharmaceutical solids is a very important test in drug product development, manufacturing and in regulatory assessment of the drug product quality. It provides essential information on the rate and extent of drug dissolution (164).

The dissolution process of solids comprehends two main steps. Firstly, the molecules at the solid-liquid interface are wetted, solvated and detached from the solid surface. Secondly, the solvated molecules diffuse away from the interface to the bulk solution. Thus, it is the diffusion rate of the molecules in the media and/or the wetting and solvation of the surface molecules that determine the dissolution profile of a certain compound (165).

The dissolution rate ($\delta M/\delta t$) of a solid in a liquid can be described by the Noyes-Whitney equation as presented below:

$$\frac{\delta M}{\delta t} = A \times \frac{D}{h} \left(C_s - C_b \right) \qquad \textbf{Eq. 2.4}$$

where, *M* is the mass; *t* is the time; *A* is the surface area of the undissolved solid in contact with the solvent; *D* is the diffusion coefficient (m^2/s); *h* is the thickness of diffusion layer; C_s is the solubility; C_b is the concentration in the bulk solution; and C_s-C_b is the concentration gradient.

The above equation assumes that the surface area and thickness of the hydrodynamic diffusion layer remain constant.

Dissolution experiments were carried out using a dissolution apparatus (AT7, Sotax, Switzerland, paddle method). Each vessel was filled with 900 ml of dissolution medium, the temperature was set at 37.0±0.5 °C and a rotation speed of 50 rpm was used. The concentration of each API through the dissolution tests was assessed spectrophotometrically at the respective wavelength of maximum absorbance, λ_{max}, using a UV spectrometry (λ= 254 nm, Hitachi U-2000, Japan).

Dissolution profiles may be considered similar by virtue of the overall profile similarity and similarity at every dissolution sample time point. The comparison of dissolution profiles may be carried out using model independent methods. A simple model independent approach uses a difference factor (f_1) and a similarity factor (f_2) to compare dissolution profiles (166). The concept of similarity factor (f_2) has been endorsed by the Food and Drug Administration (FDA) turning this factor widely adopted in formulation and development and accepted by health authorities (167). The difference factor (f_1) calculates the percentage (%) difference between the two curves at each time point and is a measurement of the relative error between the two curves:

$$f_1 = \{[\textstyle\sum_{t=1}^{n}|R_t - T_t|]/[\sum_{t=1}^{n} R_t]\} * 100 \qquad \textbf{Eq. 2.5}$$

where, n is the number of time points; R_t is the dissolution value of the reference batch at time t; and T_t is the dissolution value of the test batch at time t. The similarity factor (f_2) is a logarithmic reciprocal square root transformation of the sum of squared error and is a measurement of the similarity in the percentage (%) dissolution between the two curves:

$$f2 = 50 \times \log\left\{\left[1 + \left(\tfrac{1}{n}\right) \times \textstyle\sum_{t=1}^{n}(R_t - T_t)^2\right]^{-0.5} \times 100\right\} \quad \textbf{Eq. 2.6}$$

For 2 curves to be considered similar, f_1 values should be close to 0 and f_2 values should be close to 100. Generally, f_1 values up to 15 (0-15) and f_2 values larger than 50 (50-100) ensure sameness or equivalence of the two curves and, therefore, of the performance of the test and reference pharmaceutical products. This independent model method is most suitable for dissolution profiles comparison when more than four dissolution sampling time points are available. Furthermore, the following recommendations should also be considered (167):

- The dissolution measurements of the test and reference batches should be made under the exact same conditions. The dissolution time points for both profiles should be the same (e.g., 10, 20, 30, 60 min). The reference batch used should be the most recently manufactured product;

- Only one measurement should be considered after 85% dissolution of both products.

- To allow use of mean data, the percent coefficient of variation at the earlier time points (e.g., 15 min) should not be more than 20%, and at other time points should not be more than 10%.

To compare the dissolution profiles between 2 drug products, model-dependent approaches such as zero-order, first-order, Hixson-Crowell, Higuchi, quadratic, Weibull or logistic models may be applied.

2.6.9.1 Zero-order model

For zero-order release kinetics, the dissolution of a drug molecule is only a function of time. This model holds true only in the case of very slow drug release. For instance, this relation can be used to describe the drug dissolution of several types of modified release pharmaceutical dosage forms, such as some transdermal systems, matrix tablets with low soluble drugs, coated forms, osmotic systems, etc.

Zero-order release is therefore modeled as follows:

$$W_0 - W_t = Kt \qquad \text{Eq.2.7}$$

where, W_0 is the initial amount of drug in the pharmaceutical dosage form; W_t is the amount of drug in the pharmaceutical dosage form at time t; and K is the zero-order release constant (168).

2.6.9.2 First-order model

Nowadays most drug delivery systems present first-order drug release kinetics, where the plasma level of the drug is extremely high after administration and then decreases exponentially. This has disadvantages such as minimal therapeutic efficacy due to reduced drug levels or drug toxicity which can take place at high concentrations (169). The First-Order model is derived from First-Order release kinetics, which states that the change in concentration with respect to change in time is dependent only on concentration.

The release of the drug which followed first order kinetics can be expressed by the equation:

$$\frac{dC}{dt} = -KC \qquad \text{Eq. 2.8}$$

where, C is the concentration of the drug molecule; and K is first order rate constant expressed in units of time.

Integrating the equation, one has:

$$\ln(C_t) = \ln(C_0) + Kt \qquad \text{Eq. 2.9}$$

where, C_0 is the initial concentration of drug; C_t is the concentration of the drug at the time t; and K is the first order rate constant (168). This relationship can be used to describe the drug's

dissolution in pharmaceutical dosage forms, such as those containing water-soluble drugs in porous matrices.

2.6.9.3 Hixson and Crowell model

Hixson and Crowell proposed an equation which expresses the rate of dissolution based on the cubic root of particle weight:

$$W_0^{\frac{1}{3}} - W_t^{\frac{1}{3}} = K_s t \qquad\qquad \textbf{Eq. 2.10}$$

where, W_0 is the initial amount of drug in the pharmaceutical dosage form; W_t is the remaining amount of drug in the pharmaceutical dosage form at time t; and K is a constant incorporating the surface–volume ratio (168). This expression is applicable to pharmaceutical dosage forms in which dissolution happens in planes parallel to the drug's surface (e. g., tablets), maintaining the drug's original geometry. The equation 2.10 can be rewritten as:

$$W_0^{\frac{1}{3}} - W_t^{\frac{1}{3}} = \frac{K'N^{\frac{1}{3}}DC_s t}{\delta} \qquad\qquad \textbf{Eq. 2.11}$$

where, N is number of particles; K' is a constant related to the surface area, shape and the density of the particle; D is the diffusion coefficient; C is the solubility in the equilibrium at experience temperature; and δ is the thickness of the diffusion layer. The shape factors for cubic or spherical particles should be kept constant if the particles dissolve in an equal manner in all sides.

2.6.9.4 Higuchi model

This is the first mathematical model that describes drug release from a matrix system. This model is based on the following hypothesis: (1) initial drug concentration in the matrix is much higher than drug solubility; (2) drug diffusion takes place only in one dimension (edge effect should be avoided); (3) drug particles are much smaller than thickness of system; (4) swelling of matrix and dissolution are small or negligible; (5) drug diffusivity is constant; and (6) perfect sink conditions are always attained in the release environment (168). The study of dissolution from a planar system having a homogeneous matrix can be obtained by the equation:

$$ft = \frac{M_t}{A} = \sqrt{D(2C - C_s).C_s t} \qquad\qquad \textbf{Eq. 2.12}$$

where: M_t is the cumulative absolute amount of drug released at time t; A is the surface area of the controlled release device exposed to the release medium; C is the drug's initial concentration; C_S is the drug solubility in the matrix media; and D is the diffusivity of the drug molecules (diffusion constant) in the matrix substance (170).

2.6.9.5 <u>Korsmeyer–Peppas model</u>

Korsmeyer–Peppas model propose a simple relationship which describes the release of a drug from a polymeric system according to the following equation (171) :

$$f_t = Kt^n \qquad \text{Eq. 2.13}$$

where, f_t is fraction of drug released at time t; k is the release rate constant; and n is the release exponent. The diffusion of a drug from a controlled release polymeric system with the form of a plane sheet of thickness δ can be represented by:

$$\frac{\partial c}{\partial t} = D \left(\frac{\partial^2 c}{\partial x^2} \right) \qquad \text{Eq. 2.14}$$

where, D is the drug diffusion coefficient (concentration independent). If drug release occurs under perfect sink conditions, the following initial and boundary conditions can be assumed:

$$t = 0 \qquad -\frac{d}{2} < x < \frac{d}{2} \qquad c = c_0 \qquad \text{Eq. 2.15}$$
$$t > 0 \qquad x = \pm\frac{d}{2} \qquad c = c_1 \qquad \text{Eq. 2.16}$$

where, c_0 is the initial drug concentration in the device; and c_1 is the concentration of the drug at the polymer–water interface.

The solution equation under these conditions was developed initially by Crank:

$$\frac{M_t}{M_\infty} = 2 \left(\frac{Dt}{\delta^2} \right)^{\frac{1}{2}} \left[\pi - \frac{1}{2} + \sum_{n=1}^{\infty} (-1)^n i\ erfc\ \frac{n\delta}{2\sqrt{Dt}} \right] \qquad \text{Eq. 2.17}$$

A sufficiently accurate expression can be obtained for small values of t due to the elimination of the second term in Eq. 2.17, becoming:

$$\frac{M_t}{M_\infty} = 2 \left(\frac{Dt}{\delta^2} \right)^{\frac{1}{2}} = at^{\frac{1}{2}} \qquad \text{Eq. 2.18}$$

Hence, when the diffusion is the main drug release mechanism, a graphical representation of the drug amount released in the referred conditions versus the square root of time should form a straight line. Under certain experimental situations the release mechanism deviates from the Ficks equation, following an anomalous behavior (non-Fickian). In these cases a more generic equation can be used:

$$\frac{M_t}{M_\infty} = at^n \qquad \text{Eq. 2.19}$$

Where, n value is used to characterize different releases for cylindrical shaped matrices; in the case of cylindrical tablets, $0.45 \leq n$ corresponds to a Fickian diffusion mechanism, $0.45 < n < 0.89$ to non-Fickian transport, $n = 0.89$ to Case II (relaxation) transport, and $n > 0.89$ to super

case II transport. In order to determine the value of the exponent 'n', only the portion of the release curve where $M_t/M_\infty < 0.6$ should be used (168).

CHAPTER 3

Part of the work presented in this chapter has been <u>accepted</u> in:

Chapter 3 - Production, characterization and stability over storage of two olanzapine anhydrous polymorphic forms

3.1 Abstract

The focus of this study was the understanding of the hydrate transformations of anhydrous olanzapine forms I and II upon exposure to different moisture conditions (11, 53, 75, 93% RH) and direct contact with water (e.g. aqueous slurry) and the impact of hydration on the aqueous dissolution rates of the polymorphs. The kinetics of the transformations and the identification of polymorphs were evaluated by differential scanning calorimetry, thermogravimetry, infrared and X-ray powder diffraction. The results showed that anhydrous forms I and II have undergone water vapor phase induced transformations at 93% and 75% RH, respectively. At 93% RH, anhydrous forms I and II showed to hydrate into dihydrates D and B, respectively, the latter with a higher hydration rate. The conversion of form I into the dihydrate D showed to affect the dissolution rate of olanzapine ($f_2 < 50$). As slurries both forms showed to hydrate into a mixture of two different forms – dihydrate B and higher hydrate. The study provided an understanding of the conversion pathways of the different forms when they were exposed to humid air or aqueous environments, resembling the transformations that might occur during processing, storage or during the persecution of dissolution tests to assess the quality of dosage forms delivering olanzapine.

3.2 Introduction

Approximately one third of all compounds used in the manufacture of medicines are able to hydrate. The new unit cells, in which water is a part of the crystal, may be obtained presenting completely new properties (172).

The behavior of the anhydrous form of a drug substance in equilibrium with water can be reflected by phase diagrams which are drug substance specific (81, 173). A crystal hydrate is typically the most stable form of a drug substance in an aqueous environment, presenting as a consequence lower solubility and dissolution rates than its anhydrous counterpart (174) . Therefore, the conversion of an anhydrous form into a hydrate form, during processing or storage may modify the bioavailability of the drug, particularly when the dissolution in an aqueous environment is the rate limiting step for the absorption of that drug (5, 70).

The study of the physical stability of both anhydrous and hydrate forms of olanzapine, as a function of water vapor pressure, is important to understand and prevent a reduction on the therapeutic performance of the drug as a result of their inter-conversion (75, 175). Thus, understanding the stabilities of the different forms with a potential interplay is paramount to the selection of the appropriate storage conditions for the molecular structure to be kept stable (6). When active pharmaceutical ingredients (API) are subjected to different water vapor pressures, solid-state polymorphic transitions are likely to take place (176). A solid-state conversion requires the migration of water through the crystal lattice and a potential change in the crystal structure. Often, the kinetics of phase transition via a solid-state mechanism can be very slow, and in the early stages of drug development it is generally not possible to run an extended stability program, which enhances the difficulties to select the appropriate form of the material to progress the program (177).

Olanzapine (OLZ) is a drug that can crystallize in several forms, including various anhydrates, solvates and hydrates (18). All olanzapine crystal phases present a structural building block which is composed by a dimeric unit formed by two racemic olanzapine molecules. This racemic pairs are connected to each other through NH$^{..}$N hydrogen bonds in anhydrous forms or by solvate-mediated interactions in solvates and hydrates (18).

The first reported anhydrous form of olanzapine (referred to herein as Form II) revealed to be metastable and underwent discoloration on exposure to air and moist environments (135). This discoloration revealed to be caused by the formation of olanzapine hydrates, which present a less intense color than anhydrous olanzapine. However, the type of hydrates obtained, the moisture required, expressed as relative humidity, needed for their appearance and the impact of such phenomenon on the performance of the olanzapine solid dosage forms has not been reported, to the authors' best knowledge.

The second anhydrous polymorph to be reported (referred to herein as Form I) showed to have a higher stability and therefore is well adapted for manufacture purposes (136). However, during its production, the stress created by temperature, mechanical treatment and the use of certain solvents (e.g. methylene chloride) may result in the concomitant appearance of both anhydrous polymorphic Forms I and II as the final product (132). Because both forms have different crystalline structures, a contamination of Form I by Form II may result in changes on the physical characteristics of the final product, which may influence the therapeutic performance of olanzapine.

Although many studies have been conducted on the characterization of these two anhydrous forms (e.g. thermal behavior, infrared spectroscopy and X-ray powder diffraction, (137-139), there still is a lack of information about the hydration mechanism and rate of conversion of these anhydrous forms in response to exposure to humid environments (e.g. slurries or different relative humidity environmental conditions) and the potential ability of hydrated forms to dehydrate into the ones considered before storage or processing. The identification and quantification of such conversions is of importance to firstly understand and secondly prevent a change on the drug's structure with a deleterious impact on its therapeutic performance due to solubility differences of the different polymorphs reflecting different crystalline structures. Furthermore such knowledge can also allow the selection of the appropriate storage conditions for a particular molecular structure to be kept stable improving the final quality of the medicine

The type of hydrates, the conditions needed to promote their appearance and the impact of such phenomenon on the performance of the olanzapine solid dosage forms has not been reported, to the authors' best knowledge. Furthermore the consequences of those expositions on dosage form's performance, namely olanzapine dissolution rate have not been studied. This study, therefore, gains a special interest in the olanzapine molecule since it may crystallize into different hydrates (namely, dihydrate B, D, E and one higher hydrate form) and their mixtures.

Olanzapine is a drug commonly used in the treatment of schizophrenia, an illness which requires patients to be kept clinically stable and in good compliance with the treatment. Thus, minor changes on olanzapine's bioavailability turns patients unstable followed by a decrease on compliance. Furthermore, the small recommended dose for olanzapine (maximum dose of 20 mg per day) (178), enhances potential problems due to changes on the solubility of olanzapine with impact on the drug dissolved and then on absorption into the plasmatic stream, simply due to minor modifications of the crystalline structure of the drug.

3.3 Purpose

This study aims, firstly, to compare the stability of 2 anhydrous Forms (I and II) during storage at different relative humidity, to identify the relative humidity and the exposure time needed to promote crystalline changes in both anhydrous polymorphic structures. Secondly, to prepare two model tablet formulations containing the different forms obtained before and after exposure to humidity, focusing on the understanding of the relationship between the solid state of the drug and their dissolution rate. Finally, the conversions of the hydrates which occur due to exposure to moisture are compared with the hydrate transformations which occur in aqueous environments. The studies help to identify the phase transitions that may occur during storage or processing of olanzapine raw-materials.

3.4 Material and Methods

3.4.1 Production of the different olanzapine forms

Olanzapine anhydrous Form I (Form I), anhydrous Form II (Form II), dihydrate B (dihyd.B), dihydrate D (dihyd. D) and dihydrate E (dihyd. E) were prepared as shown in materials and methods section. Olanzapine raw-material was purchased from Pharmaorgana laboratories (India).

3.4.2 Samples preparation and storage under controlled relative humidity environment

Particle size, size distribution and habit have been shown to influence significantly the water uptake, and therefore, the approach of gentle grinding and sieving the materials was necessary to obtain the two crystal forms with similar particle size and size distribution in the same range (179). In the present study, the materials were gentle milled for 1 min with a mortar and a pestle and subsequently sieved (< 63 um) in order to obtain the two crystalline forms within the same particle size and size distribution. The materials showed not to undergo any solid phase transition during milling. After sieving, the anhydrous Forms I and II of olanzapine were stored in different controlled relative humidity environments (24 °C) in desiccators containing saturated salt solutions (155), namely, lithium chloride (11 % RH), magnesium nitrate (53 % RH), sodium chloride (75 % RH), potassium nitrate (93 % RH). Samples of olanzapine powder were collected at 0, 7, 14, 21, 30, 60 and 180 days of storage prior to characterization.

3.4.3 Preparation of tablets

Tablets containing olanzapine were prepared to evaluate the impact of moisture which might be present as absorbed/adsorbed within the tablets on the dissolution performance of olanzapine. Six sets of tablets (150 mg) were prepared and characterized for each olanzapine

polymorph (5mg) – OLZ FI, OLZ FII, prior and after 6 month storage at 93% RH condition. All olanzapine particulate samples were sieved (<63 μm) and dissolution tests conducted under sink conditions. The excipients for tableting were lactose monohydrate (145 mg, Granulac 200 Meggle, Germany) or a mixture of 40% (58 mg) of lactose monohydrate and 60% (87mg) of microcrystalline cellulose (Avicel, FMC Corp., USA). The different formulations aimed to evaluate the release profile of olanzapine in immediate and sustained release solid dosage forms. Tablets were manufactured with punches and die with 6.5 mm in diameter, at compaction forces of 20.0 kN applied by the upper punch moving at a speed of 10 mm/min, assembled in an universal mechanical press (LR 50K, Lloyd's Instruments, UK).

3.4.4 Experiments with Slurries

In order to evaluate the conversion of anhydrous forms into hydrated forms in aqueous environments, anhydrous powders where initially suspended in aqueous solutions. The olanzapine suspensions were prepared by adding 5 ml of water to 50 mg of each anhydrous olanzapine form. The slurries were stirred with an overhead mechanical stirrer at approximately 250 rpm. Samples of 50 μl were taken at 15, 30, 60, 90, 120 and 1440 min of agitation and filtered under vacuum, before their characterization carried out as described for the pure polymorphs.

3.4.5 Characterization of different OLZ polymorphic forms

Thermo Gravimetric Analysis (TGA)

Thermogravimetric analysis (Perkin-Elmer TGA 7, USA) was performed on olanzapine samples (3-4 mg) placed in an open platinum crucible heated at 10 °C/min scanning rate between 20 to 150°C. The balance chamber was kept under a positive pressure nitrogen flow (N45, Air Liquide, Portugal) of 38 cm^3/min and helium (N55, Air Liquide, Portugal) at a flow rate of 22.5 cm^3/min was used as the sample purge gas.

Differential scanning calorimetry (DSC)

Thermograms of different olanzapine forms were obtained with a Differential Scanning Calorimeter (TA instruments, Q200, USA) after calibration with indium (TA instruments, USA; T_{fus} =156.55°C, $\Delta_{fus}H$ = 28. 51 J/g). Dry N_2 was used as the purge gas (50 ml/min). For anhydrous olanzapine, 2 to 3 mg were placed in hermetic crucibles, while for stored olanzapine samples the same amount was placed only in non-hermetic crucibles. The option to use non-hermetic crucibles was made in order to avoid the possible rupture of the crucibles due to pressure of water vapor and also to prevent the appearance of metastable forms due to free water vapor in the atmosphere around the crystal (180). Samples were heated up at 10 °C/min within 0-210 °C temperature range.

Assessment of particle size distribution

The particle size distribution was measured with laser diffractometry (LD) using a Mastersizer 2000 (Malvern, Germany) equipped with a Hydro 2000S sample dispersion unit. The olanzapine powder was suspended in a dispersant solution (0.1% polysorbate in water) in order to achieve a good contact between the particles and surfactant/dispersant and to efficiently promote OLZ particle disaggregation. The suspension was shaken with a vortex prior to the measurement. The obscuration values were between 2 and 5% for the different measurements (n=6). Particle size and size distribution were obtained from the manufacturer's software (Malvern, Germany).

Hot stage microscopy

The size and shape of different olanzapine anhydrous forms were observed under the microscope with polarized light (Olympus BX51, Japan) fit with a heating stage in order to visualize of the change in shape of the crystals of form II with temperature (Linkam THMS350V, UK). The sample of anhydrous form II was heated up to 220 °C with a scan rate of 10 °C/min.

X-Ray powder diffraction (XRPD)

The X-ray powder diffractograms were recorded at room temperature by a diffractometer (equipment 1: Philips PW1730, NL). The samples were mounted on an aluminum sample holder and scans in the range of 7 to 35° (2θ) in the continuous mode, with a step size of 0.015° (2θ) and an acquisition time of 1 s/step.

Diffuse Reflectance Infrared Fourier Transformed Spectroscopy (DRIFT)

Different olanzapine samples were diluted in KBr (olanzapine concentration about 0.1 % w/w). The spectra in diffuse reflectance mode were collected on a Nicolet 6700 spectrometer (Thermo Electron Corp., Madison, WI), with 528 scans being acquired for each sample with a resolution of 2 cm^{-1}.

3.4.6 Quantification of olanzapine hydration using the DRIFT spectra

This analytical method has been effectively used in combination with a chemometric technique, partial least squares (PLS) for quantification of polymorphs.

PLS or projection to latent structures has been frequently applied in the area of chemometrics. It is a factor analysis method that relates a matrix of independent variables, X, with a matrix of dependent variables, Y. PLS decomposes both X and Y matrices, the spectral data and polymorph concentrations, respectively, into their principal components, i.e. obtaining score and loading matrices. The principal components are called latent variables or PLS components. These latent variables are obtained by maximizing the variance of the data. The

number of latent variables is much lower than the number of original variables. However, PLS may possibly extract as much of the initial information as possible while acquiring maximum correlation between the latent variables of X and Y (181).

The number of latent variables for the PLS algorithm is determined using the full cross-validation method. With cross-validation, some samples are kept out of the calibration and used for prediction. This process is repeated so that all samples are kept out once. The value for the left out sample is then predicted and compared with the known value. The prediction error sum of squares (PRESS) obtained in the cross-validation is calculated each time a new latent variable is added to the model. The optimum number of latent variables is concluded as the first local minimum in the PRESS *vs* latent variable plot. PRESS is defined as:

$$\textbf{PRESS} = \sum_{i=1}^{n}(\hat{\textbf{y}} - \textbf{y})^2 \qquad\qquad \textbf{Eq. 3.1}$$

Where ŷ is the estimated value of the *i* the object and *y* is the corresponding reference value of this object. The goodness of fit is evaluated by root mean squared error (RMSE) which is defined as:

$$\textbf{RMSE} = \sqrt{\frac{\textbf{PRESS}}{\textbf{n}}} \qquad\qquad \textbf{Eq. 3.2}$$

Where *n* is the number of samples.

For the quantification of the hydration of anhydrous Forms I and II during storage, reference samples were prepared as binary mixtures containing different fractions of OLZ FI/dihydrate D and OLZ FII/dihydrate B prepared at 10% (w/w) intervals by geometric mixing in a mortar (n=3). These samples were analyzed and their spectra collected. From this evaluations, a set of spectra collected at each concentration were set aside to form the test set. Internal cross validation (one sample removed per cycle) was performed to the calibration samples. Model equations were performed using The Unscrambler X (CAMO Software AS, Norway) software. The informative regions between 950 and 1025 cm^{-1} were selected for comparison and analysis of the anhydrous FI/dihydrate D calibration samples, whereas the regions between 740-806 cm^{-1} were selected for use in anhydrous FII/dihydrate B calibration sample.

The selection of these spectral regions for calibration was based on the wavenumber regions that showed the largest differences between the components and therefore provided the greatest contribution to the linear regression equations. The data was SNV (standard normal variate) transformed and mean centered prior to analysis (182). The quality of the model was evaluated by the root mean square error of calibration (RMEC, calibration error, i.e. the

residuals of the calibration data), prediction (RMSEP, prediction error, i.e. measured on independent testing set and compared to reference values),cross-validation (RMSECV, errors are calculated on test/train splits using a cross validation scheme for the splitting) and by the squared correlation coefficient of the experimental and predicted values (R^2) and the cross-validation squared coefficient (Q^2).

3.4.7 Dissolution tests of different olanzapine entities

Dissolution tests were performed for olanzapine tablets. The dissolution tests were carried out in a dissolution apparatus (AT7, Sotax, Switzerland), paddle method (50 rpm), 900 ml of phosphate buffer (pH= 6.80, 37 °C ± 0.5 °C, n=3). Samples were collected at time intervals of 5, 10, 15, 20, 30, 40, 50, 60, 90, 120 min for fast-released tablets (drug/lactose) and at time intervals of 5, 15, 30, 60, 90, 120, 240, 360, 480, 720, 980 for sustained release tablets (drug/MCC/lactose) . The fraction of released olanzapine was determined by UV spectrometry (λ= 254 nm, Hitachi U- 2000, Japan).

The comparison of the dissolution performances between the different olanzapine samples was based on the similarity factor (*f*). This is an independent model that measures the similarity in percentage between two profiles of dissolution (167). *f2,* which is the reciprocal logarithmic square root transformation of the square error of results (Eq. 2.6), was used to compare the dissolution profiles. When *f2* values are higher than 50 (i.e., 50–100) it indicates the equivalence of both compared profiles. In the comparative dissolution testing, only one measurement was considered after both compared profiles have reached 85% dissolution.

3.5 Results

3.5.1 Characterization of olanzapine anhydrous crystal forms

Both OLZ anhydrous forms were characterized for particle size and size distribution, thermal, infrared and X-ray powder diffraction analysis before storage. Starting materials of olanzapine presented broad particle size distributions, with spans of 2.10 and 1.64 for Forms I and II, respectively, with Form I samples presenting smaller particles size than Form II particles (Table 3.1).

Table 3.1 – Particle size distribution (µm) of crystalized OLZ FI and FII

Material	d_{10} (µm)	d_{50} (µm)	d_{90} (µm)	Span
OLZ FI	8.41 ± 0.99	18.35 ± 1.83	46.94 ± 3.79	2.10
OLZ FII	12.38 ± 2.10	22.03 ± 2.66	48.43 ± 4.78	1.64

$d_{10,\ 50,\ 90}$ - maximum particle diameter below which 10, 50, 90 % of the sample population of particles exists

The thermogram of Form I showed a melting endotherm at $Tm_{onset}=194.08 \pm 0.18$ ^{o}C with an enthalpy of $\Delta H=133.56 \pm 1.90$ J/g, whereas Form II presented 2 melting endotherms at $Tm_{onset}=177.69 \pm 0.73$ ^{o}C and at $Tm_{onset}=193.78 \pm 0.37$ ^{o}C (Figure 3.1, a).

In the thermogram of Form II, the first endotherm represents melting of the material while the second endotherm represents the melting of Form I, after recrystallization of the first form into the latter form. The exothermic event between both endotherms represents the crystallization of Form I from the melt, due to the higher thermodynamic stability of Form I in comparison to the molten Form II (137, 138). The coexistence of both forms in the thermal range of 160-180°C explains the difficulty of measuring the changes on enthalpy of the melting/recrystallization phenomena (137).

Hot-stage polarized light microscopy analysis has shown crystals of OLZ FII, which were lath-shaped (before milling), converting to plate shaped crystals when heated above their melting temperature, which can be assumed as the conversion to Form I (Figure 3.1 a).

For both forms, an amorphous state became visible when the samples were cooled down, with a glass transition at $T_g = 70.04 \pm 0.19$ °C (Figure 3.1, a) and no recrystallization occurring in the second heating run. The thermogravimetric analysis has shown that the degradation of Form I started after the melting, with degradation at $T_{onset} \approx 255$ ^{o}C, independently of the polymorphic form.

In respect to the diffraction analysis of both forms of the powders, each polymorphic form showed distinctive peaks, which could be used for their identification (2θ = 8.62°, 12.46°, 14.64° for Form I and 2θ = 10.91°, 14.01°, 18.49°, 19. 73° for Form II) (Figure 3.1 b) with the maxima being identical to data previously reported for these structures (139).

Concerning the infrared spectra of anhydrous Forms I and II, the differences in their spectra were mostly related to the atoms involved directly or indirectly with the intermolecular $N_{10}H$-N_5 hydrogen bond which is the primary intermolecular interaction of anhydrous olanzapine structures (138). For instance, the stronger intermolecular hydrogen bond in Form I results in a lower NH stretching wavenumber in Form I (3219.6cm^{-1}) than in Form II (3237.9cm^{-1}) (Figure 3.1 c). Both polymorphic forms adopt different packing arrangements of the olanzapine racemic pairs (i.e., the building block of the olanzapine crystal), therefore, the atoms which support the molecular skeleton are less sensitive to changes of the crystalline form than the atoms at the rim of the molecule (138). Hence, both forms can easily be distinguished through the maxima in the spectra at 671, 746, 887, 965 and 1009 cm^{-1} in OLZ Form I that shift to 661, 758, 904, 971, 1005 cm^{-1} in OLZ Form II.
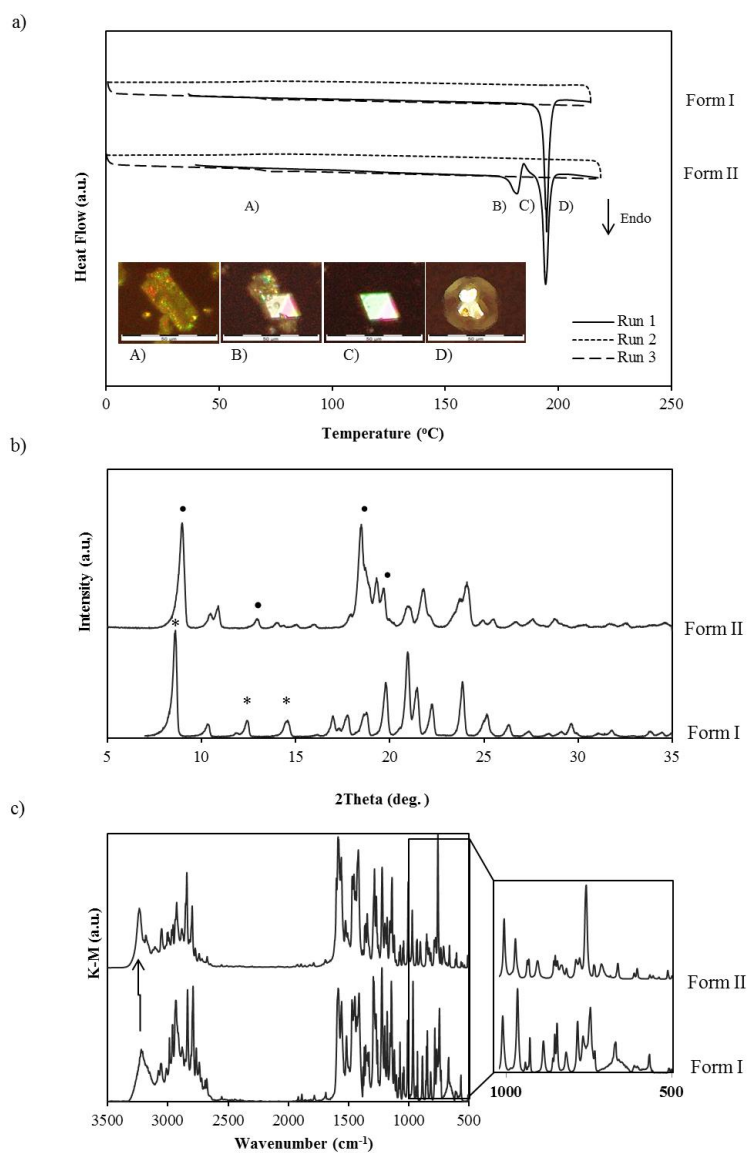
Figure 3.1 – Characterization of olanzapine forms by different techniques:

a) **Thermograms of anhydrous Forms I and II. Form II crystal shape modifications of Form II on heating.**
b) **Diffractograms (XRPD) of OLZ Form I (*) and Form II (˙)**
c) **Infrared spectra (DRIFT) of OLZ Form I and Form II. The arrow represents the shift in NH stretching band.**

3.5.2 Dihydrates of olanzapine

Three olanzapine dihydrates were produced in order to understand and characterize the crystalline changes that both anhydrous forms may undergo over their storage, at different relative humidity environments. The diffractograms produced from the 3 dihydrates by powder diffraction were shown to be in good agreement with the data previously reported for these structures (18). On the other hand, to the best of our knowledge, there is no data in the literature related to the identification by infrared spectroscopy of dihydrates B, D and E. The data obtained by DRIFT in this report revealed that this was a powerful technique for identification,

characterization and quantification of the potential presence of mixtures of olanzapine hydrate/anhydrous content in the same samples. In fact, all 3 dihydrates could be distinguished between them by their fingerprint region. As an example one may cite the out of plane bending of the benzene moiety (138) which has a distinct wavenumber for each form. This band was located respectively, at 745 cm^{-1} and 757 cm^{-1} in Forms I and II and it has shifted to 750 cm^{-1} in dihydrate D, 767 cm^{-1} in dihydrate B and 755 cm^{-1} in dihydrate E (Figure 3.2).

Comparing the infrared spectra of the dihydrate forms with the anhydrous forms, one may find several differences among them, especially in the region between 3300 and 3550 cm^{-1} (Figure 3.2). In that region, all dihydrates present two broad bands which are not observed in the anhydrous forms. The appearance of these bands was related to the OH-stretching due to hydrogen-bonded water molecules present in the crystal (183, 184).
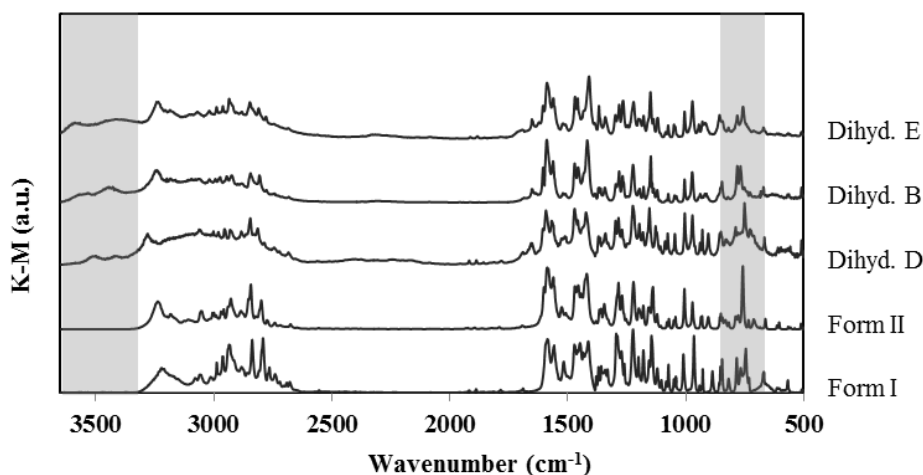
Figure 3.2 – DRIFT spectra of anhydrous OLZ Form I, Form II, dihydrate D (dihyd D), dihydrate B (dihyd B) and dihydrate E (dihyd E).
Grey bars highlight the differences between the different forms.

3.5.3 Thermogravimetric and calorimetric evaluation of Forms I and II after storage at different RH

Solid-state forms commonly differ in their moisture sorption behavior. In this study, the water sorption profiles of anhydrous Form I and Form II, when stored at 11, 53, 75 and 93 % RH for 180 days, were observed. The results revealed that in the range 11-53 % RH, both forms gained almost no moisture (< 0.1 % w/w) after 180 days. However, at 75 % RH, OLZ polymorphic Forms I and II had different moisture sorption behaviors: the mass gain due to moisture sorption was respectively 0.27 ± 0.07 % (w/w) and 7.91 ± 0.15 % (w/w) for the anhydrous Form I and Form II, (Figure 3.3, a). At 93% RH both samples increased significantly their masses, showing an increase of mass of 7.88± 0.24 % and 8.41 ± 0.28 %, respectively

(Figure 3.3, a). The water sorption by both Form I and Form II was attributed to the hydration of both forms into two different dihydrates - D and B, respectively (confirmed by X-ray diffractometry, shown below). The thermogravimetric profiles of both samples stored for 180 days at 93% RH displayed the weight loss due to dehydration that starts at lower temperatures for the stored Form II samples (T_{on}= 54.39 ± 1.08 °C) than for the stored Form I samples (T_{on}= 62.92 ± 0.93 °C, Figure 3.3b), indicating that water was more tightly bound in the dihydrate formed during the storage of Form I (dihydrate D) (21, 70).

During the 180 days at 93% RH, a higher moisture sorption rate was observed for Form II than for Form I samples (4.44 ± 0.53 *vs* 1.08 ± 0.28 % after 8 days, Figure 3.3 c), revealing that the polymorphic Form I had a longer induction period to take up water under these conditions. In spite of the higher induction period of Form I, it was in the first month of storage that the mass of both samples increased the most. For a complete conversion of anhydrous forms into dihydrates, olanzapine should absorb a maximum water content of 10.3 % w/w, which is the water ratio (w/w) in all dihydrate olanzapine forms (18). The increase of mass of about 8 % (w/w) in both samples revealed that the process of hydrate conversion during storage (180 days / 93 % RH) was not completed for all the anhydrous material. This observation was confirmed by XRPD studies (see below).

The calorimetric analysis by DSC, carried out in a crucible with a non-hermetic lid to avoid pressure build up due to the coverlid, evidenced a broad endotherm below 100 °C for both olanzapine forms stored at 93 % RH (Figure 3.3 d). The temperature (T_{max}) and enthalpy values (ΔH) of the new endotherm increased with storage time for both forms. The thermogravimetric and calorimetric curves recorded for this process had only one slope, regardless of the heating rate applied (2, 5, 10, 20, 40 °C/min), which may indicate that the dehydration occurred in a single stage. This observation suggested that all water molecules were almost simultaneously lost and there were no differences in the removal rates of the two water molecules present in the dihydrate structures. After the dehydration it was observed the melting peaks for each anhydrous form. The dehydration of each hydrate into the same original anhydrous form was confirmed by infrared analysis of the dehydrated powder (dihydrate D dehydrates to F I and dihydrate B to Form II), showing a reversible process of hydration.
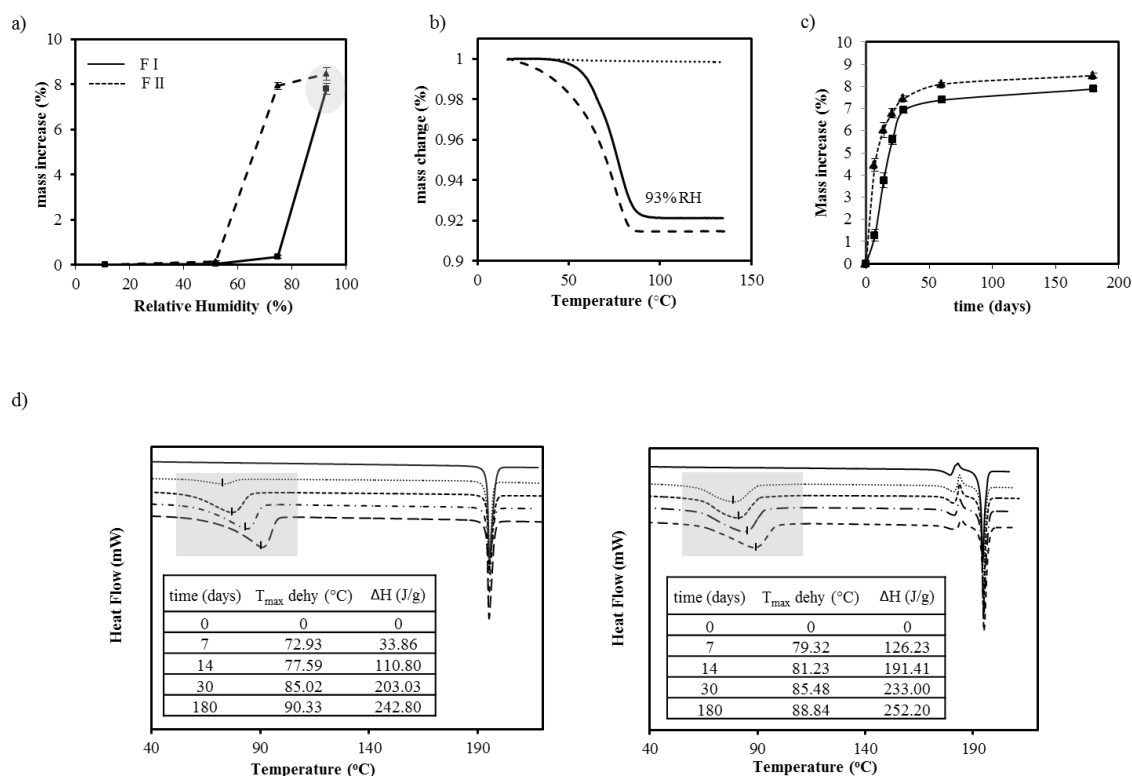
Figure 3.3 – Mass variation and calorimetric evalutation of samples

of olanzapine Forms I (——) and II (---):

a) **As a function of RH (11, 53, 75 and 93 % RH) at days 180 of storage;**

b) **Mass loss as function of temperature increase (TGA, 10 ^{0}C/min) on storage at 93% RH;**

c) **Mass increase for different time periods on storage at 93% RH;**

d) **Thermograms of Forms I and II before and after storage at 93 % RH for different days.**

3.5.4 XRPD and DRIFT characterization of Forms I and II after storage at different RH

The X-ray powder pattern of both anhydrous forms registered changes when they were stored at the highest relative humidity (93 % RH) for 180 days. However, these changes were different for each form, as a result of the hydration of each anhydrous form into different dihydrate structures (Figure 3.4, a and b). The crystalline modifications increased with storage time, which became apparent as a consequence of the gradual decrease of the peaks of the anhydrous forms and the appearance of the characteristic peaks for the dihydrates, already within one week of storage. For instance, in Form I samples the peaks at $2\theta = 8.62^o$, 14.64^o, 22.30^o tended to vanish whereas new peaks, characteristic of the dihydrate D, at $2\theta = 11.58^o$, 12.01^o, 15.55^o, 23.58^o, 26.49^o appeared. However, the peaks of the anhydrous Form I did not disappear completely after 6 months of storage ($2\theta = 8.62^o$, 23.94^o for example, Figure 3.4, a), suggesting that after 6 months under this environment a mixture of 2 different forms may be still encountered - anhydrous Form I and dihydrate D.

The samples of Form II stored at the highest RH (93 %) suffered different modifications, by comparison with the samples of Form I under the same conditions: the new peaks at 16.4^o, 19.7^o, 20.4^o, 21.3^o, 22.7^o and 23.7^o were characteristic of the dihydrate B (Figure 3.4, b). However, the hydrate conversion of this form at 75% RH was slightly different. Although 30 days of storage have not caused major crystalline changes on anhydrous Form II, the diffractograms of these samples after 180 days showed a mixture of peaks due to the presence of both dihydrates B and E (Figure 3.4, c). The presence of both dihydrates at this humidity level might be related to the notable structural similarity of both hydrates (18). However, the higher stability of the dihydrate B in comparison to the dihydrate E (18) might have accounted for its distinct appearance at a higher relative humidity. At a lower humidity (< 75% RH) both Forms I and II remained stable during the 6 months of test.
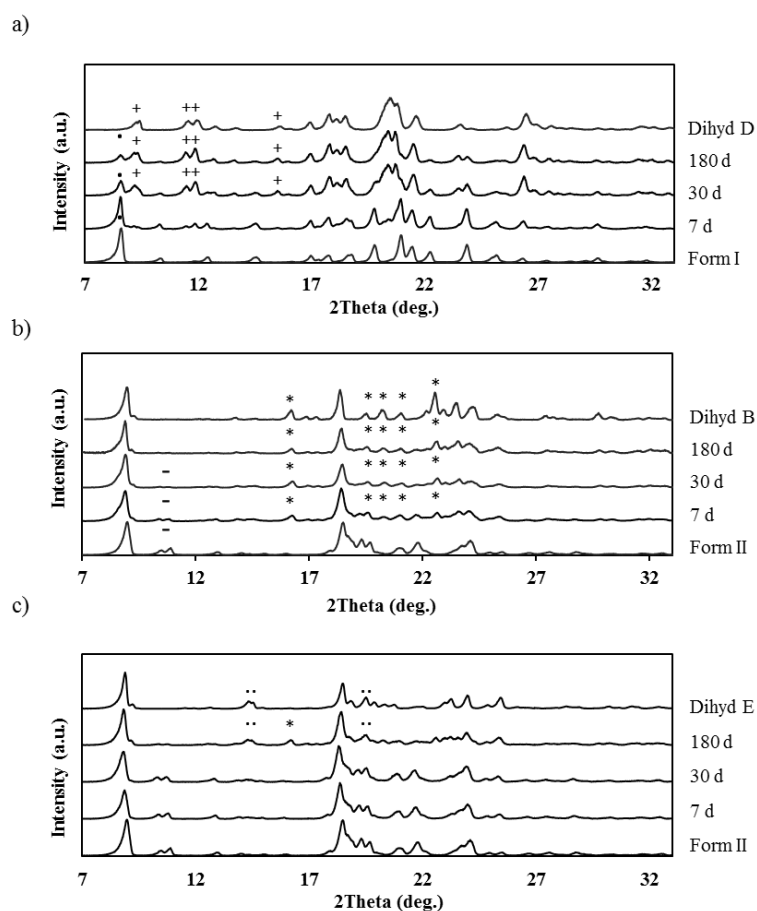
Figure 3.4 – X-ray diffractograms of OLZ Form I (FI) and OLZ Form II (FII) stored for different time periods (7, 30 and 180 days) at 93 % RH (a and b, respectively); (c) OLZ Form II (FII) stored at 75 % RH.
Different symbols are used to distinguish the characteristic peaks of each form. Peaks which appear on top of the following symbols: (.), (-), (+), (*), (..) highlight the characteristic peaks of Form I, Form II, dihydrate D, dihydrate B and dihydrate E, respectively.

After characterization of each dihydrate by infrared analysis (DRIFT analysis, Figure 3.5), it was possible to evaluate the conversions of both olanzapine anhydrous Form I and Form

II, as a result of changes on the frequency of several IR bands scattered throughout the spectra. For example, Form I bands describing the deformations of the piperazinyl group coupled to Me (2) (1009 cm^{-1}) or to the azepine and thiophene moieties (965 cm^{-1}) (138), changed to 1004 cm^{-1} and 971 cm^{-1}, respectively, at 93% RH. The out of plane deformation of the 'CH' bonds changed from 745 cm^{-1} to 750 cm^{-1} (Figure 3.5 a). The IR spectrum of the anhydrous Form II changed over storage for both environments (93 % and 75 % RH, Figure 3.5, b and c). The changes on the spectrum of OLZ F II were mainly confined to the region below 800 cm^{-1} (the so called 'fingerprint' region), and the region above 3400 cm^{-1} (due to the entrance of water molecules). The NH-stretching band in Form II (3237 cm^{-1}) did not shift, as occurred with Form I when water molecules were introduced in the crystal lattice (Figure 3.5, b vs c).
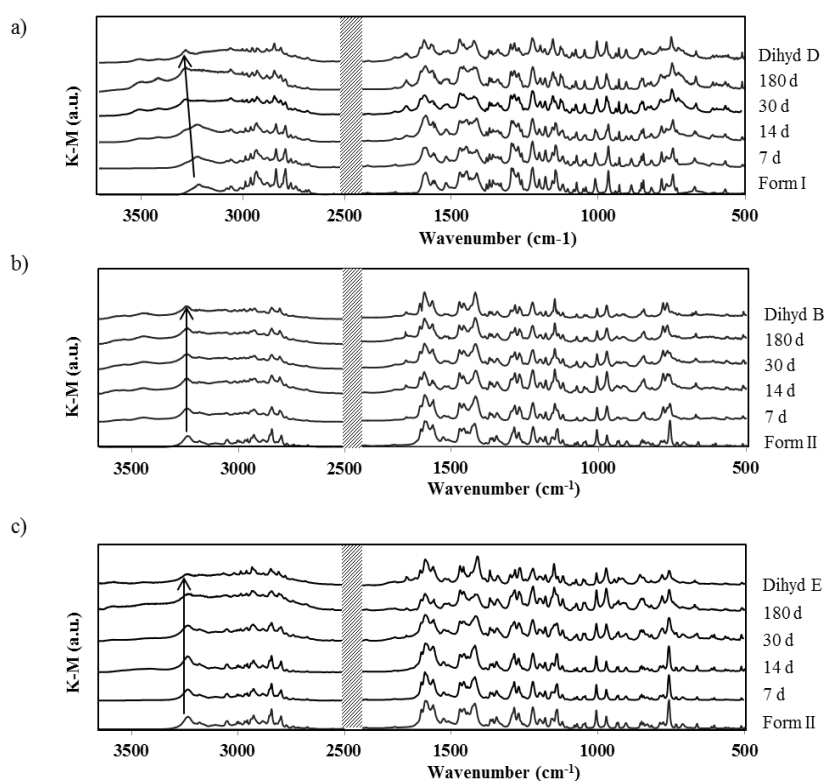
Figure 3.5 – IR spectra of OLZ Form I (FI) and OLZ Form II (FII) stored for different time periods (7, 30, 180 days) at 93 % RH (a and b, respectively); (c) OLZ FII stored at 75 % RH.

3.5.5 Quantification of OLZ hydrate conversion

The quantification of olanzapine hydrate conversion was possible to calculate from the DRIFT data (Figure 3.6, a_1 and a_2) in combination with a chemometric technique, partial least squares (PLS). The PLS regression model for FI/dihydrate D calibration curve had 1 PLS components and displayed values of 1.55%, 1.93% and 2.08% for RMSEC, RMSEP and RMSECV, respectively. The R^2 of the experimental and predicted values of polymorphic

contents of the binary mixtures was 0.997. The cross-validated R^2 (termed as Q^2) was 0.996. The regression model for the pair FII/dihydrate B had 1 PLS components and displayed values of 2.50%, 2.60% and 2.82% for RMSEC, RMSEP and RMSECV. The R^2 and Q^2 values were 0.993 and 0.992, respectively. The RMSECV below 3% for both models suggested good predictive ability of the models (182). The hydrate conversion rate is shown in (Figure 3.6, b). The mean values of the weight increase, obtained by the thermogravimetric analysis, were also converted into percentage of OLZ dihydrate existing in the samples at each time of storage (knowing that an OLZ dihydrate form presented 10.3 % w/w of water content). These results were correlated with the dihydrate content obtained by the results from the DRIFT spectroscopy, which gave rise to a regression line (R^2=0.997 and 0.998, for Forms I and II, respectively) between the two curves (Figure 3.6, c). These results suggested that most of the water taken up by the olanzapine at 93 % RH was converted in water of crystallization, giving a good correlation with a unit slope.
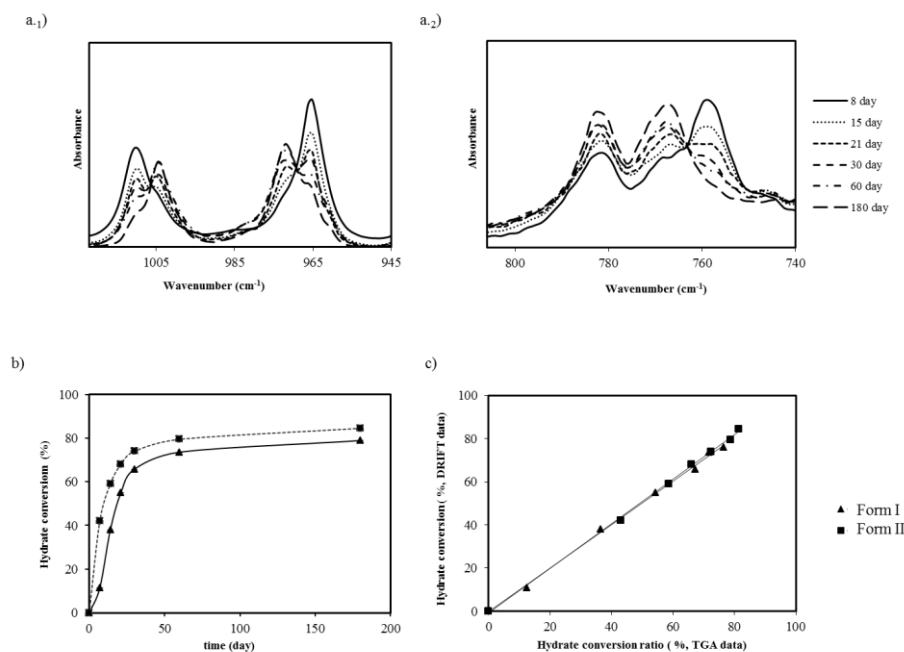
Figure 3.6 – a) Changes on IR spectra of olanzapine Form I (a.$_1$) and Form II (a.$_2$) during storage at 93% RH (a); Calculation of hydrate conversion of form I (▲) and II (■) at 93% RH from the DRIFT data using a PLS model (b); Hydrate conversion when two different methodologies were considered (TGA and DRIFT) (c).

3.5.6 Drug performance assessed by dissolution

To evaluate how (in)appropriate storage conditions of olanzapine may influence the dissolution of the drug, dissolution tests on freshly prepared tablets containing Fom I and Form II (with immediate and sustained releases), prior to and after storage (180 days at 93% RH) were carried out (Figure 3.7). For each formulation, the fraction of excipients in the formulations was the same, so the solid state of OLZ could have been assumed to be the only factor influencing the drug's dissolution rate. The drug content for both formulations containing anhydrous olanzapine was at 98.6%−100.1% of the expected values. The formulations containing olanzapine samples stored at 93% RH for 180 days presented a drug content of 91.6-92.7 % of the measured olanzapine mass. This result was consequence of the water content entrapped in the crystalline structure of both olanzapine samples that led to an increase of the sample mass. Consequently, the graphical representation of data was adjusted for the mass of olanzapine released, as anhydrous olanzapine, as a function of time. In the formulation containing lactose only (i.e., immediate release formulation), Form I and Form II prior and after storage (93% RH) showed more than 85% dissolution within 15 min of test, reflecting similarity between their dissolution profiles (167). By opposition, only 85% of Form I, stored at 93% RH, was dissolved after 90 min of test. The comparison of the dissolution profiles of stored Form I (93% RH) with the other samples' profiles was performed by the calculation of the similarity factor, f_2. The f_2 values showed to be < 50 for all the compared curves [f_2(Form I/Form I 93%) $= 23.8$; f_2(Form II/Form I 93%) $= 25.4$; f_2(Form II 93%/Form I 93%) $= 27.8$], indicating that hydration of the anhydrous Form I promoted a significant reduction on the dissolution rate of olanzapine.

For the sustained release formulations, the rank order for olanzapine dissolution rate was − Form I, Form II, Form II 93% and Form I 93% RH, for both formulations (Figure 3.7). The unstable Form II showed to dissolve more slowly than the stable Form I. However, due to the higher free energy of the unstable form, it would be expected to dissolve more rapidly than the corresponding stable form. Since both forms can hydrate when placed in contact with water, it would be expected that olanzapine would also hydrate when the tablets were placed in the dissolution medium. Therefore, the dissolution rate of anhydrous olanzapine depends on olanzapine's rate of hydration. For faster rates of hydrate conversion, the process of dissolution would have occurred predominantly from the hydrate forms formed *in situ*.
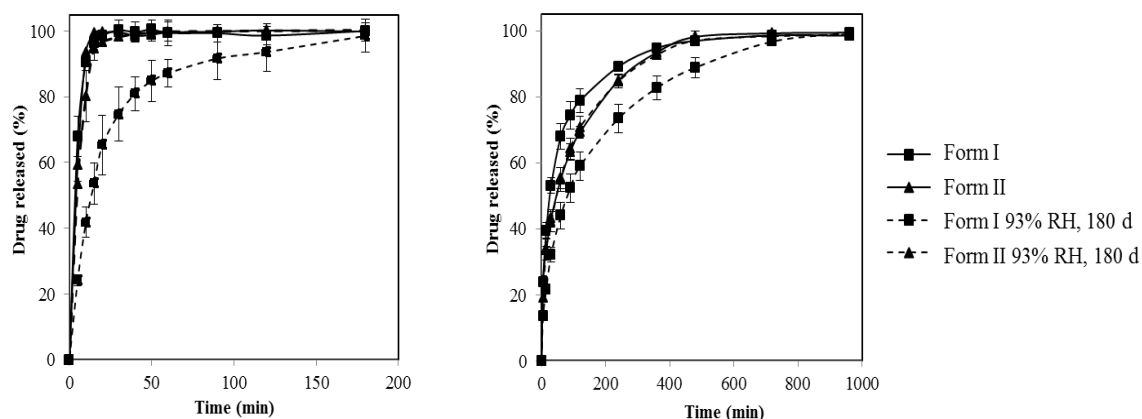
Figure 3.7 – Dissolution profiles of OLZ Form I (-■-), OLZ Form II (-▲-), OLZ Form I stored for 180 days at 93% RH (--■--) , OLZ Form II stored for 180 days at 93% RH (--▲--) considering the mass of anhydrous olanzapine. The dissolution tests were performed for tablets formulated with lactose (left) and with MCC/ lactose (right).

3.5.7 Hydration of Forms I and II in aqueous slurries

The experiments with the aqueous slurries performed for both anhydrous olanzapine forms helped to elucidate the different behaviors of hydration that each form of olanzapine might have in water. The OLZ sediment collected at different times (by filtration) was analyzed by DRIFT to evaluate the moment at which the conversion into the hydrate started to occur.

Taking into consideration the spectral bands at 782 cm^{-1} and 914 cm^{-1}, which are unique to the dihydrate B, they became visible after 15 min in the experiments carried out with the anhydrous Form II, whereas for Form I samples, those bands became visible after 60 minutes only (Figure 3.8). These results showed the rate of appearance of dihydrate B was much slower for stable form I. The continuous evaluation of the course of hydration of each form over 24h (1440 min) showed that both forms hydrated into a mixture of two different crystalline products, namely, the higher hydrate form and the dihydrate B form. A higher content of the higher hydrate form was found for the initial sample of anhydrous Form II (Figure 3.8 b, c).

The crystallization of olanzapine into these different hydrates indicates that hydrate formation of olanzapine in water has a different mechanism than when only subjected to water vapor.

a)

b)

c)
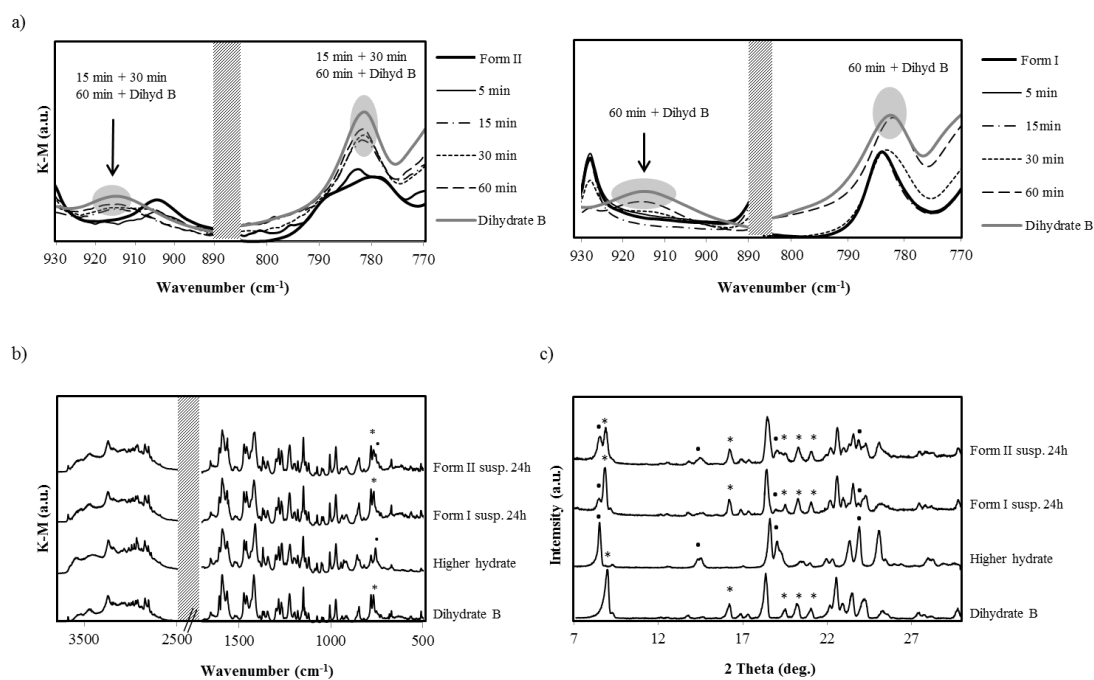
Figure 3.8 – IR spectra of OLZ FII and FI after being suspended in water for different time periods (a); IR spectra (b) and XRPD diffractograms (c) of OLZ FI and FII suspended in water for 24h.

3.6 Discussion

Water adsorbed to the surface of a crystalline material tends to be very low (< 0.1%) (185). However, one-third of APIs are known to form hydrates. For this reason, studies of the interaction of water and anhydrous APIs have received some attention in the literature (70, 173). The knowledge of the interaction of moisture with pharmaceutical solids is, therefore of a practical interest since it enables developing robust conditions for preparing and packaging the APIs, bringing them to a successful solid dosage form (4, 175).

In the present study, differences in water uptake between the two anhydrous crystal forms were clearly observable. Olanzapine Form I and Form II showed to be physically stable up to a RH of 75% and 53%, at 25 ^{0}C, respectively, since no hydrate formation was observed when these forms were stored at these RH conditions for 6 months. These results indicate that storage at room temperature and below these RHs will not promote solid –state changes of olanzapine polymorphs. This control on the formation of hydrates during the long-term storage of olanzapine is crucial to ensure that the quality attributes of the final product are not affected (186). At 93% RH and 75% RH, water molecules were absorbed in the bulk solid structures of anhydrous Form I and Form II, respectively, and hydrate formation has occurred. Since the amount of water vapor absorbed by a solid at any RH and temperature is critically dependent on the orientation and accessibility of polar functional groups, the distinct water sorption behavior of both polymorphs may be explained by their different crystal structures (179). The IR data of

both structures has shown that the differences in both spectra were mostly related to the atoms involved directly or indirectly with the intermolecular NH···N hydrogen bond, which is the primary intermolecular interaction of anhydrous olanzapine structures (138). For instance, the stronger/shorter intermolecular hydrogen bond in Form I resulted in a lower NH stretching wavenumber as compared to Form II (Figure 3.2 b). Therefore, the longer intermolecular hydrogen bonds in Form II (138, 187) may have created an easier access to water molecules through the hydrophilic sites in its structure (188-190), making this form less resistant to humidity. This lower storage stability of anhydrous Form II makes it less suitable to industrial use.

Infrared spectroscopy is very sensitive to vibrations of water O-H bonds. Comparing the infrared spectra of the dihydrates with the anhydrous forms, one may observe several differences among them, especially in the region between 3300 and 3550 cm^{-1} (Figure 3.2). In that region, all dihydrates presented two broad bands which were not observed in the anhydrous forms. The appearance of these bands is related to OH-stretching due to hydrogen-bonded water molecules present in the crystal. The wavenumber of the OH-stretching bands from the water molecules was related to the strength of the hydrogen bonds formed with the H-bond acceptors. For instance, strong hydrogen bonds weaken the covalent OH bonds causing them to vibrate at lower frequencies (183, 184). In the dihydrates of olanzapine both water molecules can establish hydrogen bonds with other water molecules and/or with the olanzapine molecules. However, both water molecules form hydrogen bonds with variable strength (18), supporting the appearance of two broad OH stretching bands at different wavenumbers in each dihydrate.

As a consequence of incorporating water molecules, the intermolecular hydrogen bonds in anhydrous forms (NH···N) are going to be disrupted by bridging water molecules (N-H···O_w-H_w···O_w-H_w···N). In all of the hydrates, the water molecules are held by two or three hydrogen-bonding interactions. The results obtained in the thermogravimetric and calorimetric analyses revealed that both dihydrates formed during storage at 93% RH have low dehydration temperatures (T_{on}< 70 ^{0}C), with a lower T_{on} for the dihydrate B formed during storage at 93% RH of OLZ F II samples. This observation may be explained by longer intermolecular hydrogen bonds of olanzapine molecules with nearby water molecules in the dihydrate B (N_{10}-H···O_1 - 2.91Å; O_1-H···N_4- 2.83Å; O_2-H···N5 - 2.99Å) than in dihydrate D crystal lattice (N_{10}-H···O_1 - 2.86Å; O_1-H···N_4- 2.82Å; O2-H···N5 2.86Å) (18) , which may weaken the interaction between the molecules and, thus, facilitate the dehydration process (191). Furthermore, the broad dehydration endotherm of both hydrates (Figure 3.3) revealed that the evaporation of water molecules exposed to the surface of crystals should provide access to the water molecules inside the crystal, resulting in a slow and continuous dehydration until all water molecules were removed. This behavior contrasts with the common behavior of isolated site hydrates (water

molecules were isolated and kept from contacting with other water molecules directly in the lattice structure), which commonly present a sharp dehydration endotherm (192).

The results have shown that the curve representing the weight increase of anhydrous Form I during storage at 93 % RH had a sigmoidal shape. In the first week, the mass increase was minimal (induction period), followed by an acceleration (8-30 days) and then a decay period, where the rate of hydrate formation was reduced (30-180 days). This behavior of hydrate conversion was slightly different from the hydrate conversion of anhydrous Form II at 93 % RH, since this form seemed to have a short or completely absent induction period indicating a lower energy barrier for hydrate nucleation in the solid state.

The decay period (30-180 days) was very long for both stored samples and even after six months of storage the final water content in the solids did not reach the stoichiometric value for the dihydrate - 10.3 % (w/w) (18). The fact that some anhydrous content was still present in the sample (XRPD and IR data), has shown that hydration was not completed. This phenomenon may be related with the wide particle size distribution in both samples, since the particles with an increased size have a reduced specific surface area exposed to water, and therefore, the reduced number of molecules/atoms at the surface of such particles available to interact with water molecules. Hence, a slower conversion rate was observed for larger than for smaller particles (188). In spite of the uncompleted hydrate conversion during this long-term storage procedure, this approach simulated the hydrate rate conversion of bulk olanzapine at room temperature and humidity, which is important to anticipate its shelf life (193). Variable fractions of hydrate/anhydrous olanzapine may result in variations in the water content of the final product, with impact on both the stability and content uniformity of the drug product. Consequently, solid dosage forms with unpredictable bulk powder properties may also be obtained (191).

The samples of olanzapine Form I stored at 93 % RH showed to hydrate directly and progressively into the dihydrate D. The crystallization of the dihydrate D from the anhydrous Form I might have been related to the similar organization of the crystal building blocks in their structures (Figure 3.9). In both cases they are aligned end-to-end and assembled directly on top of one another. In the conversion to a dihydrate D form, the water will occupy the sites between the olanzapine dimers in the lattice, changing the shape of the unit cell (18).
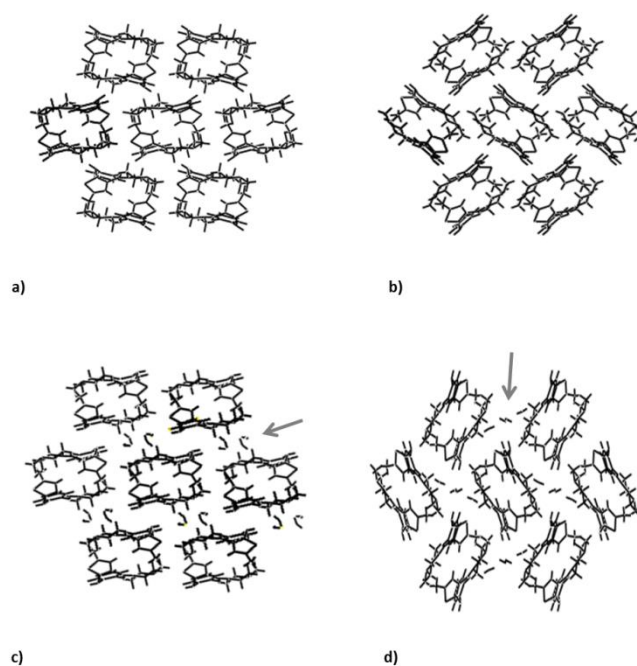
Figure 3.9 – Crystalline structure of form I (a), II (b), dihydrate D (c) and B (d) of olanzapine. Arrows highlight water molecules.

The direct conversion of the anhydrous Form I into the dihydrate D when stored at 93 % RH was different from its behavior when it was stirred directly in water with multiple conversions into other hydrated forms. The anhydrous Form II stored at 93 % RH showed to hydrate into a different form: dihydrate B. Figure 3.9 shows that olanzapine molecules in both Form II and dihydrate B adopt a herringbone arrangement, suggesting minor structural changes during the process of hydration of anhydrous Form II sample.

Hydrates of olanzapine showed to be generated by both water vapor sorption or simply by suspension of the anhydrous moieties in water. The suspension of both anhydrous forms in water led to the formation of 2 hydrates- the dihydrate B and the higher hydrate. The different hydrates formed in each environment were in accordance with the different mechanisms associated to the hydrate conversion in each environment. In the aqueous suspensions the anhydrate to hydrate transformation is expected to occur by a solution-mediated transformation (SMT) (194, 195). This transformation started with the dissolution of the metastable anhydrate form, leading rapidly to supersaturation with respect to the stable hydrate form and providing the thermodynamic driving force for nucleation of the stable hydrate. The final growth of the stable hydrate will deplete the solution concentration resulting in further dissolution of anhydrous solid. The hydrate crystal will continue to grow until all of the anhydrate material has dissolved and the concentration of the drug in solution reaches the solubility of the hydrate, as observed previously for other APIs (196, 197). Since the dissolution of the metastable phase is a

prerequisite for the transformation to take place, the solubility of the metastable form will initially provide the thermodynamic driving force for the phase transformation. Therefore, the higher rate of hydration for anhydrous Form II when suspended in water may be associated with the higher solubility of this form in relation to the anhydrous Form I, which was not unexpected, due to the higher free energy of the metastable forms (179).

The concomitant crystallization of the dihydrate B and higher hydrate in aqueous environments can be related to the simultaneous and closed nucleation rates of both forms (29). The appearance of these 2 hydrates instead of the dihydrate D form (the most stable olanzapine hydrate) at the beginning of the process can be explained by the Ostwald's Step Rule. This rule states that it is not the most stable state, with the lowest free energy, that is initially formed, but the least stable state lying nearest to the original state in free energy (50). Therefore, our results indicated that the dihydrate D form is more likely to be formed during storage, during which olanzapine Form I is exposed to low water activity for long periods, than during dissolution tests or pharmaceutical processing involving water (e.g. wet granulation), in which agitation, higher water activity and reduced contact time between olanzapine and water molecules are involved.

The dissolution profiles of both anhydrous Forms I and II in fast release tablet formulations showed almost complete dissolution within 15 min. The rapid tablet disintegration resulted in a significant fraction of olanzapine going into solution soon after coming in contact with water. The samples which were stored at 93% RH showed to have a slower dissolution rate when compared to the freshly prepared anhydrous forms. A significant decrease in the dissolution rate was observed for stored OLZ Form I, due to the higher stability of the olanzapine dihydrate D structure (18) formed during storage. Due to the fact that olanzapine is a drug whose absorption is mainly limited by its dissolution, the appearance of this dihydrate D is likely to affect the bioavailability of olanzapine present in solid dosage forms. Although Form I just hydrates at a higher RH than Form II, the hydration into the dihydrate D caused a negative impact on the bioavailability of olanzapine as compared to the conversion of Form II into the dihydrate B.

For the tablets containing microcrystalline cellulose (MCC), olanzapine molecules contacted with water for a longer period of time before coming into solution due to the sustained release promoted by MCC. During dissolution the hydrate formation of APIs can occur if the dissolution rate of anhydrous APIs is slower than the rate of transitions of anhydrous APIs into hydrates (106). In our experiments both forms showed to be hydrated in less than 60 minutes when suspended in aqueous environments, with a faster hydration rate for anhydrous Form II. Furthermore, previous studies showed olanzapine to undergo hydrate conversion during dissolution from microcrystalline pellets within 360 min (198). Therefore, in the present case,

the long period that olanzapine was in the hydrated tablet matrix before complete dissolution (940 min) could have led both olanzapine anhydrous forms to undergo, at least partially, hydrate conversion before dissolution. The faster hydrate transition of anhydrous Form II may have led to the reduction of its dissolution rate, since now it showed to reflect the dissolution profile of the hydrates formed *in situ*, presenting a similar dissolution profile to the dihydrate B formed during storage of anhydrous Form II at 93% RH.

Overall, the interconversion between the different forms is schematically shown in

. One may observe that the hydrates formed in aqueous suspensions (higher water activity) are the same for both forms, which was not the case when each form was stored at 93% RH. This shows that the slow phase transitions occurring in the solid-state are more sensitive to the different crystal conformations of the anhydrous olanzapine forms than the hydrate conversions occurring in aqueous environments.

3.7 Conclusion

The present research was performed mainly on the solid-state transformation of two known anhydrous olanzapine forms in order to provide fundamental information concerning stability of these forms over wet processing and long-term storage.

The present study showed that OLZ can be hydrated differently depending on its starting point polymorphic structure and vapor pressures to which it is submitted. Form I showed to hydrate systematically into the dihydrate D and Form II into the dihydrate B after prolonged exposition to 93% RH and not into a different hydrate. This transformation would have been different if a lower RH would have been considered. The different dihydrates formed in each anhydrous sample revealed to have similar crystalline structures to the anhydrous forms which originated them, suggesting minor structural changes during the process of hydration.

It was observed a higher stability of olanzapine Form I in comparison to Form II at 75% RH, which confirms its suitability for pharmaceutical purposes. However, the storage conditions of anhydrous Form I still need to be controlled to avoid the appearance of a lower soluble form (dihydrate D) that may have impact on the bioavailability of the drug. This study helped therefore to predict the stability of both forms upon short and long term exposure to humidity. It also highlighted the importance of a correct selection of storage conditions for both the bulk olanzapine and the final drug product (preferably below 75% RH, at room temperature), in order to prevent the appearance of new crystalline forms or variations in the content uniformity in the drug product.

Both dihydrates formed during storage showed to dehydrate at relatively low temperatures ($T_{onset} < 70$ °C) showing that water molecules form weak interactions with nearby

molecules in the crystals lattice. It was observed a reversible transformation into the anhydrous forms after dehydration without amorphization of the drug.

The anhydrate to hydrate transformations in water was found to occur by a different mechanism (solution mediated transformation). In an aqueous medium both anhydrous olanzapine forms showed to hydrate into the same hydrates (higher hydrate and dihydrate B). Worth to point out that these conversions happened within minutes to few hours before stability of the new entity is reached. These rapid hydrate transitions of both olanzapine forms in a wet environment helped to elucidate the type of conversions that olanzapine can undergo over pharmaceutical processes, such as, wet extrusion or granulation. This study also has shown that conversion of polymorphs throughout a test of dissolution may occur, in which a more soluble form converts into a less soluble one. This has implications on the assessment of the quality of the solid dosage form by dissolution testing and in vivo, olanzapine's bioavailability might be diminished.

The data obtained in this study enabled the construction of a schematic representation for the interconversion pathway between the different anhydrate and hydrate forms, thus providing an improved understanding of the role of water on the solid-state changes of this API

.

CHAPTER 4

Chapter 4 - Role of excipients on the kinetics of hydrate transformation of olanzapine Form I over storage

4.1 Abstract

The study elucidates the hydrate transformations of anhydrous olanzapine Form I (OLZ FI) when stored at a high relative humidity or suspended in an aqueous media in the presence of polymers. OLZ FI and physical mixtures (3:1 and 1:1 as powders or compacts) of olanzapine with polyethylene glycol (PEG-6000), polyvinylpyrrolidone (PVP K25) and hydroxypropylcellulose (HPC-LF) were stored (75%RH and 93%RH) for 28 days. OLZ FI and the physical mixtures were also suspended in demineralized water and stirred (200rpm/60min). Samples were collected at different time points and vacuum filtered. OLZ FI showed to hydrate at 75%RH when stored in the presence of HPC and PEG. At 93%RH all polymers affected the kinetics of hydration of OLZ FI with PVP as the only polymer with the ability to avoid the formation of the hydrate. When olanzapine was suspended in water with HPC and PVP, OLZ hydrate formation was inhibited. Compaction of the powders before storage led to an increase of the hydrate conversion rate of OLZ on the first week of storage, due to a partial amorphization of olanzapine present at the tablet surface. When stored at high humidity environments OLZ FI converted into dihydrate D and when exposed to aqueous environments in the presence of different polymers converted into dihydrates B and E. From an industrial point of view, this study highlighted the importance of the excipient's choice for OLZ formulations, so that a final OLZ product can have a consistent quality performance throughout the product's shelf life.

4.2 Introduction

A pharmaceutical solid dosage form is a combination of an active pharmaceutical ingredient (API) and excipients which are added to the formulation to ensure physical and chemical stability of the formulation, as well as its manufacturability and the bioavailability of the final product (199). During manufacture and subsequent storage of the solid dosage forms both APIs and excipients can take up unacceptable amount of moisture which are capable of altering the solid dosage form stability and lately the physical and chemical stability of the APIs (200). Therefore, it is important to know the different moisture sorption properties of both APIs and excipients in a certain formulation for an adequate selection of the excipients to be considered and the manufacturing process to be followed. Only an optimized formulation and process allow the assurance of the dosage form's stability and the prediction of the shelf-life (201).

Depending on the solid-phase of the raw materials, i.e, crystalline or amorphous solids, the interaction with water may occur by different mechanisms. Crystalline materials may interact with water by four different mechanisms: adsorption on the surface of the particles, incorporation into microporous regions by capillary condensation, formation of crystal hydrate, and deliquescence (122, 201, 202). The crystal structure, water-solubility, porous structure, and the ability to form crystal hydrates is going to determine the mechanism of water sorption into the solid (122). The water vapor in amorphous materials, on the other hand, is absorbed into their amorphous regions and not simply adsorbed on the surface: in these amorphous solids the amount of water uptake is not directly related to the specific surface area of the solid (203). Water can act as a plasticizer and increase molecular mobility due to the breakage of hydrogen bonds between molecules (204, 205). The amount of moisture absorbed by amorphous solids is commonly much larger than the one absorbed by nonhydrated crystalline materials below their critical relative humidity (RH_0) (123).

OLZ Form I is the most stable polymorphic form of this drug, being therefore well adapted for manufacture purposes (18, 136). Recent OLZ case studies (206, 207) pointed out problems on the novel generic formulations, such as undesired side effects or lack of efficiency, which authors claimed to be caused by the ability of OLZ to undergo polymorphic transformations. Consequently, excipients should play a key role in promoting the stability of OLZ in a reproducible medicine and certainly not being the cause of such instability.

For this study, different amorphous and partially amorphous excipients were selected due to their ability to sorb larger amounts of water than purely crystalline materials and due to their regular use in pharmaceutical formulations. Furthermore, amorphous or partial amorphous excipients facilitate the characterization of OLZ polymorphic transformations by X-ray diffraction. Two groups of polymers were selected for the study, namely, one partially

amorphous and water soluble polymer (PEG) and two amorphous and water soluble polymers (HPC, PVP).

4.3 Purpose

The aim of present chapter was to study the phase transitions of OLZ when exposed to different degrees of humidity in the presence of different excipients. Furthermore, the study investigates how different excipients, interacting with water vapor by different mechanisms of water sorption, may change the rate of solid phase transitions of OLZ.

It was also considered to compact (standard treatment in production of tablets) the different mixtures of drug and excipients before exposing them to different humidity conditions in order to evaluate how pressure may affect the formation of OLZ hydrates. The study aims also to provide a clarification of the mechanism of interaction between OLZ and various excipients in aqueous suspensions.

4.4 Materials and methods

OLZ anhydrous Form I was purchased from Pharmorgana, India. The different excipients were Polyethleneglycol (PEG 6000, Sigma-Aldrich, Germany), Hydroxypropylcellulose (HPC LF Pharm grade, Klucel™, Ashland, Germany), and Polyvinylpyrrolidone (PVP K25, BASF Chemicals, Germany).

4.4.1 Preparation of samples for moisture sorption studies

PEG, PVP and HPC were sieved to eliminate agglomerates of particles with collection of particles below 180 μm diameter. Approximately 1g of each polymer was placed in a 20 ml glass vial and stored at 11% RH (lithium phosphate) for 7 days prior to persecution of the vapor sorption experiments in order to decrease and normalize the water content in samples. Thereafter, these polymers were used to prepare physical mixtures with OLZ (OLZ: polymer, 25:75 w/w and 50:50 w/w, Table 4.1) by mixing OLZ and each polymer in glass vials rotating in a roller mixer for 10 min. 200 mg mixtures were prepared in triplicate and split in halves. One half (100 mg) was used to obtain compacts with 10 mm in diameter at a compaction force of 40 kN with an upper punch speed of 10 mm/min, using a universal mechanical press (Lloyd Instruments LR 50K, UK). Overall 36 samples (powder mixture and compacts) were prepared for each polymer. 6 samples (3 powder mixtures and 3 compacts) of each OLZ:polymer ratio were stored at 2 different conditions: 75%RH, and 93%RH for 28 days. These samples were analyzed periodically (7, 14, 21 and 28 days). Each polymer and OLZ (raw materials) were also stored under the same conditions and used as controls.

Table 4.1 – Formulations for moisture sorption studies

	Code	Samples	Drug/Excipient composition (mg, w/w)
Moisture Sorption Studies	A	OLZ	100:0
	B1	OLZ:PEG	50:50
	B2	OLZ:PEG	75:25
	C1	OLZ:HPC	50:50
	C2	OLZ:HPC	75:25
	D1	OLZ:PVP	50:50
	D2	OLZ:PVP	75:25
solvent-mediated conversion studies	E	OLZ	75:00
	F	OLZ:PEG	75:25
	G	OLZ:HPC	75:25
	H	OLZ:PVP	75:25

4.4.2 Preparation of samples for solvent-mediated conversion studies

Polymers (25 mg) were dissolved in 12.5 ml demineralized water (n=3). OLZ (75 mg) was suspended under agitation (200 rpm) in both water and polymer solutions (12.5 ml) for 60 min (Table 4.1). The sediment was recovered by vacuum filtration to remove excess of water and immediately transferred to XRPD for analysis.

4.4.3 Gravimetric water vapor sorption

Water vapor sorption was determined gravimetrically by storing samples at 25 °C for 28 days in desiccators containing saturated salt solutions to maintain the relative vapor pressure, namely, sodium chloride (75.29 ± 0.12 %, i.e., 75 %RH), and potassium nitrate (93.48 ± 0.55 %, i.e., 93 %RH). During this period the masses (weights) of each sample were periodically (7, 14, 21, 28 days) measured with a Mettler–Toledo analytical scale. Simultaneously, spectral (FTIR), calorimetric (DSC) and X-ray (XRPD) analysis were performed.

4.4.4 Characterization of OLZ, polymers and mixtures of thereof during storage

X-ray powder diffraction (XRPD)

The structural characterization of OLZ formulations were carried out by X-ray powder diffraction (XRPD) on an Analytical X'Pert PRO apparatus (Equipment 2). Diffractograms were obtained by continuous scanning in a 2 θ -range of 7–35° with a step size of 0.017° and scan step times of 20 s.

Differential scanning calorimetry (DSC)

Thermograms of different polymers were taken after their storage at 11% RH for 7 days. The physical mixtures of polymers and OLZ which were stored at different RH for different time periods were analyzed immediately after their removal from the container. The

OLZ particles recovered from the different polymeric solutions were allowed to dry at 25°C/53% RH for 24h prior to calorimetric analysis. The analysis was performed in a Differential Scanning Calorimeter (TA instruments, Q200, USA). Dry N_2 was used as the purge gas (Air Liquide, 50 ml/min). 2 to 3 mg were placed in pinhole crucibles. Samples were heated at 10 °C/min within 0-210 °C temperature range.

FT-Infrared spectroscopy (FTIR)

Polymers and physical mixtures before and after storage were mixed with KBr at a concentration of 0.5 w/w. The mixtures (about 200 mg) were compressed into compacts of 12 mm diameter each. The infrared spectra were obtained at the absorption mode (IR Affinity-1 Shimadzu spectrophotometer, Japan) with 64 scans with a resolution of 2 cm^{-1}. Comparisons between FTIR spectra of the OLZ:polymer samples after storage at different conditions of humidity and temperature were made possible by using a partial least square regression (PLS) a chemometric technique often used for this purpose (181). The spectral region of 875-915 cm^{-1} was selected for the PLS analysis because in this region both polymorphic forms can be distinguished due to the peaks at 886 cm^{-1} and 904 cm^{-1}, which are indicators of the existence of anhydrous Form I or dihydrate D (the one present after storage), respectively. This region was also chosen for analysis because the polymers' spectra showed not to interfere in this spectral region (208).

Physical mixtures of OLZ F I and dihydrate D of compositions ranging from 0% to 100% were used as the calibration set. The spectra were pretreated by standard normal variate transformation in order to reduce spectral noise (Unscrambler X, Camo software). From this, a set of spectra collected at each concentration were set aside to form the test set. Internal cross validation (leave-one-out) was performed to the calibration samples.

Near Infrared spectroscopy (NIR)

The polymers which were stored for a period of 1 month at different RH were analyzed by an Antaris FT-NIR spectrometer (Thermo Scientific, USA) equipped with an InGaAs detector. Each NIR spectrum was recorded between 10 000-4000 cm^{-1} with a resolution and number of scans of 8 cm^{-1} and 32 cm^{-1}, respectively.

Scanning electron microscopy (SEM)

Physical mixtures of OLZ and polymers were analyzed by scanning electron microscopy. The samples were mounted on aluminum stubs and coated with gold by ion sputtering (JEOL JFC-1200 Fine Coater) and observed under (JSM-5200 LV, JP) scanning electron microscope.

4.5 Results

4.5.1 Characterization of the starting materials

The characteristic XRPD diffraction patterns of all 4 excipients were observed using XRPD in the angular range of 7–35 (2Θ). Figure 4.1 a) shows the XRPD diffraction patterns measured for the crystalline OLZ, partially amorphous PEG and amorphous PVP and HPC compounds. Crystalline OLZ exhibited strong diffraction peaks while materials that lack long-range molecular order (PVP and HPC) scatter X-rays to produce a diffuse or ''halo'' pattern.

The evaluation of the different water sorption behaviors of each excipient contributes to elucidation on how they may alter the kinetics of hydration of OLZ in formulations due to the likely competitiveness to water molecules. The moisture uptake when various materials are exposed to 75% RH and 93% during 4 weeks is represented in Figure 4.1 b. For instance, partial crystalline PEG showed to sorb low amounts of water at 75% RH. However, the change of PEG powder's mass recorded at 93% RH was as high as 53% w/w. The amorphous and hydrophilic PVP showed to sorb considerable amounts of water when exposed to both 75% and 93% RH. HPC showed also be able to take up water vapor at a humidity of 75% RH. However, at 93% RH, this polymer was less hygroscopic lower than both, PVP and PEG.

The calorimetric analyses carried out in pin-holed crucibles lids showed a broad endotherm below 100 ^{0}C for OLZ stored at 93 %RH (Figure 4.1c). This endotherm was related with the water loss, which was confirmed by thermogravimetric analysis (data not shown). After the dehydration of the sample, one could observe the peak of melting of the anhydrous form. The thermograms of the polymers on heating showed the apearance of a broad band, between 75-120^{0}C, due to the presence of water in the sample, except for PEG. PEG's thermogram showed the disapearance of the peak of melting which result from the ability of the crystalline regions of PEG to dissolve into the water absorbed by the amorphous regions of the polymer(201).
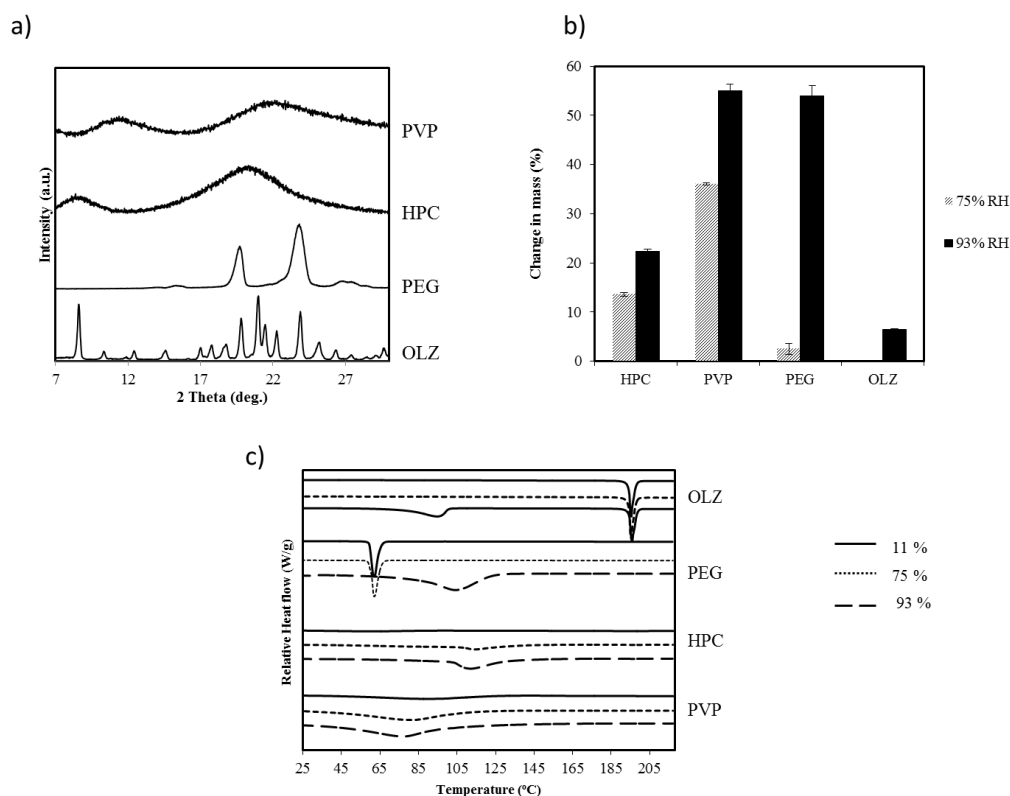
Figure 4.1 – XRPD pattern of the inicial excipients (a), their change in mass after exposed to high levels of humidity (b) and their thermal behavior after 28 days of storage at each environmental conditions (c).

The effect of moisture sorption on all excipients was investigated with NIR spectroscopy after a 4-week storage under conditions of different RH and temperature conditions. As a result of the water vapor sorption, a common feature to all spectra was the increased absorbance with an increase in water activity for wavelengths greater than 1300 nm (Figure 4.2). This trend was especially evident in the 1400-1450 nm (first overtone of -OH stretch) and 1900-1950 nm (combination of -OH stretch with -OH deformation) water absorption regions. For PVP and HPC polymers a significant increase of the absorbance observed in the spectra at the region between 1400-1450 nm could be identified for the samples stored at both 75% and 93% RH.

With regard to the position of the band due to water molecules, the 1850-1950 nm region, the maximum absorption is strongly dependent on the hydrogen-bonding reflecting the molecular mobility of water molecules. Therefore, the broadening of these bands and a decrease on their wavelength maximum indicated an increase in free water molecules (higher molecular mobility) when polymers were stored at high humidity conditions. The water absorbed to PEG was seen as a distinct absorption maximum at 1933 nm after storage at 75% RH. At 93% RH,

free water showed an absorption maximum at around 1900 nm. Furthermore, the bands related to the PEG's structure showed to reduce their intensity at 93% RH.
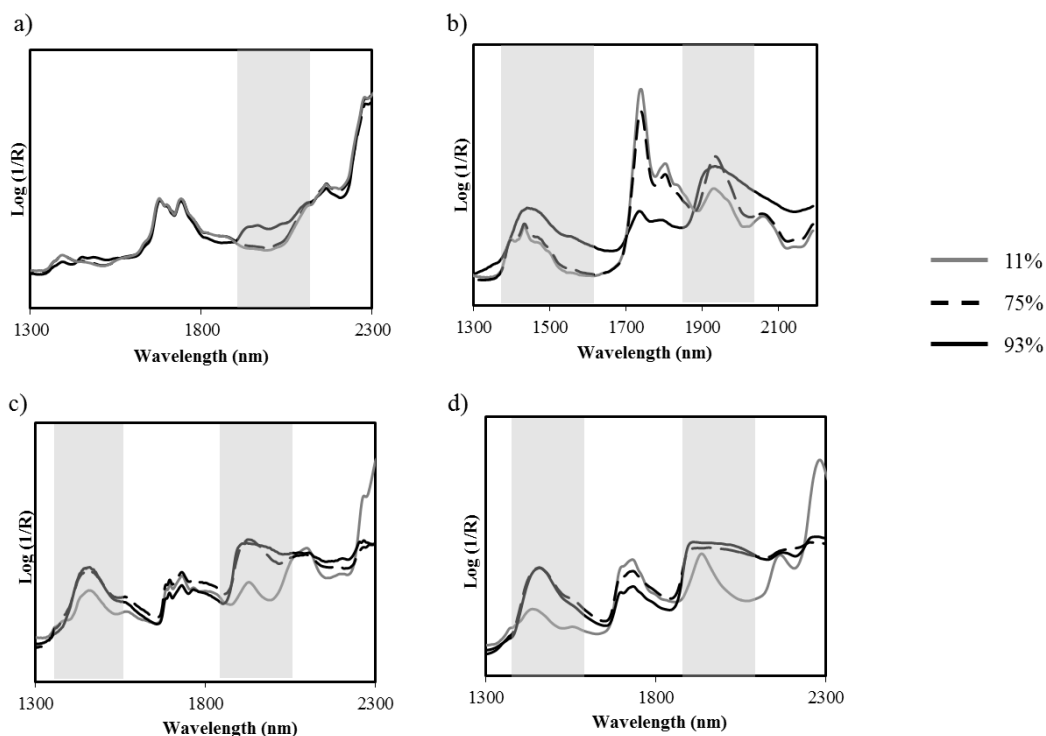
Figure 4.2 – NIR spectra of OLZ (a); PEG (b), HPC (c), PVP (d) stored at different humidity conditions (11% (─);75% RH (⋯); 93% RH (─)) for 28 days. The main shifts are represented with a grey bar.

4.5.2 Phase transformation of OLZ during storage

The effect of humidity on the different OLZ samples is shown on the Figure 4.3. At 75% RH it was possible to observe changes on the diffraction pattern of OLZ when it was physically mixed with both PEG and HPC (B1 and C1, Figure 4.3 a), due to the appearance of new crystalline peaks (grey bar) in the diffractogram. Although 3 different dihydrates of OLZ are known (Dihydrate B, D and E) (18), the characteristic peaks of OLZ dihydrate D (at $2\theta = 9.27^{o}$, 9.49^{o}, 11.62^{o}, 12.01^{o}) appeared along with the peaks of Form I in the diffractograms of these 2 OLZ:polymer samples. The dihydrate D specific peaks are more evident in OLZ:PEG XRPD profile, due to the higher content of the dihydrate D form in this sample. The presence of characteristic peaks of both anhydrous and dihydrate forms of OLZ showed that the dihydrate conversion was not completed in the time scale of the test.

At 93%RH, the X-ray powder pattern of OLZ, which was stored without any excipient, revealed a reduction of the intensity of the peaks, characteristic of the anhydrous form I, and the presence of new peaks, characteristic of the dihydrate D (Figure 4.3 b). Regarding OLZ which

was physically mixed with different excipients and stored at 93%RH, its hydration showed to have increased or decreased, depending on the polymer in which the drug was mixed. For instance, the XRPD pattern of D1 sample showed only the specific peaks of anhydrous OLZ F I, whereas the XRPD pattern of OLZ:PEG (1:1) showed only the characteristic diffraction pattern of OLZ dihydrate D.

The characteristic XRPD pattern of PEG which present 2 broad bands with maximum peaks at 2θ = 19.7 ° and 23.8 ° (Figure 4.1a) was visible in B1 samples stored at 75% RH but no longer visible in B1 samples stored at 93% RH. This may result from the dissolution of the polymer on the absorbed water, which is phenomenon that can occur with crystalline and highly soluble material (148).
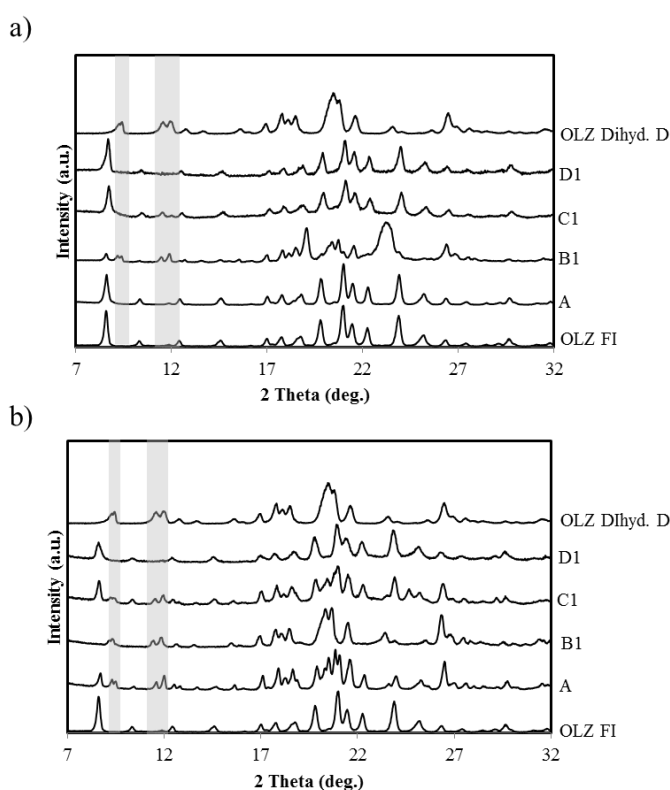
Figure 4.3 – XRPD of physical mixtures (A, B1, C1and D1) stored 28 days at 75% RH (a) and 93% (b).

The different OLZ forms can be easily distinguished by FTIR analysis, as a result of changes on the frequency of several IR bands scattered throughout the spectrum (Figure 4.4, a). When OLZ Form I was converted into the OLZ dihydrate D form, the infrared bands at 886cm^{-1} and 745cm^{-1} were shifted to 904cm^{-1} and 750cm^{-1}, respectively. The hydration of OLZ was not completed by the end of storage (28 days at 93%RH) according to the presence of characteristic bands of both OLZ anhydrous and dihydrate forms (Figure 4.4, b). At 75% RH, no changes were visible on the OLZ spectrum. The calorimetric study (Figure 4.4, c) evidenced a broad

endotherm below 100 ^{o}C for samples stored at 93% RH due to the presence of dihydrate D content within the sample.

a)

b)

c)
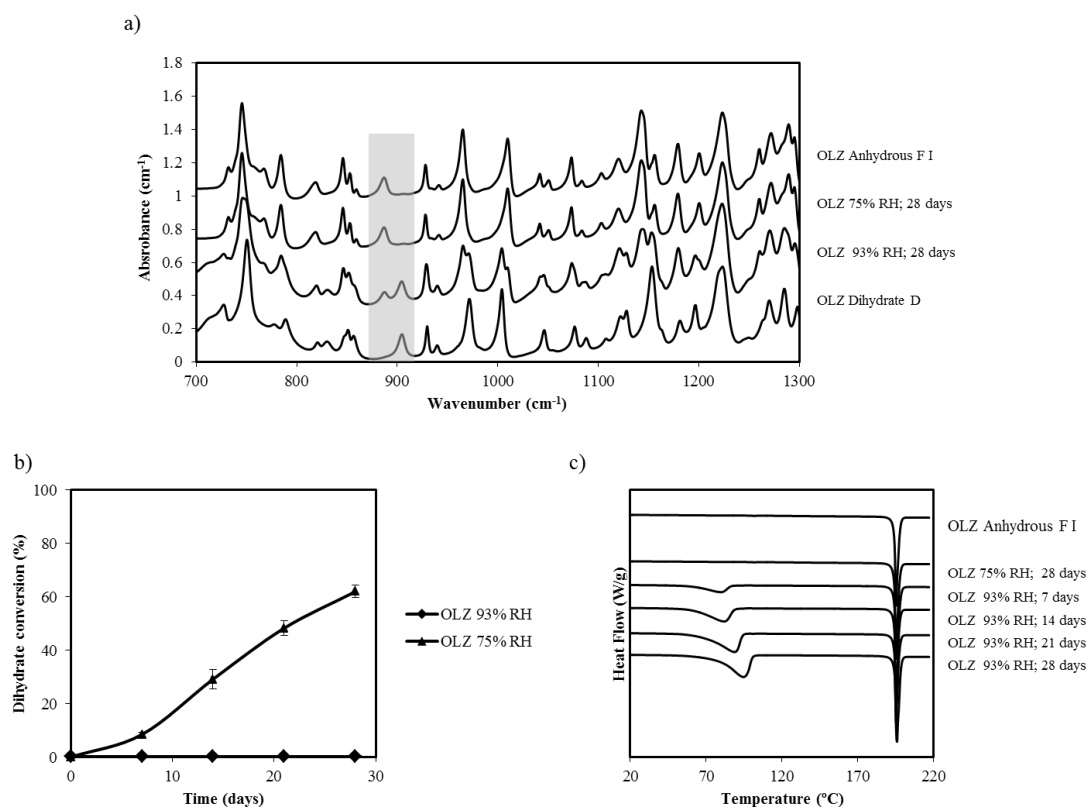
Figure 4.4 – FTIR characterization of OLZ samples (700-1300 cm^{-1}) after 28 days of storage at different RH (a), dihydrate conversion of olanzapine when stored at 75% RH and 93% RH (b) and thermograms of olanzapine after exposure to different RH for different time periods (c).

The FTIR spectra between 850cm^{-1} and 915cm^{-1} enabled the quantification of OLZ hydrate conversion in OLZ:Polymer mixtures when a multivariate analysis tool (PLS method) was used. The PLS best model contained 1 PLS component for the analysis in binary mixtures. This component captured 94% of the variance in the X-variables, demonstrating that the information contained in the spectral data was effectively used in calibration models. The correlation coefficient (R^2) of the experimental data was 0.995 and the cross-validated R^2 (also termed as Q^2) was 0.994. The root mean square errors of calibration (RMSEC) and cross validation (RMSECV) were 1.89% and 2.24 %, respectively. The value for the root mean square error of prediction (RMSEP) was 2.73 %. The region was chosen due to the absence of excipient's interference in this region.

At 75%RH/25^{0}C, OLZ dihydrate D became evident in OLZ:PEG (1:1 and 3:1) and OLZ:HPC (1:1) samples. The dihydrate D content of these 3 samples after 7, 14, 21 and 28 days

are shown in Table 4.2. After 28 days all samples presented mixtures made of OLZ anhydrous Form I and dihydrate D.

Table 4.2 – OLZ dihydrate content in samples stored at 75% RH/ 25ºC, for different days

Time (days)	Dihydrate conversion (%)		
	Formulations (API: Polymer proportions)		
	B1 (1:1)	**B2** (3:1)	**C1** (1:1)
7	0.5 ± 0.2	0.2 ± 0.0	0.3 ± 0.1
14	9.5 ± 1.6	0.5 ± 0.1	0.9 ± 0.2
21	35.2 ± 1.5	7.8 ± 0.7	10.6 ± 0.4
28	55.2 ± 2.6	20.2 ± 0.9	14.0 ± 0.7

At 93% RH, PEG showed to increase the rate of hydrate formation of OLZ; within 2 weeks OLZ was completely hydrated, regardless of the PEG content in the sample (

Table 4.3).

The hydrate conversion rate of OLZ in the presence of lower contents of HPC (OLZ:HPC, C2) showed to increase in comparison to the OLZ sample which was stored without the addition of any excipient (

Table 4.3).

Higher contents of the same polymer (OLZ:HPC, C1) showed to reduce the hydrate conversion rate significantly when these mixtures were stored at 93%RH. This suggests that changes on the HPC due to humidity may cause changes on the hydrate conversion rate.

Table 4.3 – OLZ dihydrate content present in each sample stored at 93% RH/ 25ºC for different periods

Time (day)	Dihydrate conversion (%)						
	Formulation (API: Polymer proportions)						
	A	**B1** (1:1)	**B2** (3:1)	**C1** (1:1)	**C2** (3:1)	**D1** (1:1)	**D2** (3:1)
7	8.4 ± 0.2	93.1 ± 0.4	76.1 ± 2.7	9.3 ± 0.8	8.7 ± 1.3	2.8 ± 0.5	2.0 ± 0.6
14	29.1 ± 0.2	99.4 ± 1.1	99.8 ± 1.2	25.2 ± 0.5	34.5 ± 2.1	2.6 ± 1.1	1.7 ± 0.4
21	48.2 ± 0.3	100.1 ± 0.6	100.3 ± 0.6	29.6 ± 0.8	56.2 ± 1.2	2.4 ± 1.3	1.6 ± 1.2
28	62.1 ± 0.4	99.8 ± 1.1	100.2 ± 0.4	35.0 ± 0.7	65.6 ± 1.1	2.8 ± 0.8	1.8 ± 0.6

The thermograms of the physical powder mixtures before storage showed that OLZ's enthalpy was largely reduced when physically mixed with either PEG or PVP (Figure 4.5 a and

c), showing the ability of both polymers to dissolve OLZ when the mixtures were heated, contrarily to HPC.

The samples stored at different humidity showed a broad band due to the water evaporation. These bands were broader for OLZ mixed with PEG, PVP and HPC stored at 93% RH due to the increased water sortpion ability of these polymers at this high humidity.

Figure 4.5 a) shows the elimination of the melting peak associated with PEG, when these samples were stored at 93% RH which is indicative of a polymer crystallinity loss. The B1 samples (75% RH), showed a broad band due to water evaporation after the melting of the polymer. Figure 4.5 b) revealed two overlapped broad bands between 70-110 ºC when OLZ:HPC mixtures were exposed to 75% RH and 93% RH. These two broad bands may originate from the elimination of the water molecules present in both HPC and OLZ dihydrate D structures (Figure 4.5 b). All the OLZ:HPC stored samples showed broader melting peaks for OLZ with the OLZ Tm_{onset} starting about 2 ºC before the physical mixture. The water sorption by PVP also led to the broadening of OLZ melting peak, with the Tm_{onset} of OLZ registering a decrease of about 10 ºC for all the stored D formulations. (Figure 4.5 c).
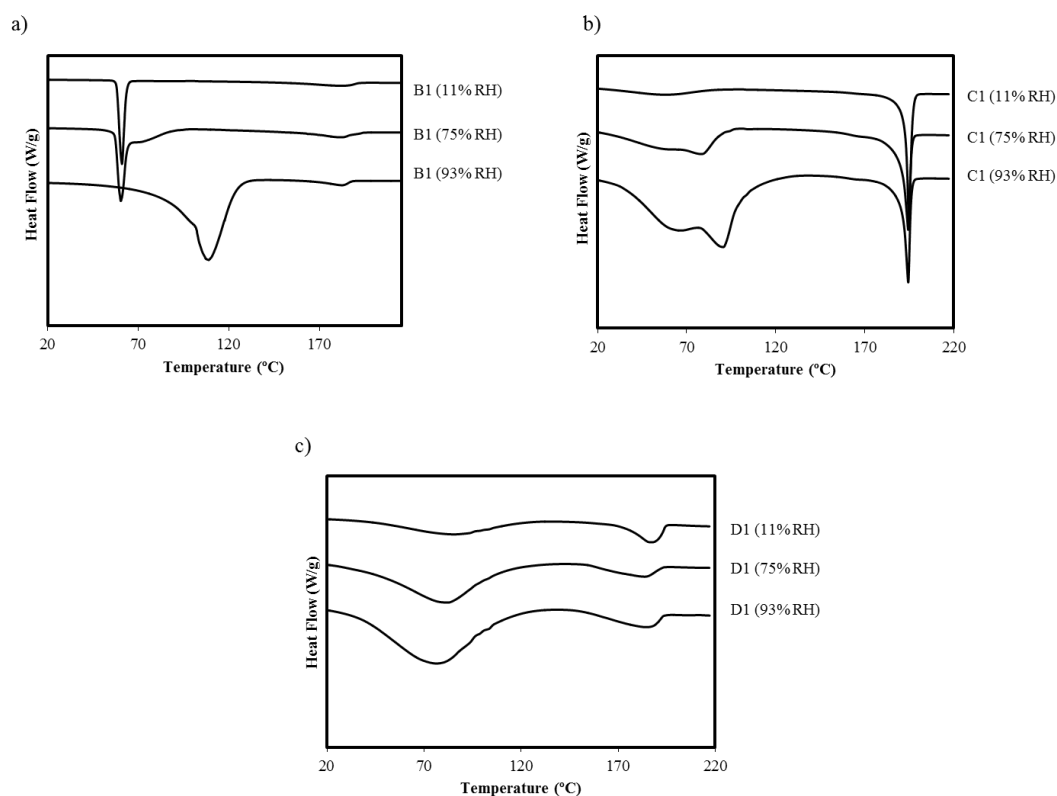
Figure 4.5 – Thermal analysis of the drug:excipient samples after being kept at different conditions of storage during 28 days. a) Formulation B1 (OLZ:PEG); b) Formulation C1 (OLZ:HPC); c) Formulation D1 (OLZ:PVP)

The observation of particles' surface by electronic microscopy (SEM) revealed that OLZ raw material presented an irregular shape. The hydrate conversion of OLZ did not lead to any

change of the particles' shape (Figure 4.6), which suggests that the phase transition occur in the solid-state without passing through intervening transient liquid phase.

The mixtures of OLZ with the 3 polymers stored at 93% RH showed that the amount of water absorbed by the polymers resulted in coverage of OLZ particles by the plasticized polymers, which did not allow observing changes on the particles surface. The optical microscopy with polarized light was useful on the observation of the OLZ particles even in the presence of the polymers. It was noticeable that OLZ particles in PEG samples can completely change their morphology; the irregular particle shape was converted to a lath shaped morphology, suggesting that the hydrate mechanism of OLZ in this sample occurred by a different mechanism.
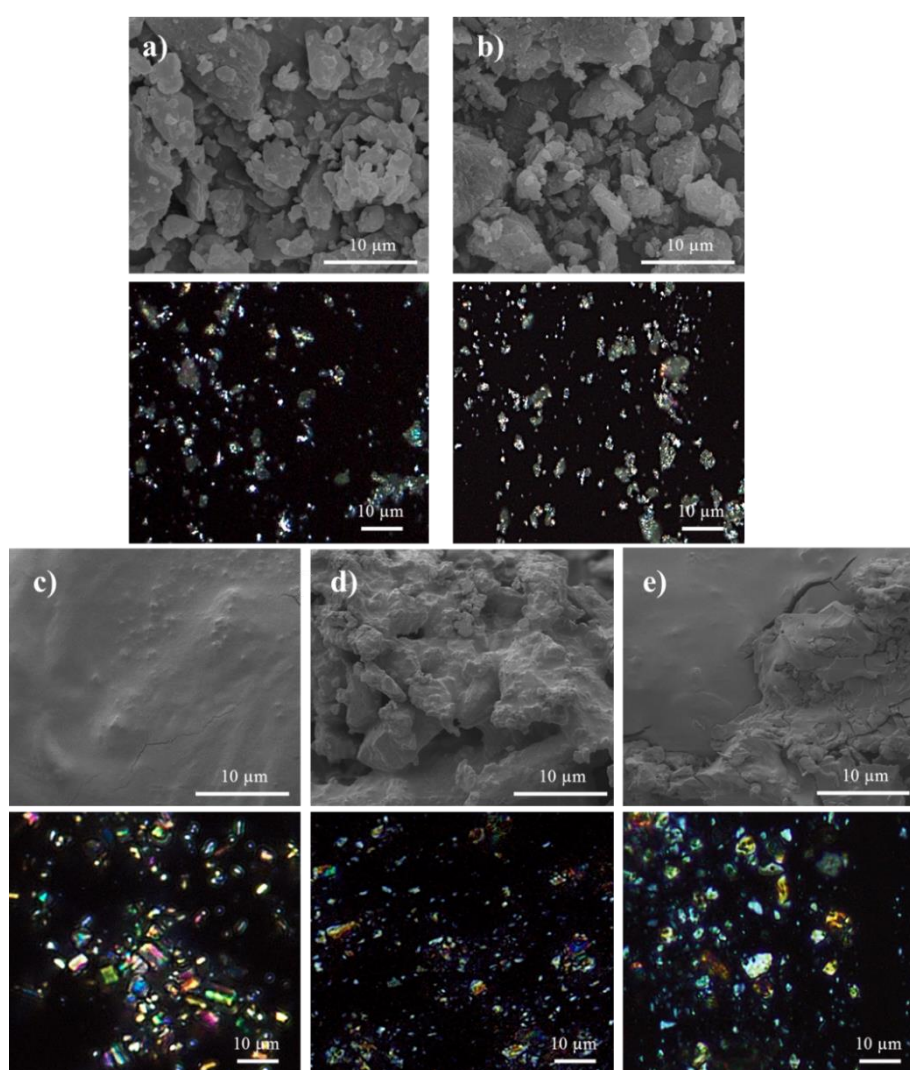
Figure 4.6 – SEM pictures and MO with polarized light pictures of the anhydrous starting materials (a), formulation A (b), formulation B2 (c), formulation C2 and D2 (e).

4.5.3 Phase transformation in compacts:

Thermograms of powders and freshly prepared compacts of formulations A, B2, C2 and D2 are presented in Figure 4.7 a). It was possible to observe a reduction of melting temperature (Tm) and melting enthalpy (ΔH) of OLZ when OLZ or the physical mixtures of OLZ:polymer were compacted. Figure 4.7 b) exhibits a reduction of the intensity of the crystalline peaks of OLZ (A P) when it is compacted (A C), reflecting a loss of crystallinity of the sample.

a)

	Tm $_{peak}$ (°C)	ΔH (J/g)
A p	195.29 ± 0.08	132.2 ± 1.09
A c	195.22 ± 0.31	120.30 ± 2.50
B2 p	191.26 ± 0.20	80.46 ± 1.77
B2 c	190.53 ± 0.61	63.916 ± 4.72
C2 p	193.42 ± 0.10	99.3 ± 1.32
C2 c	192.82 ± 0.81	84.71 ± 1.51
D2 p	194.31 ± 0.20	90.57 ± 1.80
D2 c	193.75 ± 0.01	79.82 ± 2.61

b)
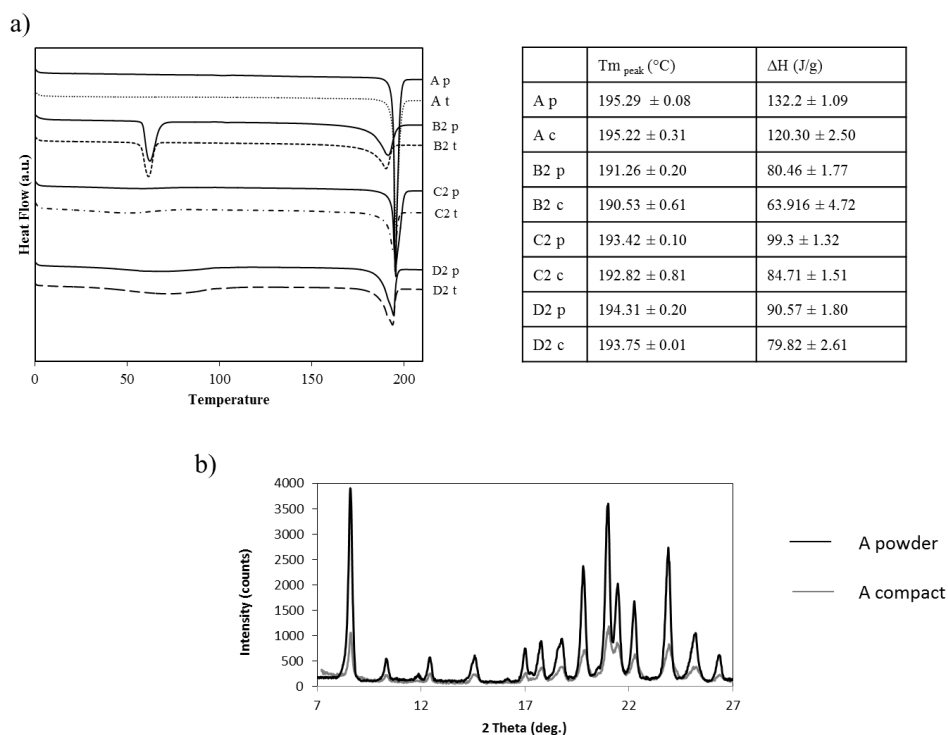
Figure 4.7 –Themograms and the respective melting temperature and enthalpy of OLZ (a) in different formulations before (powders, p) and after (compacts, c) compaction; b) shows the X-ray diffractograms of OLZ before and after compaction.

Figure 4.8 shows the OLZ dihydrate D content in different formulations (powders and compacts) after being stored for 7 and 28 days at 93% RH. OLZ, compressed alone, showed to have an increased dihydrate D content in the first days of storage when compared to the OLZ raw material stored as a powder. However, after 28 days the dihydrate D content present within the compactes showed to be about 12%, which was much lower than the dihydrate D content in OLZ powder sample (62 %).

For compacts containing mixtures of drug and polymer, a larger percentage of dihydrate D in the compacts after 7 days of storage when compared to the uncompressed material was found. In the case of OLZ:PEG compacts, a complete hydration of OLZ was observed in only one week. As found for OLZ, the compacts of physical mixtures showed a slight increase or stagnation of hydrate formation between the 7th and the 28th days.

a)

b)
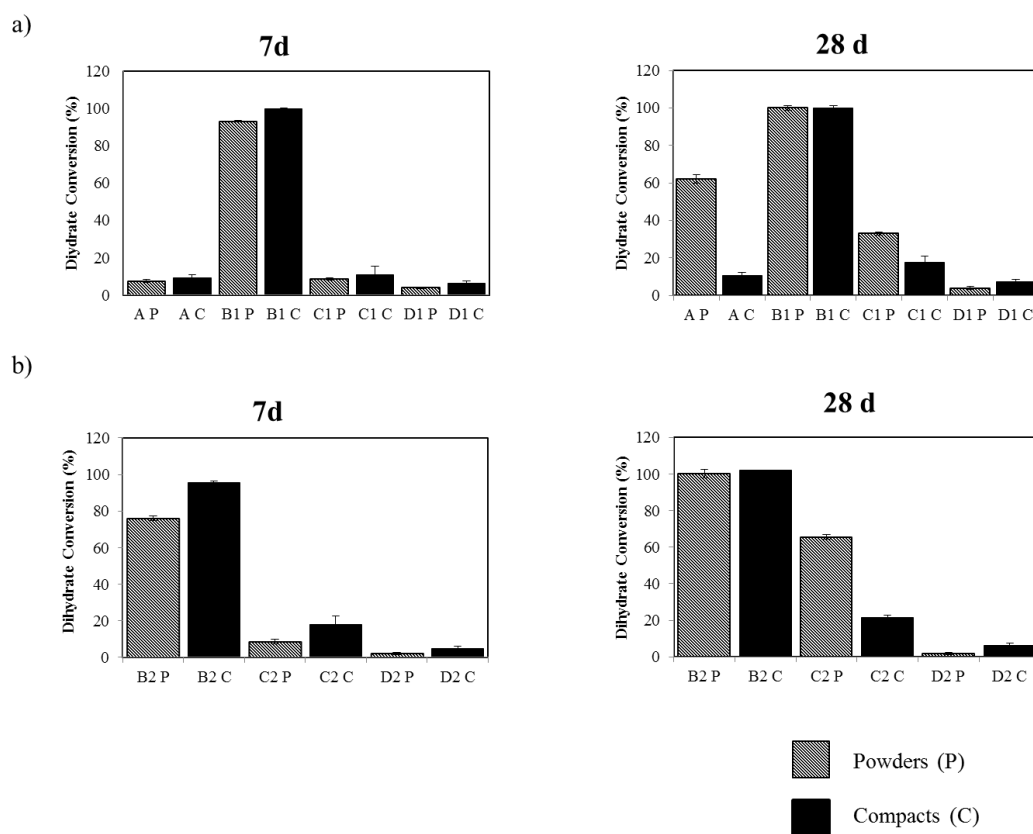
Figure 4.8 –OLZ dihydrate D content in formulations A, B1, C1 and D1 (a) and formulations B2, C2 and D2 (b), stored for 7 days and 28 days at 93% RH. The figure includes the formulations as powders or compacts.

4.5.4 Conversion kinetics of OLZ in aqueous suspensions

This study was conducted to obtain an insight into the mechanism of interaction between OLZ and various polymers in aqueous environments and to have a deeper understanding of the observed results during storage. Figure 4.9 shows the FTIR spectra of OLZ within the 720-1020 cm^{-1} range. The spectra display OLZ powders filtered after being suspended in water or polymeric solutions for different periods (15, 45 and 60 minutes) and dried at room temperature 25ºC/24h. Experiment E showed a mixture of anhydrous OLZ and dihydrate B after 45 minutes (Figure 4.9), whereas in experiment F only anhydrous OLZ was found after 45 minutes. This result revealed a slower hydration rate of OLZ when suspended in PEG solutions. The hydrates formed in this experiment were different from the ones obtained during storage at 93% RH. In spite of the aggitation (secondary nucleation is likely to take place) and the high content of free water molecules availabe to bind OLZ molecules, OLZ showed to remain anhydrous when stirred in HPC and PVP solutions (G and H) for 60 minutes.
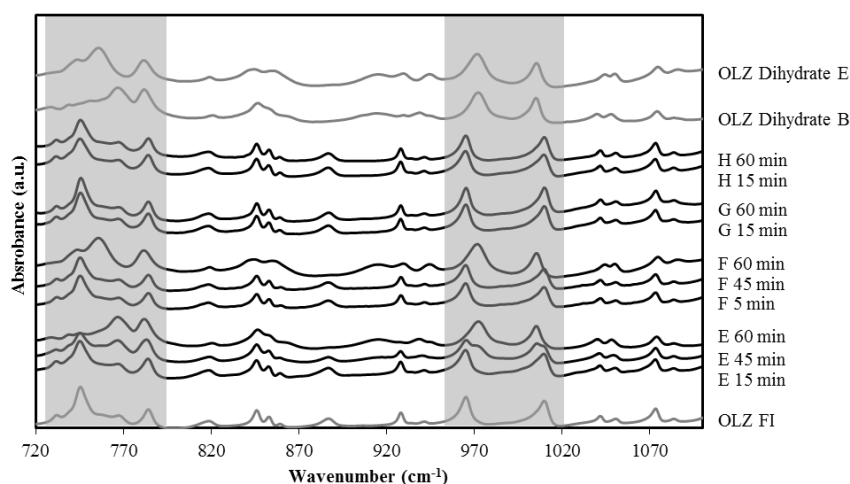
Figure 4.9 – FT-Infrared spectra of powders recovered after 15, 45 and 60 min from the different suspensions. The main shifts are represented with a grey bar.

4.6 Discussion

Pharmaceutical formulations are commonly multi-component systems. In these systems the moisture sorption may exhibit a complex and non-additive behavior (148), which needs to be understood in detail, especially when absorbed moisture may induce unexpected phase transformations with new properties in the solid-state. The physical stability of an API when exposed to high RH in the presence of hygroscopic excipients has been the focus of a number of literature reports (200, 209, 210) and it has been observed that hygroscopic excipients are prone to retard hydration kinetics under humid conditions (211). In our studies, it was observed that excipients could enhance, retard, or have little effect on the hydration rate of OLZ.

4.6.1 Polyetyleneglycol (PEG)

PEG is a semi-crystalline material (201). In addition to PEG's surface adsorption ability of, it is widely accepted that it can also absorb moisture into its amorphous regions (201). When water is absorbed into the amorphous regions of the polymer, it serves to increase the disordered fraction of PEG (148, 212), which is a mechanism that is going to be taken into consideration on the following discussion.

Results showed that PEG displayed small weight changes at 75% humidity (2.5±0.9% after 28 days) but at 93%RH, the water uptake was about 53% w/w after 28 days. Regarding the water uptake mechanism for this polymer, a number of favorable polymer–water hydrogen bonds are firstly created, forming a film of adsorbed water molecules on the polymer surface (213). It was proposed that when this first water film is formed, to allow more water uptake, the PEG chains will adapt the desired conformation of the polymer chains to be able to form extensive hydrogen bonds with water, allowing the uptake of more water. PEG's ability to sorb

large amounts of moisture results from the presence of ether oxygen atoms (–O–) in the oxyethylene polymer backbone as well as hydroxyl (–OH) end groups, both of which can form several hydrogen bonds with water (213).

Results from calorimetric experiments showed a decrease and elimination of the melting transition when PEG was exposed for 4 weeks at 75% RH/25 ℃ and 93% RH/25 ℃, respectively, which reveals loss of crystallinity. Previous studies have observed that at RH below 70% water molecules can enter in the PEG matrix forming hydrogen bonds with oxygen atoms in the PEG chains. However, water molecules do not form condensed clusters when there are still oxygen atoms in PEG available to act as an electron donor for H-bonds with water molecules (214). At RH of over 70%, the full amount of oxygen atoms in the polymer chain is taken by water molecules. For this reason, the additional water molecules will interact with the ones already absorbed in the PEG structure, forming water clusters (214). Furthermore, absorbed water also acts as a plasticizer for the polymer (214), which enables the growth of water clusters in the polymer due to the increased mobility of polymer chains and increased available space due to swelling. An increase in RH (>90%) may lead to an amount of absorbed water sufficient to dissolve the PEG (213, 215). This was observed in our experiments. The visual inspection of the PEG samples during the 28 days at 93% RH showed a solid-to-solution phase transformation of this polymer, which indicated that PEG started to dissolve on the condensed adsorbed water.

Our results revealed that OLZ could undergo hydrate formation at 75% RH when mixed with PEG, which was never observed when OLZ was stored alone. At 93% RH, OLZ samples could fully hydrate and increased PEG contents showed faster hydrate conversions. The complete conversion of anhydrous OLZ into the dihydrate D form (weight increase of 10.3 % w/w) was completed by the end of 15 days, regardless of the PEG content. The hydration of OLZ at lower relative humidity and at faster rates when physically mixed with PEG may be explained by the formation of condensed water (water clusters) within the mixture, which were available to dissolve OLZ particles. The complete change of morphology of the crystals of OLZ indicate that the transformation could potentially occur (at least partially) in solution (201), i.e, anhydrous OLZ was able to dissolve into the bulk water and the nucleation and crystal growth of the more stable dihydrate form has occurred. The higher rates of hydrate conversion of OLZ in compacts with PEG may be explained by the partial loss of crystallinity of the sample and the more intimate contact between the drug and the polymer, resulting in a complete hydrate formation in one week for both OLZ:PEG ratios used.

4.6.2 Polyvinylpyrrolidone (PVP)

PVP is an amorphous and hygroscopic polymer (216). At 25 ℃ PVP absorbs approximately 5- 10% moisture at 10% RH, but this value increases significantly as the relative

humidity above the samples is increased (126). On exposure to 93% RH, our results showed that PVP could absorb approximately 55% of moisture, based on the dry mass of the sample. Water vapor is a well-known plasticizer. Also, water molecules can influence the free volume due to the breakage of hydrogen bonds between the molecules in the solid. This can lower the glass transition temperature (Tg) to (or below) the operation temperature, changing it from a glassy to a rubbery solid-phase states (216).

The kinetics of vapor absorption for PVP samples stored at the different humidity environments were examined and it was found that PVP rapidly absorbed moisture and reached apparent equilibrium (i.e., becomes saturated with vapor) after one week of storage (data not shown). The rate of moisture sorption appears to be much shorter than the observed timescale for hydrate transformation, once PVP was able to inhibit hydrate conversion during the 28 days of storage at all three different environment conditions. This suggests that desiccant effect of PVP is not the only mechanism responsible for hydrate inhibition of OLZ. Obviously, the viscoelasticity and the volume of the polymer tremendously changes due to the glassy to rubbery transition (216). It was possible to visualize the smoothening of the surface of PVP (SEM images) due to the increased molecular mobility associated with the transitions from the glassy state to the super-cooled liquid. Therefore, the physical state of the polymer at high humidity needs to be considered (60). It was also observed that this change in polymer structure when exposed to high humidity resulted on the decrease of the tensile strength of compacts, making them soft and deformed at touch (216). Thus, this highly plasticized PVP covered OLZ particles, becoming in intimate contact with the API particles. However, contrary to PEG, no hydrate conversion was verified. In samples with PEG the dissolution of the polymer in the condensed water enhanced hydration of OLZ by providing an aqueous medium for transformation to occur in solution phase. In the case of PVP, there are a number of possible explanations for these changes to be inhibited. Firstly, the extent of dissolution into PVP should be reduced due to the higher viscosity of the plasticized polymer that showed to present a "gel-like" structure (visual inspection). This was also observed in a previous study where PVP k90 showed to form a highly viscous structure after exposure to 94% RH, reducing the contact area with the API, and, consequently, the hydrate formation (60). Secondly, in the aqueous slurries of OLZ in PVP and PEG solutions (higher contents of water available), one has observed that no hydrate transformation of OLZ was visible in the presence of PVP, showing that this polymer is a much more effective inhibitor than PEG in aqueous environments. The higher hydrogen bond ability of this polymer relatively to PEG (194) may justify the stronger inhibitory effect of PVP. The formation of hydrogen bonds between polymers and the drug inhibits the latter from establishing hydrogen bonds with water molecules. Thus, the protection of pseudopolymorphic transformations is likely to be a combination of all these factors, resulting in the observed differences.

4.6.3 Hydroxypropyl cellulose (HPC)

Water vapor absorption by HPC occurs by the same basic mechanism as it does with other types of celluloses, i.e, water is only absorbed in the non-crystalline regions of celluloses (217). Therefore, the high content of amorphous domains in the HPC excipient results in its higher water absorption ability when compared to other celluloses, such as, microcrystalline cellulose (218). In this study, OLZ showed to hydrate faster in the first week when mixed with HPC. Since moisture is commonly selectively taken up by the most hygroscopic component, the increase of OLZ hydrate formation would not be expected, which leads to a deeper understanding of water uptake by this polymer. Water-vapor sorption-desorption isotherms which were calculated to characterize the uptake of water by HPC showed to fit the Young-Nelson model (219), a model originally developed to account for water uptake by wheat. It assumes that moisture absorbed by the solid has 3 locations: monolayer adsorption (bound water), externally adsorbed moisture (normally condensed) and internally absorbed moisture. In the case of HPC, the internally absorbed moisture results from the water diffusion through pores into the core of the particle from the adsorbed monolayer (218, 220). Therefore, the absence of protection of the OLZ hydration by this hygroscopic polymer may be justified by the interaction of the condensed water molecules encountered on the surface of HPC (water molecules above the monolayer moisture, i.e, externally adsorbed moisture) with OLZ molecules. Furthermore, HPC has shown to have a lower capacity to absorb water vapor internally when compared to, for instance, other hydroxypropyl celluloses with low degrees of substitution (L-HPC) (218).

When water molecules penetrate the HPC structure they include themselves into the hydrogen-bonded links between adjacent polymer chains. As a consequence, polymer chains become more independent of each other and occupy more space, resulting in the swelling of the polymer mass (218). As a result of the swelling process, the chains are extended, resulting in more locations available for hydrogen bonding and further molecular entanglements (221). The latter process requires certain time to reach deeper layers (222). As a result of extension of chains and the increase of more hydrogen bonding locations, hydrogen bonding with OLZ may occur justifying the abrupt reduction of the hydrate formation rate, when higher contents of HPC were used in the formulation. This hydrogen bonding with OLZ may hinder the hydrogen bonding of OLZ with water molecules. When OLZ was suspended in HPC solutions it did not hydrate as occurred with PVP. The hydrogen bonding between the drug and the excipients has been pointed out as an important factor on polymorphic inhibition in aqueous solutions (194). Therefore, the presence of both hydrogen bond donor and acceptor groups in the HPC ring structure may have facilitated the interaction with OLZ molecule. Furthermore, the plasticization of the polymer seemed to form a thick gel layer around the OLZ particles, which was observed by SEM and visual inspection. The formation of this gel may also hinder OLZ

particles' dissolution into condensed water and/or prevent moisture penetration into the OLZ crystal when higher contents of HPC were used.

4.6.4 Pseudopolymorphic transformations in compacts

Tableting is a process which may potentiate the occurrence of phase transformations in either the drug or the excipients via the solid-state mechanism. Most of the data supports the idea that the transformations from one polymorphic form to another during tableting results from an intermediate amorphous phase (83). These transformations are current as exemplified by caffeine, sulfabenzamide and maprotiline hydrochloride which have been reported to undergo polymorphic transformations during compression (114).

The diffractograms of compacted OLZ showed neither missing nor new diffraction peaks of OLZ, which means that no polymorphic transformation occurred under compression. However, it was observed that, upon compression, diffraction experiments showed a loss of intensity and broadening of OLZ peaks. This was probably due to the induction of lattice disorder in the surface of anhydrate promoted by compaction. The reduction of melting temperature enthalpy of OLZ also revealed loss of crystallinity of the drug induced by application of pressure. This phenomenon was observed for both drug and drug:polymer mixtures.

For all the compacts OLZ showed to hydrate faster after 7 days of exposure to 93% RH than in the physical powder mixtures. In solids, nucleation tends to proceed from dislocations in a crystal because of their higher free energy; for this reason, the activation energy barrier for transformation is lower at these sites (114). Moreover, during compression the plastic flow induces dislocational strains in a crystal, thereby facilitating nucleation. However, the OLZ compacts showed only a minimal increase on the dihydrate D content after 28 days. The reduced hydrate conversion may be justified by the low specific surface area of the compacts in relation to the powders. This fact resulted on a reduction of the amount of molecules of OLZ in direct contact with the water vapor. Furthermore, the diffusion rate of water molecules through the OLZ crystal lattice may be compromised on the core of the tablet.

4.6.5 Conversion kinetics of OLZ in aqueous suspensions

Results showed that no hydration occurred for OLZ suspended in PVP and HPC polymeric solutions, whereas hydrate conversion was observed in PEG solution. Previous studies have shown that the effectiveness of a polymer as a crystallization inhibitor is highly dependent on its structure, due to the formation of specific intermolecular interactions between the polymers and the drugs (143, 223). These interactions have been found to contribute to the adsorption of polymer onto solids and thus, controlling a number of interfacial processes such as crystal growth. Specific intermolecular interactions (such as hydrogen-bonding) and non-specific hydrophobic drug–polymer interactions appeared to be important in determining the

impact of a given polymer on crystal growth effectiveness (143). The adsorption to the crystal surface interface promotes sterically hindrance to the access of the solute molecules to the crystal terrace.

All of these polymers have the ability to form hydrogen bonds with OLZ molecule. PEG has ether oxygen groups in its chain and two hydroxyl groups at the two ends of the polymer chain; PVP presents one acceptor hydrogen bonding group in its ring structure. However, the carbonyl oxygen of PVP is able to form stronger hydrogen bonds than the ether oxygen groups of PEG, explaining its stronger protection against crystal growth (194). In other study with acetaminophen, the stronger inhibitory effect of PVP was also attributed to lower mobility of the functional groups involved in specific polymer-drug interactions when compared to PEG.

HPC is constituted by a cellulose derivative polymer, with both hydrogen bond donor and acceptor groups in its ring structure, also presenting a certain hydrophobic nature that showed to have an impact on avoiding and retarding the hydrate conversion of a few of other drugs (194, 196).

The effect of these polymers on crystallization of OLZ is going to be explored in the next chapter in more detail.

4.7 Conclusion

This study provided an insight into the role of hygroscopic polymeric additives on the stabilization of OLZ anhydrous Form I. The study showed that the stabilization of anhydrous OLZ in humid environments was dependent on the type of polymer and the amount of polymer present in the formulation. For example, both PEG and HPC showed to induce hydrate transformations of OLZ at a relative humidity of 75%. Since OLZ cannot hydrate at this humidity when it is stored alone, this result highlighted the importance of the right choice of formulation design in order to maintain the drug stable in the final product. At 93% RH, PEG showed to absorb high contents of moisture, which allowed OLZ to undergo a solvent-mediated transformation, accelerating the hydrate conversion rates of OLZ. PVP also showed to uptake high moisture contents but, contrary to PEG, PVP was able to protect OLZ from undergoing hydrate transformation. In aqueous environments, when a higher content of free water molecules was available to bind OLZ, PVP also showed to protect OLZ from hydration. It was therefore possible to extrapolate that PVP could form specific interactions with the drug, which inhibited OLZ to form hydrogen bonds with the water molecules. Regarding HPC, the protector effect of this polymer seemed to be related to the content of this polymer within the sample. Since during the swelling of the polymer there are more hydrogen bond locations available to bind with the OLZ molecule, this process was amplified when there were more molecules of HPC in the system available to bind with the OLZ molecule. Compaction of OLZ revealed to

slightly reduce its crystallinity, inducing a faster hydrate formation in the first days of storage. Compaction also led to close contact between OLZ and polymers, which resulted in an acceleration of hydrate formation when OLZ was mixed with PEG.

Overall, since the choice of the formulation design is important, in order to produce a product with a consistent quality performance throughout the product's shelf life, attention should be payed to the excipients used in the formulation, helping to avoid the formation of metastable phases that may affect the final product quality. Furthermore, being OLZ a drug commonly used in the treatment of schizophrenia, an illness which requires patients to be kept clinically stable and in good compliance with the treatment, minor changes on the bioavailability could affect the stability of the patients, with a decrease on their compliance.

CHAPTER 5

Chapter 5 - An insight into the impact of polymers on the hydrate conversion of olanzapine Form I in aqueous suspensions

5.1 Abstract

Hydrate conversion of anhydrous drugs may occur during wet agglomeration processes (e.g. fluidized bed granulation). The objective of this study was to assess the polyethyleneglycol's (PEG-6000/ PEG-40000), polyvinylpyrrolidone' s (PVP K30) and hydroxypropylcellulose' s (HPC LF) potential to inhibit the hydration process of OLZ in an aqueous environment (e.g. suspension), thus understanding their mechanims of action. OLZ Form I (OLZ FI) was suspended either in double-distilled water (A) or in aqueous polymer solution (2, 0.2, 0.02 and 0.002%) [PEG 6000 (B), PEG 40000 (C), HPC LF (D) or PVP K30 (E)] and stirred at 200 rpm for 3h. Samples were collected at different times and were filtered and analyzed by different techniques (XRPD, FTIR, DSC, ^{1}H-NMR). The results suggested that OLZ suspended in PEG solutions (B and C) showed to hydrate regardless of the polymer chain and concentration considered. OLZ hydrate conversion showed to be faster in water than in PEG solutions. OLZ recovered from D and E suspensions remained anhydrous at concentrations of 2-0.02%. The nuclear magnetic resonance measurements revealed that all of these polymers are able to establish hydrogen bonding with the OLZ molecule. It was found that all of these polymers can increase the OLZ saturation solubility. Only HPC LF and PVP K30 showed to increase the wettability of the OLZ particles after exposure to the respective solutions, suggesting binding of these polymers to the surface of OLZ crystal surfaces. The inhibition of the process of hydration by both polymers showed to be related to both the H-bond ability and the stronger bonding of these polymers to the crystal surfaces of the hydrate nuclei / first crystals, preventing the crystal growth. This study provided an insight into the main mechanisms of hydrate protection of OLZ by polymers confirming the advantage of using either PVP K30 or HPC LF as excipients in granulation processes to prevent OLZ hydrate formation, in aqueous solutions in concentrations as low as 0.02%.

5.2 Introduction

The previous chapter showed that different polymers may interact differently with OLZ Form I (OLZ FI) in aqueous environments. Since in wet agglomeration processes, such as wet granulation or extrusion in particular, the formation of hydrates may pose severe problems during manufacturing (79) (80). The study of the interactions of OLZ with polymers in aqueous environments is, thus, important to be explored in more detail. Furthermore, the small recommended dose for OLZ (maximum dose of 20 mg per day) (178) enhances potential problems due to changes on its solubility, with an impact on the amount of drug dissolved and consequently on the absorption into the plasmatic stream, which may simply be due to minor modifications of the crystalline structure of the drug (e.g. hydrate formation).

In recent years, the study of the impact of addition of polymeric excipients on the preventing the hydrate formation of APIs in aqueous environments has attracted some attention (196, 224, 225). Polymers may inhibit crystallization at both the nucleation and growth stages and several mechanisms may be involved (194, 197). For instance, polymers can change viscosity, solubility or the properties of the hydrodynamic boundary layer surrounding the crystal, thereby decreasing the rate of diffusion of the drug molecules to the crystal nuclei (226). They can also adsorb into the crystals surface interface, due to hydrophobic and hydrogen bonding type interactions, blocking the access of the solute molecules to the crystal terrace (39, 196, 227). The different inhibitory behaviors therefore result from the type of interactions between drug and polymer, which may vary for each polymer and API. Nuclear magnetic resonance (NMR) has been shown to be a powerful tool to detect intermolecular interactions between different components and to characterize the type of interactions between the drugs and excipients. NMR has already been used to detect specific binding between drugs and cyclodextrines, surfactants or polymers (143, 228, 229).

OLZ is commonly used in the treatment of schizophrenia, an illness which requires patients to be kept clinically stable. The small recommended dose for OLZ (maximum dose of 20 mg per day) enhances potential problems due to changes on its solubility, with an impact on the amount of drug dissolved and consequently on the absorption into the plasmatic stream, which may simply be due to modifications of the crystalline structure of the drug (e.g. hydrate formation).

5.3 Purpose

The purpose of this study was to explore the OLZ hydrate transformation in an aqueous medium and the mechanism of interaction between OLZ and various polymers in aqueous suspension. For this study, OLZ was suspended in different polymer solutions, namely polyethyleneglycol (PEG), hydroxypropylcellulose (HPC) and polyvinylpyrrolidone (PVP). In particular, this study aims: (1) to characterize the potential hydrate conversions of OLZ in

polymeric solutions over time; (2) to detect changes in the wettability of the powders collected due to potential binding to polymers; and (3) to understand the mechanisms of inhibition of hydrate formation by the polymers through the study of the rheological properties of the polymeric solutions and the saturation solubility of OLZ in each polymeric solution.

5.4 Materials and methods

OLZ anhydrous Form I [OLZ FI, molecular weight (Mw) = 312.43 g/mol] was purchased from Pharmorgana, India. The polymers considered in the study were polyethylene glycol with different molecular weights (PEG, Mw = 6000 and 40000, Sigma-Aldrich, Germany), hydroxypropyl cellulose (HPC LF Pharm grade, Mw = 95000, Klucel™, Ashland, Germany) and polyvinylpyrrolidone (PVP, Kollidon 30, 44000 < Mw < 54000, BASF Chemicals, Germany). Other chemical were supplied by Sigma-Aldrich, Germany.

5.4.1 Preparation of samples for solvent-mediated conversion studies

OLZ (100 mg) was dispersed in triplicate into 5 mL aqueous solutions/polymer solution with different polymer concentrations (Table 5.1) during 180 min. Suspensions were agitated using a magnetic stir bar (200 rpm) and then recovered by vacuum filtration to remove excess of water. The powders were transferred into XRPD sample holders and analyzed immediately.

Table 5.1– Formulations for hydrate conversion studies.

Polymers	Formulation code
No polymer	A
PEG 6000	B
PEG 40000	C
HPC LF	D
PVP K30	E

Experiments	1	2	3	4
OLZ:Polymer ratio	1:1	10:1	100:1	1000:1
Polymer concentration (%, w/v)	2%	0.2%	0.02%	0.002%

Each formulation with a different polymer has a different letter (formulation code) and each OLZ:polymer ratio used has a different number

5.4.2 Characterization of the different formulations

X-ray Powder Diffraction (XRPD)

The structural characterization of OLZ formulations were carried out by X-ray powder diffraction (XRPD) on an Analytical X'Pert PRO apparatus, NL (Equipment 2, chapter 2). Diffractograms were obtained by continuous scanning in a 2θ range of 7–35 with a step size of 0.017° and scan step times of 20 sec. X-ray diffraction characterization was performed to the different formulations before and after the end of the study (180 min) in order to observe the hydrate conversions of OLZ in each sample.

Differential Scanning Calorimetry (DSC)

Thermograms of different samples were obtained with a Differential Scanning Calorimeter (TA instruments, Q200, New Castle, USA). Dry N was used as the purge gas (Air Liquide, mL/min). OLZ was allowed to dry at room humidity and temperature (55% RH/25 ºC) before analysis in order to remove the excess of water. Samples (2–3 mg) were placed in pinhole crucibles and heated at 10 ºC/min within 0–210 ºC temperature range.

FT-Infrared Spectroscopy (FTIR)

Each sample was mixed with KBr in a 1:100 proportion and the mixture (200 mg) compacted into compacts (12 mm diameter). The infrared spectra were collected in the absorption mode (IR Affinity-1Shimadzu spectrophotometer, Kyoto, Japan) based on 64 scans with a resolution of 2 cm^{-1}.

Scanning Electron Microscopy (SEM)

OLZ powders were analyzed by scanning electron microscopy. The samples were mounted on aluminum stubs and coated with gold by ion sputtering (JEOL JFC-1200 Fine Coater, Tokyo, Japan) and observed under scanning electron microscope (JSM-5200 LV, Tokyo, Japan).

5.4.3 Wettability Measurements

In order to measure the wettability of OLZ before and after being exposed to polymeric solutions, the contact angles in bi-distilled water were measured (Wilhelmy plate technique, Krüss Tensiometer K12, Hamburg, Germany). Samples of powders were made to adhere on a rectangle shape substrate (20 x 20 mm) uniformly coating its surface. All measurements were performed at a controlled temperature of 25 ± 0.5 ºC by flowing water from a circulator (Krüss).

5.4.4 Viscosity studies

The viscosity of the polymeric solutions at 2% and 0.2% w/v was measured. The capillary measurement method was used. The constant of the viscometer (k) is 0.02978 mm/s^2 and the equation used, based on the Poiseuille's Law, was: $\eta = k.t.\rho$, where: η represents the viscosity of the solution; k is the constant of the viscometer; t represents the time the liquid takes from going from A to B (2 points marked in the viscometer); and ρ represents the density of the solution, measured beforehand with a densitometer.

5.4.5 Determination of OLZ solubility in different solutions

An excess of OLZ powder (approximately 10 mg) was placed into 4 ml Eppendorf cups and 2 ml of the respective stabilizing medium was added (PVP, HPC and PEG solutions at 2%, 0.2%. 0.02%, 0.002% w/v). The cups were sealed and placed into a water bath at 25 ºC shaking at 100 rpm. After 36 h the Eppendorf cups were centrifuged at 12000 rpm for 20 min (Sigma

202K, Germany). The concentrations of dissolved OLZ were determined with a UV apparatus 254 nm (Higuchi, Japan).

5.4.6 ^{1}H- RMN measurements

A solution of OLZ (10 mg) in 0.5 mL of deuterated chloroform (CDCl$_3$) was prepared. Afterwards, a solution of the polymer (10 μL, 1.0 mg/mL) was added to the OLZ solution and the latter was allowed to stabilize for 5 min before the ^{1}H-NMR spectra measurement (OLZ:polymer 1000:1). A solution of the polymer (10 uL, 9.0 mg/mL) was added to the previous solution. This solution was allowed to stabilize for 5 min and the ^{1}H-NMR spectra was measured (OLZ:polymer 100:1). To the above solution, 0.9 mg of the polymer was added and allowed to stabilize for 5 min before the ^{1}H-NMR spectra measurement (OLZ:polymer 10:1). Finally, to the previous solution 9.0 mg of the polymer was added and allowed to stabilize for 5 min before the ^{1}H-NMR spectra measurement (OLZ:polymer 1:1).

NMR spectra were recorded in a Bruker Avance II 300 Ultrashield Plus. The ^{1}H- RMN spectra was obtained at 25 ºC.

5.5 Results

5.5.1 Conversion of OLZ in aqueous suspensions

This study was conducted to obtain an insight into the mechanism of interaction between OLZ and various polymers in aqueous environments. Figure 5.1 shows the X-ray diffractograms of different OLZ forms. The diffractograms for the recovered samples from 180 min suspensions are shown in Figure 5.1. The characteristic peaks of dihydrate B (higher proportion) and higher hydrate (lower proportion) can be observed in OLZ which was suspended in water (A1). Regarding OLZ recovered from PEG solution (B1), it could be observed that it was selectively hydrated into the higher hydrate form (Figure 5.1). This form showed to dehydrate into the dihydrate E in a few hours when stored at room humidity and temperature (25 ºC/55% RH). OLZ showed to remain anhydrous when stirred in HPC and PVP solutions (Figure 5.1). The DSC analyses showed that the different OLZ hydrates recovered from water (A1) and PEG solution (B1 and C1) had different dehydration temperatures (Figure 5.1).
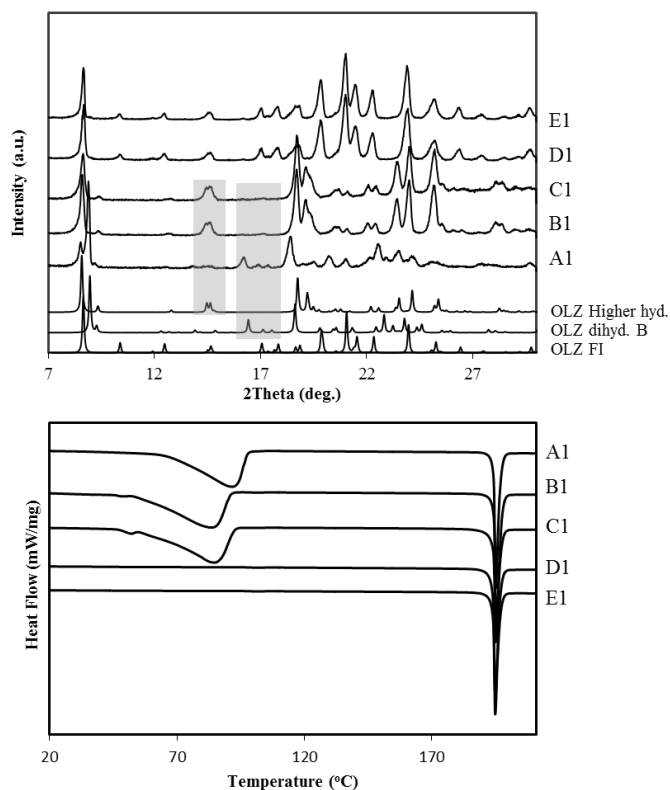
Figure 5.1 – Diffractograms and thermograms of powders filtered from the different suspensions after 180 min. Grey bar highlights the characteristic peaks of OLZ hydrates.

Figure 5.2 shows the FTIR spectra of all of the recovered samples within the 720 cm^{-1}-1020 cm^{-1} range. In this region, the band patterns of the OLZ hydrates and anhydrous Forms I can be easily distinguished. OLZ recovered from the formulations B and C after 180 min showed to hydrate in all of the different samples, regardless of the PEG content in the formulations. OLZ recovered from polymer solutions D and E showed to remain anhydrous when the polymer concentration was 2%, 0.2% and 0.02%.
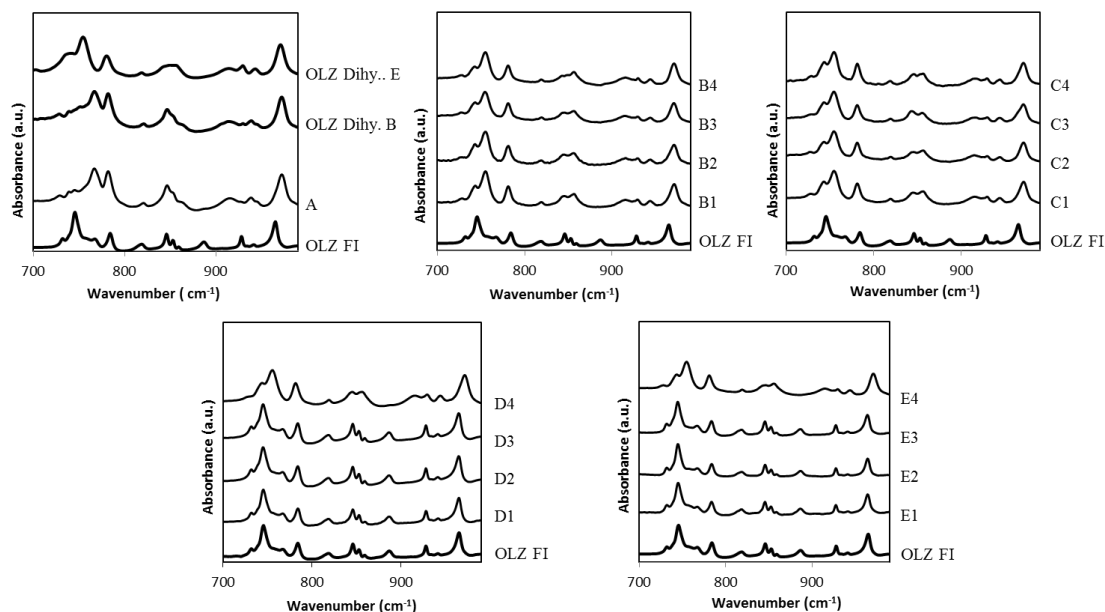
Figure 5.2 – FT-Infared analyzes of OLZ recovered from the different polymeric solutions (A, B1-B4, C1-C4, D1-D4, E1-E4).

Figure 5.3 shows the rates of OLZ hydration in water and PEG solutions. It was possible to observe that hydrate formation is faster in water and slower in PEG 40000 solution. In PEG 40000 solution, hydrate formation was visible only after 180 min of stirring.
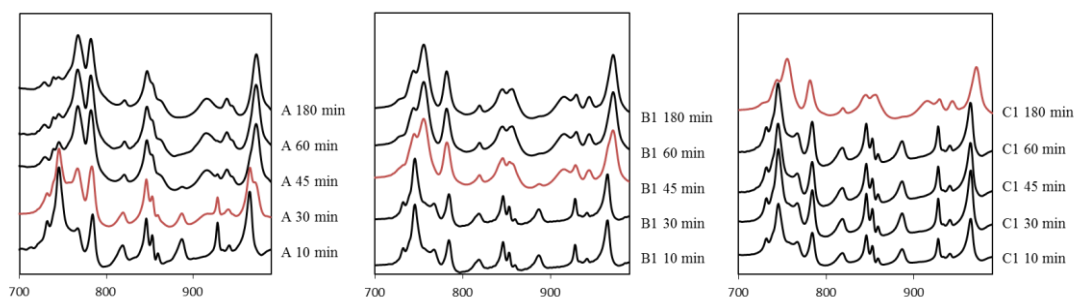
Figure 5.3 – FT-Infared analyzes of OLZ recovered from the polymeric solutions A, B1 and C1 at different time periods.

Figure 5.4 a) shows a SEM micrograph of OLZ raw-material, which is characterized by having an irregularly shape. Regarding OLZ particles which were suspended in PEG solutions for 180 min (Figure 5.4 b and c), one may observe that OLZ particles had their morphology changed due to hydrate formation. In contrast, formulations D1 and E1 showed no modifications on OLZ particles' morphology over the same period (Figure 5.4 d) and e).
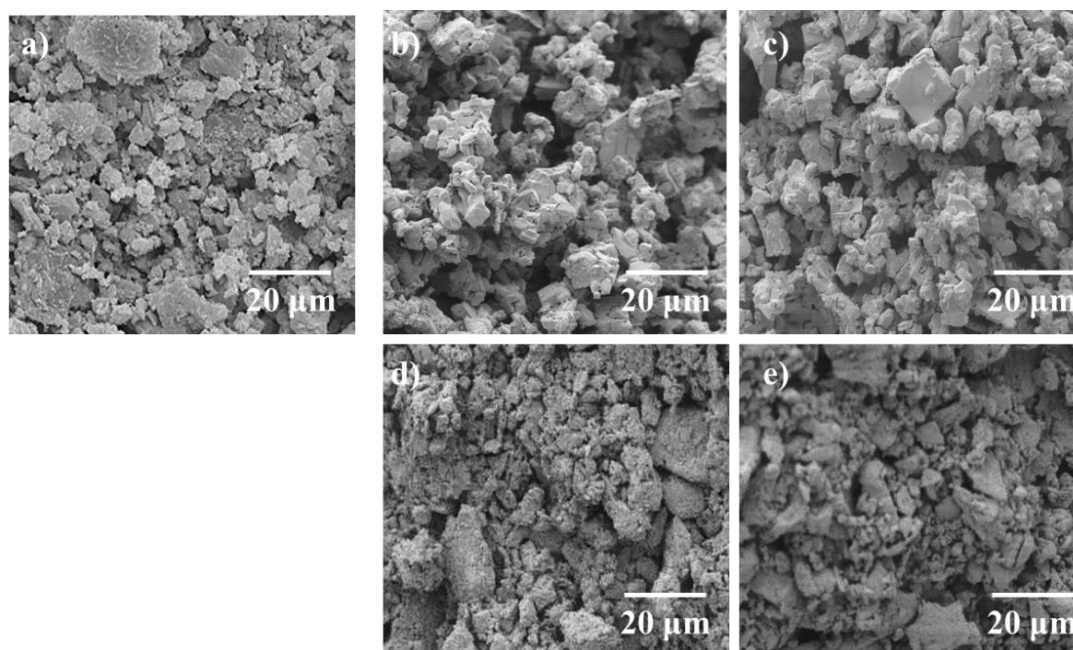
**Figure 5.4 – SEM micrographs of (a) OLZ Form I (raw material)
and formulations B1, C1, D1and E1.**

5.5.2 Viscosity

Table 5.2 shows the viscosity of polymeric solutions at the highest concentrations: 2% and 0.2%. Results showed that HPC polymer solutions present the highest viscosity. At 0.2% all solutions presented low viscosity values (< 1.2 mPa.s). Polymer solutions can be ordered in terms of their viscosity in the following manner for both concentrations: HPC<PEG 40000<PVP k30< PEG 6000.

Table 5.2 – Viscosity measurements of the two most concentrated polymer solutions

Solutions	Viscosity (mPa.s) of the polymer solutions
Water	-
PEG 40000 (2%)	1.686
PEG 40000 (0.2%)	1.104
PEG 6000 (2%)	1.186
PEG 6000 (0.2%)	1.006
HPC (2%)	7.394
HPC (0.2%)	1.144
PVP (2%)	1.292
PVP (0.2%)	1.009

5.5.3 Wettability of the recovered OLZ

Table 5.3 shows the contact angle of the raw-materials and filtered OLZ particles (t=180 min in water or polymeric solution) with water. While the contact angle of the filtered OLZ particles in formulations B1, C1 and E1 showed a contribution of the contact angles of both polymers and OLZ raw-materials, the contact angle of OLZ particles in formulation D1 (OLZ filtered from HPC solution) seemed to solely be due to the contribution of HPC. Furthermore, the contact angle observed for these particles showed a lower contact angle than the values measured for the polymer alone (76.4 ° vs 91.84 °). This suggests that, as a result of changes in polymer chain conformation, this polymer was not only completely covering the crystalline particles of OLZ but also decreasing the number of hydrophobic groups exposed on the surface of the particles. OLZ recovered from the formulations D showed to have a contact angle inferior to the polymer in experiments D1, D2 and D3, which were the formulations where OLZ remained anhydrous during the 180 minutes. OLZ recovered from the formulations E showed to have contact angles between the drug and the polymer in formulations where hydrate formation of OLZ has not occurred (E1, E2 and E3). Formulations B and C showed to have a contact angle similar to OLZ raw-material in formulations 2, 3 and 4.

Table 5.3 – Contact angle and standard deviation of the filtered powders (t=180 min) from different solutions (A, B1-B4, C1-C4, D1-D4, E1-E4) and raw materials

Drug:polymer ratio	Contact angle ± SD (θ / °) of recovered samples (180 min)					Raw Materials	Contact angle ± SD (θ / °)
	1:0	1:1 (1)	1:10 (2)	1:100 (3)	1:1000 (4)		
No polymer	104.8± 0.5	-	-	-	-	OLZ	104.6 ± 0.6
PEG 6000	-	100.9 ±1.0	104.8 ±1.8	105.8 ±1.1	106.2 ±1.3	PEG 6000	63.6 ± 2.0
PEG 40000	-	100.2 ± 0.9	104.7 ± 0.9	105.2 ± 1.2	105.9 ±1.0	PEG 40000	64.3 ± 1.9
HPC LF	-	76.4 ± 2.1	81.7 ± 0.9	88.1 ± 0.8	104.9 ±1.5	HPC	91.8 ± 0.4
PVP K30	-	97.3 ± 1.7	99.1 ± 1.8	101.1± 1.0	105.3 ±1.3	PVP	75.7 ± 2.2

5.5.4 Saturation solubility of OLZ

After 36h of bath-shaking of the OLZ suspensions, the OLZ solubility in each polymer solution at different concentrations was evaluated and the concentration of OLZ dissolved was plotted against each polymer concentration (Figure 5.5). It was observed that PVP K30 and PEG 40000 had the highest impact on the saturation solubility of OLZ. Both polymers showed to induce a linear increase in the solubility of OLZ, with an increase of their concentrations. PVPk30 at a concentration of 2.0% showed to increase at values 10 times higher than the solubility of OLZ in water, whereas PEG 40000 at the same concentration showed to increase five times the solubility of OLZ.

The solubilization of the drug proved to be quite low by the HPC and PEG 6000. The filtration of the suspended OLZ powders after the test and their further solid-state characterization showed that OLZ was hydrated after being kept for 36h in all PEG 6000 and PEG 40000 solutions. In contrast, OLZ suspended in HPC and PVP solutions remained anhydrous at polymer concentrations of 2%, 0.2% and 0.02%. This suggests that the protection of OLZ from hydration by HPC or the absence of protection by PEG 40000 is not related to the drug solubilizing effect of the polymers.
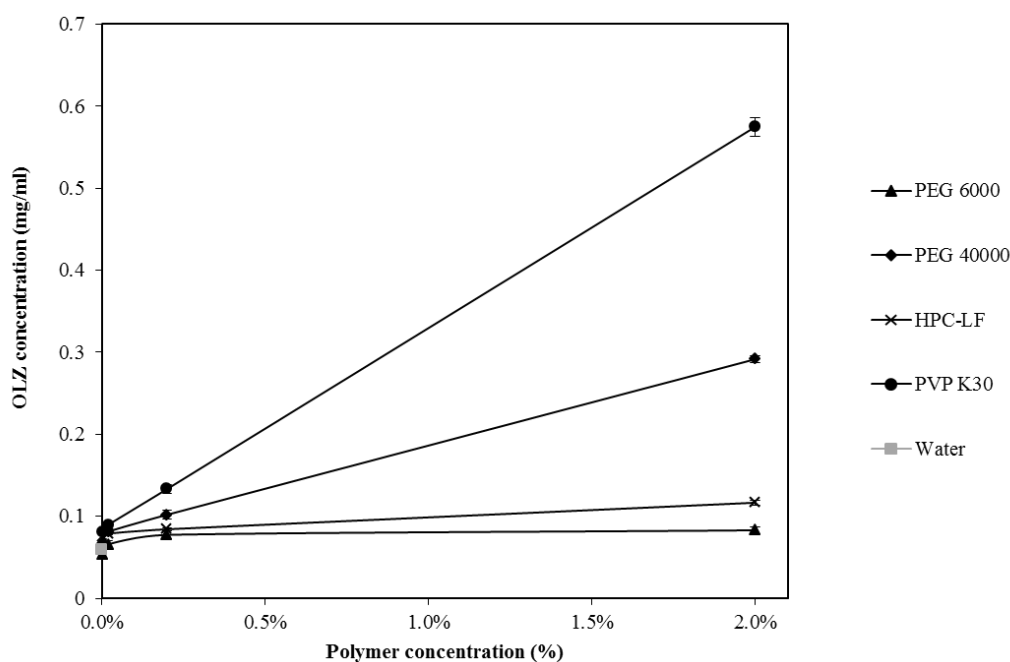
**Figure 5.5 – OLZ saturation solubility measured in water
and different polymeric solutions at 25ºC.**

5.5.5 Evaluation of molecular state of OLZ in polymer solutions by ^{1}H-NMR studies

^{1}H-NMR measurements were done to OLZ mixed with different proportions of different polymers. Although several attempts have been undertaken to collect these spectra in aqueous environments, the low solubility of OLZ in both H_2O and D_2O did not allow a proper OLZ spectrum collection. A previous ^{1}H-NMR work which have studied the stabilities of hydrogen bonds in aprotic environments compared to water, concluded that the electronic perturbations due to the hydrating water molecules (which are able to form additional hydrogen bonds with the solute), have a low impact on the length of solute−solute hydrogen bonds (230). Other studies have also used aprotic organic solvents, either alone or mixed with D_2O, in order to understand if polymers can affect the chemical environment around the drugs and, therefore, understand how polymers may affect the crystallization of drugs (63, 143).

Deuterated chloroform (CDCl$_3$) was chosen for this study because it is an aprotic solvent, which means that it will not exchange the NH proton of OLZ. In addition, CDCl$_3$ will not interact with the potential hydrogen bonding between OLZ and polymers (63) – therefore, the impact of each polymer on OLZ ^{1}H-NMR spectra could be comparable.

The increase of the signs at 3.66 ppm, 3.64 ppm, 3.5 ppm, 3.21 ppm, resulted from the increase of PEG 6000, PEG 40000 HPC and PVP concentrations, respectively.

The ^{1}H-NMR of OLZ in CDCl$_3$ shows a singlet at 4.98 ppm (integration to one proton), which corresponds to the amino group (231). This signal shifted downfield with the increased addition of each polymer. A similar effect has already been observed in previous studies as a result of the formation of hydrogen bonds between the polymers and the drugs (143, 232). The chemical environment of OLZ showed also to depend on polymer concentrations.
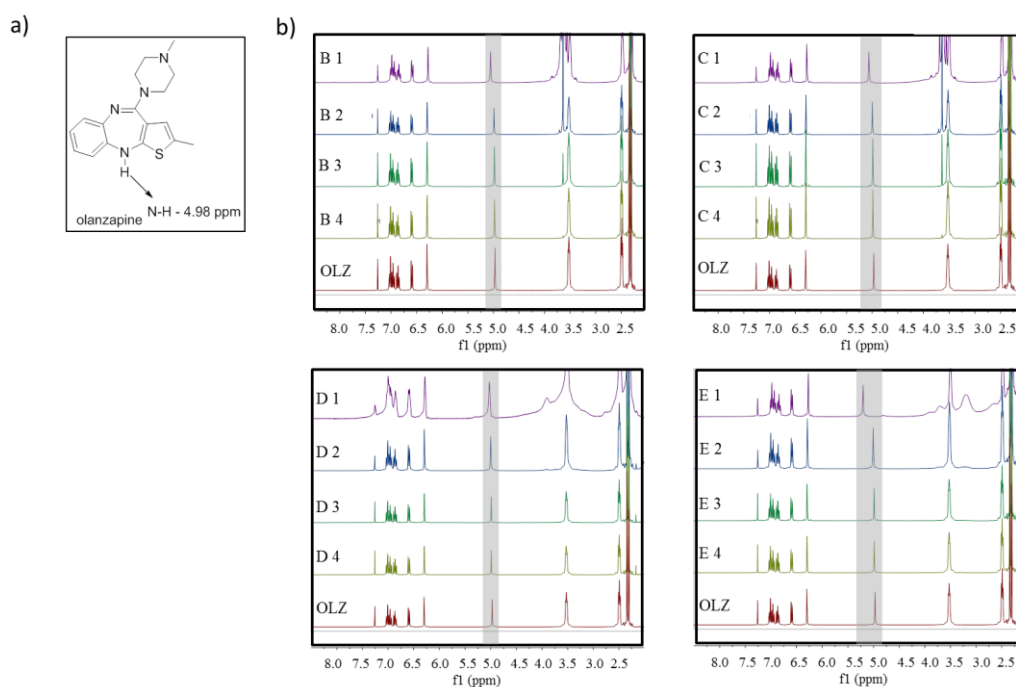
Figure 5.6 – OLZ molecule showing the H responsible for the peak at 4.98 ppm (a) and proton NMR spectra for pure OLZ and the OLZ:Polymer mixtures (B1-B4, C1-C4, D1-D4, E1-D4) (b).

Figure 5.7 shows the NH proton shifts in more detail. It is noted that the downshift of the peak was larger for higher polymer fractions. OLZ:PEG 6000, OLZ:PEG 40000, OLZ:PVP and OLZ:HPC showed a downshift of 0.08, 0.10, 0.23 and 0.06 ppm, respectively, when the highest drug:polymer ratios were used. HPC showed to promote the lowest shift in the singlet at 4.98 ppm of OLZ. However, this polymer showed to not completely dissolve for the highest polymer concentration and therefore the polymer:OLZ proportions dissolved were not the same as compared to the other polymers. For this reason, we could not consider this value.

Nevertheless, the downshift was visible for lower HPC concentrations, indicating that this polymer can actually interact with the drug.

The interactions between the NH proton with the acceptor hydrogen bonding group in the PVP ring structure may explain the strongest shift in the singlet at 4.98 ppm of OLZ (63). Furthermore, the shift became larger with the increase of PVP concentration.
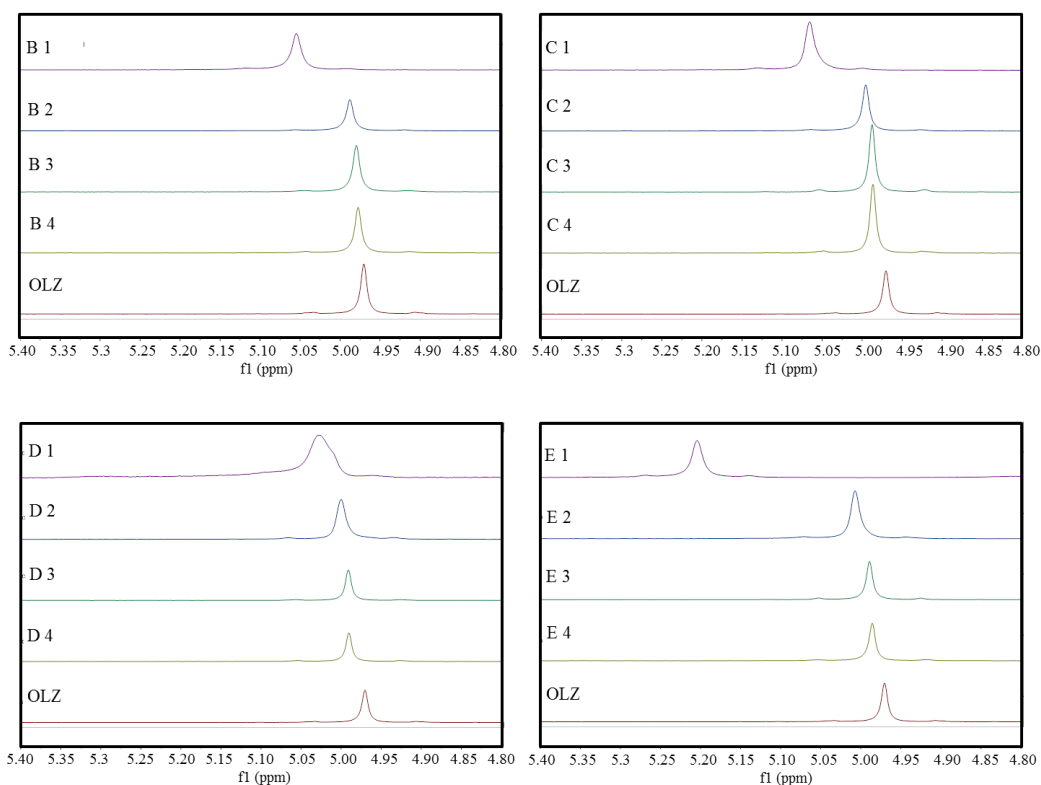
Figure 5.7 – Higher magnification of proton NMR spectra for pure OLZ and the OLZ:Poymer mixtures within the range of 5.40-4.80 ppm (a).

5.6 Discussion

The different crystalline forms of OLZ are built through the assemblage of OLZ centrosymmetric racemic pairs and these pairs connect to each other through hydrogen bonds, either from atoms like in the OLZ structure (e.g. anhydrous form) or by water molecules (e.g. hydrate forms). In an aqueous environment, anhydrous OLZ tends to hydrate in few minutes. The hydrate conversion is likely to occur as a solvent-mediated transformation (116, 117). In these transformations three steps are involved: dissolution of the metastable phase into the solution to reach and exceed the solubility of the stable phase; nucleation; and crystal growth of the stable phase coupled with the continuous dissolution of the metastable phase (6).

In this study, the addition of soluble excipients (polymers) was analyzed in detail in order to understand their effect on crystallization of OLZ hydrates.

The results showed that, when OLZ was suspended in water, its XRPD pattern OLZ exhibited mixed reflections of 2 different hydrates, whereas in the presence of PEG the XRPD diffractograms showed a pure pattern of the higher hydrate form. In other study, a similar phenomenon was observed for nitrofurantoin, where the formation of hydrogen bonds with the polymer led to the formation of an isolated hydrate form (227). In the present work PEG polymers showed to also be able to retard hydrate formation, which might have affected the kinetics of nucleation with an impact on the final hydrate phase formed.

The ^{1}H-NMR results showed that all the different polymers have affinity to form hydrogen bonds with OLZ. The possible interaction between the drug and the polymers is the proton that is located on the nitrogen atom (amine group) of the drug. Previous studies have demonstrated that, besides the electrostatic and van der Waal's forces, hydrogen bonds between the drug and the polymers are likely to be involved in the increase of drug's solubility (63).

In the present study, the saturation solubility values of crystalline OLZ at 25 °C were determined to be 0.059 mg/ml in water. At concentrations above 0.02% all polymers were able to increase the saturation solubility of OLZ by the following rank order: PVP K30>PEG 40000>HPC LF> PEG 6000. Loftsson et al., 1994 (233) showed that the addition of 0.25% (w/v) PVP to water results in an average increase of 64% in the aqueous solubility of nine different drugs and that an addition of 0.25% (w/v) carboxymethylcellulose (also a cellulose derivative) resulted in an average increase of 53% in the aqueous solubility of 16 different drugs. PEG has also shown to increase the solubility of several drugs since it can form hydrogen bonds between its ether oxygens and the drug's amino groups (143). Our results showed that OLZ had the highest solubility enhancement in PVP and PEG 40000 polymer solutions, which were the polymers that induced the strongest shift in OLZ ^{1}H-NMR N-H signal.

In another work, ^{1}H-NMR studies were performed to understand the interaction between PVP, diphenylhydantoin and dimethylphenytoin and the relationship between these interactions and the solubilization efficacy of PVP on each drug. It was observed that PVP could promote much larger chemical shifts on the diphenylhydantoin molecule. This molecule also showed to have higher solubility in PVP solutions, leading the authors to conclude that the intermolecular interaction of PVP with diphenylhydantoin could be stronger than with dimethylphenytoin, resulting in increased solubilization efficiency of the former by PVP (143). As such, the increment of solubility seems to be related to the hydrogen bonding interactions between drug and polymer through the formation of a soluble complex between the drug and polymers in aqueous media (63). The stronger hydrogen bonding ability of PVP is likely to be associated with the ability of carbonyl oxygen of povidone to form stronger hydrogen bonds with drug's amine groups when compared to the ether oxygen groups of PEG (194, 234).

PEG 6000 showed to slightly increase the OLZ solubility. The lower viscosity of PEG 6000 and its reduced capacity to increase OLZ's solubility may explain the faster hydrate

conversion of OLZ in presence of this polymer when compared to PEG 40000. The increase of solubility by interactions with polymers has been pointed out as one of the mechanisms of reducing crystallization of hydrate forms, since these interactions showed to lead to a reduction on the amount of freely dissolved drug to undergo crystallization (143). However, although all polymers have shown to increase the solubility of OLZ, only PVP and HPC have showed to be able to inhibit the crystallization of hydrates.

Previous studies have demonstrated that the effectiveness of a polymer as a crystallization inhibitor is highly dependent on the hydrogen bond ability and hydrophobicity of the polymer (143, 223, 224). However, it has been difficult to understand the relative importance of both factors.

Polymers which are more hydrophobic are less present in the aqueous phase, having more ability to bind to hydrophobic crystals' surfaces. When absorbed at relevant growth sites these polymers may block the growth of the forming crystals. The measured contact angles of the raw materials with water have shown that HPC is the most hydrophobic excipient and PEG is the most hydrophilic one. The recovered particles of OLZ showed that particles that were filtered from HPC solution presented a contact angle lower than HPC. This suggested that the higher hydrophobic nature of HPC may have been led to the adsorption of this polymer on the hydrophobic crystal surfaces of OLZ, leaving its most hydrophilic groups in contact with water molecules. It was only at the lowest concentration of HPC (formulation D4), when the polymer could not avoid the hydrate formation, that OLZ particles showed to have their contact angles with water similar to the OLZ raw-material. These results demonstrated that HPC could avoid hydrate formation due to its higher affinity towards the newly formed OLZ hydrophobic surfaces formed in HPC solution, stabilizing them against the crystal growth. HPC also revealed to be the polymer which could increase the most the viscosity of the system, which could have also contributed to restrain the diffusivity of the drug molecules.

PVP exhibits moderate hydrophobicity and the surface of OLZ crystals filtered from most concentrated PVP solutions showed contact angles between the OLZ raw material and the polymer. No differences on OLZ protection were observed between PVP and HPC, since both polymers showed to protect OLZ hydrate formation when OLZ was suspended in solutions of 0.02% w/v but unable to protect OLZ hydrate formation when polymers were at a concentration of 0.002% m/v.

In order to explain this phenomenon the molar ratios between dissolved OLZ in each polymer solution and the polymer repeat units dissolved in each system (2, 0.2, 0.02 and 0.002% m/w) in saturation stability studies were taken under consideration. The molar ratios in the investigated systems were calculated as presented in the following table:

Table 5.4 – OLZ:Polymer molar ratios of investigated systems

Polymer concentration (% m/w)	Polymer repeat units:OLZ dissolved (molar ratios)	
	PVP:OLZ	**HPC:OLZ**
2	97.90	146.36
0.2	42.19	20.28
0.02	6.27	2.16
0.002	0.70	0.23

The results showed that when PVP and HPC polymers were in solution at 0.02% w/v, there were approximately 6 and 2 polymer monomers of PVP and HPC for each dissolved OLZ molecule, whereas, at polymer concentration of 0.002% m/v the number of OLZ molecules dissolved were higher than the number of polymer monomers in solution. It can be therefore concluded that up to a polymer concentration of 0.02% (w/v), the amount of polymers is adequate to interact with the whole amount of dissolved OLZ, resulting in OLZ hydrate protection.

PEG polymers showed to be the most hydrophilic tested polymers. OLZ particles after being in contact for 180 min with these polymers displayed similar contact angles to the OLZ raw-material. This may result from the low ability of PEG to attach to the OLZ crystal surfaces and, therefore, the low ability to bind to surfaces of new nucleus of hydrates formed during stirring, leading us to conclude that the hydrophobicity of the polymers is an important factor to protect the drug from undergoing hydrate transformations.

5.7 Conclusion

This study provided an insight into the role of polymer additive on the crystallization of hydrates of OLZ in aqueous slurries. The results confirmed that polymers can affect crystallization by both hydrogen bonding with the drug and hydrophobicity. The secondary amine NH of OLZ has a relatively strong H-bond donor, which showed the highest potential for H-bonding with the oxygen atom of the polymers. The hydrogen bonding interaction between OLZ and polyethylene glycol showed to retard the hydrate conversion and to crystallize OLZ into only one hydrate form – higher hydrate. The insufficient hydrophobicity of PEG seems to explain the absence of hydrate protection by this polymer. PVP showed to have the ability to form hydrogen bonds with the drug and to increase OLZ solubility in aqueous phase but also sufficient hydrophobicity to adsorb into the crystals surface interface, blocking access to the solute molecules to the crystal terrace. Cellulose polymer, on the other hand, showed to slightly increase the solubility of OLZ, being its effect on the inhibition of OLZ hydrate formation mainly related to its strong hydrophobic nature.

The understanding of the interactions between OLZ and polymers, at a molecular level, helps to optimize the selection of excipients to be used in OLZ formulations, reducing problems during manufacturing of the final dosage form.

CHAPTER 6

Chapter 6 - Effect of RESS and RESSAS technologies on the particle size reduction, solid-state form and dissolution rate of olanzapine

6.1 Abstract

The purpose of the work was to understand the impact of rapid expansion of supercritical solution (RESS) and rapid expansion of supercritical solution into aqueous solution (RESSAS) processes on the particle size reduction, polymorphism and dissolution rate of olanzapine (OLZ) particles. A pilot scale unit for supercritical fluid processing was used for the production of RESS OLZ particles and RESSAS suspensions. Supercritical OLZ-solution (scCO$_2$, 20MPa/50°C) was expanded into air (RESS) or into an aqueous solution (HPMC, PEG, PEG+SLS, or Polysorbate 80, RESSAS). Nanoparticles and nanosuspensions were produced and characterized for particle size, particle size distribution and zetapotential. After freeze-drying nanosuspensions, nanoparticles were further evaluated for FTIR, in order to control the olanzapine polymorphic structure present in the nanoparticles. Their dissolution rate was also characterized. RESS OLZ could be produced with a mean particle size of 191.4±9.6nm, *i.e.*, a 200 fold size reduction compared to the original anhydrous material. The material was partially amorphous, as confirmed by DSC and FTIR. The particle size of RESSAS OLZ nanosuspensions was in the same range. The highest stability (size and solid-phase) of nanosuspensions before and after freeze-drying was achieved when PEG+SLS were considered. In conclusion, the preparation of OLZ nanoparticles with improved dissolution rate and known changes on the solid-state forms were achieved by RESS and RESSAS processes.

6.2 Introduction

Particle size reduction is one of the oldest strategies for improving dissolution rate of the APIs. As the particle size becomes smaller, the surface area to volume ratio increases, thus increasing the surface area available for solvation (87). In the traditional RESS process, the supercritical fluid is used as a crystallization solvent. In fact, the solute is firstly dissolved in the supercritical fluid and then rapidly expanded, by sudden depressurization through a nozzle to ambient pressure (235-236). Due to the sudden pressure drop upon expansion, a very high rate of supersaturation causes the precipitation of the dissolved material as submicron or micron particles (237). Like most techniques that lead to the production of fine particles, particle harvesting is difficult in the traditional RESS process. Since the precipitated particles travel at high speed after expansion, they are carried with the gaseous stream and therefore recovering is difficult. Many studies reporting the production of micron particles and low process yields may do so as a consequence of losing the fine fraction of submicron particles due to insufficient separation from the expansion jet (238). The typically reported micron-sized particles also result from particle growth processes of condensation and coagulation during the residence time in the expansion vessel, since theoretical modeling of the traditional RESS process predicts the formation of particles with initially less than 50 nm (239).

In the case of water insoluble drugs, a viable approach is therefore spraying the RESS product directly into an aqueous solution containing a stabilizing agent. This technique, also called RESSAS (rapid expansion of supercritical solution into aqueous solutions), enables to form nanosuspensions of active pharmaceutical ingredients (API) in a suitable stabilizing medium, which can contain polymers or surfactants as steric and electrostatic stabilizers (240) (241) (242, 243). If the particles suspended are partially or fully crystalline, they are referred as nanocrystals. The formulation of nanocrystals is an important tool to enhance the bioavailability after oral or parenteral administration of poorly water soluble drugs with high lipophilicity (244). The use of a liquid at the receiving end in RESSAS technology has been thought to inhibit particle agglomeration and coagulation in the expansion jet (238, 245). A challenge in this process is however the loss of stabilizing medium due to the force of expansion into the liquid, which complicates the use of excipients with surface activity that stabilize foams with the expanding CO_2. In this study, we therefore focused on using highly viscous media as stabilizers on the receiving end.

The administration of nanosized OLZ is interesting because it classifies as a BCS (Biopharmaceutical Classification System) class II drug with low aqueous solubility. In addition, OLZ shows pH dependent solubility since it is a weak base (pK_a = 7.4). For drugs with pH dependent solubility, a reduced variability of the fed-fasted bioavailability was observed in previous studies when formulated as nanosuspensions (246). Compared to classic bottom-up techniques for the formulation of nanoparticles, the risk of precipitating OLZ solvates is

eliminated in the RESS and RESSAS process, since no organic solvents are used (247, 248). The formulation of OLZ as an aqueous nanosuspension, and later freeze dried nanoparticles is however challenging regardless of the chosen method of production, since olanzapine may hydrate during the process. The choice of a stabilizer is therefore crucial to suppress recrystallization of the precipitated material, not only to prevent particle growth but also crystal conversion of the nanodispersed material.

6.3 Purpose

This chapter aims to study the effect of the unique expansion conditions provided by RESS and RESSAS on the size, solid-state form and dissolution of OLZ. For the RESSAS technology this study aims in particular, on finding the best stabilizer conditions to suppress recrystallization of the precipitated OLZ.

6.4 Materials and methods

Olanzapine was purchased from Vega Pharma (China), India. Polyethylenglycol (PEG) 40000 was supplied by Serva (Amstetten, Austria), polysorbate 80 (Psb) by Croda (Nettetal, Germany); hydroxypropylmethylcellulose (HPMC; Pharmacoat 615) by Syntapharm (Mülheim a.d. Ruhr, Germay); sodium lauryl sulphate (SLS; Texapon K12 G) was purchased from Cognis (Düsseldorf, Germany) and carbon dioxide (CO_2) from Air Liquide (Düsseldorf, Germany).

6.4.1 Pilot unit for supercritical fluid processing

A pilot unit designed for high-pressure extractions and RESS-technique (Sietec-Sieber, Zürich, Switzerland) was used for particle design (Figure 6.1). Carbon dioxide was used as solvent in all experiments. The equipment comprises a tank, where CO_2 is present in the liquid state. It is conveyed via a high-pressure pump into the extraction vessel with a volume of 5 l, at supercritical conditions. After dissolution of the material placed inside the extraction vessel is completed, or an equilibrium between solid and dissolved material is reached, the supercritical solution is passed through a micro valve, which regulates the flux through the 150 μm nozzle. Upon passage of the nozzle, the supercritical solution is expanded inside the expansion chamber. To compensate for the cooling effect inside the expansion chamber, the mantle temperature was set to 70 °C for RESS experiments and to 55 °C for RESSAS experiments. The pressure of the expansion chamber was kept at atmospheric conditions (1 bar and room temperature). All RESS and RESSAS experiments were conducted during 1 h of expansion time with a medium CO_2 flow rate between 1.5 and 3.5 kg/h.
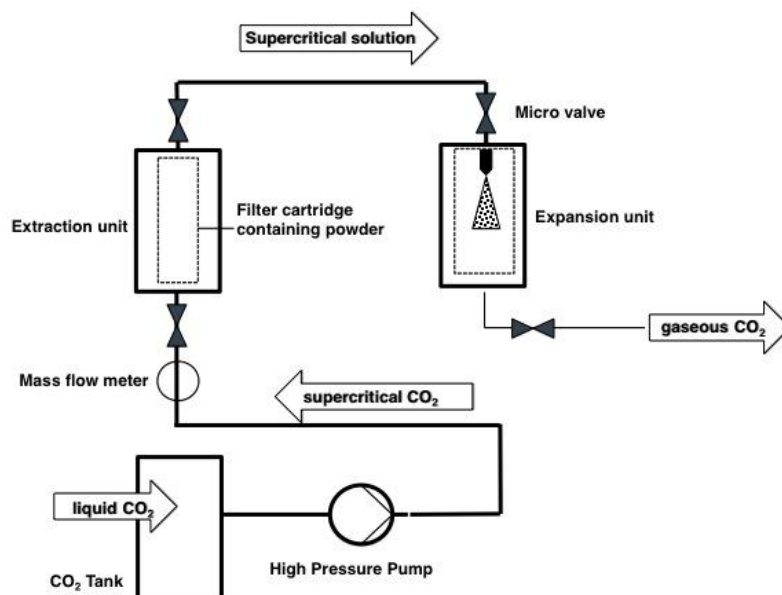
Figure 6.1 – Functional sketch of the extraction equipment.

6.4.2 Solubility of OLZ in supercritical carbon dioxide

An amount of 5.0 g of OLZ powder was weighed and placed inside the extraction chamber, which was consequently flooded with CO_2, heated to 50 °C and pressurized to 200 bar. The solution was left to equilibrate for 24 h prior to expansion. In that time span, 236 ± 13.1 mg of OLZ were dissolved in $scCO_2$, corresponding to a mole fraction of $y = 8.67*10^{-6}$.

6.4.3 Production of OLZ nanoparticles with the RESS process

For the collection of OLZ nanoparticles, a filter cartridge was attached to the lid of the expansion chamber, which contained paper filters for the collection of the nanoparticles (Figure 6.2 a). The nozzle in this setup was placed shortly under the lid of the expansion chamber. The expansion chamber was allowed to reach room temperature before collecting the product to prevent condensation of air moisture on the products.
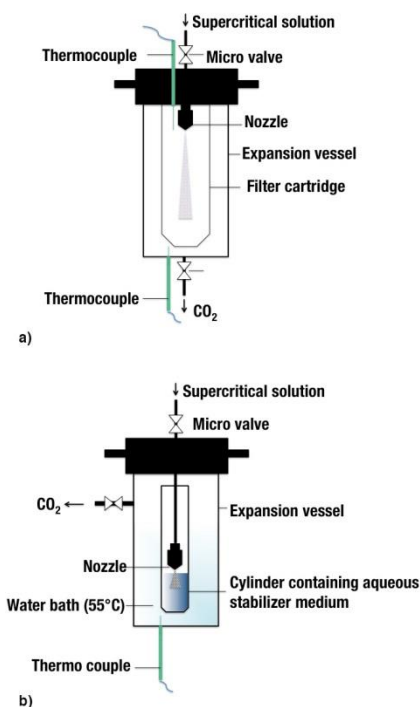
Figure 6.2 – Schematic of expansion setups for a) classic RESS process and b) RESSAS process.

6.4.4 Production of OLZ nanosuspensions with the RESSAS process

For the production of RESSAS nanosuspensions, a cylinder containing the aqueous stabilizer solution was placed inside the expansion chamber (Figure 6.2 b). The volume of stabilizer medium was 100 ml. The stabilizers were dissolved in phosphate buffer pH 7.4 in order to prevent a pH drift of the stabilizing medium due to dissolved CO_2 and consequent dissolution of OLZ nanoparticles in the medium. In cases when SLS was added as co-stabilizer, 3.3 ml of a stock solution of 10% w/w SLS were added to 30 ml of the freshly produced nanosuspension to yield a final concentration of 1% w/w SLS.

6.4.5 Freeze-drying

3 ml of the nanosuspensions were transferred to 10 ml glass vials and pre-frozen at -18 °C for 24 h prior to freeze-drying. The nanosuspensions were freeze-dried at -20 °C for 12 h, followed by a secondary drying phase of 12 h at 20 °C using a Lyovac GT2 freeze-dryer (Finn-Aqua/GEA Pharma Systems, Hildesheim, Germany). The freeze dried particles obtained were characterized by FTIR. For the characterization of the particle size distribution after freeze-drying, the cakes were reconstituted with demineralized water (3 ml).

6.4.6 Determination of drug content in freeze-dried nanosuspensions

The freeze-dried cakes were reconstituted with demineralized water and diluted 1:100 in 0.1N HCl to dissolve the drug present in the cakes. The solutions were analyzed

spectrophotometrically at 255 nm. It was ensured that at this dilution and the given wavelength, the stabilizing agents did not interfere with the OLZ absorption.

6.4.7 Measurement of particle size and zeta potential

The particle size, particle size distribution (PSD) and zeta potential of OLZ nanosuspensions were measured using a Zetasizer Nano (Malvern, Herrenberg, Germany) with dynamic light scattering (DLS) for a 1.709 refraction index. The samples were diluted 1:4 and equilibrated during 120 s at a cell temperature of 20 °C. Each sample was measured 3 times for the size and 5 times for the zeta potential and the average values are reported. The particle sizes of the unprocessed material and that of freeze-dried suspensions, where particle growth to the micron range was observed, were measured with laser diffractometry (LD) using a Mastersizer 2000 (Malvern, Herrenberg, Germany) equipped with a Hydro 2000S sample dispersion unit. The unprocessed powder was suspended in demineralized water containing 0.1% Polysorbate as surfactant to ensure a good dispersion of the hydrophobic OLZ particles in water. Freeze-dried suspensions were re-dispersed with demineralized water. Prior to the measurement cycles, ultrasound was applied to de-agglomerate the particles. 3 measurements were performed and the average values are reported.

6.4.8 Differential scanning calorimetry (DSC)

Measurements were performed using a DSC system (TA 8000, DSC 820, Mettler Toledo, Germany). The samples (1.5 – 2.0 mg) were placed in perforated 40 μl aluminum standard pans and crimped with punched lids. An empty aluminum sample pan was used as reference. The heating rate was set to 10 K/min to determine melting points (onset temperature, T_{on}) and the heat of fusion (ΔH).

6.4.9 Scanning electron microscopy (SEM)

The surface morphology and particle shape were examined using a scanning electron microscope (DSM 940 A, Zeiss, Oberkochen, Germany). Pictures were taken using the Orion 5 frame grabber system (E.L.I. Microscopy, Charleroi, Belgium). Each sample was fixed on double-sided adhesive tape and coated with gold with a sputter coater (E5100, BioRad, München, Germany). All samples were sputtered 4 times over 60 s at 2.1 kV and 20 mA.

6.4.10 Fourier Transform Infrared Spectroscopy (FTIR)

Measurements were performed using a Nicolet 380 FT-IR spectrometer in absorbance mode (Thermo scientific, Karlsruhe, Germany). A total of 30 scans was performed over a range of 4000-400 cm^{-1} at a scan speed of 0.5 cm/s. The second derivative of the FTIR spectra was calculated.

6.4.11 Determination of saturation solubility

An excess of OLZ powder (approximately 10 mg) was placed into 2 ml Eppendorf cups and 1 ml of the respective stabilizing medium was added. The cups were sealed and placed into a water bath at 37 °C shaking at 50 rpm. After 48 h, the Eppendorf cups were centrifuged at 13,400 rpm for 20 min. The concentrations of dissolved OLZ were determined with a UV microplate reader at 255 nm (Synergy HT, Biotek, Bad Friedrichshall, Germany).

6.4.12 Dissolution studies

Dissolution studies were conducted with a Pharmatest PT-DT 7 (Hainburg, Germany). A paddle apparatus (USP apparatus 2) at 37.0 °C was used. The freeze-dried cakes of OLZ RESSAS nanosuspensions were reconstituted with 3 ml of the dissolution medium and immediately added to the dissolution vessels containing 900 ml of phosphate buffer pH 6.8 providing concentrations between 8.0 and 11.3 µg/ml. These samples were compared with unprocessed OLZ and with OLZ in physical mixtures with PEG, HPMC and Psb. The rotation speed of the paddles was set to 50 rpm. Samples were drawn at preset time intervals and filtered through a 5 µm sintered filter. The removed sample volume was immediately replaced by fresh medium. The dissolution testing was carried out under sink conditions. The concentration of the samples was analyzed with a UV microplate reader at 255 nm (Synergy HT, Biotek, Bad Friedrichshall, Germany). Results between different release profiles were compared for significance using an independent mathematical approach model for calculating a similarity factor (f_2).

6.5 Results

6.5.1 Production of olanzapine nanoparticles with the RESS technique

Precipitation of OLZ from supercritical solutions resulted in the production of a very fine powder, which complicated the separation of the product from the expansion jet. Most particles were likely to be removed with the air stream in the outlet, resulting in a process yield below 10%. SEM images of the precipitated material showed that the particle size of RESS OLZ was distinctly below 500 nm (Figure 6.3).
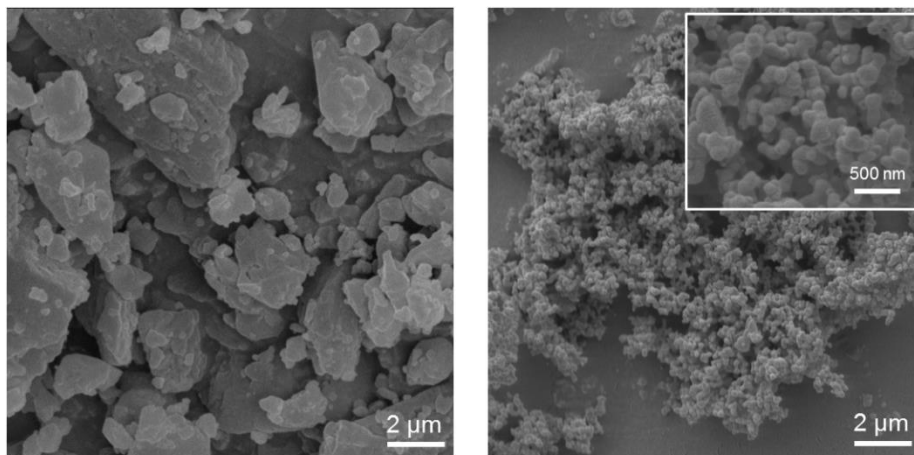
Figure 6.3 – SEM images of unprocessed (left) and RESS (right) OLZ.

The collected particles had a round shape with a mean diameter of roughly 200 nm and appeared partly agglomerated merged. The particle size measurement of RESS OLZ revealed that they had a D_{i50} of 191.4 ± 9.6 nm and a span of 1.08 ± 0.15 (Figure 6.4). The unprocessed OLZ powder had a D_{v50} of 39.3 ± 1.0 µm (Figure 6.4), showing that the size reduction via RESS was about 200 fold.
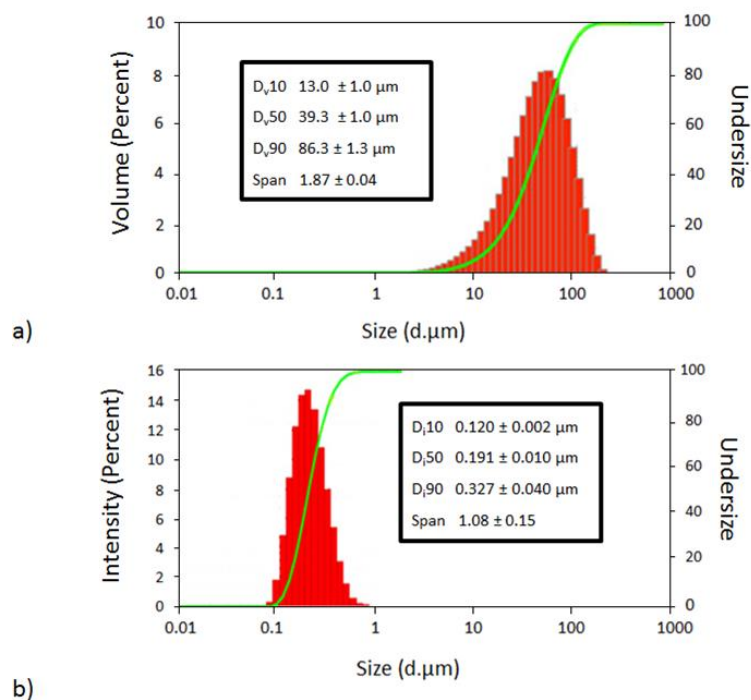
Figure 6.4 – Particle size distribution of a) RESS OLZ measured in aqueous suspension with DLS; b) unprocessed OLZ powder measured in aqueous suspension with laser diffractometry (LD).

DSC analysis indicated that RESS OLZ showed a distinct reduction of the heat of fusion from 135.0 ± 2.7 mJ/g to 102.2 ± 6.3 mJ/g (Figure 6.5), indicating a reduced crystallinity of RESS OLZ. The onset temperature of the melting peak of the RESS precipitated material showed a reduction from 194.3 ± 0.9 °C of the unprocessed material (OLZ anhydrous form I) to 190.7 ± 1.1 °C (Figure 6.5). Since this melting temperature does not belong to other polymorphic forms of OLZ, this depression maybe caused by the high ratio of surface area to volume for smaller OLZ particles.
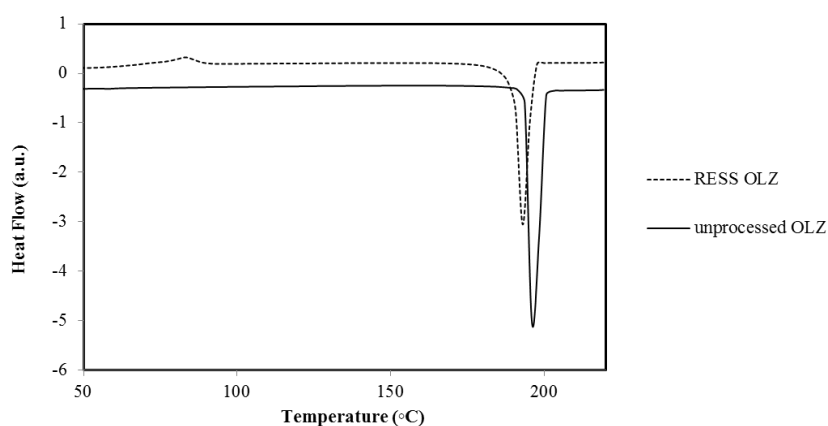
Figure 6.5 – DSC Thermograms of unprocessed OLZ (solid line) and RESS OLZ (dotted line).

To confirm that OLZ remained in anhydrous Form I, but with a reduced crystallinity, the second derivative of the FTIR spectra of the anhydrous form, the amorphous form and RESS OLZ were compared in the range of 900 cm^{-1} to 1100 cm^{-1} (Figure 6.6). The amorphous form showed an additional band at 998 cm^{-1}, which also appeared in the spectra of RESS OLZ. The band at 965 cm^{-1} in the amorphous form was distinctly broader than in the anhydrous form, which could also be observed in the spectra of RESS OLZ. In addition, the sharp peak of the anhydrous form at 927 cm^{-1} could also be found in spectra of RESS OLZ. This analysis confirmed that the material was indeed partially precipitated in the amorphous form.
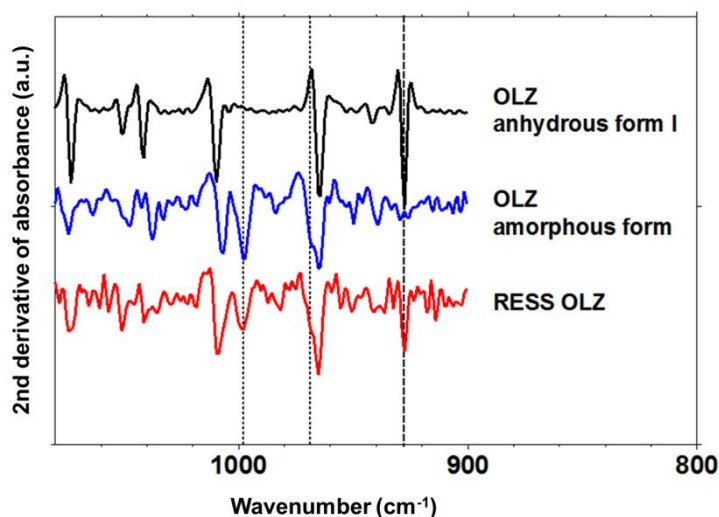
Figure 6.6 – Second derivative of FTIR spectra of anhydrous, amorphous and RESS OLZ.

6.5.2 Production of Olanzapine nanosuspensions with the RESSAS technique

Various stabilizing media were chosen after pre-studies concerning the saturation solubility of OLZ in the various stabilizing media, their viscosity and tendency to foam with the expanding CO_2. The optimized stabilizer concentrations are presented in Table 6.1. The solubility of the drug in the stabilizer plays an important role in the formulation of nanosuspensions, since an increased solubility can induce agglomeration and/or Ostwald ripening of the colloidal system (249). The stabilizer should thus have little effect on the solubility of the formulated drug. None of the tested stabilizers increased significantly the solubility of OLZ in comparison to the medium phosphate buffer pH 7.4. In combination with sodium lauryl sulfate (SLS), a distinct increase of the saturation solubility of OLZ was seen, especially for HPMC (1.62 ± 0.2 mg/ml).

Table 6.1 – Viscosity (η) of different stabilizing media and saturation solubility (S) of OLZ

Stabilizer	Stabilizer concentration (% w/w)	S (mg/ml)	S + 1% SLS (mg/ml)	η (cSt)	Foaming tendency [a]
Buffer pH 7.4	-	0.11 ± 0.06	1.82 ± 0.05	0.81 ± 0.001	-
Psb 80	0.1	0.10 ± 0.00	n.a.	0.72 ± 0.001	+
PEG	2	0.13 ± 0.01	0.8 ± 0.01	1.63 ± 0.001	-
HPMC	2	0.12 ± 0.01	1.62 ± 0.20	7.27 ± 0.005	+

All means reported are the means of 3 individual experiments
[a] Assessed by visual inspection
n.a.: not analyzed

The importance of the viscosity and the ability to stabilize foam for the precipitation of the nanoparticles into the stabilizing medium has been seen in preliminary studies (data not shown). Since OLZ has a rather low solubility in $scCO_2$, the ratio of dissolved drug to fluid is very low and thus, a high amount of fluid needs to be processed into the stabilizing medium for the collection of particles in reasonable number. A low viscosity on the one hand, and a good ability to stabilize foams on the other, can cause loss of the medium due to the force of expanding gas, which can carry the medium out of the collecting cylinder and destabilize the process. Of the tested stabilizers, Psb and HPMC presented distinct foaming abilities when $scCO_2$ was expanded into the solutions, whereas PEG did not show a high tendency to form foams (Table 6.2). The process conditions were therefore least subjected to variability when PEG was used (Table 6.2). The mean mass flow of CO_2 could be adjusted to 3.01 ± 0.34 kg/h, which was the highest possible in the conducted experiments. Therefore, the concentration of OLZ in nanosuspensions stabilized with PEG was also the highest with the smallest variation compared to the other tested stabilizers. With this stabilizer, it was also possible to recover almost 100 % of the drug that was dissolved in $scCO_2$ (Table 6.2), indicating no drug loss by the CO_2 stream.

Table 6.2 – Overview of RESSAS experiments

Stabilizer	Dissolved OLZ in $scCO_2$ (mg)	Mass flow of CO_2 (kg/h)	CO_2 density in extraction chamber (kg/m^3)	Temperature in expansion vessel (°C)	Volume of final suspension (ml)	c OLZ in final suspension (mg/ml)	Recovery of OLZ (% w/w)[a]
Psb 80 0.1%	221	1.55 ± 0.54	904.8 ± 19.5	40.5 ± 2.3	30 ± 11	3.3 ± 1.4	44.8
PEG 2%	237.5	3.01 ± 0.34	877.8 ± 3.5	39.2 ± 2.2	70 ± 5	3.4 ± 0.4	98.4
HPMC 2%	245.1	2.59 ± 0.77	886.1 ± 11.91	41.9 ± 2.2	45 ± 10	2.4 ± 1.3	44.1

[a] Recovery of OLZ in nanosuspensions in relation to the dissolved mass in scCO2.
All means reported are means of 3 individual RESSAS experiments. There is no standard deviation given for the dissolved mass of OLZ, since this value was calculated from the dissolved mass in the extraction chamber after 3 individual expansions.

6.5.2.1 <u>Particle size</u>

The smallest particle size of the colloidal OLZ suspensions after production was achieved with Psb as stabilizing agent giving a D_{i50} value of 158.7 ± 12.7 nm and a narrow size distribution (span = 1.15 ± 0.12; Figure 6.7). The largest particles were obtained with HPMC, which had a D_{i50} of 341.3 ± 42 nm and a broader size distribution with a span of 1.48 ± 0.37 (Figure 6.7). The particle size of PEG stabilized nanosuspensions was between that of Psb 80 and HPMC with a D_{i50} of 213.8 ± 23.7 nm and a narrow span of 0.99 ± 0.08 (Figure 6.7).
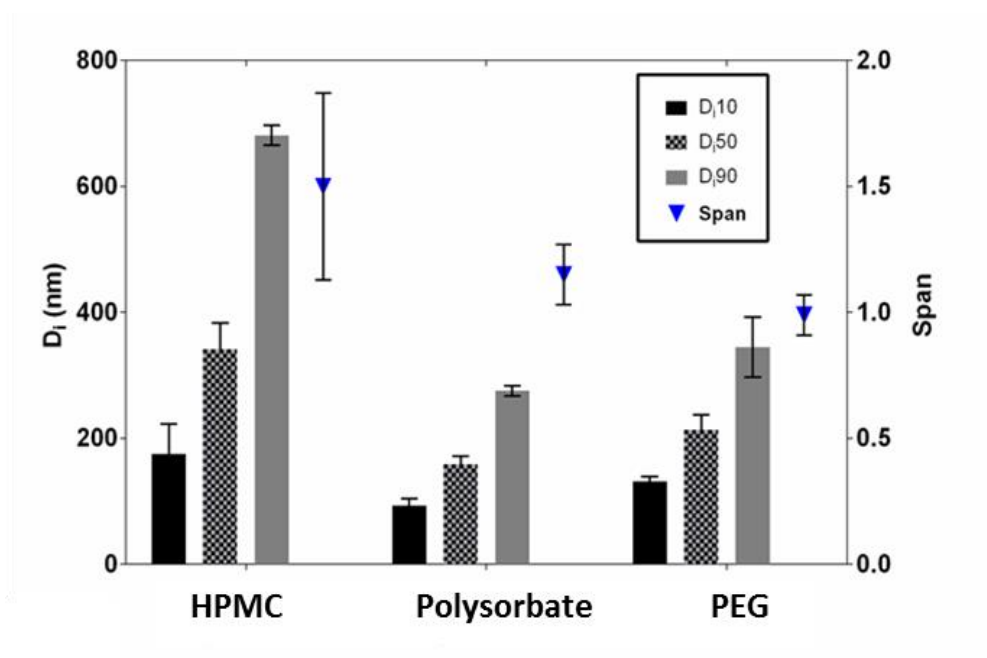
Figure 6.7 – Medium D_i values and spans of nanosuspensions produced with different stabilizing agents directly after production.

The Psb 80 and PEG suspensions only remained macroscopically stable for a few hours after production. After 12h at room humidity and temperature it was possible to observe flocculation of the nanosuspensions and the flocculated material was observed under FTIR (Figure 6.8). This recovered material showed to correspond to the dihydrate B form of OLZ. Therefore, freeze drying of the nanosuspensions was performed immediately after their production to avoid particle growth.
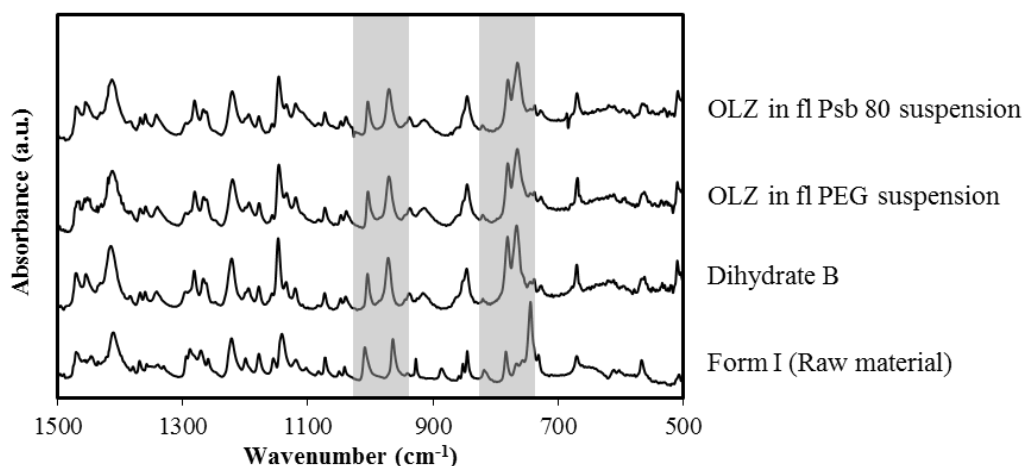
Figure 6.8 – Infrared spectra of Flocculated material recovered from the Pbs 80 and PEG suspension after resting 8h at room temperature.

After freeze-drying and reconstitution of the nanosuspensions however, the particle size was distinctly increased to the micron range (D_{v50} of 8.5 ± 0.9 µm for PEG and 15.1 ± 2.6 µm

for Psb; Figure 6.9). For both stabilizers, the size distribution range was also distinctly increased after freeze-drying, showing particle growth during freezing. For HPMC, only a slight particle growth was detected ($324.2.5 \pm 8.7$ nm before freeze-drying vs. 341.3 ± 42 nm after freeze-drying; Figure 6.9). This shows that steric stabilization with Psb and PEG was not sufficient for the formulated drug. For HPMC only a slight increase of the particle size was observed.

6.5.3 Effect of electrostatic co-stabilization with SLS

Since the steric stabilization achieved with the polymeric agents employed in this study was not entirely effective for the colloidal suspensions, it was attempted to add sodium lauryl sulfate (SLS) as an electrostatic co-stabilizer after the actual precipitation process. The co-stabilizer was added after the actual production of the particles and before freeze-drying, since it distinctly increased the foam formation of the media, destabilizing the process and resulting in increased loss of the stabilizer medium. At a concentration of 1 % w/w of SLS, the solubility of OLZ was increased to 0.8 ± 0.01 mg/ml in combination with PEG, and to 1.62 ± 0.2 mg/ml in combination with HPMC (Table 6.2). The increase of solubility due to surfactants is a known problem and can cause Ostwald ripening and agglomeration of the particles in suspension (250). Therefore, the attempt seemed only feasible for PEG stabilized suspensions, considering the drug load of approximately 3 mg/ml in the RESS suspensions. With the addition of 1% SLS, it was possible to suppress the drastic particle growth observed in suspensions that were only stabilized by PEG (Figure 6.9). With SLS, only a slight increase of the particle size was observed after freeze-drying and reconstitution. The addition of 1% SLS decreased the zeta potential of the suspensions from -1.58 mV to about -33 mV, which reflects the physical stability of the co-stabilized suspensions (Figure 6.9).
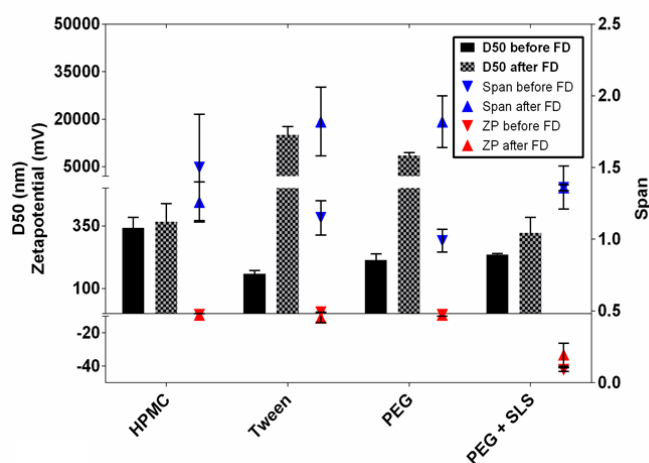
Figure 6.9 – Comparison of D_{50} values and spans immediately after production and after freeze drying; D_{50} values reported for HPMC and PEG+SLS are medium Di50; values reported for Psb and PEG are medium Dv50.

6.5.4 Solid-state characterization

Solid-state characterization of OLZ was performed via FTIR by analyzing the freeze-dried cakes of the nanosuspensions. With the second derivative of the FTIR spectra, it was possible to enhance the resolution of overlapping and complex band contours in the original spectra. A range of the spectrum (950 - 1050 cm^{-1}) was chosen, where the stabilizers did not interfere with the OLZ spectra (Figure 6.10). Hydration to the dihydrate B became apparent from two peak shifts of the anhydrous from at 965 $^{-1}$ and 1009.6 cm^{-1} to 1003.8 cm^{-1} and 971 cm^{-1}, respectively. OLZ filtered from the flocculated nanosuspensions with PEG and polysorbate 80 was completely transformed in the dihydrate B (Figure 6.10). After freeze-drying, the hydrated form was maintained by OLZ in PEG suspensions, while in Polysorbate 80 suspensions was dehydrated during the drying process so that the solid remnant again contained the anhydrous Form I.

Judging by the appearance of double bands in OLZ spectra of freeze dried HPMC nanosuspensions the drug was probably partially hydrated (Figure 6.10). OLZ in freeze-dried nanosuspensions stabilized with PEG and SLS showed no trace of hydrate formation. This combination of stabilizers could thus effectively suppress both particle growth of the colloidal system and hydrate formation. This also became apparent macroscopically, since the RESS OLZ suspensions only stabilized with PEG lost the yellow color and transparency after freeze-drying and reconstitution, while suspensions stabilized with PEG and SLS showed no macroscopic change after freeze-drying and reconstitution compared to the freshly prepared samples (Figure 6.11). Particle growth and hydrate formation coincided in the insufficiently stabilized nanosuspensions.
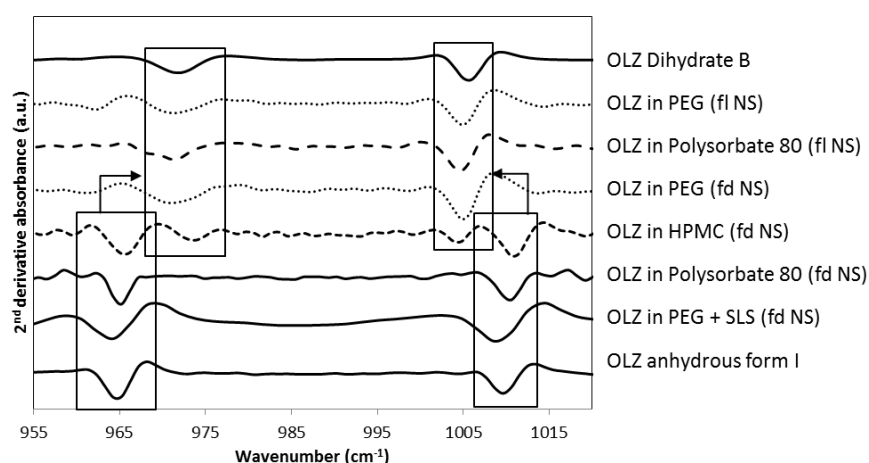
Figure 6.10 – Second derivative of FTIR spectra of Freeze-dried olanzapine (OLZ) in flocculated nanosuspensions (fl NS) or freeze-dried nanosuspensions (fd NS) with different stabilizing agents.
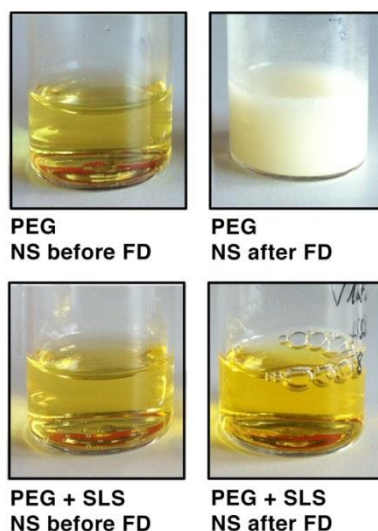
Figure 6.11 – Comparison of nanosuspensions (NS) before and after freeze-drying (FD) with and without the addition of SLS.

6.5.5 In vitro drug dissolution

All RESSAS OLZ suspensions were found to show a strongly increased dissolution rate when compared to the unprocessed OLZ, regardless of the drastic particle growth observed in Psb and PEG stabilized suspensions (Figure 6.11, Figure 6.12). Only for HPMC suspensions, a slower release than for the other ones was observed, which is probably related to the increased viscosity of these suspensions in comparison to the other stabilizing media (Table 6.2). Since the stabilizing agents all possess more or less pronounced surface activity, their influence on the dissolution of raw OLZ was also investigated (Figure 6.12 b-d). The release of the unprocessed drug suspended in the stabilizing media was highly accelerated in comparison to the unprocessed powder, which shows that the effect of these agents on the solubility of OLZ cannot be underestimated. The effect of the size reduction was, however, still apparent in all RESSAS suspensions, with HPMC showing the highest differentiation between the release profiles of RESSAS suspensions and suspensions of the unprocessed drug in the stabilizing medium (Figure 6.12 c). Significant improvements on the release rates between OLZ RESSAS and OLZ in physical mixtures were observed, reaching the maximum significance with unprocessed OLZ.
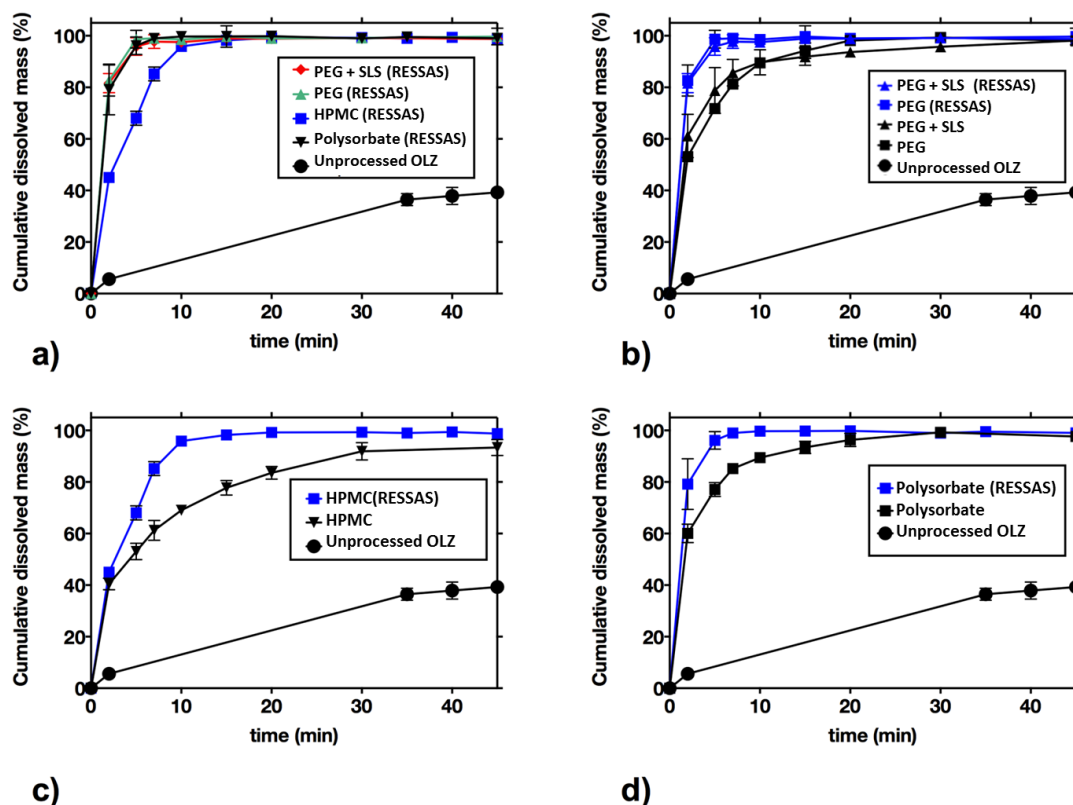
Figure 6.12 – Dissolution profiles in phosphate buffer pH 6.8, USP apparatus II (Paddle). Dissolution profile of RESSAS OLZ suspended in different stabilizers is compared to the dissolution profile of unprocessed OLZ.

6.6 Discussion

6.6.1 Production of RESS OLZ nanoparticles

OLZ nanoparticles were produced by RESS technique. Polymorphic conversion during the RESS process has been shown before and is related to the processing conditions such as extraction and expansion pressure and temperature (251-253). In the present study, the original material was apparently not subjected to polymorphic conversion, since the RESS product was found to be the thermodynamically stable OLZ Form I. There are few reports about supercritical fluid processing of OLZ in the literature. However, US patent US20070021605 reports a RESS process for the production of OLZ Form II (metastable OLZ form) (254). Therein, a low temperature range of 30 - 50 °C at the time of depressurizing the fluid have to be used, in order to prevent conversion to OLZ Form I (the most stable form), which is obtained when higher temperatures are used. The results from this work were not in accordance with those from the procedure described therein, once our experiments yielded OLZ Form I nanoparticles, which were apparently not entirely crystalline. The particle morphology studied by SEM and DSC analysis suggested the formation of an amorphous layer on the nanoparticles. Due to the very

fast nucleation period and the rapid crystallization in RESS, the formation of an at least partially amorphous phase seems likely and has been shown before (255). In most RESS experiments, however, the formation of mostly crystalline material with particle sizes in the micron range has been reported, which can be ascribed to the initially colloidal (and possibly amorphous) material undergoing immediate recrystallization and particle growth during the residence time in the expansion vessel (245, 256). This is also in agreement with the Ostwald law of stages, which describes the conversion of initially crystallized metastable forms to more stable forms (257). Many researchers report a reduction in the PXRD peak intensities of RESS precipitated material in comparison to the unprocessed bulk powder, which is however an effect that could be related to the decreased particle size of RESS products and is therefore inconclusive for judging a possible reduction of crystallinity (251, 252, 258-262). Our results, however, confirm the formation of a partially amorphous product.

Compared to usual bottom-up techniques such as liquid antisolvent precipitation, with the RESS process, there is no risk of precipitating a solvate or hydrate during the manufacturing process, since scCO$_2$ returns to the gaseous state after expansion, resulting in a solvent residue free product. Solvent removal in established bottom-up techniques is critical, since solvent residues can cause crystal growth, physical or chemical instabilities of the formulation, and increase the potential toxicity of the formulation (249). Furthermore, no thermal or mechanical stresses are induced during RESS, which can cause degradation of the drug or crystal defects (249).

6.6.2 Characterization of OLZ nanosuspensions and freeze-dried nanoparticles

The RESSAS process for the production of nanosuspensions is comparable to bottom-up techniques such as liquid antisolvent precipitation. A fast adsorption process and slow desorption of the stabilizer molecules onto the freshly created drug surface are therefore crucial to ensure fast and complete surface coverage of the precipitated nanoparticles and therefore a well stabilized system. PEG and polysorbate suspensions remained macroscopically stable for a couple of hours after the production process showing reduced mean D$_i$ values immediately after production, in comparison with the particles suspended in HPMC solution which showed an increased size (Figure 6.7). However, leaving the PEG nanosuspensions to rest at 20°C/ 65% RH for several hours, the transparent PEG and polysorbate suspensions started to turn cloudy and flocculation became visible. The same was reported for nanosuspensions produced with RESSAS, which were stabilized by PEG and PVP (258). The authors suggested that the RESSAS process can be divided into two related processes, the first being the actual precipitation step and the suppression of particle growth by the receiving medium and the second step being the stabilization of the particles. Our results suggest that such a division is at least partly reasonable, considering that the addition of SLS to PEG suspensions after the actual

precipitation process still results in the desired effect of preserving the colloidal particle size (no precipitation was visible). It is however likely to assume that by the time the co-stabilizer is added, the system is already undergoing a certain degree of agglomeration, since the co-stabilizer is not present at the actual precipitation process to immediately reduce the interfacial tension by covering the freshly created surface (257). The larger nanoparticles and broader PSD obtained with HPMC, compared with Psb and PEG, where the particle size and PSD were in the range of the material precipitated in the classic RESS process, clearly demonstrates the influence of stabilizer on the primary particle formation (Figure 6.4and Figure 6.7).

Regarding the stabilizers used, although the HPMC stabilizer showed to create nanosuspensions with particles larger than the ones obtained with Psb and PEG (immediately after the RESSAS process, Figure 6.7), the freeze-drying of the nanosuspensions and subsequent reconstitution of the cakes, showed just a slight particle size growth. These results showed that both the stabilizer used (HPMC) and the freeze-drying process applied to dry the nanosuspension did not lead to agglomeration or precipitation macroscopically visible (Figure 6.9). HPMC therefore seems to at least detain the particle growth of the nanoparticles, which could additionally be attributed to the higher viscosity of HPMC suspensions compared to PEG and Psb, thus reducing the diffusivity of the drug particles in suspension (Table 6.2).

A drastic particle growth was observed in PEG suspensions after freeze-drying. One of the main challenges in nanosuspension technology is prevention of particle agglomeration or aggregation and crystal growth (263). At the nanometer scale, attractive van der Waals and dispersive forces between particles come into play. These attractive forces increase dramatically as particles approach each other, which ultimately results in irreversible aggregation (264, 265). The success for the drug nanoparticle technology is the compensation of the extra free energy of freshly exposed surfaces (266). The tendency of the smaller particles in a suspension to dissolve and re-crystallize on the larger particles represents a mode of instability, termed Ostwald ripening. In general, the speed of Ostwald ripening is governed by molecular diffusion or surface reaction. Irrespective of the mechanism, particle growth can be prevented or at least minimized by steric hindrance and/or electrostatic repulsion. Therefore, addition of hydrophobic polymers during the preparation of nanosuspensions have shown to adsorb on hydrophobic surfaces of insoluble nanoparticles providing steric stabilization effect (266, 267) The lower hydrophobicity of PEG in relation to HPMC, decreases the likehood of interactions of PEG with OLZ crystal surface, leading to insufficient stabilization of the this polymer. Furthermore, the amount of polymeric excipient not only determines its adsorption onto the drug substance particles, but also contributes to the viscosity of the suspension medium, thereby increasing the diffusion barrier for particle-particle interaction (268). HPMC showed to strongly increased the viscosity of the medium, thus constraining the diffusivity of the drug molecules. It therefore seems plausible that the protective effect of HPMC is more pronounced than that of PEG.

The recrystallization of the drug and the hydrate formation in suspensions with mere steric stabilization also explain why no amorphous trace of the material could be detected after freeze-drying, even though the existence of amorphous material was confirmed for OLZ that was precipitated in the classic RESS process. It is likely that the partially amorphous material that is originally precipitated during RESS dissolved in the aqueous suspension medium due to its enhanced solubility, thus accelerating the supersaturation and recrystallization of the dihydrate B that was detected in the freeze-dried cakes of the OLZ RESSAS nanosuspensions (Figure 6.8). For PEG nanosuspensions that were co-stabilized with SLS, neither particle growth nor crystal conversion to the Dihydrate B was observed. This indicates that particle growth and hydrate formation of OLZ coincide in the insufficiently stabilized colloidal suspensions. Since the suppression of particle growth and hydrate formation are both mechanistically related to a surface interaction of the drug with the excipient in suspension, it seems likely to assume that these processes are also related.

Polysorbate 80, on the other hand, as a non-polymeric small molecule prevented neither particle growth nor hydrate formation. OLZ in Psb nanosuspensions showed to hydrate which is easily explained by the classic nucleation theory, which refers that crystal nucleation increases with decreasing interfacial tension by the inclusion of surfactants like Psb 80 in the medium. After freeze-drying, OLZ showed to be anhydrous which may be due to the very low Psb concentration used, which was not able to prevent the dehydration phenomenon during the secondary drying of the freeze-drying process. Therefore, the most stable anhydrous Form I was always obtained in the final dried cake.

6.7 Conclusion

In this study, rapid expansion of supercritical solutions (RESS) and rapid expansion of supercritical solutions into aqueous solutions (RESSAS) was successfully employed for the production of nanoparticles and nanosuspensions of OLZ, a poorly soluble BCS class II compound. With RESSAS, OLZ nanosuspensions with an increased dissolution rate could be produced. As anticipated it was paramount to find a compromise between process operability and formulation stability when using RESSAS as a tool for the production of nanosuspension. This study showed that the choice of stabilizer has a critical influence on both the stability of nanosuspensions, particle size distribution and the expansion process itself. Polymeric stabilizers showed to be better choice from a processing standpoint, but steric repulsion is often not a sufficient stabilizing mechanism for nanosuspensions. On the other hand, it could be shown that retroactive electrostatic stabilization (e.g. SLS) will still lead to preservation of the nanosized particles. Consequently, the work shows that the combination of PEG with SLS provides the best stabilization system to OLZ. Both the suppression of particle growth and

hydrate formation showed to be mechanistically related to a surface interaction of the drug with the excipient used in suspension, being those processes related

The beneficial features of the RESSAS process lie on the mild process conditions and the absence of organic solvents, but especially on its ability to produce particles with small sizes and narrow particle size distributions. It was concluded that RESSAS process may present a superior alternative to other bottom up techniques for the production of pharmaceutical nanosuspensions.

CHAPTER 7

Part of the work presented in this chapter has been published in:

Paisana M, Wahl MA, Pinto JF. Olanzapine solid-state transformations throughout the process of extrusion-spheronisation. 6th International Granulation Workshop, Sheffield. 2013; (proceedings paper)

Chapter 7 - Impact of extrusion process on the physical properties of olanzapine and pellets

7.1 Abstract

A fine control should be considered when APIs are exposed to either hydrating or dehydrating conditions during pharmaceutical processing. This may lead to the detection of polymorphic changes during processing, which may have an impact on the APIs solubility and bioavailability. This study focused on the ability of anhydrous olanzapine (OLZ) to hydrate during the manufacture of pellets by extrusion and spheronisation and the impact of hydrated OLZ on the pellets' characteristics. Extrudates were made of OLZ (0, 15, 30% w/w), microcrystalline cellulose (MCC, 90, 75, 60% w/w), polyethylene glycol 6000 (PEG 6000, 10% w/w) and water (75% w/w) in a ram extruder (200 mm/min) prior to spheronisation (5 min, radial plate). Half of the wet mass was extruded immediately, whereas the remainder was stored in a hermetic container for 6 hours prior to extrusion. A placebo formulation was manufactured with calcium phosphate replacing olanzapine. Pellets were dried in a fluid bed drier (45 °C, for 30, 60, 90, 180 min). XRPD and FTIR analyses were performed to detect and characterize different solid phases of OLZ in all manufacturing steps. Physical characteristics (size, crushing stress and moisture) of the pellets were also evaluated. The results showed that OLZ was able to hydrate in a mixture of 2 hydrates (dihydrate B and a higher hydrate) when the wet mass was left to equilibrate for 6 h. Drying of pellets for 60 min was sufficient to remove the higher hydrate but not sufficient to remove the dihydrate B. The presence of the dihydrate B showed to have a negative impact on OLZ's dissolution. Furthermore, the hydration of OLZ during resting of the wet mass was able to affect the force required for extrusion, the pellets' sizes, the mechanical strength and residual moisture after drying. Overall, the study enhanced the need to have highly controlled processes to minimize anhydrate-hydrate conversions of OLZ.

7.2 Introduction

Several particles' agglomeration processes are well known, namely wet granulation, which encompasses a variety of different steps, such as wetting, mechanical stressing and sieving which may promote crystalline changes of a drug. The solid state transformations that are more likely to occur during this process are solvent-mediated transformations to a more stable polymorphic form or the formation of solvated forms (typically a hydrate). However, the kinetics of such transformations, together with the drug loading in the dosage form, the quantity of liquid used for granulation and the time of exposure of the solid to the liquid determine whether or not the changes will occur or be completed during the wet granulation process (83). The hydrated forms can dehydrate throughout the subsequent process of drying, depending on the drying conditions (e.g. water vapor, temperature, or mechanical stress) and the dehydration mechanisms of the crystal. The dehydration process may result in the formation of an amorphous form, a lower hydrate, a stable or metastable anhydrous form or even a mixture of different forms (105, 210). When an Active Pharmaceutical Ingredient (API) has multiple anhydrous or hydrated forms, the control over the final solid-form can become even more complex (85). Extrusion and spheronisation of wet masses also involves the wetting and drying steps of the materials, together with mechanical stresses, which are all likely to promote solid-state modifications of an API. Furthermore, the amount of wetting liquid used in this process is relatively high when compared to other processes, namely fluidized bed granulation. Therefore, APIs which will be included in pellets manufactured by extrusion of wet masses are more prone to undergo structural transformations than APIs manufactured otherwise (111).

Olanzapine (OLZ) is practically insoluble in water and has only 60% oral bioavailability. Based upon individual patient characteristics, dosage adjustments may be required (269). The need for long term therapy of OLZ (270), can turn small variations of OLZ's solubility (due to molecular structural transformations, for instance) into significant changes on the dissolution rates from pellets, thus affecting OLZ bioavailability. The latter can generate high instability on patient behavior and quality of life.

7.3 Purpose

This section aims to study the manufacture of pellets with OLZ form I (the most stable anhydrous form) and to evaluate its solid-state modifications during all of the process of extrusion/spheronisation, mainly the wetting and drying steps, which are the most critical ones. The influence of crystalline changes of OLZ on the physical characteristics of the pellets and on OLZ performance when dissolved into an appropriate aqueous environment is investigated in this chapter.

7.4 Materials and Methods

7.4.1 API and excipients

Olanzapine Form I (OLZ FI, Pharmorgana, India), microcrystalline cellulose (MCC, Avicel 101, FMC corporation, USA), polyethylene glycol 6000 (PEG, Sigma-Aldrich, Germany) and tricalcium phosphate (CP, Sigma-Aldrich, Germany) were used for pellets manufacture. MCC and PEG-6000 were chosen due to their common application on the production of solid dosage forms (271-273) and on the grounds of the poor crystallinity shown, thus their X-ray powder diffraction profiles allowed the visualization of OLZ solid-state transformations throughout processing. Freshly demineralized water was used as a solvent.

7.4.2 Manufacture of pellets

The different raw materials (50 g) were dry-mixed in a planetary mixer (Kenwood, Hampshire, UK) for 10 min (Table 7.1, formulations A-D) prior to the addition of water and mixing for another 10 min (wet massing). Half of the wet mass was extruded immediately (1) whereas the other half was allowed to rest for 6 h (2) in a hermetically closed polyethylene bag before extrusion. During the resting period, it is expected that the water is better spread over the components, becoming more plastic (274). The extrudates were manufactured in a ram extruder (Lurga, Sacavém, Portugal) adjusted to a universal testing machine (LR 50K, Lloyds Instruments, Leicester, UK) fitted with a load cell to allow the collection of data for the applied force to the ram and its displacement (200 mm/min). The wet mass was forced to pass through a die (L/D=6) and the extrudates placed immediately after extrusion in a spheroniser (Caleva, radial friction plate rotating at 500 rpm) for 5 min. The wet pellets were dried in a fluid bed drier (Aeromatic-Fielder AG, Switzerland) at 45 $^{\circ}$C and samples were collected after 30, 60, 90 and 180 min of drying.

Pellets were characterized for size and size distribution (sieving, Retsch, Haan, Germany) and the fraction of pellets between 1.00 and 1.40 mm was considered for physical and dissolution studies. The mechanical resistance of pellets for each formulation (A-D dried for 30, 60, 90 and 180 min) was assessed by crushing them between two parallel flat plates approaching at a constant speed of 0.5 mm/s (n=20, Texture Analyser, XT Plus, Stable Microsystems, Godalming, UK).The residual water content in the pellets after drying was found by determination of the water loss on drying using an infrared moisture analyzer (n=6, Sartorius Moisture Analyzer, Germany).

Table 7.1 – Design of extrusion formulations

Formulation	OLZ:MCC (w/w)	PEG-6000 (w/w)	CP (w/w)	Water level (w/w dry powders)	Resting time of the mass (h)
A1	0:60	10	30	75	0
A2	0:60	10	30	75	6
B1	0:90	10	0	75	0
B2	0:90	10	0	75	6
C1	15:75	10	0	75	0
C2	15:75	10	0	75	6
D1	30:60	10	0	75	0
D2	30:60	10	0	75	6
E1	100:0	0	0	75	0
E2	100:0	0	0	75	6

7.4.3 Preparation of a wet mass without addition of excipients

The preparation of a wet mass which only contains the API (Table 7.1, formulation E) was performed in a smaller scale: water (7.5 g) was added to OLZ (1 g) and the wet massing of OLZ was carried out in a mortar with a pestle prior to storage in a sealed vial. After 6 h the wet OLZ was analyzed by X-ray powder diffraction (XRPD), Fourier transform infrared spectroscopy (FTIR) and hot stage microscopy (HSM). For the contact angle measurements and scanning electron microscopy (SEM), the wet mass of OLZ was filtered and dried at 45 ºC for 15 min and 180 min. No extrusion was performed for this formulation.

7.4.4 Characterization of the wet masses, wet pellets and dried pellets

Crystalline changes of OLZ over wetting, extrusion, spheronisation and drying, and the impact of excipients on the changes were monitored by X-ray powder diffraction (XRPD) and Fourier transform infrared spectroscopy (FTIR) complemented by hot plate microscopy (HSM) and dissolution studies.

X-ray powder diffraction (XRPD)

The XRPD was performed in equipment 1 (described in chapter 2). The X-ray powder diffractograms were recorded at room temperature by a diffractometer with automatic data acquisition software using a Cu Kα radiation source. The tube amperage was 30 mA and the tube voltage 40 kV. For the characterization of the OLZ crystalline structures in each process stage the XRPD patterns were compared with the XRPD pattern of crystalline structures of

anhydrous OLZ FormI, dihydrate B and higher hydrate obtained from the Cambridge Structural Database and visualized using the Mercury 1.4.2 software (Cambridge Crystalographic Data Centre, Cambridge, UK) (18).

FT-IR Spectroscopy (FTIR)

The wet masses and pellets were analyzed by FT-IR Spectroscopy (IR Affinity-1 Shimadzu spectrophotometer, Japan). Each sample was mixed with KBr at a concentration of 0.5 w/w. The mixtures (200 mg) were compressed into a tablet of 10 mm diameter. The second-derivative of the absorbance spectra was applied to improve the visualization of the specific bands of the different OLZ forms.

Hot stage microscopy (HSM)

HSM was used to provide a visual insight on hydrate to anhydrate OLZ transformation crystals obtained from the formulation E2. The dehydration of the crystals obtained from this wet mass were monitored under a microscope with polarized light (Olympus BX51, JP) fitted with a heating stage plate (Linkam THMS350V, UK). The sample was heated up to 45 °C at a rate of 20 °C/min and was kept at this temperature for 150 min.

Particle size distribution (PSD)

The PSD of the unprocessed/processed material were measured with laser diffractometry (LD) using a Mastersizer 2000 (Malvern, Herrenberg, Germany) equipped with a Hydro 2000S sample dispersion unit. The OLZ powder was suspended in demineralized water containing 0.1% Polysorbate as surfactant to ensure a good dispersion of the hydrophobic OLZ particles in water.

7.4.5 Dissolution testing

Dissolution studies were performed for pellets dried for 60 min and 180 min. The dissolution media was a phosphate buffer (pH= 6.8), used to mimic the pH of the intestinal fluid. The pellets were placed in each dissolution vessel in order to have 5 mg of OLZ per vessel. The amount of water present in the pellets was considered (Sartorius Moisture Analyzer, Germany), since pellets extruded immediately and pellets extruded 6 h after the wet massing retained different fractions of water. OLZ was quantified by UV spectrometry (λ= 254 nm, Hitachi U- 2000, Japan) and a comparison of dissolution profiles was possible by application of the similarity factor f2.

7.4.6 Statistical analysis

Results of the extrusion force and the fraction of pellets in the 1.00-1.40 mm range were considered and analysed by ANOVA (SPSS v.17, USA). This test was applied to explore

significant differences between the force values needed to extrudate the wet masses and the size of the pellets when the wet mass was left to equilibrate for 0 h or 6 h.

7.5 Results

7.5.1 Wet massing step

In order to study the crystal modification of OLZ during the extrusion process, the XRPD diffractograms of the OLZ formulations after different steps of extrusion process were plotted together with the reference XRPD patterns of OLZ for a better comparison. Reference XRPD patterns for 3 crystalline forms of OLZ (anhydrous OLZ F I, OLZ dihydrate B and OLZ higher hytdrate) are shown in Figure 7.1 (a, b and c). Figure 7.1 a) shows the raw materials used for the pellets production. The XRPD patterns of wet mass C1 revealed that OLZ presents the characteristic peaks of OLZ F I (Figure 7.1 b). However, wet mass D1 presented distinct XRPD reflections for anhydrous OLZ FI and OLZ dihydrate B (grey bar, Figure 7.1 2b), indicating that in a formulation with a higher OLZ/MCC ratio, the hydration of OLZ could not be prevented during the wet massing. Although for formulation C1 no hydrate conversion has occurred in the time scale of the wet massing, the presence of OLZ hydrates in wet masses C2 revealed that hydration of OLZ is dependent on the time that the drug is in contact with water. Figure 7.1 c) shows that the diffraction pattern of OLZ in wet masses C2, D2 and E2 no longer had traces of OLZ F I. In these wet masses, the diffraction patterns showed characteristic peaks of 2 different hydrates of OLZ - OLZ higher hydrate and OLZ dihydrate B.

In order to understand the impact of using different ratios of OLZ:MCC on the rate of OLZ hydration, infrared analyzes were performed for wet masses C and D at different time periods (Figure 7.2). The second derivate of absorbance in the 958-980 cm^{-1} region allowed the observation of anhydrate to hydrate conversion of OLZ in wet masses during 6 h. The anhydrous OLZ band at 965 cm^{-1}, related to the deformation of the piperazinyl group coupled to the azepine and thiophene moieties (138), reduced its intensity and shifted to higher wavenumbers when hydration occurred. Formulation C (15 OLZ: 75 MCC) showed a slower reduction of the intensity of this band due to slower hydrate formation in this wet mass.

a)

b)

c)
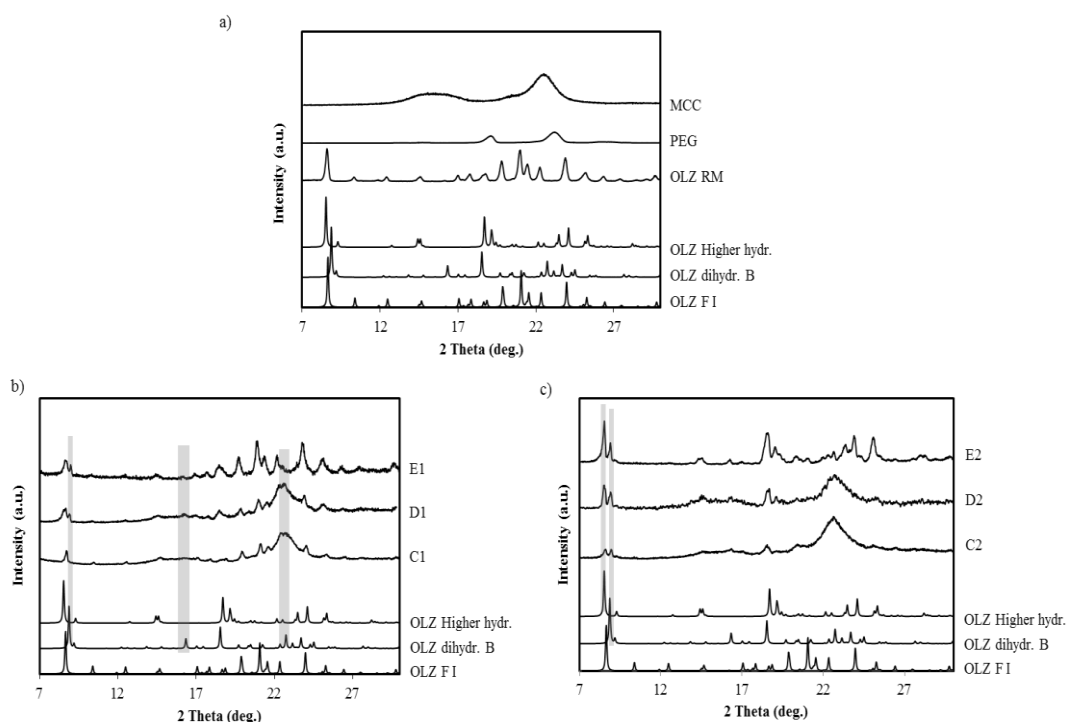
Figure 7.1 – The diffraction patterns for the three forms of olanzapine calculated from single-crystal data of anhydrous olanzapine form 1 (OLZ FI), olanzapine dihydrate B (OLZ dihydr. B) and olanzapine higher hydrate (OLZ Higher hydr.) are followed by the XRPD pattern of (a) raw materials olanzapine raw materials (OLZ RM, PEG and MCC), (b) wet mass C1, D1 and E1 and (c) wet mass C2, D2 and E2. The characteristic diffraction peaks of OLZ dihydrate B and OLZ higher hydrate are indicated with a grey bar.

a)

b)

c)
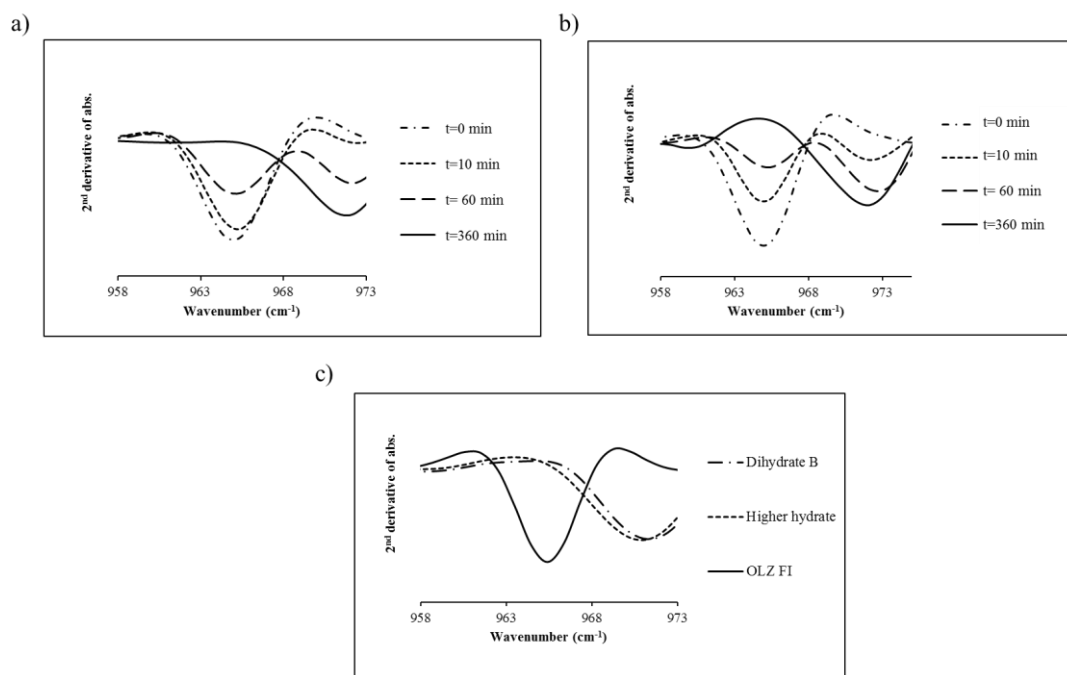
Figure 7.2 – 2nd derivative of FTIR of the region 958-972cm^{-1} of wet mass C (15 OLZ: 75 MCC, a) and D (30 OLZ: 60 MCC, b) at different time periods (0, 10, 60, 360 min). Different OLZ crystal forms are shown in c).

154

Formulation E was formulated without excipients in order to study the morphological changes of OLZ particles during the wetting process. OLZ raw-material particles (OLZ FI) showed to be irregularly shaped. However, after being kept for 6 h in direct contact with water (wet mass E2), hydrate formation has occurred (mixture of 2 hydrates), thus affecting the particles' morphology, which changed to plate-like shaped crystals (Figure 7.3 a.1, a.2, b.1 and b.2).

The hot stage microscopy showed that the new crystals formed were transparent and showed birefringence (Figure 7.3, b2). After heating for 180 min at 45 ºC, the crystals became darker (Figure 7.3 b.2). The optical property changes of crystals accompanying dehydration events have already been reported for other drugs (275, 276). Figure 7.3 shows that dehydration starts with a darkening of the crystal which is slowly propagated throughout the crystal's body, revealing that dehydration did not occur uniformly. The XRPD pattern of this dehydrated sample showed that an anhydrous phase became apparent after dehydration (Figure 7.3 c) but with a lower crystallinity (reduction of the peak's intensity). A higher magnification of the SEM microphotographs of OLZ crystals before and after dehydration showed that the crystals present several cracks at the surface. This change of the surface may result from the breaking up of the crystal into numerous small crystallites that lead to its loss of transparency as a result of light scattering on the surfaces of the numerous crystallites.

Figure 7.3 d) shows the change of crystal size distribution due to the hydrate formation. The growth of the crystals during the resting of the wet masses led to the formation of particles with increased particle sizes.
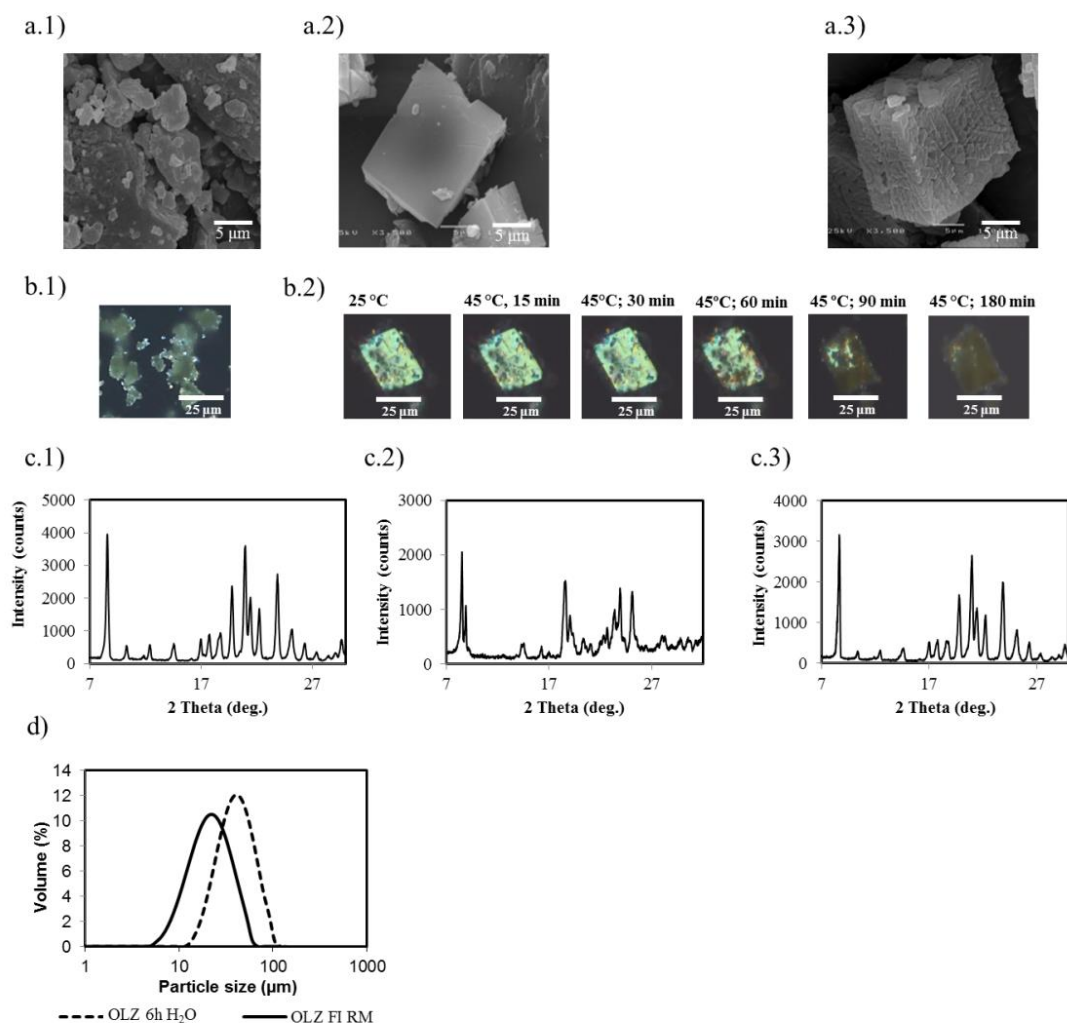
Figure 7.3 – OLZ F I RM and Formulation E were observed by SEM (a), HSM (b) and XRPD (c) The particle size distribution of OLZ raw material(RM) and formulation E (t=360 min) is represented in d)

a) **OLZ FI RM particles (a.1); Particles from formulation E dried at 25 ºC (a.2) and 45ºC for 180 min (a.3); after being kept 6h in direct contact with water**

b) **OLZ FI RM particles (b.1) and particles from formulation E (t=360 min) subjected to an isothermal at 45ºC for 180 min (b.2) under the HSM**

c) **Diffractograms of olanzapine RM (c.1), formulation E (wet paste, t=360 min) (c.2) and formulation E dried 45ºC for 180 min (c.3)**

d) **Particle size distribution (d) of OLZ FI RM and formulation E (t=360 min).**

7.5.2 Extrusion and drying

During the manufacture of pellets using the extrusion-spheronisation technique, the steps following the wet massing of the powders is the extrusion of the moist mass, spheronisation and drying. Formulation C1 (containing lower content of OLZ) showed to not hydrate during all of the extrusion process, therefore OLZ showed to remain anhydrous after pelletisation (Figure 7.4). This result led to the suggestion that the time required for the

immediate extrusion (around 20 minutes), together with the ratio of OLZ:MCC considered in this experiment, were adequate in preventing hydrate formation.

With regard to the wet pellets C2, where a concomitant crystallization of 2 hydrate forms have occurred, the drying process did not initiate a total retransformation of the hydrates to anhydrate at 45 ºC. This drying temperature is not high enough to discharge the dihydrate B in the first 60 minutes of drying and the dihydrate B remains within the core of the pellet. However, these drying conditions of 45 ºC for 60 min were sufficient to convert the OLZ higher hydrate into the dihydrate B (Figure 7.4). By increasing the drying time up to 180 min, dehydration of the dihydrate-B occurs (Figure 7.4).
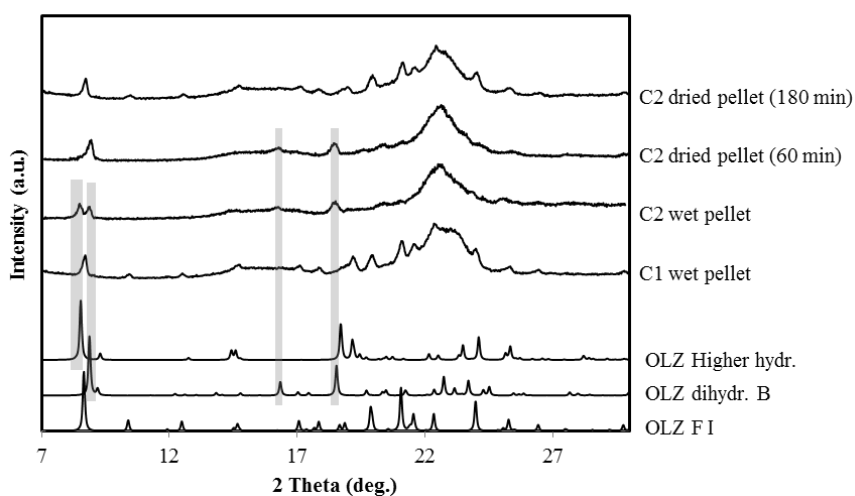
Figure 7.4 – Diffractograms of anhydrous OLZ form I, OLZ dihydrate-B, OLZ higher hydrate, wet pellets C1, wet pellets C2, and pellets C2 dried for 60 min and 180 min. The characteristic diffraction peaks of OLZ dihydrate B and higher hydrate are indicated with a grey bar.

The process of hydration and dehydration of OLZ present in the different pellets' formulations could also be monitored by IR spectroscopy. OLZ FI showed to present a distinct IR spectrum when compared to OLZ hydrates in the spectral regions between 1800-400 cm^{-1} (Figure 7.5). In spite of the presence of MCC, the bands of anhydrous OLZ or hydrated OLZ could be clearly distinguished in the wet and dried pellets of the different formulations (Figure 7.5 A1 and B1, b-e). The 2nd derivative of the absorbance data allowed for a detailed observation of three distinct absorption maxima for the anhydrous OLZ FI (928, 965 and 1010 cm^{-1}), which were present in wet and dried pellets C1 and absent in wet pellets C2. For the formulation D, the pellets D1 showed to present bands at 928, 965 and 1010 cm^{-1}, characteristic of OLZ FI, but also bands at 971 and 1004 cm^{-1}, specific of both OLZ dihydrate B and higher hydrate, showing once again, a mixture of crystalline phases in pellets with a higher ratio of OLZ/MCC.
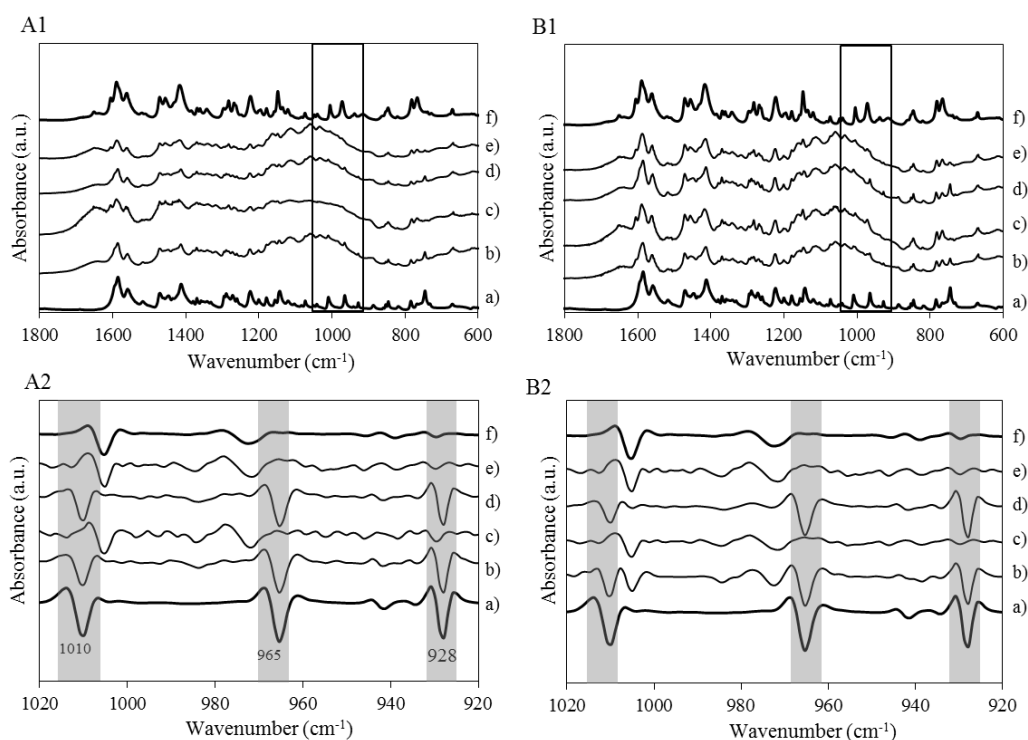
Figure 7.5 – Infrared spectra (A1) and second derivative of infrared spectra (A2) of: (a) anhydrous OLZ F1; (b) wet pellets C1; (c) wet pellets C2; (d) pellets C1 dried for 60 min; (e) pellets C2 dried for 60 min; and (f) dihydrate B.
Infrared spectra (B1) and second derivative of: (a) infrared spectra (B2) of OLZ F1; (b) wet pellets D1; (c) wet pellets D2; (d) pellets D1 dried for 60 min; (e) pellets D2 dried for 60 min; and (f) dihydrate B.
Grey bars show the specific bands of anhydrous OLZ FI

Figure 7.6 shows the surface and the cross section of the pellets C1 produced immediately after wet massing (t=0) and pellets whose wet mass rested for 360 min. Although the pellets surfaces look similar in both processing approaches, it was possible to distinguish the hydrated OLZ crystals when the pellets were cross sectioned. The appearance of plate-like crystals of OLZ in the inner part of the pellet (t=360 min) shows that the changes in shape of OLZ particles due to hydrate formation are also occurring in the formulations containing excipients.
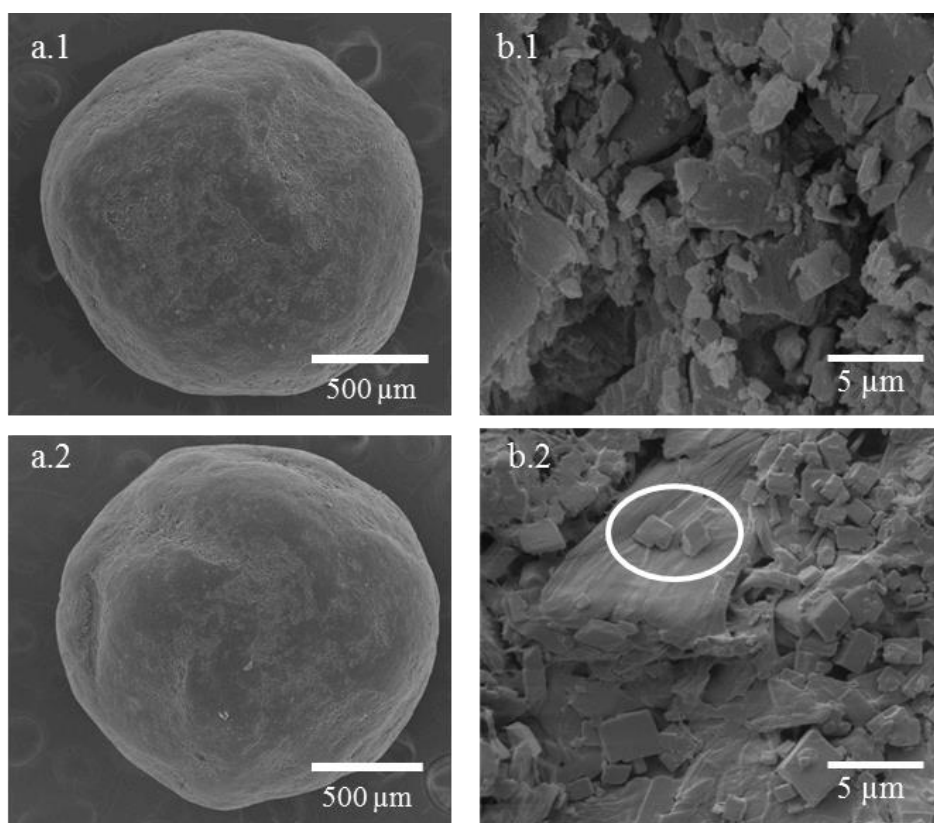
Figure 7.6 – SEM micrographs of formulation C1 t=0 min (1) and C2 A t=360 min (2). The pellet's surface is shown in figure a) and the cross section of pellets is represented in b).

7.5.3 Mechanical characterization of the wet mass and dried pellets

The hydrate conversion of OLZ, together with the change of shape and size, may have a significant impact on several physical and mechanical characteristics of the pellets.

7.5.3.1 Extrusion force

The extrusion force required to obtain the extrudates depends on the rheological properties of the wet mass (113). For this study, formulations A and B (without OLZ) were also taken into consideration.

As a result of MCC being an excipient which presents a high water retention ability, the wet mass B (higher MCC fraction and the same amount of wetting liquid) showed to require an increased force in order to be extruded due to its lower degree of water mobility (Table 7.2). Increasing the OLZ or calcium phosphate content (A, C, D) and therefore reducing the ratio of MCC/water in the wet mass, lowers the force needed for the extrusion of the masses.

Rheological properties of the wet masses may be improved by allowing the wet mass to equilibrate for a few hours prior to extrusion in order to improve the water's capability of hydrating the microcrystalline cellulose (MCC), making it more plastic (113). This fact was observed in pellets without OLZ (A and B) since the mass that rested for 6 h (2) showed to

require slightly less force to be extruded (Table 7.2). However, the differences between them were not statistically significant. Concerning the formulations containing OLZ (C and D), they showed the opposite result since they required lower forces to be extruded immediately after the wet massing as compared to extrusion after 6h. A significant increase of the force necessary for extrusion was verified between the pairs C1 *vs* C2 and D1 *vs* D2.

Table 7.2 – The effect of formulation on the extrusion force needed to extrudate the wet masses and analysis of variance of the extrusion force values needed to extrudate the formulations with different periods of resting of wet mass (0h and 6h)

Formulation	Extrusion force at steady state (N)[a]	p- value [b]
A1	4233.3 ± 107.84	0.08
A2	3824.4 ± 286.35	
B1	7188.6 ± 226.54	0.56
B2	7089.1 ± 155.11	
C1	5572.6 ± 449.25	0.02
C2	6878.7 ± 390.50	
D1	4406.8 ± 369.65	<0.01
D2	6372.2 ± 108.16	

[a] Mean value of extrusion force (n=3)

[b] α=0.05

7.5.3.2 <u>Pellet size</u>

Calcium phosphate pellets (A) generated pellets with similar sizes to the formulation D1. This excipient has low higrosocpicity and does not hydrate during the wet massing. By opposition to formulation D, pellets with increased sizes are observed after the resting period. Formulation B showed to have a higher fraction of pellets in 1.0 - 1.4 mm size range when the wet mass rested for 6 h.

As opposed to the previous formulations, OLZ pellets showed to have pellets with reduced sizes when the wet masses rested for 6 h (C1 vs C2 and D1 vs D2, Table 7.3). This resulted in a higher fraction of pellets in the 1.0 and 1.4 mm size range. When the percentage of the pellets in the size range of 1.0-1.4 mm was compared to the formulations C1 *vs* C2 and D1 *vs* D2 (3 different batches for each formulation) the differences showed to be significant (α<0.05).

Table 7.3 – Interquartile range and percentage of pellets within 1.0-1.4 mm (n=3 batches). The percentage of pellets in the 1.0-1.4 mm range was compared between batches and the statistical significance calculated

Formulations	Interquartil range IQR	Pellets in 1.0 –1.4 mm fraction (%)	p-value [a]
A1	0.33	68.9 ± 1.87	0.06
A2	0.35	65.0 ± 1.89	
B1	0.27	81.7 ± 1.64	0.80
B2	0.28	82.0 ± 1.09	
C1	0.28	79.3 ± 2.28	0.03
C2	0.23	85.9 ± 2.74	
D1	0.31	67.5 ± 2.17	0.01
D2	0.22	80.2 ± 3.37	

[a] $\alpha=0.05$

7.5.3.3 Pellet mechanical strength

The values of the mechanical strength, expressed as the crushing force of the pellets obtained with the different preparations, are shown in Table 7.4. The strength was determined on pellets in the same size fraction, 1.0-1.4 mm. The value of the strength of the pellets obtained with the different preparations showed to increase proportionally with the increase of the drying time of the pellets. Considering the preparations with 15% and 30% of OLZ, the average values of the crushing force needed to break the pellets C2 and D2 showed to be higher than for pellets C1 and D1, regardless of the drying period (Table 7.4), which was not verified for pellets without OLZ. Comparing the mean extrusion force needed to extrudate wet masses containing 0%, 15% and 30% of OLZ (B, C and D) and the mean crushing force needed to crush the pellets obtained from the same masses, one may observe that the mechanical strength changes in the same manner as the force needed to extrudate the wet masses.

Table 7.4 – Analysis of the effect of formulation on the mechanical strength of pellets

Formulation	Mean crushing force after different drying times (N)				
	15 min	30 min	60 min	90 min	180 min
A1	6.55 ± 0.67	7.73 ± 1.13	8.88 ± 0.94	9.64 ± 1.41	9.49 ± 1.36
A2	6.54 ± 0.43	8.15 ± 1.02	8.64 ± 1.18	9.19 ± 1.30	9.36 ± 1.41
B1	7.82 ± 1.62	8.82 ± 1.18	9.13 ± 0.83	9.25 ± 1.27	9.69 ± 1.68
B2	7.51 ± 1.15	8.67 ± 1.19	9.24 ± 0.81	9.14 ± 0.82	9.44 ± 0.98
C1	7.01 ± 0.46	7.59 ± 0.73	8.16 ± 0.60	8.48 ± 0.87	8.78 ± 1.15
C2	7.66 ± 0.69	8.41 ± 0.94	9.07 ± 0.84	9.29 ± 0.96	9.42 ± 1.29
D1	6.33 ± 0.51	7.01 ± 1.09	7.55 ± 0.83	7.95 ± 0.71	8.36 ± 0.81
D2	7.47 ± 0.46	8.11 ± 0.89	8.75 ± 0.66	9.06 ± 1.18	9.33 ± 1.04

Figure 7.7 shows the schematic representation of the extrusion force necessary to extrude wet masses, pellet size distribution and crushing force necessary to crush the dried pellets of one single batch of formulations B, C and D. This figure sums up the results showed above, allowing for a better visualization of the differences between the formulations which were allowed to rest in a hermetic container and the formulations that were extruded immediately after their preparation. For the 3 different characterizations referred above, formulations B1 and B2 registered almost no differences when compared to formulations C and D.
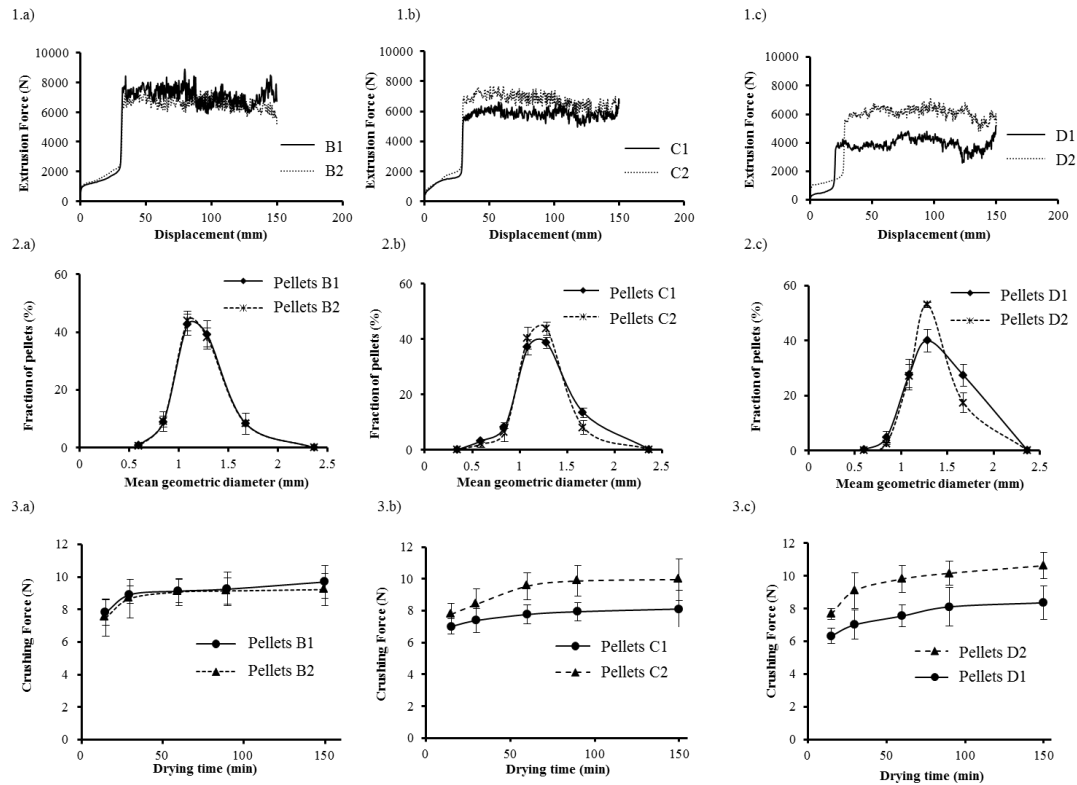
Figure 7.7 – (1) Extrusion force necessary to extrude wet masses; (2) pellet size distribution; and (3) crushing forces necessary to crush the pellets produced from the formulations (a) B, (b) C, and (c) D.

7.5.3.4 Water content

Pellets A and B showed to have the same kinetics of water removal during drying, irrespective of the time elapsed between the wet massing and extrusion steps (Figure 7.8). Regarding formulations C and D, one could observe higher residual moisture for pellets C2 and D2 when the pellets are dried for periods inferior to 180 minutes.
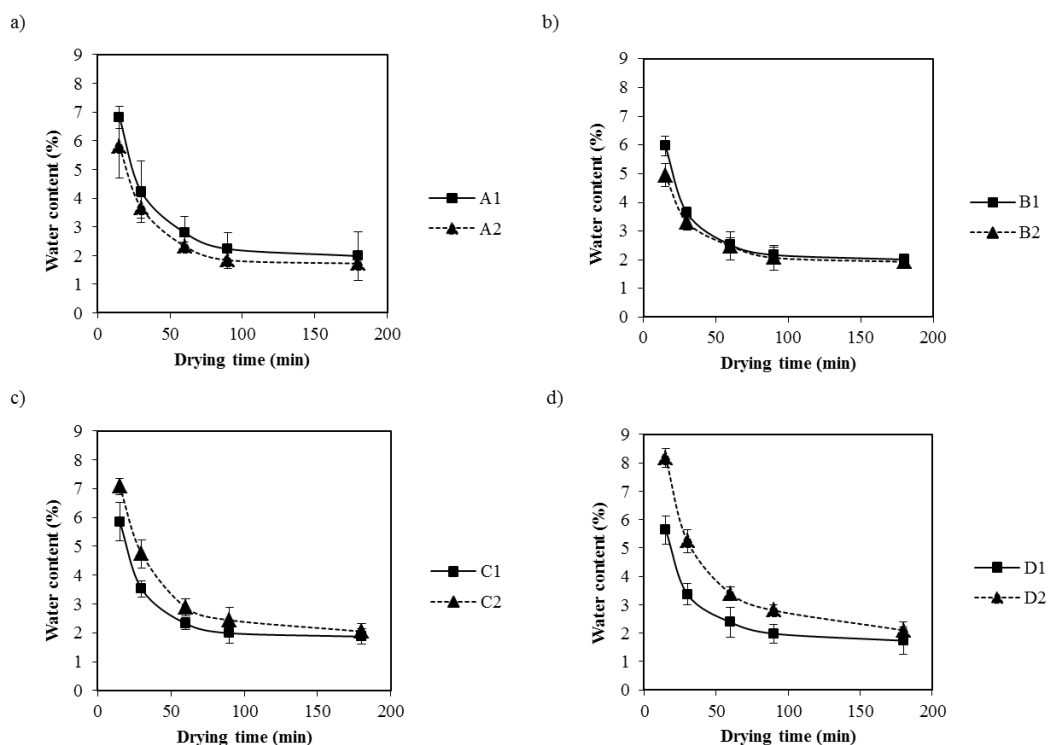
Figure 7.8 – Moisture content (% wt/wt) of pellets: (a) A1 and A2, (b) B1 and B2, (c) C1 and C2 and (d) D1 and D2, dried for different periods of time. Samples measured with an Infrared dryer (n=6).

7.5.4 Drug performance assessed by dissolution

The extent of OLZ dissolution after 12 h was lower than 65% for all of the different formulations (Figure 7.9). A cross section of the pellets after the dissolution test showed that the core of the pellets was yellow (which is the color of OLZ), proving that OLZ was retained in the interior of the pellet. In another approach, pellets were crushed after the end of the test, which enabled the release of 100% of OLZ. This demonstrated that there was no degradation of OLZ during the test. The release of OLZ from pellets (C2 and D2) dried for 60 or 180 minutes presented different behaviors. For pellets C2 and D2 dried for 60 minutes (Figure 7.9 A and B) the OLZ dissolution rate was decreased in relation to the pellets C1 and D1. The same was not verified for pellets C2/D2 dried for 180 min (Figure 7.9 C).

The comparison of the dissolution data was possible through the calculation of $f2$ values. Generally, a similarity factor $f_2 > 50$ indicates an average difference of no more than 10% at the sample time points. The dissolution of OLZ in formulations C1/C2 and D1/D2 (dried for 60 min) in the buffer with the higher pH revealed to be about 50 ($f2= 49$ and 51), which is the threshold for similarity. Moreover, formulations C2 and D2 showed to release about 10% less of OLZ than their counterparts (C1 and D1) after 12 h ($\approx$ 50% of release). An increase of similarity of the curves was observed when OLZ in pellets C2 and D2 dehydrated again into the

anhydrous form I (Figure 7.9 c).Therefore, in the pellets C2 and D2 dried for 150 min, a higher similarity was found with their respective pair (*f2*=81 for the pair C1/C2 and *f2*=79 for the pair D1/D2).
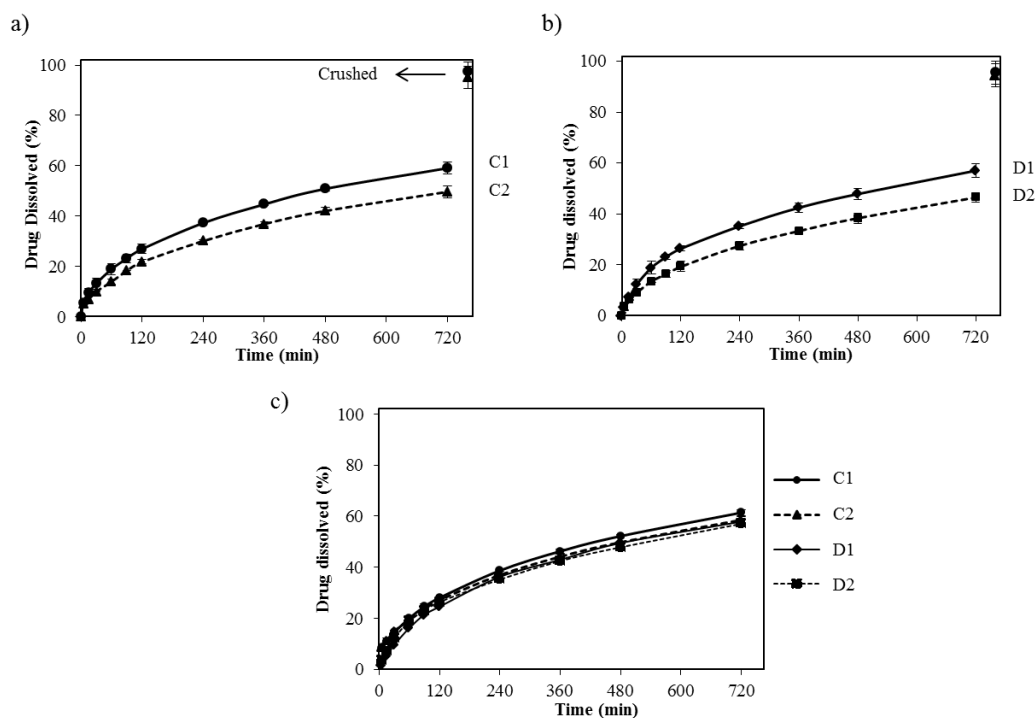
Figure 7.9 – Release of olanzapine from pellets: (a) C and (b) D dried for 60 min and from (c) pellets C and D dried for 180 minutes

7.6 Discussion

Hydrate formation in aqueous environments is expected to occur through solvent-mediated transformations. These transformations start with the dissolution of the metastable anhydrate form (step 1) in the solvent used for the wetting process, leading to supersaturation with respect to the stable hydrate form and providing the thermodynamic driving force for nucleation (step 2) of the stable hydrate. The final growth (step 3) of the stable hydrate will deplete the solution concentration, resulting in further dissolution of anhydrous solid. The hydrate crystal will continue to grow until all of the anhydrous material has dissolved and the concentration of the drug in the solution reaches the solubility of the hydrate (197).

The presence of excipients in the formulation may provide the surfaces or interfaces necessary to promote heterogeneous nucleation, which happens at low driving forces, and the favorable dissolution properties of the metastable drug may be lost due to the fast nucleation of the stable form (42). At the same time, water activity (a_w), which has shown to affect the hydration kinetics (69), may be changed by certain excipients due to their dissolution on the

water used for the agglomeration of the powders, or the ability of excipients to absorb water (195).

Our results showed that the rate for OLZ hydrate formation is dependent on the OLZ/microcrystalline cellulose ratio in the formulation. Due to the ability of MCC to absorb water, its addition to the formulation led to a decrease in the water activity experienced by the hydrate forming drug. When water interacts with MCC, new pores are formed as the cellulose particles swell. At low moisture contents, water molecules are adsorbed on the cellulose surfaces and they bind to the free hydroxylgroups of cellulose chains through hydrogen bonds. At high relative humidity, capillary condensation takes place and the porous cellulose can hold appreciable amounts of water between its fibrils and fibers (210). Thus, the formulation with higher MCC content (formulation C1) showed not to hydrate during all of the extrusion process, whereas formulation D1 showed to have features of both anhydrous and hydrated phases of OLZ in the wet pellets. The faster hydrate formation in formulation D1 can also be explained by the fact that lower content of MCC could have left OLZ molecules more exposed to shear forces during the wet massing, decreasing the time to supersaturation, which is a prerequisite for nucleation and growth.

The time scale of the wetting process revealed to have an impact on OLZ hydrate formation. As nucleation is a stochastic process, and events are usually expressed as a rate or the number of events occurring in unit time, the probability of such an event occurring increases with time, and the transformations in a water environment is therefore most effective if continued over an extended period. Hence, both formulations whose wet mass was left to equilibrate during 6 h showed to be depleted of anhydrous OLZ content, showing instead a mixture of two different hydrate forms (dihydrate B and higher hydrate). The concomitant crystallization of both dihydrate B and higher hydrate may be associated with the similar nucleation rate of the two hydrates in these experimental conditions in which the nucleation takes place (29). Although dihydrate D is the most stable hydrate form of OLZ, it was not the form encountered in the wet mass. These results are easily explained by the Ostwald's rule of Stages (50), which states that when a given chemical system leave a metastable state it does not seek out the most stable state, rather the nearest metastable one that can be reached without loss of free energy.

When the pellets were dried, an easier elimination of the OLZ higher hydrate as compared to the OLZ dihydrate B was observed. This may be related to the fact that the higher hydrate is only stable in wetcakes of OLZ, rapidly losing its stability when dried, as suggested by Reutzel-Edens et al. (18). The increase of the peak at 16.3 ° (2Θ), which is only characteristic of the dihydrate B, and the reduction of the peaks' intensity at 14.4 ° and 14.6 ° (2Θ), characteristic of the higher hydrate form (18), indicated that the higher hydrate form (2.5 water molecules) dehydrated into a lower hydrated form – the dihydrate B (2 water molecules).

Commonly, due to the dissolution or partial dissolution of drugs during wet massing, the subsequent solvent removal induces phase transformations. After the removal of the solvent, the solid which is regenerated from the solution may not be the same original phase (6). The phase obtained is therefore dependent on the rate of solvent removal, the ease of nucleation and crystal growth under processing conditions and the undissolved drug may act as seed during the dehydration (6). Therefore, prior to the dehydration into the anhydrous OLZ FI, the presence of the dihydrate B may have acted as a seed for the dehydration of the higher hydrate into this dihydrate B structure.

The SEM pictures of OLZ in formulation E before and after hydration show that OLZ changes its morphology by changing from an irregular shape to a plate-like shape structure. The hydrate crystals revealed to form cracks over the entire surface when dehydrated. The XRPD analysis of the dehydrated material revealed that OLZ had a slightly lower crystallinity than the raw-material. Therefore, if OLZ hydrates during wetting and dehydrates during drying, even though the final polymorphic form is the same, the particles have a completely different shape and reduced crystallinity. This modification of the shape during the process seems to have an implication on the physical and mechanical characteristics of the extrudates/pellets. For instance, the forces needed for the extrusion of the wet masses containing OLZ showed to be affected by the OLZ hydrate formation since an increment on the force needed was observed when OLZ wet masses rested for 6 h. As observed previously, the hydration of OLZ was a slow process, being the OLZ hydrate conversion only completed in the wet masses which were kept in a hermetic container for 6h. The integration of part of the water available in the wet mass into OLZ crystal lattice may have caused its removal from the surface of the particles and, thus, a reduction on the liquid bridges between the particles has occurred (277). This fact, together with the change of the size and shape of OLZ crystals, may justify the significant increase in force needed for the extrusion of wet masses containing higher contents of OLZ (formulation D1 *vs* D2).

Regarding the placebo formulations, one could observe that formulation B containing higher contents of MCC (90% w/w) showed to need higher forces to be extruded when compared to wet masses containing both MCC and calcium phosphate (60:30 % w/w, A). This can be related to the high water absorption of water by MCC, as opposed to calcium phosphate, which is not hygroscopic and has a poor solubility. Calcium phosphate may behave as a "shield" in the wet mass, resulting in a higher amount of free water available in the formulation. Hence, the wet mass becomes softer and lower forces are needed to extrudate calcium phosphate masses. (278). For these 2 formulations, A and B, lower forces were observed for wet masses which were left to equilibrate for 6 h. This shows that a better spreading of the water throughout the excipients was verified and a higher plasticity of the mass was achieved.

The factors that influenced the extrusion force may also be related to the pellet size distribution, since an increased amount of pellets within the 1-1.4 mm range was found for the wet masses which were extruded with increased forces. Accordingly, the reduction of the free water in the formulations C2 and D2 due to hydration of OLZ resulted in a reduced size and narrow distribution of the pellet size.

During dehydration, the water inside the structure of OLZ molecule may have had more difficulty to be removed than the water just absorbed by the other components of the wet pellets. This explains the higher residual moisture in the pellets containing hydrated OLZ, which were dried for periods inferior to 180 min. The residual moisture between pellets (C1 *vs* C2 and D1 *vs* D2) became similar after 180 minutes of drying, when the dehydration of OLZ hydrates was completed.

The increase on the pellet strength with the increase of extrusion force may be attributed to the fact that wet masses with a lower plasticity are squeezed with higher pressures, leading to a higher compaction of the mass that will generate the pellets (278). Furthermore, the morphological changes of OLZ crystals during the resting of the mass may cause abrupt modifications to particle's surface and to interparticle bonds, affecting the strength of the pellets.

Regarding the dissolution profile of the different formulations, it was visible that OLZ dissolved after 12 h was lower than 65% for all of the different formulations. However, the crushing of the pellets at the end of the test showed the total release of the OLZ from the pellet. The low solubility and wettability of OLZ, together with the increased amounts of cellulose used in the formulations, can explain the slow release of OLZ.

Lower dissolution rates of the drug were found for pellets containing OLZ dihydrate B (C2 and D2, dried for 60 minutes). As it has been discussed before, the hydration of OLZ was also accompanied by variations in crystal morphology. Morphological/size modifications are able to change the dissolution rate of the drug as a result from a combination of changes to the size and number of crystal faces exposed to the dissolution medium, as well as the nature of those faces, which in turn will influence the wettability and subsequent dissolution of drug (73). Furthermore, dissolution rate of dihydrate B showed to be slightly lower than anhydrous Form I, as verified in chapter 3. Therefore, the reduction on the dissolution rate of the drug may have been related to the changes of both molecular and morphological properties of OLZ during the resting time of the drug. An increase of similarity of the curves was observed when the hydrated species of OLZ were dehydrated. The dehydration of OLZ is also accompanied by changes on its morphology since cracks appear at the surface. These cracks, resultant from dehydration, may increase the fragility of the crystal, resulting in the production of powder-like crystals with an increased surface area, as it was observed for other drugs, such as naproxen (275).

7.7 Conclusion

In summary, the low water solubility of OLZ (practically insoluble in water) results in low wetting properties, which makes the formation of its hydrates more difficult when it is in contact with water for a short period of time (e.g., immediate extrusion). The higher ratio of MCC in the formulations showed to retard the hydrate conversion of OLZ due to a completion effect, as a consequence of the higher affinity of water with the amorphous regions present in the molecular structures of this excipient.

The dehydration of OLZ was possible when a low temperature of drying was applied (45 ^{0}C). However, 180 minutes were needed to complete the dehydration of the dihydrate B structure. In spite of the presence of excipients in the pellets' formulations, the FTIR and XRPD analysis showed to be able to detect the formation of the hydrates of OLZ over the process of extrusion. This revealed the suitability of the utilization of these excipients (MCC and PEG-6000) when alterations of a crystalline drug need to be studied over a pharmaceutical process.

The presence of the dihydrate B in the dried pellets showed to affect OLZ's dissolution rate. Being OLZ a drug whose absorption is dependent on the dissolution rate, the presence of the dihydrate B in the final dosage form may have a negative impact on the bioavailability of the drug. The changes in crystalline structure of OLZ during the process showed to affect the rheology of the wet mass, and the pellet's size and strength.

Hence, the structural changes related to the hydration/dehydration process can strongly affect the technological performance, the bioavailability and the drug stability. These results suggest that attention should be given to the pseudopolymorphism of the drugs before the selection of the excipients and conditions for a new pharmaceutical process.

This study confirms the importance of monitoring the crystalline changes of a drug when water and temperature need to be applied during processing.

CHAPTER 8

Part of the work presented in this chapter has been published in:

Chapter 8 - Role of excipients on the stabilization of olanzapine during extrusion and dissolution

8.1 Abstract

Hydrate formation is a phase transition which can occur during manufacturing processes involving water. This work considers the prevention of olanzapine (OLZ) hydrate conversions in the presence of water and polymers [polyethyleneglycol (PEG); hydroxypropylcellulose (HPC); polyvinylpyrrolidone (PVP)] in forming pellets by wet extrusion and spheronisation and during dissolution testing of dried pellets. Our previous results showed the potential that HPC and PVP may have on preventing hydrate formation, therefore, in this study they are going to be added to pellet's formulations. Anhydrous OLZ was added to water with or without those polymers prior to extrusion with microcrystalline cellulose. Assessment of OLZ conversion was made by XRP-Diffraction; FTIR spectroscopy; calorimetry (DSC) and microscopy (SEM for crystal size and shape). The wettability and the surface energy of the powders before and after being exposed to hydrating conditions were evaluated. Both PVP and HPC prevented the hydrate transformations of the anhydrous drug; the latter even in the presence of hydrate seeds. The higher ability of HPC to spread over the OLZ particles was observed. The addition of microcrystalline cellulose needed for the pellets production (final product) did not eliminate the protector effect of both HPC and PVP during pellets' processing and dissolution evaluation.

8.2 Introduction

Active pharmaceutical ingredients (API) may undergo solvent mediated polymorphic transformations when they are present in certain pharmaceutical manufacturing processes e.g. wet granulation/wet extrusion (279) which can affect the drug's dissolution rate which can ultimately result in variations in bioavailability (57, 280) . The excipients used in the formulation may affect the rate of hydrate conversions of the API during a wet granulation or wet extrusion process. It would be desirable to avoid as many phase transitions as possible by using inhibitors like excipients in the formulation (224, 279).

Microcrystalline cellulose is a common excipient used in solid dosage forms and the effect of MCC on the reduction of the hydrate formation of the drugs during the wet massing step was shown to be originating from its ability to hold large amounts of water in its internal structure, which can retard the hydrate formation (210, 211). However, the use of high contents of water (e.g., 60%–80% w/w) may reduce the protection of MCC on retarding the hydrate formation. The addition of other excipients to the formulation (e.g., polymers) may reduce the amount of water needed for the powder to agglomerate and avoid hydrate formation during the wet massing. (60, 281). Therefore, depending on the API and excipients used, hydrate

formation may take place during the wetting step (111), which may or may not be reversible after the drying step.

In the literature, one may find some examples where polymers showed to inhibit hydrate formation of pharmaceutical crystals in aqueous slurries (196, 282). For instance, polyvinylpyrrolidone (PVP) has been demonstrated to inhibit partial or completely the growth rate of sulfathiazole single crystals in solutions (282). The cross-linked poly(acrylic acid) (PAA) has been shown to completely inhibit the caffeine anhydrate to hydrate transformation in aqueous environments (196). Cellulose derivatives (e.g. HPC and HPMC) have been shown to be successful in inhibiting the hydrate conversion of carbamazepine but exhibit no effect on the transformation kinetics of anhydrous sulfaguanidine (196). The different inhibitory behaviors of different polymers, and the same polymer with different APIs, reveal that there is no single polymer which promotes the inhibition of hydrate conversions in all APIs. This may be a consequence of different specific interactions that the polymer may establish with individual crystal surfaces (150, 194).

Our previous studies showed that anhydrous OLZ form is unstable under humid conditions or in aqueous dispersions and converts rapidly to its dihydrates/higher hydrated forms when exposed to water. Therefore, a rigorous process monitoring and control of the existing form at each step of its manufacture is necessary to ensure the quality of the final products.

To the best of our knowledge, studies on the monitoring of the polymorphic transitions of OLZ during the entire extrusion-spheronisation process have not been reported previously. Furthermore, there is a lack of information about how excipients may control the OLZ transformations that are likely to take place during the pharmaceutical processes involving water.

8.3 Purpose

The previous section showed the impact of hydrate formation during processing on the physical characteristics of the pellets. Also, in chapter 5, it was observed that certain polymers are more prone to protect OLZ from hydration. In this study, the material is going to be wet massed for a short period of time and it will be evaluated how long can OLZ be kept stable before drying. The protector effect of polymers is also evaluated during dissolution. This study aims, in particular, (1) to access the time needed for OLZ to undergo hydrate conversion in wet masses, (2) to study whether polymers (e.g. PEG, HPC, PVP) with different molecular weights can affect the hydrate conversions of OLZ during and after the wet massing step, (3) to characterize different hydrate crystal forms of OLZ that may be generated during processing, (4) to find a formulation which allows the maintenance of the original crystal form of the API

throughout the entire extrusion-spheronisation process and dissolution. For a more complete study, PEG and PVP with different molecular weights were taken into consideration.

To address these goals, wet masses of OLZ with different polymers are produced and their characterization is carried out using different techniques such as, FTIR, XRPD, calorimetry and microscopy. The contact angle and surface energy of the mixtures is also considered. The dissolution rate of OLZ in each pellet's formulation is assessed and fitted into different dissolution models.

8.4 Materials and methods

8.4.1 Olanzapine and polymers

Olanzapine anhydrous Form I (OLZ FI) was purchased from Pharmorgana, India.

The polymers considered in the study were polyethyleneglycol with different molecular weights (PEG, Mw = 6000 and 40000, Sigma-Aldrich, Germany), hydroxypropylcellulose (HPC LF Pharm grade, Mw = 95,000, Klucel™, Ashland, Germany) and polyvinylpyrrolidone (PVP, Kollidon 12, 2600 < Mw < 5500 and Kollidon 30, 44,000 < Mw < 54,000, BASF Chemicals, Germany). Other chemical were supplied by Sigma-Aldrich, Germany. The following OLZ forms were produced in order to identify the transformations that OLZ FI may undergo during processing:

8.4.2 Conversion of OLZ FI during wet massing in the presence of polymers

Four wet masses were prepared using anhydrous OLZ Form I (OLZ FI, 15 g, *"formulation A"*) or physical mixtures of OLZ with each one of the different polymers, belonging to the three groups described above, namely PEG-6000/ PEG 40000 (group I, *"formulation B1 and B2"*, 10 g), HPC-LF (group II, *"formulation C"*, 10 g) and PVP k12/ PVP k30 (group III, *"formulation D1 and D2"*, respectively", 10 g) (Table 8.1).

Formulations A-D had the same OLZ:polymer ratio as the formulations produced in the previous section (15:10). However, for a better understanding of the mechanism of hydrate protection by the polymers, we also tried different OLZ:Polymer ratios (15:5, 15:0.5 and 15:0.1) in this section. Moreover, seeding experiments were performed, where 5% of anhydrous OLZ was replaced by OLZ dihydrate, to promote crystal growth within the anhydrous OLZ containing formulations. These experiments were performed for better characterization of the mechanisms of the interaction between the polymer and OLZ.

OLZ or physical mixtures of OLZ and polymer were blended for 5 min in a planetary mixer (Kenwood, Hampshire, UK). Demineralized water (75 g, 5 times the OLZ mass) was added for 1 min to the blends. For a homogenization of results and better comparison with the previous data we tried to use the same proportion OLZ: water.

The wet masses were mixed thoroughly for 10 min and then placed into sealed glass vials filled to the top. Samples were taken at different time periods (t= 0, 30, 60, 180 and 360 min) after production. A fraction of each sample was analyzed immediately by XRPD and the remaining portion was dried in Petri dishes (24h at 25°C/55% RH, until constant weight) and analyzed by infrared spectroscopy (FTIR), thermal analysis (calorimetry, DSC) and microscopy (SEM).

8.4.3 Manufacture of Pellets Containing Polymers

Taking into consideration the same fractions of both API and excipients, 75 g MCC was added to the blends described previously (Table 8.1), to turn the manufacture of pellets possible:OLZ:MCC (AM), OLZ:MCC:PEG 6000/40000 ($B1_M$ and $B2_M$, respectively), OLZ:MCC:HPC (C_M) or PVP k12/k30 ($D1_M$ and $D2_M$ respectively) were dry-mixed in a planetary mixer (Kenwood, UK) for 5 min prior to the addition of 75 g (5 times the OLZ mass) of demineralized water. Each wet mass (175 g) was further mixed for another 10 min. Half of the wet mass was extruded immediately (#1) whereas the other half was allowed to equilibrate for 360 min (#2) in a sealed polyethylene bag before extrusion. The storage of wet masses to equilibrate for several hours is commonly considered in daily practice to ensure a uniform distribution of water (283) and in the present case to promote hydration of OLZ. All measurements were performed off-line at defined time points after wet massing (t = 0, 30, 60, 180, and 360 min) by FTIR and XRPD. Extrudates were manufactured from 2 wet masses (#1 and #2) in a ram extruder (Lurga, Portugal) adjusted to an universal testing machine (LR 50K, Lloyds Instruments, UK) fitted with a load cell to allow the collection of data for the applied force to the ram and its displacement (200 mm/min). The wet mass was forced to pass through a die (Length/Diameter = 6) and, after extrusion, the extrudates were immediately placed in a spheroniser (radial friction plate rotating at 500 rpm, Caleva, UK) for 5 min. The wet pellets were dried in a fluid bed drier (Aeromatic-Fielder AG, Bubendorf, Switzerland) at 45 °C for 60 min. Dried pellets were evaluated for powder diffraction (XRPD) infrared spectroscopy (FTIR) and OLZ dissolution studies into an aqueous solution.

Table 8.1 – Formulations considered in polymer screening and pellets manufacture

Formulation	Components (g)		
	OLZ	**Polymer**	**MCC**
A	15	-	-
B_1	15	10 (PEG-6000)	-
B_2	15	10 (PEG-40000)	-
C	15	10 (HPC- LF)	-
D_1	15	10 (PVP k12)	-
D_2	15	10 (PVP k30)	-
A_M	15	-	85
B_{1M}	15	10 (PEG-6000)	75
B_{2M}	15	10 (PEG-40000)	75
C_M	15	10 (HPC- LF)	75
D_{1M}	15	10 (PVP k12)	75
D_{2M}	15	10 (PVP k30)	75

8.4.4 Characterization of Blends and Pellets

X-Ray powder diffraction (XRPD)

The X-ray powder diffractograms were recorded at room temperature on an Analytical X'Pert PRO apparatus (Equipment 2). X-ray diffraction characterization was performed to the different formulations (A, B1, B2, C, D1, D2) before and after the end of the study (360 min) in order to observe the hydrate conversions of OLZ in each sample. For the characterization of the OLZ crystalline structures in each wet mass the XRPD patterns were compared with the XRPD pattern of crystalline structures of anhydrous OLZ Form I(CSD refcode: UNOGIN), dihydrate B (CSD refcode: AQOMAU01) and higher hydrate (CSD refcode: AQOMEY) obtained from the Cambridge Structural Database and visualized using the software Mercury 1.4.2 (Cambridge Crystalographic Data Centre, Cambridge, UK) (18).

FT-IR Spectroscopy (FTIR)

Each OLZ formulation was mixed with KBr in a 1:1 proportion and the mixture (200 mg) compacted (2 Tons) into compacts (12 mm diameter). The infrared spectra were collected in the absorption mode (IR Affinity-1 Shimadzu spectrophotometer, Kyoto, Japan).

Differential Scanning Calorimetry (DSC)

Thermograms of different OLZ forms were obtained with a Differential Scanning Calorimeter after calibration with indium. Dry N_2 was used as the purge gas. Dried samples (2

to 3 mg) were placed in pinhole crucibles and heated at 10 °C/min within 0-210 °C temperature range.

Scanning electron microscopy (SEM)

Different formulations were mounted on aluminum stubs and coated with gold by ion sputtering and observed under scanning electron microscope (JSM-5200 LV, Japan).

8.4.5 Wettability and surface energy measurements

In order to measure the wettability and the surface energy of the powders before and after being exposed to hydrating conditions, the contact angles in two liquids (bi-distilled water, Strom and diiodometane, Sigma, Germany) of the samples were measured (Wilhelmy plate technique, Krüss Tensiometer K12, Germany). Samples of powders were made to adhere on a rectangle shape substrate (20X20 mm) uniformly coating its surface. All measurements were performed at a controlled temperature $25 \pm 0.5°C$, by flowing water from a circulator (Haake, Germany). The surface energy of the polymers and OLZ was measured according to the Wu equation (284).

8.4.6 Dissolution studies

Dissolution studies were performed for OLZ (5 mg) from dried pellets (60 min / 45ºC, size of 1-1.4 mm). Tests were performed in a dissolution apparatus (paddle method, 50 rpm, 900 ml of phosphate buffer at 6.8, $37\pm0.5°C$, n=6, AT7, SOTAX, Switzerland) with collection of samples at time intervals (t= 5 to 1440 min). The residual water present in the pellets was taken into consideration (Sartorius Moisture Analyser, Germany). OLZ was quantified by UV spectrophotometry ($\lambda= 254$ nm, Hitachi U- 2000, Japan) and the analysis of OLZ release and dissolution profiles was possible by comparison of dissolution models. Simultaneously, dissolution tests were performed with pellets A_M, $B1_M$, C_M and $D2_M$ for off-line FT-Infrared evaluation of the anhydrate to hydrate transformations occurring in non-dissolved fraction of OLZ present in the pellets (t=0 min, 30 min, 60 min, 180 min and 360 min). Each sample collected for FT-IR analysis was recovered from a different vessel.

8.5 Results

8.5.1 Polymer screening method to identify polymers that can stabilize OLZ FI during wet massing

The different polymers used in this work may be classified into three categories according to their molecular structure. In group I polyethylene glycol with different molecular weights (PEG 6000 and 40000) were considered; this polymer has both hydrogen bond donor and acceptor groups at the two ends of the polymer chain. Group II is constituted by a cellulose derivative polymer, hydroxypropylcellulose (HPC) with both hydrogen bond donor and

acceptor groups in their ring structure. Group III includes polyvinylpyrrolidone (PVP K12 and PVP k30) which present only one acceptor hydrogen bonding group in their ring structure.

The X-ray powder diffraction (XRPD) patterns for OLZ, OLZ:Polymer physical mixtures and the respective wet/dried masses, are represented in Figure 8.1. In order to characterize the changes in the crystal structure of OLZ in each formulation, the XRPD patterns were compared to the XRPD patterns of different crystal structures of OLZ, such as, anhydrous form I, dihydrate B, dihydrate E and higher hydrate.

Figure 8.1 A shows the XRPD pattern of OLZ and recovered OLZ after 360 min in contact with water. The XRPD diffractograms show that OLZ was able to hydrate into the dihydrate-B form. However, the peaks at 8.58°, 19.20°, 24.14° 2θ, which are characteristic of the higher hydrate form suggests a concomitant crystallization of both hydrates, although in different proportions. The subsequent resting of the wet mass at 25ºC/55% RH for 24h was followed by the elimination of the higher hydrate form.

OLZ which was physically mixed with PEG 6000 /PEG 40000 was shown to hydrate selectively into the higher hydrate form (Figure 8.1 B). The product from the dehydration of the higher hydrate (2.5 mol water per mol of OLZ) was the dihydrate E. The XRPD study of the wet material enabled the observation of the intermediate higher hydrate form which is generated and only stable in a wet environment. Similar diffraction patterns of OLZ before and after wetting suggests a complete inhibition of hydrate transformations of OLZ during the time of experiment in formulation C. However, a slight widening of the OLZ peaks was observed after drying the OLZ: HPC wet mass (Figure 8.1 C). Similarly OLZ: PVP mixtures also failed to show transformations of OLZ. No peaks due to excipients were observed after the manufacture of physical mixtures with PVP k12, PVP k30 and HPC LF reflecting the amorphous nature of these polymers.
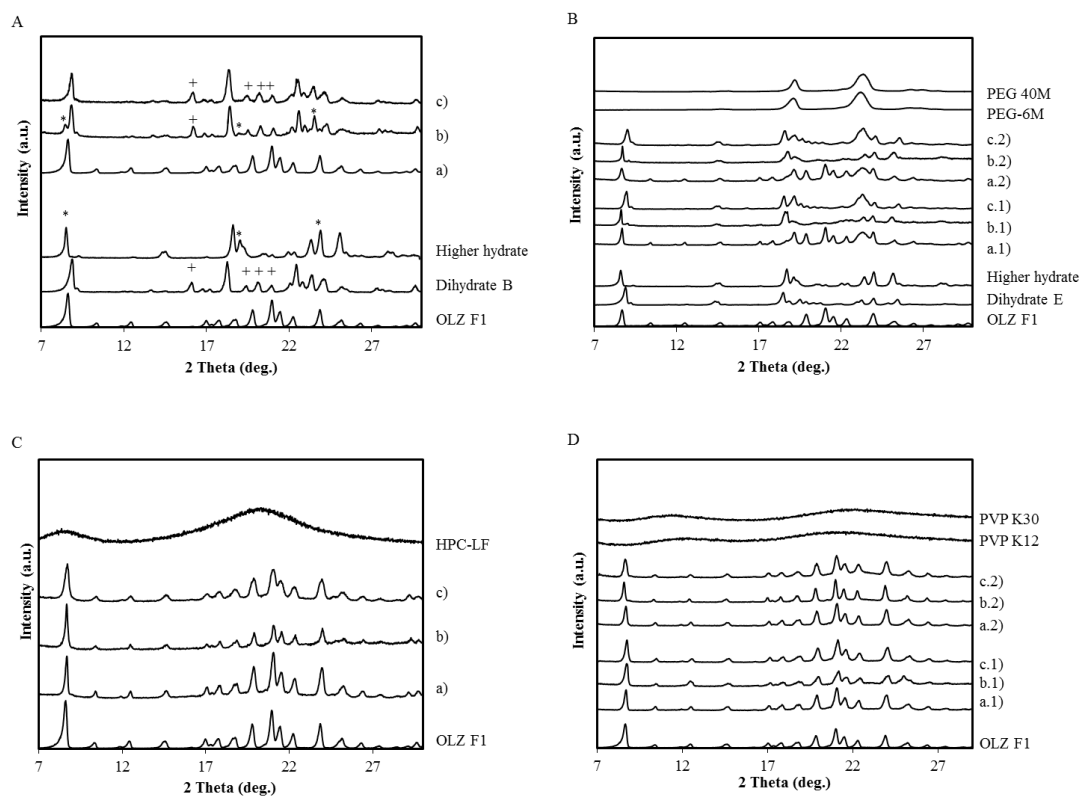
Figure 8.1– Diffractograms of 6 formulations before wetting, after wetting and after drying. The wet samples were analyzed after storage in a sealed container for 360 min.

A) OLZ before (a) and after wetting (b) and drying (c); (+) represents the characteristic peaks of the OLZ dihydrate B and (*) represents the characteristic peaks of the OLZ higher hydrate.

B) Formulations B1 and B2 physical mixture (a.1 and a.2), after wetting (b.1 and b.2) and after drying (c.1 and c.2).

C) Formulation C physical mixture (a), after wetting (b) and after drying (c).

D) Formulation D1 and D2 physical mixture (a.1 and a.2) after wetting (b.1 and b.2) and after drying (c.1 and c.2).

The region 720-780 cm^{-1} was selected to distinguish the different hydrate conversion occurrences in OLZ wet masses containing no polymer (A) or the PEGs (B1 and B2) as excipients. The out of plane deformation of the CH bond of the benzene group at 745 cm^{-1} was no longer present in both wet masses after 360 min. Wet mass A revealed a new absorption maximum at 767 cm^{-1} specific for the dihydrate B whereas wet masses B1 and B2 presented a new band at 754 cm^{-1}, characteristic of the dihydrate E.

In Figure 8.2 A, the fraction of the polymer was reduced by 1, 1.5 and 2 orders of magnitude in relation to formulations B, C and D. The ratio of OLZ:Polymer varied between 15:1, 15:0.5 and 15:0.1. Figure 8.2 A displays the spectra of the wet masses collected 360 min after their preparation. The reduction on the polymers fraction in formulations containing PVP was reflected by the hydrate conversion (especially for the formulation containing PVP k12), which started to hydrate after 360 min in a sealed container. By opposition, no hydrate

transformation was observed in formulation C containing a low percentage of HPC in the wet mass. Hydration in OLZ:PEG formulations, was verified for all the OLZ:polymer ratios.

Seeding experiments were carried out to determine if the HPC and PVP could still prevent the transformation in the presence of nuclei, and to better understand the inhibitory mechanism of these polymers. Five percent of the anhydrous API was thus replaced by OLZ dihydrate E before the wetting step. Shifts in the spectra of samples based on formulations D1 and D2 were observed and assumed to be related to hydration of anhydrous OLZ, whereas samples of formulation C did not produce shifts in the characteristic bands (Figure 8.2 B).
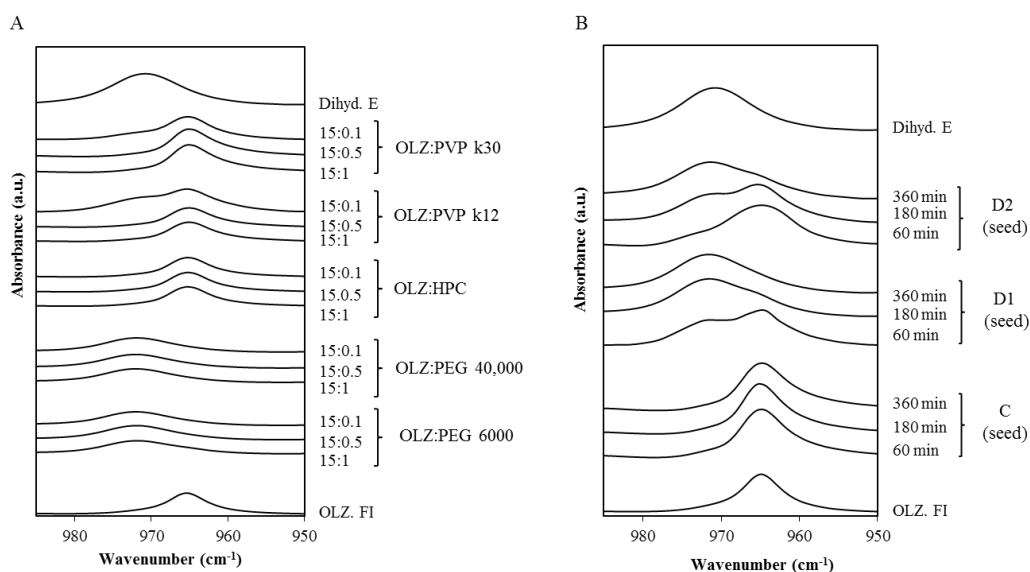
Figure 8.2– Spectra (FTIR) in the region (990-950 cm^{-1}) for the different OLZ:polymer formulations.
A) Wet masses collected 360 min after wet mass preparation. The OLZ:polymer ratio varied from 15:1 to 15:0.1.
B) Wet masses C, D1 and D2 with seeds (5%). The spectra were collected at 60, 180 and 360 min after the wet mass preparation.

Figure 8.3 A1 shows that immediately after wet massing (t=0), OLZ particles were irregularly shaped and agglomerated. OLZ particles, alone (A) or in the presence of PEG (B1), after 360 min in direct contact with water, had their morphology changed to plate-like shaped crystals (Figure 8.3 A2) characteristic of the hydrate and the size of the latter larger than OLZ particles alone (Figure 8.3 B2). By opposition, formulations C and D1 showed no transformation of OLZ particles over the same period (Figure 8.3, C and D).
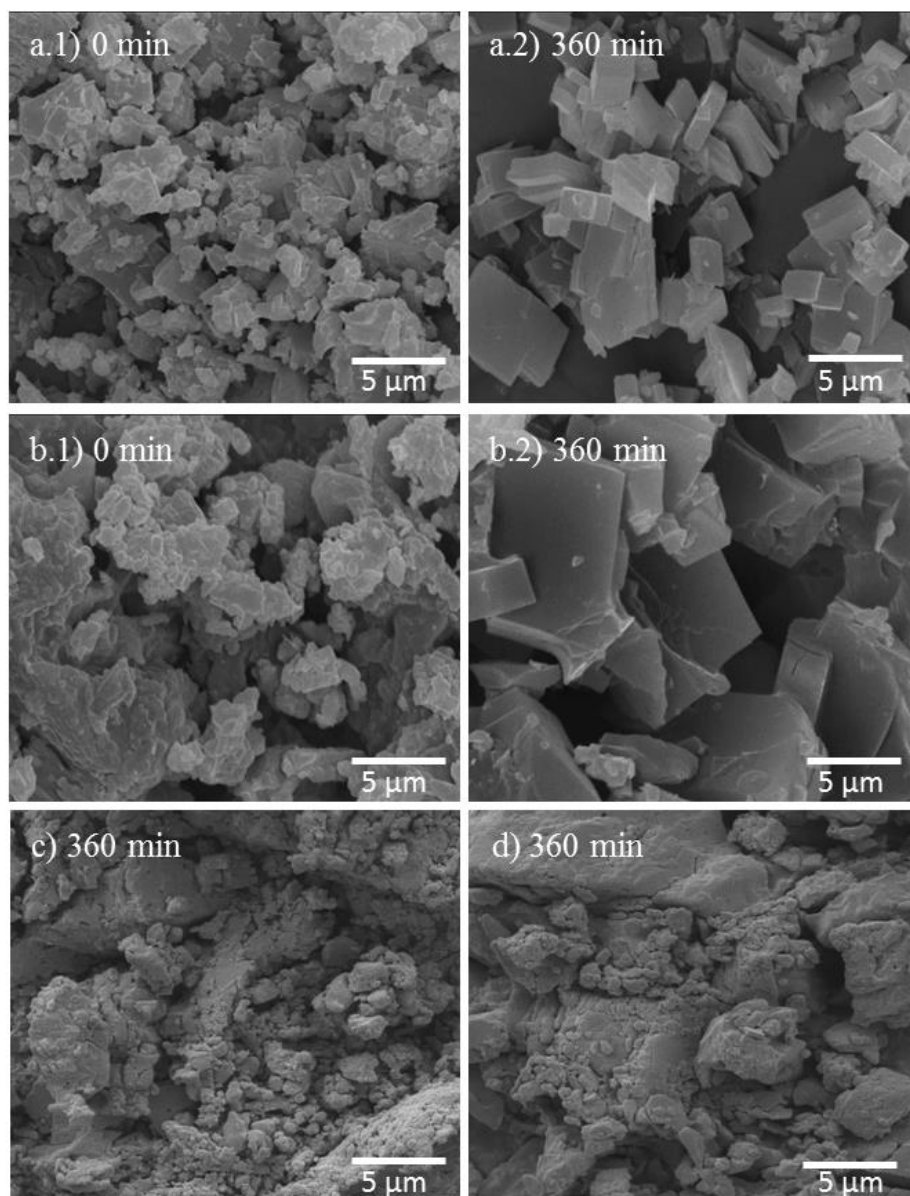
Figure 8.3 – Micrographs of wet masses for formulations A, B1, C and D1.
Formulation A (t=0 min, a1 and t=360 min, a2); Formulation B1 (t=0 min, b1 and t=360 min, b2);
Formulation C (t=360 min, c); Formulation D1 (t=360 min, d).

The thermal behavior of anhydrous OLZ and physical mixtures of formulations B1, B2 C, D1 and D2 are shown in Figure 8.4 (line 1, A to D) in which thermograms 2 and 5 correspond to the samples recovered immediately after the wet massing (t=0 min) and the curves 3 and 6 correspond to the samples which were kept in a sealed container (t=360 min).

Figure 8.4 A1 (OLZ raw-material) shows only one endotherm event at 195.29 °C due to the melting of OLZ. Thermograms A2 and A3 reveal a new endotherm at lower temperatures corresponding to the release of water in the molecular structure, as a result of the presence of OLZ hydrate in the samples. The small fraction of the hydrate content in OLZ samples which

were produced immediately after the wet massing (a mixture of anhydrous and hydrous content is present, Figure 8.4 resulted in a water loss endotherm with a low enthalpy.

curve	Tm (°C)	ΔH (J/g)
A.1)	195.29 ± 0.08	132.05 ± 1.01
A.2)	194.95 ± 0.27	128.52 ± 1.33
A.3)	194.95 ± 0.05	113.02 ± 1.31
B.1)	185.64 ± 1.69	55.58 ± 3.70
B.2)	186.89 ± 1.85	53.29 ± 5.01
B.3)	187.42 ± 1.83	55.776 ± 4.84
B.4)	184.66 ± 1.22	55.80 ± 2.54
B.5)	186.22 ± 0.10	50.46 ± 2.589
B.6)	186.06 ± 1.52	50.48 ± 2.77

curve	Tm (°C)	ΔH (J/g)
C.1)	194.79 ± 0.06	76.20 ± 2.51
C.2)	192.28 ± 0.89	62.62 ± 3.52
C.3)	192.45 ± 0.13	66.04 ± 2.63
D.1)	190.72 ± 1.14	60.01 ± 0.63
D.2)	188.22 ± 0.90	52.77 ± 2.17
D.3)	189.83 ± 1.95	52.64 ± 1.83
D.4)	186.95 ± 1.67	59.77 ± 1.44
D.5)	182.09 ± 1.54	52.07 ±2.34
D 6)	181.01 ± 1.88	51.74 ± 1.25

Figure 8.4 – Thermograms of formulations A (A), B_1 (B, curves 1-3), B_2 (B, 4-6), C (C), D_1 (D, 1-3) and D_2 (D, 4-6).
Curve 1 (physical mixture of raw materials), curves 2 and 5 (wet masses at t=0 min), curves 3 and 6 (wet masses at t=360 min).
Tables present the melting point of OLZ and the respective enthalpy of fusion (T_{max} and ΔH) for each formulation (grey shadow in figures).

Figure 8.4 (B1 and B4) shows that the physical mixtures (PM) obtained from formulations B1 and B2 present 2 endothermic peaks due to the melting of both PEG and OLZ. The depression on OLZ melting temperature and enthalpy result from the solubilization of the drug within the molten PEG during heating. Figure 8.4 (B2 and B5) shows no traces of water evaporation allowing the assumption that no hydrate was present in the sample. However, curves B3 and B6, reveal an endothermic peak due to dehydration of the dihydrate E. Furthermore, a reduction on the melting temperature of the PEG polymers was also registered in thermograms B3 and B6 (Figure 8.4), suggesting conformational changes of the polymer chains with an impact on its melting temperature. This is in line with the ability of the PEG chains to adapt its conformation when in contact with water to establishing extensive hydrogen bonds. In a different experiment OLZ was heated up to 120 °C with dehydration, cooled and heated again (Figure 8.4, B3 and B6).These samples revealed an increase of the PEG melting temperature in

line with its initial value (data not shown). This finding suggests reversibility of the conformational changes of the polymer chains occurred after removal of water in the sample.

There was no apparent conversion to the OLZ dihydrate for the samples which were formulated in the presence of both PVP and HPC, however some adsorbed water created a broad endotherm (Figure 8.4, C and D). In thermograms C) (curves 2 and 3) and D) (curves 2, 3, 5 and 6) the OLZ endotherm due to melting became broader, with a lower enthalpy and temperature than those observed in the physical mixture (curve 1). This shift towards lower temperatures indicates a higher miscibility of drug in the polymer after the wet massing process.

Table 8.2 shows the surface energy and the polarity for each polymer in the formulation. The results show the ranking for the measured hydrophobicity as HPC>PVP>PEG. Generally, for the binder (polymer) to spread over the substrate (API) in a wet massing process, the work of cohesion of the binder must be lower than that of the substrate, allowing the spreading of the first on the latter. This occurred just for HPC, only. These results were in line with the results obtained for the contact angles (Table 8.3) which have shown the wettability of the powders, as measured by the contact angle (°) of the substances in water. Table 2 shows the contact angle of the raw-materials separately and the contact angle obtained after the wet massing. While the contact angle of the particles in formulations B1, B2, D1 and D2 after wet massing showed a contribution of the contact angles of both polymers and OLZ, the contact angle of particles in formulation C1 (OLZ with HPC) seemed to account only on the contribution of HPC (Table 8.3). Furthermore, a slightly lower contact angle was observed for these particles than for the isolated HPC suggesting that this polymer was not only completely covering the crystalline particles of OLZ, but also a decreasing number of hydrophobic groups were exposed on the surface of the particles, as a result of polymer chain conformation.

Table 8.2 – Surface energy of OLZ and polymers.

	$\gamma^{d\ 1}$ (mN/m)	γ^{p} (mN/m)	γ^{1} (mN/m)	Polarity (%)	W_{c}^{2} (mJ/m^2)	W_{a}^{2} (mJ/m^2)	W_a-W_c (mJ/m^2)
OLZ	41.31	1.19	42.50	3	85.00		
PEG 6000	35.71	14.62	50.33	29	100.66	81.01	-19.65
PEG 40000	34.78	12.93	47.71	27	95.42	79.89	-15.53
PVP k12	43.22	7.48	50.71	15	101.42	88.59	-12.83
PVP k30	40.46	6.73	47.19	14	94.38	85.81	-8.57
HPC LF	31.90	4.80	36.70	13	73.40	75.81	2.41

[1] Surface free energy (γ) and its dispersive (γ^{d}) and polar (γ^{p}) components.
[2] W_c and W_a are, respectively, the work cohesion and the work of adhesion (to OLZ).
[3] W_a-W_c reflect the spreading coefficient (λ).

Table 8.3 – Contact angles of the raw materials and different formulations

Raw-Material	Contact angle* $(\theta / °)$	Formulations after massing t=0	Contact angle* $(\theta / °)$
OLZ	104.65 ± 0.64	A	104.87 ± 0.74
PEG 6000	63.60 ± 2.05	B1	81.24 ± 2.98
PEG 40000	64.30 ± 1.95	B2	79.52 ± 1.07
HPC-LF	91.84 ± 0.47	C	87.41 ± 1.72
PVP k12	56.46 ± 1.36	D1	79.73 ± 1.54
PVP K30	75.77 ± 2.17	D2	89.14 ± 3.40

*Contact angle measured in water (n=6)

8.5.2 Characterization of OLZ wet masses and pellets containing microcrystalline cellulose

For the formulations containing MCC, the ratio OLZ:polymer was maintained, as well as the amount of liquid used for the wet massing. The examination of the diffractograms acquired off-line after the wet massing (t=360 min) (Figure 8.5) revealed that the contact with the liquid binder triggered the hydrate formation in formulations A_M, $B1_M$ and $B2_M$ (Figure 8.5, A and B). In all these formulations, both OLZ dihydrate B and OLZ higher hydrate were observed in the wet mass. For formulations $B1_M$ and $B2_M$, the conversion of the anhydrous OLZ into 2 hydrates, instead of only one hydrate (B1 and B2), suggests that PEG was not interacting with the drug at the same extent as occurring without the MCC. Drying the pellets (Figure 8.5, A c and B c1 and c2) at 45ºC for 60 min was not sufficient to remove the dihydrate B, which was visible in both OLZ formulations (Figure 8.5, A c and B c1 and C2).
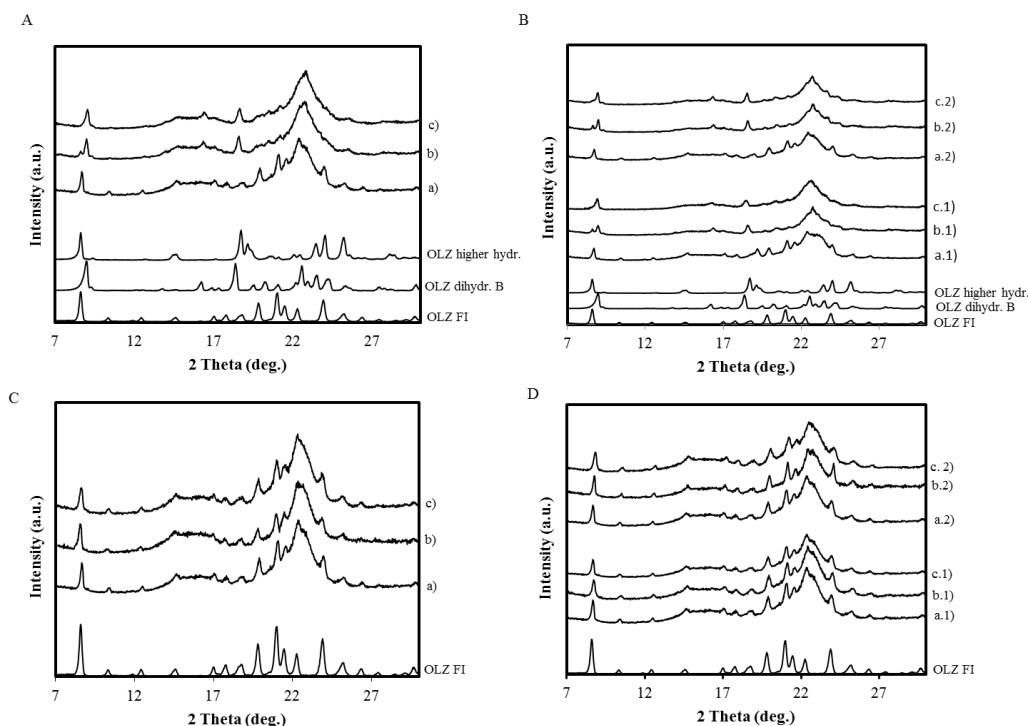
**Figure 8.5 – Diffractograms of formulations as physical mixtures (a),
as wet masses (t=360 min, b) and dried pellets (c).**
A) Formulation A_M;
B) Formulation $B1_M$ (a.1-c.1) and $B2_M$ (a.2-c.2);
C) Formulation C_M;
D) Formulation $D1_M$ (a.1-c.1) and $D2_M$ (a.2-c.2).

Figure 8.6 (A) shows the dissolution curves of OLZ released from pellets prepared immediately before the test. For each formulation, dissolution profiles were obtained from A_M, $B1_M$ (PEG 6000), C_M (HPC) and $D2_M$ (PVP k30) pellets made from non-stored (#1, i.e., t=0) and stored (#2, i.e., t=360 min) wet masses. A significant change on OLZ dissolution rate (p< 0.05) was observed between #1 and #2 pellets for A_M and $B1_M$ formulations. On contrary, no significant differences on the OLZ dissolution rate from pellets #1 and #2 from formulations C_M (HPC) and $D2_M$ (PVP), although a slight increase on OLZ dissolution rate was verified for pellets #2.

During dissolution it was possible to characterize the OLZ solid-state form remaining in the pellets. The 2nd derivative from FTIR absorbance spectra of the pellets taken from the dissolution media, have shown that PVP and HPC can also have a suppressing effect on the OLZ hydrate conversion in the dissolution media, by opposition to pellets A_M (no polymer) and $B1_M$ (PEG) in which OLZ suffered hydration. This observation strongly suggests that HPC and PVP, which had shown a strong protection of OLZ over the production of wet masses, also stabilize the anhydrous OLZ over the release from pellets into the dissolution medium.
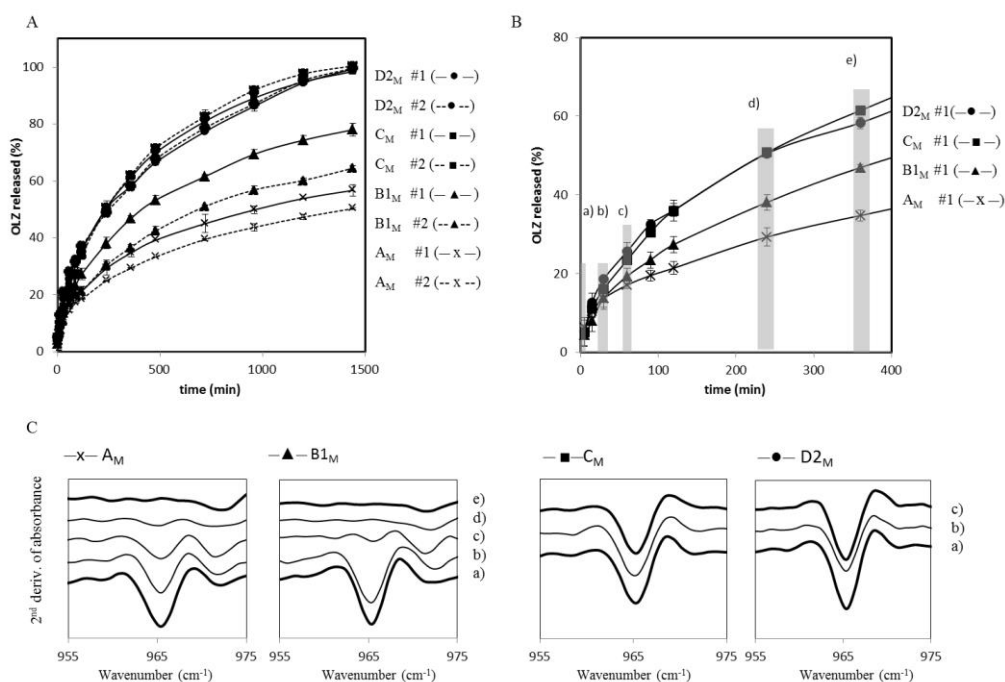
Figure 8.6 – Dissolution profiles of OLZ from pellets (top) and Spectra (FTIR) analysis made from different formulations (A_M, $B1_M$, C_M and $D2_M$).
A) Dissolution profiles of OLZ from pellets #1 (t=0 min) and #2 (t=360 min);
B) Formulations and the time periods (a-e) in which pellets were collected for FTIR chacterization;
C) Second derivative of FTIR absorbance spectra from collected samples (times a-e for
formulations AM and B1M and times c-d for formulations C_M and $D2_M$).

Table 8.4 summarizes the results of OLZ release modelling for the pellets under investigation. The goodness of fit for the various models ranked in the order: Korsmeyer-Peppas > Higuchi > First-order for the formulations A_M, $B1_M$ and C_M. For formulation $D2_M$, the goodness of fit for first-order model was better than for Higuchi model. The fact that drug release from pellets follows Korsmeyer-Peppas model and the values of the exponent *n are* lower than 0.5 (0.383–0.441) indicate that the OLZ, independently of the polymorphic form present in the pellets follows a diffusion controlled release.

Table 8.4 – Fitting of dissolution models to OLZ release data for pellets

Formulation		First-order Model			Higuchi Model			Korsmeyer-Peppas Model			
		Adj R^2	MSE root	K_1	Adj R^2	MSE root	k_H	Adj R^2	MSE root	k_{KP}	n
A_M	#1	0.669	9.946	0.001	0.952	3.797	1.648	0.997	0.958	3.585	0.383
	#2	0.706	8.624	0.001	0.970	2.728	1.441	0.995	1.127	2.676	0.407
$B1_M$	#1	0.820	10.15	0.002	0.962	4.674	2.218	0.994	1.794	4.442	0.395
	#2	0.839	8.466	0.001	0.986	2.464	1.821	0.995	1.554	2.703	0.441
C_M	#1	0.951	6.910	0.002	0.986	3.810	2.696	0.995	2.226	4.450	0.431
	#2	0.926	8.408	0.003	0.973	5.044	2.755	0.995	2.353	4.966	0.411
D_M	#1	0.972	5.697	0.003	0.958	6.991	2.995	0.980	4.801	5.510	0.408
	#2	0.978	5.115	0.003	0.956	7.321	3.069	0.981	4.658	5.494	0.410

#1 and #2 represent pellets manufactured at t=0 min and t=360 min of wet masses, respectively.

8.6 Discussion

The different crystalline forms of OLZ are built through the assemblage of (OLZ) centrosymmetric racemic pairs and then connected to each other through hydrogen bonds, either from atoms like in the OLZ structure (e.g. anhydrous form) or by water molecules (e.g. hydrate forms). In form I the hydrogen bond interactions between the amine and imine (NH-N) are responsible for the connection of two different OLZ pairs (18). When the hydrate formation occurs the NH-N interactions are disrupted and replaced by water bridging molecules between the dimmers. The presence of water balances the hydrogen bond donor/acceptor ratio of OLZ, thus making 2 acceptors able to participate in hydrogen-bonding, which was not possible in the anhydrates. Therefore, in OLZ hydrates, a single hydrogen-bond donor (NH) and two good acceptors (imine and piperidine) may participate in hydrogen bonding with water. In manufacturing processes in which water is added (e.g. wet extrusion) OLZ is exposed to conditions in which the hydrate forms are expected to be the most stable due to high water activity (224). Consequently, starting from the addition of water until the final drying, the API may undergo an anhydrate to hydrate transformation which may or, may not, be completed by the end of the process. The API transformations in an aqueous environment are expected to occur via a solvent-mediated transformation (SMT) (224) which encompasses a three stage process. Firstly, the metastable phase starts to dissolve, in this work the anhydrous OLZ. Since the dissolution of the metastable phase is a prerequisite for the transformation to take place, the solubility of the metastable form will initially provide the thermodynamic driving force for the phase transformation. Dissolution under non-sink conditions will lead to a supersaturation with

respect to the stable hydrate phase and provide a thermodynamic driving force for nucleation of the stable phase (hydrate). The next stage involves nucleation of the stable hydrate once supersaturation has been reached. During wet massing of powders, which can be regarded as a suspension, there is an abundance of particles in the form of the anhydrate phase, which might aid heterogeneous nucleation (285). By opposition to homogeneous nucleation, heterogeneous nucleation lowers the thermodynamic free energy barrier. Thus, heterogeneous nucleation can occur at lower driving forces (44). Finally, once nuclei of the stable form are present in the solution, growth of that form continues until all the metastable phase has dissolved. Therefore, the growth of the stable phase (hydrate) is maintained by the supersaturation created by the dissolution of the metastable phase (286). The kinetics of solvent-mediated transformations is therefore governed by dissolution of the unstable phase and nucleation and growth of the stable phase. It follows that, if nucleation of the hydrate phase could not be inhibited by polymers, then crystal growth could occur, i.e., inhibition of crystal growth only became important if seeding crystals were present.

When observing the XRPD data obtained from the masses without the presence of excipients, one could observe that hydration of all of the material was not finished in the time scale of the wet massing step and that a concomitant crystallization of both dihydrate B and higher hydrate took place on the OLZ wet mass A. This phenomenon may be associated with the similar nucleation rates of both forms, favoring the concomitant crystallization of both hydrates (44). The kinetics of this process was controlled by the dissolution rate of the unstable form, the rate of crystallization of the more stable form and their relative solubilities. It means that in wet massing, the extent of hydrate formation is proportional to the solubility of the anhydrate and the volume of the wetting liquid used (82). Furthermore, since that wetting of powders is a factor governing hydrate formation kinetics (287), it is clear that the APIs with poor wettability will require an excessive amount of moisture and/or prolonged contact with wet massing liquid for the hydrate to form. Thus, the short wet massing period together with the low wettability of OLZ ($\theta \approx 104°$) led to the incomplete hydrate conversion of OLZ during wet massing. Furthermore its low solubility (288) (a small quantity of OLZ can be dissolved in the liquid at any time) resulted in a slower hydrate rate conversion, which contrasts with other drugs such as theophylline (solubility in water of 12 mg/mL) (224) or sulfaguanidine (solubility in water of 1.38 mg/mL) that showed to hydrate in less than 5 minutes during wet granulation processes (224).

The presence of the polymers in the wet mass can cause stabilization of OLZ anhydrous phase by increasing the local viscosity, impeding diffusion of drug molecules, and increasing thermodynamic and kinetic barriers for nucleation. Furthermore, polymers can kinetically stabilize the supersaturated state by forming intermolecular interactions with the drug via hydrogen bonding or hydrophobic interactions. They can also promote steric hindrance to the

crystallization process (224). The addition of PEG 6000 and 40000 to the formulations, respectively B1 and B2, has retarded the hydrate conversion without no concomitant crystallization into two different hydrates. The disappearance of the XRPD pattern of the PEG (semi-crystalline nature, which facilitates its distinction when compared with other amorphous polymers) was observed in the PEG wet masses (B1 and B2), which was indicative of its dissolution into the wet massing medium. Therefore, an increase on the viscosity of the binding liquid is expected due to the high network associations of these polymers. This change on the reological properties of solvent, contributes to restraints the diffusivity of the API. A reduction on the drug's diffusivity, reduces the degree of supersaturation (118), affecting both nucleation and crystal growth rates (44) (118).

The effect of the viscosity of the medium on the nucleation rate has been described by Turnbull and Fisher (289) The frequency of atomic or molecular transport at the nucleus-liquid interface (v) is inversely related to the bulk viscosity, η, with the Stokes-Einstein relation:

$$V = \frac{kT}{3\pi a_0^3 \eta(T)}$$

Eq.8.1

Where a_0 is the mean effective diameter of the diffusing species, k, is a constant and T is temperature. If the viscosity dependence on temperature is described by Arrhenius behavior, then:

$$J = \frac{K}{\eta_0} \exp\left(\frac{-\Delta G^* - \Delta G_a}{K_B T}\right)$$

Eq. 8.2

J is the number of nuclei formed per unit time per unit volume, ΔG* is the maximum in Gibbs free energy change for the formation of clusters, at a certain size. ΔGa is the activation energy for transport across the nucleus-liquid interface.

Therefore, the addition of PEG may have changed the nucleation kinetics, favoring the appearance of a single form – higher hydrate- which is never obtained as an isolated form in water environments without any additive.

On the other hand, a complete inhibition of OLZ hydration was achieved by addition of both HPC and PVP. According to the literature, there are two major factors that lead to an efficient hindrance of the hydrate formation by the polymeric excipients: the capacity to form hydrogen bonds with the drug and a sufficient hydrophobicity (194). Both these features prevent the drug from binding with water and force it to bind with the polymer instead (194, 224, 290), which are important factors affecting the nucleation and growth rates of crystals.

The capacity to form hydrogen bonds can affect the nucleation rates. For nucleation to occur, drug–polymer hydrogen bonds have to be broken so that drug molecules may diffuse and form a nucleus. The strength of the drug–polymer association determines the time required for the nucleation to take place (194). Furthermore, the ability of polymers to adsorb to the crystal

surface interface (also by formation of hydrogen bonding between the polymer and the drug) are able to block the crystal growth by preventing the access of the solute molecules to the crystal terrace (39). In the wet masses with HPC (C) and PVP (D) OLZ molecules may interact with the polymer molecules to form OLZ–polymer hydrogen bonds in the aqueous environment. These interactions may, then, inhibit or retard the formation of nuclei due to collisions or/and block the growth of the crystals.

When the content of HPC, PVP k30 and PVP k12 was reduced by two orders of magnitude in formulations C, D1 and D2, respectively, only HPC has shown to continue to inhibit hydrate conversion which can easily be explained by both the hydrogen's bond ability of the involved polymers and spreading over OLZ particles. In a different experiment, where hydrate seeds were added to the wet masses, transformation times decreased for PVPs. When hydrate seeds were added to the HPC formulation the hydrate transformation continued to be inhibited during the 6 h of the test, indicating that HPC can effectively inhibit the crystal growth. Although PVP was not successful on preventing transformations, polymer Mw had an impact (formulations D1 and D2). In both cases the nucleation step was no longer a limiting factor but nuclei grew at different rates: faster for PVP k12 (more hydrophilic) than for PVP k30. This was also observed by other authors (194) for which the inhibition effect of polymers on carbamazepine was also related to their hydrophobicity, since polymers with a higher hydrophobicity had a stronger interaction with the carbamazepine crystal surface. Also, the slower hydration rate of OLZ in presence of PVP k30 can be attributed to an increase in the number of available functional groups on the polymer chains (39).

Data has shown that HPC had a lower polarity (higher hydrophobicity), and a lower work of cohesion than the work of adhesion to the OLZ molecules. This showed the ability of this polymer to spread over the OLZ crystal surfaces. The other more hydrophilic polymers were not so successful on spreading on OLZ surfaces. These results indicate affinity of this polymer to OLZ surfaces, which when absorbed at relevant growth sites may have led to a blockage of the growth of the nuclei.

The addition of cellulose (MCC) to the wet masses as an excipient did not have an effect on the inhibition of hydrate conversion, and the respective formulations AM, B1M and B2M, OLZ were shown to hydrate in the same manner as had occurred in formulations without HPC or PVP. However, while in formulation B1 and B2 only one hydrate was obtained (higher hydrate), in formulations with cellulose (B1M and B2M), two hydrates were visible in the wet mass (dihydrate B and higher hydrate). This loss of selectively of hydrate conversion indicates a reduction of the close contact between the polymer (PEG) and the drug.

A better understanding of the dissolution process can be accomplished by analyzing not only the drug in the liquid dissolution medium but also in the solid state of the dissolving sample, which provides a more complete understanding of the dissolution behavior.

The fast and similar dissolution rate of OLZ present in all the different pellets formulations at the very beginning can be partly explained by the dissolution of OLZ anhydrate before the hydrates began to crystallize. Moreover, the dissolution of OLZ particles on the surface of the pellet can promote the burst effect during the first few minutes.

The mechanism by which OLZ hydrates in the dissolution vessel is expected to be the same as the one that occurs when OLZ is subjected to the wet massing process, since in this situation the drug is also exposed to a solvent. Aaltonen et al. (291) reported hydration by solvent-mediated phase transformation of theophylline and nitrofurantoin during dissolution in purified water. The FTIR absorbance spectra of OLZ present in the pellets after being for different periods in the dissolution medium (not dissolved OLZ fraction) showed that both PVP and HPC had a suppressing effect on the OLZ hydrate formation during the dissolution test, which coincides with the best performance of OLZ.

During the dissolution process of the pellets, several processes competing with each other may take place simultaneously, such as: dissolution of OLZ, recrystallization of anhydrous OLZ to OLZ hydrated, swelling of the polymer and dissolution of the polymer. The polymers that were shown to strongly interact with the drug during the wet massing of OLZ may also stabilize the anhydrous OLZ during the dissolution by inhibiting aggregation due to a stronger interaction between the drug and polymer in the dissolution media. Therefore, the interaction with the polymers prevents the formation of the hydrate crystals, thus rendering the drug dispersed in the matrix of the polymer easier to dissolve.

8.7 Conclusion

In an attempt to clarify the mechanisms underlying the effect of polymeric excipients on the hydrate conversion of anhydrous OLZ in aqueous environments, the impact of various polymers on the hydration of OLZ in wet masses was investigated. The polymer screening methodology used to identify polymers that could stabilize OLZ during wet massing proved to be useful to identify which polymers may have the strongest effect of inhibition of OLZ. In general all polymers promoted the inhibition of the transformation with different degrees of success, provided the contact time of OLZ anhydrous with water was low (e.g., less than 30 min). PEGs delayed the conversion of OLZ, but after 360 min of storage in a moist environment, conversion was observed. The HPC had the strongest effect on protecting the hydrate conversion of OLZ. The major reduction of the wettability of the OLZ powders in a blend with HPC revealed that this polymer can adsorb to OLZ's surface inhibiting the water attack and, therefore, causing a hydrate formation.

The presence of microcrystalline cellulose in formulations, needed for the pellets production, neither improves the protection against water nor did it eliminate the protector effect of both PVP and HPC. Conversion of the anhydrous form into hydrate was partially reversible

and occurred during the wetting, and dissolution test in which the anhydrous form was converted into a hydrate. The combination of data retrieved from the different analytical techniques (FTIR spectroscopy, XRPD, calorimetry and microscopy) was successfully used to investigate the hydrate conversion of OLZ in various excipients allowing visualizing the different hydrate conversions that OLZ may undergo in the presence of excipients.

The results of this work are relevant to industrial practice as they can orient choice towards the most appropriate excipients for industrial production of OLZ and support the preparation of extrudates at lower cost, with lower risks of lot-to-lot variability and with improvements in biopharmaceutical properties.

CHAPTER 9

Conclusions and Future work

Chapter 9 - Conclusions and suggestions for future work

9.1 Concluding Remarks

The research of polymorphism and pseudopolymorphism of APIs provides important information about the stability of the drugs during pharmaceutical processing. Health Authorities require manufacturers to provide evidence of the polymorphic form of the drug and its stability. When different excipients are combined with the API to allow the manufacturing of a medicine they can contribute to changes on the molecular organization of a drug molecule. It is therefore in the interest of regulators and industry that the polymorphic changes of an API are well characterized and documented in order to prevent problems in the process and final products.

The work presented in this Thesis was focused on the characterization of different molecular organizations of OLZ. The impact of polymorphism/pseudopolymorphism on OLZ's technological performance and dissolution was evaluated.

Overall, this work has highlighted the importance of studying OLZ when it is exposed to different environmental conditions (e.g. temperature, humidity and pressure) and processing techniques, such as tableting (a dry process run at room temperature), extrusion (a wet process requiring drying) and RESS/RESSAS (a supercritical fluid is used as a solvent) to evaluate their stability and rate of conversion into a different polymorph. During the processing of the polymorphic drugs, special attention was paid to the excipients used in the formulations, namely polymers. This strategy was important to understand how some excipients may stabilize the drug, inhibiting polymorphic conversions during pharmaceutical processing.

Therefore, the characterization of the different polymorphic transformations was performed by using several techniques, such as calorimetry (DSC, TGA, DMA), powder diffractometry (XRPD), infrared spectroscopy (FTIR, Raman), microscopy (optical, electronic, hot stage and atomic force) and surface free energy analyses.

In the chapter 3 of this Thesis one has focused on the environmental conditions that can affect the stability of anhydrous forms of OLZ. In this study we aimed to predict if high relative humidity could induce hydrate transformations and the impact of those conversions on the dissolution of the drug. Our results showed that anhydrous forms could not hydrate at RH below 75% (anhydrous Form I) and 53 % (anhydrous Form II) at room temperature. At 93% RH and 75% RH, pseudopolymorphic transitions can occur for form I and II, respectively. The dihydrate conversion of the anhydrous forms revealed to decrease their rate of dissolution. This revealed to be significant for OLZ Form I, which proved to hydrate into the most stable dihydrate form – Dihydrate D. These results clarified the negative impact that the appearance of these hydrated forms may have if the RH during the storage of the raw materials is not controlled.

During the same study it was possible to develop a method to measure the hydration of anhydrous Form I and II during storage through DRIFT analysis. This method was achieved due to visible differences between the IR spectra of both anhydrous forms and dihydrates.

In chapter 4 the interplay between Form I, humidity and excipients was analyzed. The effect of compaction on water sorption of OLZ in presence of excipients was also characterized. The kinetics of hydrate formation showed to be highly affected if polymeric excipients are physically mixed with the drug. Polymeric excipients, such as PEG and HPC showed to induce hydrate transformation at 75% RH, which was a RH where OLZ was not able to hydrate when stored by itself. PVP showed to avoid hydrate conversions at 93% relative humidity, whereas PEG accelerated hydrate conversion at the same humidity. The OLZ dihydrate formed during storage was always the same, the dihydrate D form, which is the dihydrate form of OLZ with the lowest dissolution rate. Storing the physical mixtures as powders or tablets proved to have an impact on hydrate formation rates. Tableting showed to accelerate the hydrate formation during the first week of storage due to a reduction of crystallinity of the OLZ material when subjected to pressure. Also, the higher contact interaction between OLZ and the polymers enabled PEG to induce the complete dihydrate conversion of OLZ material in only 7 days of storage at 93% RH. In tablets, however, the lower surface area exposed to humidity retarded the hydration of OLZ during the further days of storage in comparison to the powders. This study emphasized the importance of the right choice of polymers in order to maintain the drug stable both during formulation and shelf life.

In chapter 5 the process of OLZ hydrate transformations in an aqueous medium and the mechanism of interaction between OLZ and various polymers in aqueous suspension was explored. The results showed that polymers were able to affect OLZ hydration by both hydrogen bonding with OLZ and sufficient hydrophobicity to adsorb into the crystals surface interface, blocking access of the solute molecules to the crystal terrace.

Chapter 6 showed that SCF technology produces OLZ particles with submicron size and increased dissolution rate. Production and stabilization of OLZ nanoparticles and nanosuspensions was achieved by using RESS and RESSAS technologies. RESSAS enabled to decrease the particle size of OLZ with a final recovery of almost 100% of the drug that was dissolved in $scCO_2$, thus indicating no drug loss by the CO_2 stream. However, when RESSAS approach was used as a tool to obtain particles in the nanoscale, it was paramount to find a compromise between process operability and formulation stability. This study showed that the choice of stabilizer had a critical influence on the stability of nanosuspensions, particle size distribution and the expansion process itself. The particle growth and hydrate formation of OLZ showed to coincide with the insufficiently stabilized colloidal suspensions. The suppression of particle growth and hydrate formation showed to be mechanistically related to a surface interaction of the drug with the excipient used in suspension, being those processes related

Extrusion and spheronisation of wet masses involves both wetting and drying, which are steps that could promote solid-state modifications of OLZ. In Chapter 7 it was possible to observe that anhydrous OLZ Form I hydrated into 2 different hydrates (dihydrate B and higher hydrate) when exposed to aqueous environments involved in wet extrusion process. Higher ratios of MCC in the formulations showed to retard the hydrate conversion of OLZ, as a consequence of the higher affinity of water to the amorphous regions present in the molecular structures of this excipient. PEG proved to be an excipient which could not protect hydrate formation during extrusion. Applying low temperatures of drying (45^0C) for less than 60 minutes proved to be ineffective in eliminating the dihydrate B. The presence of this hydrate showed to reduce OLZ's dissolution rate. The changes in crystalline structure of OLZ during the process showed to affect the rheology of the wet mass and the size and strength of the dried pellets. These results suggested that attention should be given to the pseudopolymorphism of the drugs before the selection of the excipients and process conditions for a new pharmaceutical process. Thus, in chapter 8, attention was payed to the ability of polymeric excipients to avoid the crystalline changes of OLZ when wetting of the OLZ is required during the pharmaceutical processing. Chapter 8 also aimed to determine whether the protector effect by excipients was also present during the dissolution of OLZ from the formulated pellets or not. The results showed that when using PVP and HPC polymers in extrusion process the hydrate formation in wet masses is avoided, even in the presence of other excipients (eg. MCC). Hydrophobicity and surface energy calculations helped to elucidate why HPC was the best polymer to be used in a wet extrusion process. The inhibition of the conversion of OLZ into lower soluble dihydrate forms during both wet extrusion and dissolution testing showed to have a favorable impact on the dissolution profile of the drug. Since OLZ is a drug used in mental disorders (e.g. schizophrenic and bipolar disorders) and very often used in prolonged therapies, small variations on its solubility may delay the fraction of API dissolved from the dosage form. Therefore, absorption may be compromised with a negative impact on the patients' behavior.

Overall, one could conclude that polymorphic/pseudopolymorphic changes of OLZ can occur during storage and pharmaceutical processing, with an impact on the drug's performance. Furthermore, these solid-phase transformations of OLZ could be easily monitored by infrared techniques (FTIR/DRIFT), even in the presence of excipients. On the other hand, interaction between the drug and excipients could be studied at the molecular level using nuclear magnetic resonance. The prevention of hydration of OLZ, showed to be easily avoided by the right choice of excipients.

In-depth knowledge of hydrated forms of OLZ and their stability under different experimental conditions is essential to the development of successful drug products. From an industrial point of view, changes in process variables (process parameters, equipment used, excipient characteristics and their amount) should be carefully studied in order to validate the

processes in use and reduce the risks of variability between batches. The results of this work are relevant to the industrial practice as they can orient choice towards the most appropriate excipients for industrial production of OLZ and support the preparation of tablets/extrudates at lower cost and with improvements in their biopharmaceutical properties, for example.

9.2 Recommendations for Future Work

The work developed, regardless of the findings described in this Thesis, can be considered as a starting point for new projects as it only addresses a part of the challenges facing the polymorphism study during pharmaceutical development. This work aimed to understand the main challenges when processing olanzapine, however, the results showed us that there were some results that need to be studied in more detail.

In order to continue this research path it would be very important to explore the following areas:

1- Control and characterization of the conversion kinetics of olanzapine polymorphs to the hydrate forms in aqueous suspensions using RAMAN (online) technology.
   The conversions of olanzapine could be monitored and the kinetics of transformation characterized in more detail. RAMAN technology can be used in the presence of solvents (e.g. wet granulation). Furthermore, it does not need any sample preparation, is non-destructive and avoids water interference;

2- Using a combination of molecular dynamics (MD) simulations and docking calculations to model and predict polymer-drug interactions and therefore understand the subtle structural features that can significantly affect the effectiveness of the protection of hydration by polymers. The computational calculations of polymer-drug pairs hold the potential of becoming a powerful pre-screening tool in the excipients selection process for a new solid-dosage form, with an impact on the stabilization of the drug;

3- Determine adsorption isotherms to quantify the amount of polymer adsorbed onto the API crystals. Different experimental techniques can probe the interactions between drug and polymers. For example, NMR relaxation time measurements can determine the fraction of stabilizer molecule "bound" to the interface. This method distinguishes adsorbed polymer chains from those in bulk solution. NMR can discriminate between highly mobile (liquid-like) and immobile (solid-like) protons on the basis of magnetic relaxation times. Other analytical techniques have been developed for monitoring polymer solution concentrations. Some are specific to a given polymer or group of polymers (e.g., complex formation to give species which adsorb in the visible/uv part of the electromagnetic spectrum). Other techniques, such as solution depletion method are used to quantify adsorption of polymers

to drug seed crystals using size exclusion chromatography (SEC-HPLC) to measure polymer concentrations adsorbed per crystal unit surface area;

4- Preparation of solid dispersions of olanzapine with the same polymers used in this study. The preparation of these solid dispersions has shown a considerable potential for the solubility enhancement of various active pharmaceutical ingredients belonging to BCS class II.

CHAPTER 10

Appendices

Table A.1– Values for axis length a, b and c and angles α, β and γ of the unit cell of both forms I and II of olanzapine. Standard errors are represented in the second line.

	a	b	c	α	β	γ
Form I	10.436	14.902	10.605	90	100.630	90
	0.039	0.013	0.033	0	0.729	0
Form II	9.8448	16.340	9.983	90	98.280	90
	0.0289	0.0187	0.0201	0	0.368	0

Table A.2– Integer Miller indices (h, k, l) of both forms I and II of olanzapine

	h	k	l	2θ (obs)	2θ (Calc)	diff.
Form I	1	0	0	8.6145	8.6203	-0.0058
	0	1	1	10.3515	10.3566	-0.0051
	-1	1	1	12.4325	12.4429	-0.0104
	0	2	1	14.5455	14.6129	-0.0674
	0	0	2	16.9906	17.0129	-0.0223
	2	0	0	17.3087	17.2899	0.0188
	1	2	1	17.7287	17.7763	-0.0476
	-1	1	2	18.602	18.596	0.006
	-2	1	1	18.784	18.7872	-0.0032
	0	3	1	19.7972	19.7978	-0.0006
	-1	3	1	20.9595	20.9814	-0.0219
	-2	2	1	21.4366	21.4612	-0.0246
	1	3	1	22.2487	22.2566	-0.0079
	0	4	0	23.8707	23.8834	-0.0127
	2	3	0	24.9511	24.954	-0.0029
	-1	3	2	25.1814	25.1799	0.0015
	0	1	3	26.3205	26.3388	-0.0183
	1	4	1	27.3922	27.3727	0.0195
	-3	1	2	29.1066	29.0947	0.0119
	2	4	0	29.6388	29.636	0.0028
	1	4	2	31.7919	31.667	0.1249
	1	3	3	33.8474	33.9244	-0.077
	0	0	4	34.4653	34.4159	0.0494
Form II	0	0	1	8.9400	8.9510	-0.011
	0	1	1	10.4222	10.4635	-0.0413
	0	2	0	10.8337	10.828	0.0057
	-1	1	1	12.9082	12.9908	-0.0826
	0	1	2	18.8031	18.7667	0.0364
	-1	1	2	19.6433	19.7068	-0.0635
	0	2	2	20.9526	21.0156	-0.063
	0	4	0	21.715	21.7543	-0.0393
	2	1	1	22.1463	22.1562	-0.0099
	1	4	0	23.65	23.615	0.035
	2	2	1	24.0757	24.104	-0.0283
	-1	4	1	24.8946	24.8189	0.0757
	2	0	2	27.5207	27.5066	0.0141
	2	1	2	28.0913	28.0538	0.0375
	0	5	1	28.7343	28.7719	-0.0376
	0	2	3	29.3155	29.2387	0.0768
	1	1	3	30.3208	30.3738	-0.053
	-2	1	3	30.9986	30.9958	0.0028
	-2	2	3	32.4926	32.4509	0.0417

References

1. Cui Y. A material science perspective of pharmaceutical solids. International Journal of Pharmaceutics 2007;339(1-2):3-18.

2. Singh D, Marshall PV, Shields L, York P. Solid-state characterization of chlordiazepoxide polymorphs. Journal of Pharmaceutical Sciences. 1998;87(5):655-62.

3. Qi S, Avalle P, Saklatvala R, Craig DQ. An investigation into the effects of thermal history on the crystallisation behaviour of amorphous paracetamol. European Journal of Pharmaceutics and Biopharmaceutics : official journal of Arbeitsgemeinschaft fur Pharmazeutische Verfahrenstechnik eV. 2008;69(1):364-71.

4. Hancock BC, Zografi G. Characteristics and significance of the amorphous state in pharmaceutical systems. Journal of Pharmaceutical Sciences 1997;86(1):1-12.

5. Singhal D, Curatolo W. Drug polymorphism and dosage form design: a practical perspective. Advanced Drug Delivery Reviews. 2004;56(3):335-47.

6. Zhang GG, Law D, Schmitt EA, Qiu Y. Phase transformation considerations during process development and manufacture of solid oral dosage forms. Advanced Drug Delivery Reviews. 2004;56(3):371-90.

7. Hancock BC. Disordered drug delivery: destiny, dynamics and the Deborah number. The Journal of Pharmacy and Pharmacology. 2002;54(6):737-46.

8. Cullity BD, Stock SR. Elements of X-Ray Diffraction (3rd Edition): Prentice Hall; 2001.

9. Guillory K. Generation of polymorphs, hydrates, solvates, and amorphous solids. In: Brittain HG, editor. Polymorphism in Pharmaceutical Solids. New York: Marcel Dekker; 1999. p. 183-226.

10. Nichols G. Light Microscopy. In: Hilfiker R, editor. Polymorphism: in the Pharmaceutical Industry. Wiley-VCH Verlag GmbH & Co. KGaA; 2006. p. 167-209.

11. USP 27 2004 TUSP. Mongraph 776 (Optical Microscopy). 12601 Twinbrook, Parkway, Rockvillw, MD 20852: United States Pharmacopeial Convention, Inc.

12. Moriyama K, Furuno N, Yamakawa N. Crystal face identification by Raman microscopy for assessment of crystal habit of a drug. International Journal of Pharmaceutics. 2015;480(1–2):101-6.

13. Schorsch S, Hours J-H, Vetter T, Mazzotti M, Jones CN. An optimization-based approach to extract faceted crystal shapes from stereoscopic images. Computers & Chemical Engineering. 2015;75:171-83.

14. Pingali KC, Shinbrot T, Cuitino A, Muzzio FJ, Garfunkel E, Lifshitz Y, et al. AFM study of hydrophilicity on acetaminophen crystals. International Journal of Pharmaceutics. 2012;438(1–2):184-90.

15. Haleblian J, McCrone W. Pharmaceutical applications of polymorphism. Journal of Pharmaceutical Sciences. 1969;58(8):911-29.

16. Yu L, Reutzel-Edens SM, Mitchell CA. Crystallization and Polymorphism of Conformationally Flexible Molecules: Problems, Patterns, and Strategies. Organic Process Research & Development. 2000;4(5):396-402.

17. Roy S, Aitipamula S, Nangia A. Thermochemical Analysis of Venlafaxine Hydrochloride Polymorphs 1−5†. Crystal Growth & Design. 2005;5(6):2268-76.

18. Reutzel-Edens SM, Bush JK, Magee PA, Stephenson GA, Byrn SR. Anhydrates and Hydrates of Olanzapine: Crystallization, Solid-State Characterization, and Structural Relationships. Crystal Growth & Design. 2003;3(6):897-907.

19. Haisa M, Kashino S, Maeda H. The orthorhombic form of p-hydroxyacetanilide. Acta Crystallographica Section B. 1974;30(10):2510-2.

20. Haisa M, Kashino S, Kawai R, Maeda H. The Monoclinic Form of p-Hydroxyacetanilide. Acta Crystallographica Section B. 1976;32(4):1283-5.

21. Lee AY, Erdemir D, Myerson AS. Crystal polymorphism in chemical process development. Annual Review of Chemical and Biomolecular Engineering. 2011;2:259-80.

22. Giron D. Thermal analysis and calorimetric methods in the characterisation of polymorphs and solvates. Thermochimica Acta. 1995;248:1-59.

23. Burger A, Lettenbichler A. Polymorphism and preformulation studies of lifibrol. European Journal of Pharmaceutics and Biopharmaceutics. 2000;49(1):65-72.

24. Guideline for Submitting Supporting Documentation in Drug Applications for the Manufacture of Drug Substances, FDA. 1987.

25. Specifications: test procedures and acceptance criteria for new drug substances and new drug products: chemical substances. ICH Harmonised Tripartite Guideline. Q6A. 1999.

26. Burger A, Ramberger R. On the polymorphism of pharmaceuticals and other molecular crystals. I. Mikrochimica Acta. 1979;72(3-4):259-71.

27. Yu L, Reutzel SM, Stephenson GA. Physical characterization of polymorphic drugs: an integrated characterization strategy. Pharmaceutical Science & Technology Today. 1998;1(3):118-27.

28. Rodríguez-Spong B, Price CP, Jayasankar A, Matzger AJ, Rodríguez-Hornedo Nr. General principles of pharmaceutical solid polymorphism: A supramolecular perspective. Advanced Drug Delivery Reviews. 2004;56(3):241-74.

29. Bernstein J, Davey RJ, Henck JO. Concomitant Polymorphs. Angewandte Chemie (International ed in English). 1999;38(23):3440-61.

30. Volmer M. Kinetik der Phasenbildung. Steinkopf, Leipzig. 1939.

31. Stranski I, Totomanov D. Zeitschrift für Physikalische Chemie. 1933; A163: 399.

References

32. Avramov I, Rüssel C, Avramova K. Conditions for metastable crystallization from undercooled melts. Journal of Non-Crystalline Solids. 2004;337(3):220-5.

33. Myerson A. Crystallization basics In: Myerson A, editor. Molecular modeling applications in crystallization. New York: Cambridge University Press; 1999. p. 55–105.

34. Beckmann W. Seeding the Desired Polymorph: Background, Possibilities, Limitations, and Case Studies. Organic Process Research & Development. 2000;4(5):372-83.

35. Rodríguez-Hornedo N, Kelly RC, Sinclair BD, Miller JM. Crystallization: General Principles and Significance on Product Development. In: Swarbrick J, editor. Encyclopedia of Pharmaceutical Technology. 3rd ed. New York: Informa Healthcare; 2006. p. 834-57.

36. Fujiwara M, Nagy ZK, Chew JW, Braatz RD. First-principles and direct design approaches for the control of pharmaceutical crystallization. Journal of Process Control. 2005;15(5):493-504.

37. Togkalidou T, Tung H-H, Sun Y, Andrews A, Braatz RD. Solution Concentration Prediction for Pharmaceutical Crystallization Processes Using Robust Chemometrics and ATR FTIR Spectroscopy. Organic Process Research & Development. 2002;6(3):317-22.

38. Braatz RD. Advanced control of crystallization processes. Annual Reviews in Control. 2002;26(1):87-99.

39. Warren DB, Benameur H, Porter CJ, Pouton CW. Using polymeric precipitation inhibitors to improve the absorption of poorly water-soluble drugs: A mechanistic basis for utility. Journal of Drug Targeting. 2010;18(10):704-31.

40. Perepezko JH. Nucleation reactions in undercooled liquids. Materials Science and Engineering: A. 1994;178(1):105-11.

41. Gunton JD. Homogeneous Nucleation. Journal of Statistical Physics. 1999;95(5-6):903-23.

42. Blagden N, de Matas M, Gavan PT, York P. Crystal engineering of active pharmaceutical ingredients to improve solubility and dissolution rates. Advanced Drug Delivery Reviews. 2007;59(7):617-30.

43. Florence A, Attwood D. Physicochemical Principles of Pharmacy. 4th ed. London: Pharmaceutical Press; 2006. 492 p.

44. Rodríguez-Hornedo N, Murphy D. Significance of controlling crystallization mechanisms and kinetics in pharmaceutical systems. Journal of Pharmaceutical Sciences. 1999;88(7):651-60.

45. Davey RJ, Allen K, Blagden N, Cross WI, Lieberman HF, Quayle MJ, et al. Crystal engineering - nucleation, the key step. CrystEngComm. 2002;4(47):257-64.

46. Sangwai K. Morphology and size distribution of crystals. In: Sangwai K, editor. Additives and crystallization processes From Fundamentals to applications: Wiley; 2007.

47. Veesler S, Lafferrère L, Garcia E, Hoff C. Phase Transitions in Supersaturated Drug Solution. Organic Process Research & Development. 2003;7(6):983-9.

48. Lafont S, Veesler S, Astier JP, Boistelle R. Solubility and prenucleation of aprotinin (BPTI) molecules in sodium chloride solutions. Journal of Crystal Growth. 1994;143(3):249-55.

49. Boistelle R, Astier JP, Marchis-Mouren G, Desseaux V, Haser R. Solubility, phase transition, kinetic ripening and growth rates of porcine pancreatic α-amylase isoenzymes. Journal of Crystal Growth. 1992;123(1):109-20.

50. Nývlt J. The Ostwald Rule of Stages. Crystal Research and Technology. 1995;30(4):443-9.

51. Hamiaux C, Perez J, Prange T, Veesler S, Ries-Kautt M, Vachette P. The BPTI decamer observed in acidic pH crystal forms pre-exists as a stable species in solution. Journal of Molecular Biology. 2000;297(3):697-712.

52. Mullin JW. Crytallization. Oxford: Butterworth-Heinemann; 2001.

53. Tung H-H, Paul EL, Midler M, McCauley JA. Crystallization of Organic Compounds: An Industrial Perspective: John Wiley & Sons, Inc.; 2008.

54. Lee EH, Byrn SR, Carvajal MT. Additive-induced metastable single crystal of mefenamic acid. Pharmaceutical research. 2006;23(10):2375-80.

55. Lopez-Mejias V, Knight JL, Brooks CL, 3rd, Matzger AJ. On the mechanism of crystalline polymorph selection by polymer heteronuclei. Langmuir : the ACS journal of surfaces and colloids. 2011;27(12):7575-9.

56. Rodriguez-Hornedo N, Murphy D. Surfactant-facilitated crystallization of dihydrate carbamazepine during dissolution of anhydrous polymorph. Journal of Pharmaceutical Sciences. 2004;93(2):449-60.

57. Tian F, Sandler N, Aaltonen J, Lang C, Saville DJ, Gordon KC, et al. Influence of polymorphic form, morphology, and excipient interactions on the dissolution of carbamazepine compacts. Journal of Pharmaceutical Sciences 2007;96(3):584-94.

58. Airaksinen S, Karjalainen M, Kivikero N, Westermarck S, Shevchenko A, Rantanen J, et al. Excipient selection can significantly affect solid-state phase transformation in formulation during wet granulation. AAPS PharmSciTech. 2005;6(2):E311-22.

59. Leveque N, Raghavan SL, Lane ME, Hadgraft J. Use of a molecular form technique for the penetration of supersaturated solutions of salicylic acid across silicone membranes and human skin in vitro. International Journal of Pharmaceutics 2006;318(1-2):49-54.

60. Salameh AK, Taylor LS. Physical stability of crystal hydrates and their anhydrates in the presence of excipients. Journal of Pharmaceutical Sciences. 2006;95(2):446-61.

61. Mirza S, Miroshnyk I, Heinämäki J, Rantanen J, Antikainen O, Vuorela P, et al. Hydroxypropyl Methylcellulose-Controlled Crystallization of Erythromycin A Dihydrate Crystals with Modified Morphology. Crystal Growth & Design. 2008;8(10):3526-31.

62. Loftsson T, Fri∂riksdóttir H, Gu∂mundsdóttir TK. The effect of water-soluble polymers on aqueous solubility of drugs. International Journal of Pharmaceutics. 1996;127(2):293-6.

References

63. Karavas E, Ktistis G, Xenakis A, Georgarakis E. Effect of hydrogen bonding interactions on the release mechanism of felodipine from nanodispersions with polyvinylpyrrolidone. European Journal of Pharmaceutics and Biopharmaceutics. 2006;63(2):103-14.

64. Bansal SS, Kaushal AM, Bansal AK. Molecular and Thermodynamic Aspects of Solubility Advantage from Solid Dispersions. Molecular pharmaceutics. 2007;4(5):794-802.

65. Bhugra C, Pikal MJ. Role of thermodynamic, molecular, and kinetic factors in crystallization from the amorphous state. Journal of Pharmaceutical Sciences. 2008;97(4):1329-49.

66. DiNunzio JC, Miller DA, Yang W, McGinity JW, Williams RO, 3rd. Amorphous compositions using concentration enhancing polymers for improved bioavailability of itraconazole. Molecular Pharmaceutics. 2008;5(6):968-80.

67. Vandecruys R, Peeters J, Verreck G, Brewster ME. Use of a screening method to determine excipients which optimize the extent and stability of supersaturated drug solutions and application of this system to solid formulation design. International Journal of Pharmaceutics. 2007;342(1–2):168-75.

68. Brittain HG. Polymorphism and solvatomorphism 2005. Journal of Pharmaceutical Sciences 2007;96(4):705-28.

69. Byrn SR, Pfeiffer RR, Stowell JG. Solid-state chemistry of drugs. 2nd ed. West Lafayette: SSCI, Inc.; 1999.

70. Vippagunta SR, Brittain HG, Grant DJ. Crystalline solids. Advanced Drug Delivery Reviews. 2001;48(1):3-26.

71. Zhou D, Schmitt EA, Zhang GG, Law D, Wight CA, Vyazovkin S, et al. Model-free treatment of the dehydration kinetics of nedocromil sodium trihydrate. Journal of Pharmaceutical Sciences 2003;92(7):1367-76.

72. Zhou D, Schmitt EA, Zhang GG, Law D, Wight CA, Vyazovkin S, et al. Model-free treatment of the dehydration kinetics of nedocromil sodium trihydrate. Journal of Pharmaceutical Sciences. 2003;92(7):1367-76.

73. Griesser UJ. The Importance of Solvates. Polymorphism: Wiley-VCH Verlag GmbH & Co. KGaA; 2006. p. 211-33.

74. Doherty R. The application of computational chemistry to the study of molecular materials. In: Myerson A, Green D, Meenan P, editors. Crystal Growth of Organic Materials. Washington DC: American Chemical Society; 1996. p. 2-14.

75. Bernstein J. Polymorphism in Molecular Crystals. Oxford: Clarendon Press; 2002. 297-307 p.

76. Niazi SK. Handbook of Bioequivalence Testing. 2 ed: CRC Press; 2015.

77. Grant DJW, Higuchi T. Solubility behaviour of organic compounds. New York: John Wiley & Sons, Inc. ; 1990. p. 600.

78. Shefter E, Higuchi T. Dissolution behavior of crystalline solvated and nonsolvated forms of some pharmaceuticals. Journal of Pharmaceutical Sciences. 1963;52(8):781-91.

79. Ando H, Ishii M, Kayano M, Ozawa H. Effect of moisture on crystallization of theophylline in tablets. Drug Development and Industrial Pharmacy. 1992;18(4):453-67.

80. Han J, Suryanarayanan R. Influence of environmental conditions on the kinetics and mechanism of dehydration of carbamazepine dihydrate. Pharmaceutical Development and Technology. 1998;3(4):587-96.

81. McMahon LE, Timmins P, Williams AC, York P. Characterization of dihydrates prepared from carbamazepine polymorphs. Journal of Pharmaceutical Sciences. 1996;85(10):1064-9.

82. Davis TD, Peck GE, Stowell JG, Morris KR, Byrn SR. Modeling and monitoring of polymorphic transformations during the drying phase of wet granulation. Pharmaceutical Research. 2004;21(5):860-6.

83. Morris KR, Griesser UJ, Eckhardt CJ, Stowell JG. Theoretical approaches to physical transformations of active pharmaceutical ingredients during manufacturing processes. Advanced Drug Delivery Reviews. 2001;48(1):91-114.

84. Wikstrom H, Marsac PJ, Taylor LS. In-line monitoring of hydrate formation during wet granulation using Raman spectroscopy. Journal of Pharmaceutical Sciences. 2005;94(1):209-19.

85. Morris KR, Nail SL, Peck GE, Byrn SR, Griesser UJ, Stowell JG, et al. Advances in pharmaceutical materials and processing. Pharmaceutical Science & Technology Today. 1998;1(6):235-45.

86. Newman AW, Byrn SR. Solid-state analysis of the active pharmaceutical ingredient in drug products. Drug Discovery Today. 2003;8(19):898-905.

87. Williams HD, Trevaskis NL, Charman SA, Shanker RM, Charman WN, Pouton CW, et al. Strategies to address low drug solubility in discovery and development. Pharmacological Reviews. 2013;65(1):315-499.

88. Vehring R. Pharmaceutical Particle Engineering via Spray Drying. Pharmaceutical Research. 2008;25(5):999-1022.

89. Chieng N, Zujovic Z, Bowmaker G, Rades T, Saville D. Effect of milling conditions on the solid-state conversion of ranitidine hydrochloride form 1. International Journal of Pharmaceutics. 2006;327(1–2):36-44.

90. Crowley KJ, Zografi G. Cryogenic grinding of indomethacin polymorphs and solvates: assessment of amorphous phase formation and amorphous phase physical stability. Journal of Pharmaceutical Sciences. 2002;91(2):492-507.

91. Shekunov BY, York P. Crystallization processes in pharmaceutical technology and drug delivery design. Journal of Crystal Growth. 2000;211(1–4):122-36.

References

92. Shekunov BY, Chattopadhyay P, Seitzinger J, Huff R. Nanoparticles of poorly water-soluble drugs prepared by supercritical fluid extraction of emulsions. Pharmaceutical Research. 2006;23(1):196-204.

93. Edwards AD, Shekunov BY, Kordikowski A, Forbes RT, York P. Crystallization of pure anhydrous polymorphs of carbamazepine by solution enhanced dispersion with supercritical fluids (SEDS). Journal of Pharmaceutical Sciences 2001;90(8):1115-24.

94. Martín A, Cocero MJ. Micronization processes with supercritical fluids: Fundamentals and mechanisms. Advanced Drug Delivery Reviews. 2008;60(3):339-50.

95. Tom JW, Debenedetti PG. Particle formation with supercritical fluids—a review. Journal of Aerosol Science. 1991;22(5):555-84.

96. York P. Strategies for particle design using supercritical fluid technologies. Pharmaceutical Sciences & Technology Today. 1999;2(11):430-40.

97. Jung J, Perrut M. Particle design using supercritical fluids: Literature and patent survey. The Journal of Supercritical Fluids. 2001;20(3):179-219.

98. Tozuka Y, Miyazaki Y, Takeuchi H. A combinational supercritical CO_2 system for nanoparticle preparation of indomethacin. International Journal of Pharmaceutics. 2010;386(1-2):243-8.

99. Huang Z, Sun G-B, Chiew YC, Kawi S. Formation of ultrafine aspirin particles through rapid expansion of supercritical solutions (RESS). Powder Technology. 2005;160(2):127-34.

100. Young TJ, Mawson S, Johnston KP, Henriksen IB, Pace GW, Mishra AK. Rapid expansion from supercritical to aqueous solution to produce submicron suspensions of water-insoluble drugs. Biotechnology Progress. 2000;16(3):402-7.

101. Kordikowski A, Shekunov T, York P. Polymorph control of sulfathiazole in supercritical CO_2. Pharmaceutical Research. 2001;18(5):682-8.

102. Chen F, Li T, Li S, Hou K, Liu Z, Li L, et al. Preparation and Characterization of Tripterygium wilfordii Multi-Glycoside Nanoparticle Using Supercritical Anti-Solvent Process. International Journal of Molecular Sciences. 2014;15(2):2695-711.

103. Stephenson GA, Stowell JG, Toma PH, Dorman DE, Greene JR, Byrn SR. Solid-State Analysis of Polymorphic, Isomorphic, and Solvated Forms of Dirithromycin. Journal of the American Chemical Society. 1994;116(13):5766-73.

104. Otsuka M, Onoe M, Matsuda Y. Physicochemical stability of phenobarbital polymorphs at various levels of humidity and temperature. Pharmaceutical Research. 1993;10(4):577-82.

105. Wong MWY, Mitchell AG. Physicochemical characterization of a phase change produced during the wet granulation of chlorpromazine hydrochloride and its effects on tableting. International Journal of Pharmaceutics. 1992;88(1–3):261-73.

106. Phadnis NV, Suryanarayanan R. Polymorphism in anhydrous theophylline--implications on the dissolution rate of theophylline tablets. Journal of Pharmaceutical Sciences 1997;86(11):1256-63.

107. Dukić-Ott A, Thommes M, Remon JP, Kleinebudde P, Vervaet C. Production of pellets via extrusion–spheronisation without the incorporation of microcrystalline cellulose: A critical review. European Journal of Pharmaceutics and Biopharmaceutics. 2009;71(1):38-46.

108. Trivedi NR, Rajan MG, Johnson JR, Shukla AJ. Pharmaceutical approaches to preparing pelletized dosage forms using the extrusion-spheronization process. Critical Reviews in Therapeutic Drug Carrier Systems. 2007;24(1):1-40.

109. Vervaet C, Baert L, Remon JP. Extrusion-spheronisation A literature review. International Journal of Pharmaceutics. 1995;116(2):131-46.

110. Chatchawalsaisin J, Podczeck F, Newton JM. The preparation by extrusion/spheronization and the properties of pellets containing drugs, microcrystalline cellulose and glyceryl monostearate. European Journal of Pharmaceutical Sciences. 2005;24(1):35-48.

111. Sandler N, Rantanen J, Heinamaki J, Romer M, Marvola M, Yliruusi J. Pellet manufacturing by extrusion-spheronization using process analytical technology. AAPS PharmSciTech. 2005;6(2):E174-83.

112. Hagsten A, Casper Larsen C, Møller Sonnergaard J, Rantanen J, Hovgaard L. Identifying sources of batch to batch variation in processability. Powder Technology. 2008;183(2):213-9.

113. Sousa JJ, Sousa A, Podczeck F, Newton JM. Factors influencing the physical characteristics of pellets obtained by extrusion-spheronization. International Journal of Pharmaceutics 2002;232(1-2):91-106.

114. Chan HK, Doelker E. Polymorphic Transformation of Some Drugs Under Compression. Drug Development and Industrial Pharmacy. 1985;11(2-3):315-32.

115. Gu CH, Young V, Jr., Grant DJ. Polymorph screening: influence of solvents on the rate of solvent-mediated polymorphic transformation. Journal of Pharmaceutical Sciences 2001;90(11):1878-90.

116. Cardew PT, Davery RJ. The kinetics of solvent-mediated-phase-transformations. Proc R Soc London A Math Phys Eng Sci. 1985;398:415-28.

117. Rodriguez-Honredo N, Lechuga-Bellesteros D, Wu HJ. Phase transition and heterogeneous/epitaxial nucleation of hydrated and anydrous theophyline crystals. International Journal of Pharmaceutics. 1992;85:149-62.

118. Otsuka M, Ohfusa T, Matsuda Y. Effect of binders on polymorphic transformation kinetics of carbamazepine in aqueous solution. Colloids and Surfaces B: Biointerfaces. 2000;17(3):145-52.

References

119. Jackson K, Young D, Pant S. Drug–excipient interactions and their affect on absorption. Pharmaceutical Science & Technology Today. 2000;3(10):336-45.

120. Moreton RC. Tablet Excipients to the Year 2001: A Look into the Crystal Ball. Drug Development and Industrial Pharmacy. 1996;22(1):11-23.

121. Szakonyi G, Zelkó R. The effect of water on the solid state characteristics of pharmaceutical excipients: Molecular mechanisms, measurement techniques, and quality aspects of final dosage form. International Journal of Pharmaceutical Investigation. 2012;2(1):18-25.

122. Airaksinen S, Karjalainen M, Shevchenko A, Westermarck S, Leppanen E, Rantanen J, et al. Role of water in the physical stability of solid dosage formulations. Journal of Pharmaceutical Sciences. 2005;94(10):2147-65.

123. Kontny M, Zografi G. Sorption of water by solids. In: Brittain H, editor. Physical characterization of pharmaceutical solids. New York: Marcel Dekker Inc.; 1995. p. 387-418.

124. Yu L. Amorphous pharmaceutical solids: preparation, characterization and stabilization. Advanced Drug Delivery Reviews. 2001;48(1):27-42.

125. Reutzel-Edens SM, Newman AW. Physical characterization of hygroscopicity in pharmaceutical solids. In: Hilfiker R, editor. Polymorphism in the Pharmaceutical Industry. Weinheim, Germany: Wiley-VCH; 2006. p. 235-58.

126. Fitzpatrick S, McCabe JF, Petts CR, Booth SW. Effect of moisture on polyvinylpyrrolidone in accelerated stability testing. International Journal of Pharmaceutics 2002;246(1-2):143-51.

127. Andronis V, Zografi G. The molecular mobility of supercooled amorphous indomethacin as a function of temperature and relative humidity. Pharmaceutical Research. 1998;15(6):835-42.

128. Fulton B, Goa KL. Olanzapine. A review of its pharmacological properties and therapeutic efficacy in the management of schizophrenia and related psychoses. Drugs. 1997;53(2):281-98.

129. European Pharmacopeia. Council of Europe. Strasbourg, France 2011.

130. Bhardwaj RM, Price LS, Price SL, Reutzel-Edens SM, Miller GJ, Oswald IDH, et al. Exploring the Experimental and Computed Crystal Energy Landscape of Olanzapine. Crystal Growth & Design. 2013;13(4):1602-17.

131. Cavallari C, Santos BP, Fini A. Olanzapine solvates. Journal of Pharmaceutical Sciences. 2013;102(11):4046-56.

132. Bunnell CA, Hendriksen BA, Larsen SD. Olanzapine polymorph crystal form. US 5736541 A; 1998.

133. Wawrzycka-Gorczyca I, Koziol AE, Glice M, Cybulski J. Polymorphic form II of 2-methyl-4-(4-methyl-1-piperazinyl)-10H-thieno- 2,3-b 1,5 benzodiazepin e. Acta Crystallographica Section E-Structure Reports Online. 2004;60:O66-O8.

134. Bunnell CA, Hendriksen BA, Larsen SD. Crystal forms of a thieno(2,3-B)(1,5) benzodiazepine derivative and process for their preparation. EP 0733635 B1; 2001.

135. Cochran GR, Morris TC. Oral olanzapine formulation. EP0733367 B1; 2001.

136. Perc S, Banko I, Kolenc I. Pharmaceutical formulation of olanzapine. US 20110319395 A1; 2004.

137. Polla GI, Vega DR, Lanza H, Tombari DG, Baggio R, Ayala AP, et al. Thermal behaviour and stability in Olanzapine. International Journal of Pharmaceutics 2005;301(1-2):33-40.

138. Ayala AP, Siesler HW, Boese R, Hoffmann GG, Polla GI, Vega DR. Solid state characterization of olanzapine polymorphs using vibrational spectroscopy. International Journal of Pharmaceutics 2006;326(1-2):69-79.

139. Tiwari M, Chawla G, Bansal AK. Quantification of olanzapine polymorphs using powder X-ray diffraction technique. Journal of Pharmaceutical and Biomedical Analysis. 2007;43(3):865-72.

140. Callahan JC, Cleary GW, Elefant M, Kaplan G, Kensler T, Nash RA. Equilibrium Moisture Content of Pharmaceutical Excipients. Drug Development and Industrial Pharmacy. 1982;8(3):355-69.

141. Bühler V. Kollidon, Polyvinylpyrrolidone excipients for the pharmaceutical industry. 9 ed. Germany: BASF SE; 2008.

142. Torres VM, Posa M, Srdjenovic B, Simplicio AL. Solubilization of fullerene C60 in micellar solutions of different solubilizers. Colloids and surfaces B, Biointerfaces. 2011;82(1):46-53.

143. Otsuka N, Ueda K, Ohyagi N, Shimizu K, Katakawa K, Kumamoto T, et al. An Insight into Different Stabilization Mechanisms of Phenytoin Derivatives Supersaturation by HPMC and PVP. Journal of Pharmaceutical Sciences. 2015;104(8):2574-82.

144. Olorunsola EO, Adedokun MO. Surface activity as basis for pharmaceutical applications of hydrocolloids: A review. Journal of Applied Pharmaceutical Sciences. 2014;4(10):110-6.

145. Koltzenburg S. Formulation of problem drugs-and they are all problem drugs. In: Reintjes T, editor. Solubility Enhancement with BASF Pharma Polymers. Lampertheim, Germany: Pharma Incredients and Services.; 2011. p. 130.

146. Rowe RC, Sheskey PJ, Quinn ME. Handbook of Pharmaceutical Excipients. 6th ed. London, UK: Pharmaceutical Press; 2009.

147. Taylor LS, Langkilde FW, Zografi G. Fourier transform Raman spectroscopic study of the interaction of water vapor with amorphous polymers. Journal of Pharmaceutical Sciences 2001;90(7):888-901.

References

148. Baird JA, Olayo-Valles R, Rinaldi C, Taylor LS. Effect of molecular weight, temperature, and additives on the moisture sorption properties of polyethylene glycol. Journal of Pharmaceutical Sciences. 2010;99(1):154-68.

149. Cohen S, Marcus Y, Migron Y, Dikstein S, Shafran A. Water sorption, binding and solubility of polyols. Journal of the Chemical Society, Faraday Transactions. 1993;89(17):3271-5.

150. Katzhendler I, Azoury R, Friedman M. Crystalline properties of carbamazepine in sustained release hydrophilic matrix tablets based on hydroxypropyl methylcellulose. Journal of Controlled Release : official journal of the Controlled Release Society. 1998;54(1):69-85.

151. Katzhendler I, Mader K, Azoury R, Friedman M. Investigating the structure and properties of hydrated hydroxypropyl methylcellulose and egg albumin matrices containing carbamazepine: EPR and NMR study. Pharmaceutical Research. 2000;17(10):1299-308.

152. Thoorens G, Krier F, Leclercq B, Carlin B, Evrard B. Microcrystalline cellulose, a direct compression binder in a quality by design environment—A review. International Journal of Pharmaceutics. 2014;473(1–2):64-72.

153. Majka Z, Stawinski T. Process for removing impurity S from olanzapine polymorphic form I. EP1581537 B1; 2007.

154. Cavallari C. Thermal Study of Anhydrous and Hydrated Forms of Olanzapine. Pharmaceutica Analytica Acta. 2013;04(05).

155. Greenspan L. Humidity Fixed Points of Binary Saturated Aqueous Solutions Journal of research of the National Bureau of Standards- A Physics and Chemistry 1977;81A:89-96.

156. Zhang M, Wilson DI, Ward R, Seiler C, Rough SL. A comparison of screen and ram extrusion–spheronisation of simple pharmaceutical pastes based on microcrystalline cellulose. International Journal of Pharmaceutics. 2013;456(2):489-98.

157. Craig DQM, Reading M. Thermal analysis of pharmaceuticals. London: CRC Press/Taylor & Francis; 2007.

158. Differential Scanning Calorimetry. In: Martinho Simões JA, Minas da Piedade ME, editors. Molecular Energetics - Condensed-Phase Thermochemical Techniques. New York: Oxford University Press; 2008.

159. Vitez IM, Newman AW, Davidovich M, Kiesnowski C. The evolution of hot-stage microscopy to aid solid-state characterizations of pharmaceutical solids. Thermochimica Acta. 1998;324(1-2):187-96.

160. Barth A. Infrared spectroscopy of proteins. Biochimica et Biophysica Acta (BBA) - Bioenergetics. 2007;1767(9):1073-101.

161. Koenig JL. Infrared and Raman Spectroscopy of Polymers: Rapra Tecnhology Limited; 2001. 152 p.

162. Kubelka P, Munk F. Ein Beitrag Zur Optik Der Farbanstriche. Zeitschrift für Technische Physik. 1931;12:593-601.

163. Gilmore CJ. X-Ray Diffraction. In: Storey RA, Ymén I, editors. Solid State Characterization of Pharmaceuticals. Chichester, UK: John Wiley & Sons; 2011.

164. Lee S, Raw A, Yu L. Dissolution Testing. In: Krishna R, Yu L, editors. Biopharmaceutics Applications in Drug Development: Springer US; 2008. p. 47-74.

165. Hörter D, Dressman JB. Influence of physicochemical properties on dissolution of drugs in the gastrointestinal tract. Advanced Drug Delivery Review. 2001;46(1–3):75-87.

166. Moore JW, Flanner HH. Mathematical comparison of curves with an emphasis on dissolution profiles. Pharmaceutical Technology. 1996;20(6):64-74.

167. Guidance for industry: dissolution testing of Immediate Release Solid Oral Dosage Forms. U.S. Department of Health and Human Services, Center for Drug Evaluation and Research, (August 1997).

168. Costa P, Sousa Lobo JM. Modeling and comparison of dissolution profiles. European Journal of Pharmaceutical Sciences. 2001;13(2):123-33.

169. Moodley K, Pillay V, Choonara YE, du Toit LC, Ndesendo VMK, Kumar P, et al. Oral Drug Delivery Systems Comprising Altered Geometric Configurations for Controlled Drug Delivery. International Journal of Molecular Sciences. 2012;13(1):18-43.

170. Siepmann J, Peppas NA. Modeling of drug release from delivery systems based on hydroxypropyl methylcellulose (HPMC). Advanced drug delivery reviews. 2001;48(2–3):139-57.

171. Korsmeyer RW, Gurny R, Doelker E, Buri P, Peppas NA. Mechanisms of solute release from porous hydrophilic polymers. International Journal of Pharmaceutics. 1983;15(1):25-35.

172. Threlfall TL. Analysis of organic polymorphs. A review. Analyst. 1995;120(10):2435-60.

173. Giron D, Goldbronn C, Mutz M, Pfeffer S, Piechon P, Schwab P. Solid State Characterizations of Pharmaceutical Hydrates. Journal of Thermal Analysis and Calorimetry. 2002;68(2):453-65.

174. Huang LF, Tong WQ. Impact of solid state properties on developability assessment of drug candidates. Advanced Drug Delivery Reviews. 2004;56(3):321-34.

175. Krzyzaniak JF, Williams GR, Ni N. Identification of phase boundaries in anhydrate/hydrate systems. Journal of Pharmaceutical Sciences 2007;96(5):1270-81.

176. Matsuo K, Matsuoka M. Solid-State Polymorphic Transition of Theophylline Anhydrate and Humidity Effect. Crystal Growth & Design. 2007;7(2):411-5.

177. Ticehurst MD, Storey RA, Watt C. Application of slurry bridging experiments at controlled water activities to predict the solid-state conversion between anhydrous and hydrated forms

using theophylline as a model drug. International Journal of Pharmaceutics. 2002;247(1–2):1-10.

178. Shrivastava A, Johnston M, Terpstra K, Stitt L, Shah N. Atypical antipsychotics usage in long-term follow-up of first episode schizophrenia. Indian Journal of Psychiatry. 2012;54(3):248-52.

179. Carvajal MT, Staniforth JN. Interactions of water with the surfaces of crystal polymorphs. International Journal of Pharmaceutics. 2006;307(2):216-24.

180. Saunders M, Gabbott P. Thermal Analysis – Conventional Techniques. Solid State Characterization of Pharmaceuticals: John Wiley & Sons, Ltd; 2011. p. 135-86.

181. Tantishaiyakul V, Permkam P, Suknuntha K. Use of Drifts and PLS for the Determination of Polymorphs of Piroxicam Alone and in Combination with Pharmaceutical Excipients: A Technical Note. AAPS PharmSciTech. 2008;9(1):95-9.

182. Tian F, Zeitler JA, Strachan CJ, Saville DJ, Gordon KC, Rades T. Characterizing the conversion kinetics of carbamazepine polymorphs to the dihydrate in aqueous suspension using Raman spectroscopy. Journal of Pharmaceutical and Biomedical Analysis. 2006;40(2):271-80.

183. Anderton CL. Vibrational spectroscopy in pharmaceutical analysis. In: Lee DC, Webb ML, editors. Pharmaceutical Analysis. Oxford: Blackwell Publishing Ltd; 2003. p. 216-26.

184. Tang X, Pikal M, Taylor L. A Spectroscopic Investigation of Hydrogen Bond Patterns in Crystalline and Amorphous Phases in Dihydropyridine Calcium Channel Blockers. Pharmaceutical Research. 2002;19(4):477-83.

185. Kontny MJ, Grandolfi GP, Zografi G. Water vapor sorption of water-soluble substances: studies of crystalline solids below their critical relative humidities. Pharmaceutical Research. 1987;4(2):104-12.

186. Koradia V, Fontelonga de Lemos AF, Allesø M, Lopez de Diego H, Ringkjøbing-Elema M, Müllertz A, et al. Phase transformations of amlodipine besylate solid forms. Jounal of Pharmaceutical Sciences. 2011;100:2896-910.

187. Dong Z, Salsbury JS, Zhou D, Munson EJ, Schroeder SA, Prakash I, et al. Dehydration kinetics of neotame monohydrate. Journal of Pharmaceutical Sciences 2002;91(6):1423-31.

188. Sakata Y, Shiraishi S, Otsuka M. Characterization of dehydration and hydration behavior of calcium lactate pentahydrate and its anhydrate. Colloids and surfaces B, Biointerfaces. 2005;46(3):135-41.

189. Amado AM, Nolasco MM, Ribeiro-Claro PJ. Probing pseudopolymorphic transitions in pharmaceutical solids using Raman spectroscopy: hydration and dehydration of theophylline. Journal of Pharmaceutical Sciences 2007;96(5):1366-79.

190. Sheth AR, Zhou D, Muller FX, Grant DJ. Dehydration kinetics of piroxicam monohydrate and relationship to lattice energy and structure. Journal of Pharmaceutical Sciences 2004;93(12):3013-26.

191. Di Martino P, Barthelemy C, Joiris E, Capsoni D, Masic A, Massarotti V, et al. A new tetrahydrated form of sodium naproxen. Journal of Pharmaceutical Sciences 2007;96(1):156-67.

192. Censi R, Martena V, Hoti E, Malaj L, Di Martino P. Sodium ibuprofen dihydrate and anhydrous. Journal of Thermal Analysis and Calorimetry. 2013;111(3):2009-18.

193. Dalton CR, Clas S-D, Singh J, Khougaz K, Bilbeisi R. Investigating the hydrate conversion propensity of different etoricoxib lots. Journal of Pharmaceutical Sciences. 2006;95(1):56-69.

194. Tian F, Saville DJ, Gordon KC, Strachan CJ, Zeitler JA, Sandler N, et al. The influence of various excipients on the conversion kinetics of carbamazepine polymorphs in aqueous suspension. The Journal of pharmacy and pharmacology. 2007;59(2):193-201.

195. Jorgensen AC, Airaksinen S, Karjalainen M, Luukkonen P, Rantanen J, Yliruusi J. Role of excipients in hydrate formation kinetics of theophylline in wet masses studied by near-infrared spectroscopy. European journal of pharmaceutical sciences : official journal of the European Federation for Pharmaceutical Sciences. 2004;23(1):99-104.

196. Gift AD, Luner PE, Luedeman L, Taylor LS. Influence of polymeric excipients on crystal hydrate formation kinetics in aqueous slurries. Journal of Pharmaceutical Sciences. 2008;97(12):5198-211.

197. Tian F, Sandler N, Gordon KC, McGoverin CM, Reay A, Strachan CJ, et al. Visualizing the conversion of carbamazepine in aqueous suspension with and without the presence of excipients: A single crystal study using SEM and Raman microscopy. European Journal of Pharmaceutics and Biopharmaceutics. 2006;64(3):326-35.

198. Paisana M, Wahl M, Pinto J. Role of Polymeric Excipients in the Stabilization of Olanzapine when Exposed to Aqueous Environments. Molecules (Basel, Switzerland). 2015;20(12):22364-82.

199. Campisi B, Chicco D, Vojnovic D, Phan-Tan-Luu R. Experimental design for a pharmaceutical formulation: optimisation and robustness1. Journal of Pharmaceutical and Biomedical Analysis. 1998;18(1–2):57-65.

200. Heidemann DR, Jarosz PJ. Preformulation studies involving moisture uptake in solid dosage forms. Pharmaceutical Research. 1991;8(3):292-7.

201. Marsac PJ, Romary DP, Shamblin SL, Baird JA, Taylor LS. Spontaneous crystallinity loss of drugs in the disordered regions of poly(ethylene oxide) in the presence of water. Journal of Pharmaceutical Sciences. 2008;97(8):3182-94.

References

202. Ahlneck C, Zografi G. The molecular basis of moisture effects on the physical and chemical stability of drugs in the solid state. International Journal of Pharmaceutics. 1990;62(2–3):87-95.

203. Zografi G. States of Water Associated with Solids. Drug Development and Industrial Pharmacy. 1988;14(14):1905-26.

204. Zhang J, Zografi G. Water vapor absorption into amorphous sucrose-poly(vinyl pyrrolidone) and trehalose-poly(vinyl pyrrolidone) mixtures. Journal of Pharmaceutical Sciences. 2001;90(9):1375-85.

205. Rumondor AC, Marsac PJ, Stanford LA, Taylor LS. Phase behavior of poly(vinylpyrrolidone) containing amorphous solid dispersions in the presence of moisture. Molecular pharmaceutics. 2009;6(5):1492-505.

206. Galarneau D. A case of teeth discoloration upon transition from zyprexa to generic olanzapine. The Ochsner journal. 2013;13(4):550-2.

207. Samuel R, Attard A, Kyriakopoulos M. Mental state deterioration after switching from brand-name to generic olanzapine in an adolescent with bipolar affective disorder, autism and intellectual disability: a case study. BMC psychiatry. 2013;13:244.

208. Chakravarty P, Govindarajan R, Suryanarayanan R. Investigation of solution and vapor phase mediated phase transformation in thiamine hydrochloride. Journal of Pharmaceutical Sciences. 2010;99(9):3941-52.

209. Otsuka M, Matsuda Y. The Effect of Humidity on Hydration Kinetics of Mixtures of Nitrofurantoin Anhydride and Diluents. Chemical & Pharmaceutical Bulletin 1994;42(1):156-9.

210. Airaksinen S, Luukkonen P, Jorgensen A, Karjalainen M, Rantanen J, Yliruusi J. Effects of excipients on hydrate formation in wet masses containing theophylline. Journal of Pharmaceutical Sciences. 2003;92(3):516-28.

211. Salameh AK, Taylor LS. Physical stability of crystal hydrates and their anhydrates in the presence of excipients. Journal of Pharmaceutical Sciences. 2006;95(2):446-61.

212. Byrn SR, Xu W, Newman AW. Chemical reactivity in solid-state pharmaceuticals: formulation implications. Advanced Drug Delivery Reviews. 2001;48(1):115-36.

213. Thijs HML, Becer CR, Guerrero-Sanchez C, Fournier D, Hoogenboom R, Schubert US. Water uptake of hydrophilic polymers determined by a thermal gravimetric analyzer with a controlled humidity chamber. Journal of Materials Chemistry. 2007;17(46):4864.

214. Chan KLA, Kazarian SG. Visualisation of the heterogeneous water sorption in a pharmaceutical formulation under controlled humidity via FT-IR imaging. Vibrational Spectroscopy. 2004;35(1–2):45-9.

215. Kitano H, Ichikawa K, Ide M, Fukuda M, Mizuno W. Fourier Transform Infrared Study on the State of Water Sorbed to Poly(ethylene glycol) Films†. Langmuir : the ACS journal of surfaces and colloids. 2001;17(6):1889-95.

216. Kiekens F, Zelko R, Remon JP. Effect of the storage conditions on the tensile strength of tablets in relation to the enthalpy relaxation of the binder. Pharmaceutical Research. 2000;17(4):490-3.

217. Mihranyan A, Llagostera AP, Karmhag R, Stromme M, Ek R. Moisture sorption by cellulose powders of varying crystallinity. International Journal of Pharmaceutics 2004;269(2):433-42.

218. Alvarez-Lorenzo C, Gomez-Amoza JL, Martinez-Pacheco R, Souto C, Concheiro A. Interactions between hydroxypropylcelluloses and vapour/liquid water. European journal of pharmaceutics and biopharmaceutics : official journal of Arbeitsgemeinschaft fur Pharmazeutische Verfahrenstechnik eV. 2000;50(2):307-18.

219. Young JH, Nelson GH. Theory of hysteresis between sorption and desorption isotherms in biological materials. Transaction of ASAE. 1967;10:260-3.

220. Joshi HN, Wilson TD. Calorimetric studies of dissolution of hydroxypropyl methylcellulose E5 (HPMC E5) in water. Journal of Pharmaceutical Sciences 1993;82(10):1033-8.

221. Ju RT, Nixon PR, Patel MV, Tong DM. Drug release from hydrophilic matrices. 2. A mathematical model based on the polymer disentanglement concentration and the diffusion layer. Journal of Pharmaceutical Sciences 1995;84(12):1464-77.

222. Dios P, Pernecker T, Nagy S, Pal S, Devay A. Influence of different types of low substituted hydroxypropyl cellulose on tableting, disintegration, and floating behaviour of floating drug delivery systems. Saudi Pharmaceutical Journal : the official publication of the Saudi Pharmaceutical Society. 2015;23(6):658-66.

223. Ilevbare GA, Liu H, Edgar KJ, Taylor LS. Impact of Polymers on Crystal Growth Rate of Structurally Diverse Compounds from Aqueous Solution. Molecular Pharmaceutics. 2013;10(6):2381-93.

224. Wikstrom H, Carroll WJ, Taylor LS. Manipulating theophylline monohydrate formation during high-shear wet granulation through improved understanding of the role of pharmaceutical excipients. Pharmaceutical Research. 2008;25(4):923-35.

225. Gift AD, Luner PE, Luedeman L, Taylor LS. Manipulating hydrate formation during high shear wet granulation using polymeric excipients. Journal of Pharmaceutical Sciences. 2009;98(12):4670-83.

226. Patel DD, Anderson BD. Adsorption of Polyvinylpyrrolidone and its Impact on Maintenance of Aqueous Supersaturation of Indomethacin via Crystal Growth Inhibition. Journal of Pharmaceutical Sciences 2015;104(9):2923-33.

References

227. Tian F, Baldursdottir S, Rantanen J. Effects of polymer additives on the crystallization of hydrates: a molecular-level modulation. Molecular Pharmaceutics. 2009;6(1):202-10.

228. Ueda K, Higashi K, Yamamoto K, Moribe K. Inhibitory effect of hydroxypropyl methylcellulose acetate succinate on drug recrystallization from a supersaturated solution assessed using nuclear magnetic resonance measurements. Molecular Pharmaceutics. 2013;10(10):3801-11.

229. Lindfors L, Forssen S, Westergren J, Olsson U. Nucleation and crystal growth in supersaturated solutions of a model drug. Journal of Colloid and Interface Science. 2008;325(2):404-13.

230. Sigala PA, Ruben EA, Liu CW, Piccoli PMB, Hohenstein EG, Martínez TJ, Schultz AJ, Herschlag D. Determination of Hydrogen Bond Structure in Water versus Aprotic Environments To Test the Relationship Between Length and Stability. Journal of the American Chemical Society. 2015;137(17):5730-5740.

231. Zhang YK, Plattner JJ, Freund YR, Easom EE, Zhou Y, Ye L, et al. Benzoxaborole antimalarial agents. Part 2: Discovery of fluoro-substituted 7-(2-carboxyethyl)-1,3-dihydro-1-hydroxy-2,1-benzoxaboroles. Bioorganic & medicinal chemistry letters. 2012;22(3):1299-307.

232. Ma JH, Guo C, Tang YL, Zhang H, Liu HZ. Probing paeonol-pluronic polymer interactions by 1H NMR spectroscopy. The Journal of Physical Chemistry B. 2007;111(47):13371-8

233. Loftsson T, Frikdriksdóttir H, Sigurkdardóttir AM, Ueda H. The effect of water-soluble polymers on drug-cyclodextrin complexation. International Journal of Pharmaceutics. 1994;110(2):169-77.

234. Teberekidis VI, Sigalas MP. Theoretical study of hydrogen bond interactions of felodipine with polyvinylpyrrolidone and polyethyleneglycol. Journal of Molecular Structure: Theochem. 2007;803(1–3):29-38.

235. Debenedetti PG, Tom JW, Sang-Do Y, Gio-Bin L. Application of supercritical fluids for the production of sustained delivery devices. Journal of Controlled Release. 1993;24(1):27-44.

236. Charoenchaitrakool M, Dehghani F, Foster NR, Chan HK. Micronization by Rapid Expansion of Supercritical Solutions to Enhance the Dissolution Rates of Poorly Water-Soluble Pharmaceuticals. Industrial & Engineering Chemistry Research. 2000;39(12):4794-802.

237. Türk M. Formation of small organic particles by RESS: experimental and theoretical investigations. The Journal of Supercritical Fluids. 1999;15(1):79-89.

238. Sun YP, Meziani MJ, Pathak P, Qu L. Polymeric nanoparticles from rapid expansion of supercritical fluid solution. Chemistry (Weinheim an der Bergstrasse, Germany). 2005;11(5):1366-73.

239. Weber M, Thies MC. A simplified and generalized model for the rapid expansion of supercritical solutions. The Journal of Supercritical Fluids. 2007;40(3):402-19.

240. Patravale VB, Date AA, Kulkarni RM. Nanosuspensions: a promising drug delivery strategy. Journal of Pharmacy and Pharmacology. 2004;56(7):827-40.

241. Rabinow BE. Nanosuspensions in drug delivery. Nature Reviews Drug Discovery. 2004;3(9):785-96.

242. Türk M, Lietzow R. Formation and stabilization of submicron particles via rapid expansion processes. The Journal of Supercritical Fluids. 2008;45(3):346-55.

243. Pathak P, Meziani MJ, Desai T, Sun Y-P. Formation and stabilization of ibuprofen nanoparticles in supercritical fluid processing. The Journal of Supercritical Fluids. 2006;37(3):279-86.

244. Müller RH, Peters K. Nanosuspensions for the formulation of poorly soluble drugs: I. Preparation by a size-reduction technique. International Journal of Pharmaceutics. 1998;160(2):229-37.

245. Sun Y-P, Meziani MJ, Pathak P, Qu L. Polymeric Nanoparticles from Rapid Expansion of Supercritical Fluid Solution. Chemistry- A European Journal. 2005;11(5):1366-73.

246. Mou D, Chen H, Wan J, Xu H, Yang X. Potent dried drug nanosuspensions for oral bioavailability enhancement of poorly soluble drugs with pH-dependent solubility. International Journal of Pharmaceutics. 2011;413(1–2):237-44.

247. Verma S, Gokhale R, Burgess DJ. A comparative study of top-down and bottom-up approaches for the preparation of micro/nanosuspensions. Int J Pharm. 2009;380(1-2):216-22.

248. Mahesh KV, Singh SK, Gulati M. A comparative study of top-down and bottom-up approaches for the preparation of nanosuspensions of glipizide. Powder Technology. 2014;256:436-49.

249. Wang Y, Zheng Y, Zhang L, Wang Q, Zhang D. Stability of nanosuspensions in drug delivery. Journal of Controlled Release. 2013;172(3):1126-41.

250. He W, Lu Y, Qi J, Chen L, Hu F, Wu W. Food proteins as novel nanosuspension stabilizers for poorly water-soluble drugs. International Journal of Pharmaceutics. 2013;441(1-2):269-78.

251. Lin P-C, Su C-S, Tang M, Chen Y-P. Micronization of ethosuximide using the rapid expansion of supercritical solution (RESS) process. Journal of Supercritical Fluids. 2012;72(0):84-9.

252. Gosselin PM, Thibert R, Preda M, McMullen JN. Polymorphic properties of micronized carbamazepine produced by RESS. International Journal of Pharmaceutics. 2003;252(1-2):225-33.

References

253. Bolten D, Türk M. Micronisation of carbamazepine through rapid expansion of supercritical solution (RESS). J Supercrit Fluids. 2012;62(0):32-40.

254. Keltjens R, Thijs L, inventorsA process and composition for making olanzapine form (i). US 20070021605. 2007 Jan 25.

255. Perrut M, Jung, J., Leboeuf, F., editor Solid state morphology of particles prepared by supercritical fluid processes. Proceedings of the Fourth International Symposium on High Pressure Process Technology and Chemical Engineering; 2002; Venice.

256. Türk M, Hils P, Helfgen B, Schaber K, Martin HJ, Wahl MA. Micronization of pharmaceutical substances by the Rapid Expansion of Supercritical Solutions (RESS): a promising method to improve bioavailability of poorly soluble pharmaceutical agents. The Journal of Supercritical Fluids. 2002;22(1):75-84.

257. Rabinow BE. Nanosuspensions in drug delivery. Nature Reviews Drug Discovery. 2004;3(9):785-96.

258. Pathak P, Meziani MJ, Desai T, Sun Y-P. Formation and stabilization of ibuprofen nanoparticles in supercritical fluid processing. The Journal of Supercritical Fluids. 2006;37(3):279-86.

259. Asghari I, Esmaeilzadeh F. Formation of ultrafine deferasirox particles via rapid expansion of supercritical solution (RESS process) using Taguchi approach. International Journal of Pharmaceutics. 2012;433(1-2):149-56.

260. Thakur R, Gupta RB. Formation of phenytoin nanoparticles using rapid expansion of supercritical solution with solid cosolvent (RESS-SC) process. International Journal of Pharmaceutics. 2006;308(1-2):190-9.

261. Hezave AZ, Esmaeilzadeh F. Micronization of drug particles via RESS process. The Journal of Supercritical Fluids. 2010;52(1):84-98.

262. Baseri H, Lotfollahi MN. Formation of gemfibrozil with narrow particle size distribution via rapid expansion of supercritical solution process (RESS). Powder Technology. 2013;235(0):677-84.

263. Merisko-Liversidge E, Liversidge GG, Cooper ER. Nanosizing: a formulation approach for poorly-water-soluble compounds. European Journal of Pharmaceutical Sciences. 2003;18(2):113-20.

264. Peukert W, Schwarzer H-C, Stenger F. Control of aggregation in production and handling of nanoparticles. Chemical Engineering and Processing: Process Intensification. 2005;44(2):245-52.

265. Kesisoglou F, Panmai S, Wu Y. Nanosizing — Oral formulation development and biopharmaceutical evaluation. Advanced Drug Delivery Reviews. 2007;59(7):631-44.

266. Choi J-Y, Yoo JY, Kwak H-S, Uk Nam B, Lee J. Role of polymeric stabilizers for drug nanocrystal dispersions. Current Applied Physics. 2005;5(5):472-4.

267. Lee J, Choi JY, Park CH. Characteristics of polymers enabling nano-comminution of water-insoluble drugs. International Journal of Pharmaceutics. 2008;355(1-2):328-36.

268. Ploehn HJ, Russel WB. Interactions Between Colloidal Particles and Soluble Polymers. In: James W, editor. Advances in Chemical Engineering. Volume 15: Academic Press; 1990. p. 137-228.

269. Lerner V. High-dose olanzapine for treatment-refractory schizophrenia. Clinical Neuropharmacology. 2003;26(2):58-61.

270. Lipkovich I, Deberdt W, Csernansky JG, Buckley P, Peuskens J, Kollack-Walker S, et al. Predictors of risk for relapse in patients with schizophrenia or schizoaffective disorder during olanzapine drug therapy. Journal of Psychiatric Research. 2007;41(3-4):305-10.

271. Sonaglio D, Bataille B, Ortigosa C, Jacob M. Factorial design in the feasibility of producing Microcel MC 101 pellets by extrusion/spheronization. International Journal of Pharmaceutics. 1995;115(1):53-60.

272. Fielden KE, Newton JM, Rowe RC. A comparison of the extrusion and spheronization behaviour of wet powder masses processed by a ram extruder and a cylinder extruder. International Journal of Pharmaceutics. 1992;81(2–3):225-33.

273. Leonardi D, Barrera MG, Lamas MC, Salomón CJ. Development of prednisone: Polyethylene glycol 6000 fast-release tablets from solid dispersions: Solid-state characterization, dissolution behavior, and formulation parameters. AAPS PharmSciTech. 2007;8(4):221-8.

274. Pinto JF, Lameiro MH, Martins P. Investigation on the co-extrudability and spheronization properties of wet masses. International Journal of Pharmaceutics 2001;227(1-2):71-80.

275. Kim Y-s, Paskow HC, Rousseau RW. Propagation of Solid-State Transformations by Dehydration and Stabilization of Pseudopolymorphic Crystals of Sodium Naproxen. Crystal Growth & Design. 2005;5(4):1623-32.

276. Byrn SR, Lin CT. Letter: The effect of crystal packing and defects on desolvation of hydrate crystals of caffeine and L-(--)-1,4-cyclohexadiene-1-alanine. Journal of the American Chemical Society. 1976;98(13):4004-5.

277. Jorgensen AC, Luukkonen P, Rantanen J, Schaefer T, Juppo AM, Yliruusi J. Comparison of torque measurements and near-infrared spectroscopy in characterization of a wet granulation process. Journal of Pharmaceutical Sciences 2004;93(9):2232-43.

278. Knight PE, Podczeck F, Newton JM. The rheological properties of modified microcrystalline cellulose containing high levels of model drugs. Journal of Pharmaceutical Sciences. 2009;98(6):2160-9.

279. Jorgensen A, Rantanen J, Karjalainen M, Khriachtchev L, Rasanen E, Yliruusi J. Hydrate formation during wet granulation studied by spectroscopic methods and multivariate analysis. Pharmaceutical Research. 2002;19(9):1285-91.

References

280. Tian F, Zhang F, Sandler N, Gordon KC, McGoverin CM, Strachan CJ, et al. Influence of sample characteristics on quantification of carbamazepine hydrate formation by X-ray powder diffraction and Raman spectroscopy. European journal of pharmaceutics and biopharmaceutics : official journal of Arbeitsgemeinschaft fur Pharmazeutische Verfahrenstechnik eV. 2007;66(3):466-74.

281. Jørgensen A, Rantanen J, Karjalainen M, Khriachtchev L, Räsänen E, Yliruusi J. Hydrate Formation During Wet Granulation Studied by Spectroscopic Methods and Multivariate Analysis. Pharmaceutical Research. 2002;19(9):1285-91.

282. Simonelli AP, Mehta SC, Higuchi WI. Inhibition of sulfathiazole crystal growth by polyvinylpyrrolidone. J Pharm Sci. 1970;59(5):633-8.

283. Majidi S, Motlagh GH, Bahramian B, Kaffashi B, Nojoumi SA, Haririan I. Rheological evaluation of wet masses for the preparation of pharmaceutical pellets by capillary and rotational rheometers. Pharmaceutical development and technology. 2013;18(1):112-20.

284. Wu S. Calculation of interfacial tension in polymer systems. Journal of Polymer Science Part C: Polymer Symposia. 1971;34(1):19-30.

285. Wikström H, Rantanen J, Gift AD, Taylor LS. Toward an Understanding of the Factors Influencing Anhydrate-to-Hydrate Transformation Kinetics in Aqueous Environments. Crystal Growth & Design. 2008;8(8):2684-93.

286. Cardew PT, Davey RJ. The Kinetics of Solvent-Mediated Phase Transformations1985 1985-04-09 00:00:00. 415-28 p.

287. Otsuka M, Ishii M, Matsuda Y. Effect of surface-modification on hydration kinetics of nitrofurantoin anhydrate. Colloids and Surfaces B: Biointerfaces. 2002;23(1):73-82.

288. Thakuria R, Nangia A. Polymorphic form IV of olanzapine. Acta crystallographica Section C, Crystal structure communications. 2011;67(Pt 11):o461-3.

289. Turnbull D, Fisher JC. Rate of Nucleation in Condensed Systems. The Journal of Chemical Physics. 1949;17(71).

290. Raghavan SL, Trividic A, Davis AF, Hadgraft J. Crystallization of hydrocortisone acetate: influence of polymers. International Journal of Pharmaceutics. 2001;212(2):213-21.

291. Aaltonen J, Heinanen P, Peltonen L, Kortejarvi H, Tanninen VP, Christiansen L, et al. In situ measurement of solvent-mediated phase transformations during dissolution testing. Jounal of Pharmaceutical Sciences. 2006;95(12):2730-7.